T H E U N I V E R S I T Y O F T U L S A

THE GRADUATE SCHOOL

UNIFIED TRANSIENT MODEL FOR GAS-OIL-WATER FLOW IN WELLS AND PIPELINES

by
Fahad B. A. Almudairis

A Dissertation submitted in partial fulfillment of

the requirements for the degree of Doctor of Philosophy

in the Discipline of Petroleum Engineering

The Graduate School

The University of Tulsa

2018

T H E U N I V E R S I T Y O F T U L S A

THE GRADUATE SCHOOL

UNIFIED TRANSIENT MODEL FOR GAS-OIL-WATER FLOW IN WELLS AND PIPELINES

by
Fahad B. A. Almudairis

A DISSERTATION

APPROVED FOR THE DISCIPLINE OF

PETROLEUM ENGINEERING

By Dissertation Committee

Hong-Quan Zhang, Chair
Mohan Kelkar
Mauricio Prado
Brenton McLaury
Zhihua Wang

COPYRIGHT STATEMENT

ABSTRACT

Fahad B. A. Almudairis (Doctor of Philosophy in Petroleum Engineering)

Unified Transient Model for Gas-Oil-Water Flow in Wells and Pipelines

Directed by Dr. Hong-Quan Zhang

162 pp., Chapter 6: Conclusions and Recommendations

(285 words)

Many transient phenomena are encountered in the oil industry during daily operations. In a production system, transient multiphase flow can be initiated from production rate change, sudden perturbation of steady-state flow, or due to special pipeline geometries such as severe slugging in pipeline-riser system and developing slug flow in hilly-terrain pipelines. Operating a well or a pipeline under these transient conditions can cause significant production fluctuations, and reduce the efficiency of the production system. Therefore, these transient operation processes need to be predicted and analyzed.

This study presents a three-phase gas-oil-water model for the simulation and analysis of various steady-state and transient production processes. In three-phase flow, when the two liquids are separated, the two-phase models cannot be used, and new flow patterns are formed. The new transient mechanistic models are developed based on mass and momentum conservation principles for each flow pattern. The partial differential equations are solved using the finite difference method for both spatial and time discretization. A new solution algorithm is adopted to achieve a stable and full transient model. The flow patterns are determined based on two-phase gas-liquid flow pattern transition criteria along with the oil and water mixing status.

The fluid properties at each time step are calculated using either black oil or compositional model. The additional variables are calculated using closure relationships.

The present model can predict the detailed multiphase flow hydrodynamic behaviors including pressure, temperature, local flow pattern, liquid holdup, and fluid velocities. The present simulator is comprehensive and can be used for various transient phenomena. Moreover, practical situations are considered, including complex pipeline and wellbore geometries, and a wide range of operating conditions. The model is validated through comparisons with experimental results and commercial software simulations.

ACKNOWLEDGEMENTS

Thanks to whom thanks are due. Dr. Hong-Quan Zhang is an exceptional advisor and with his great intellect, insight, knowledge, and kindness deserves most of the credit for the successful completion of this work. I would also like to extend my sincere appreciation for sparing a lot of his time and effort in advising me both professionally and personally.

I am grateful to Dr. Mohan Kelkar, Dr. Mauricio Prado, Dr. Brenton McLaury, and Dr. Zhihua Wang for serving as members of the Dissertation Committee and for offering their valuable input and constructive ideas.

I wish to thank all the Tulsa University Artificial Lift Projects (TUALP) personnel and especially the project assistant, Mrs. Donna Trankley, for her sincerity and continuous care and help.

Kuwait University is acknowledged for the great scholarship, and TUALP members are recognized for their contributions and feedbacks.

Kuwait Oil Company (KOC) is also thanked for providing numerous and valuable data that helped shape and validate this study.

I dedicate this study to my dearest ones—my father, Bader Almudairis, and my brother, Abdullah Almudairis. My daily exchanges with them made the long distance feel like a few miles. I hope this achievement makes them proud.

TABLE OF CONTENTS

LIST OF TABLES

LIST OF FIGURES

CHAPTER 1

INTRODUCTION

Three-phase gas-oil-water flow is a common occurrence in petroleum production and during transportation through wells and pipelines. When the reservoir is depleted with time, water and condensate may increase, resulting in a higher probability of three-phase flow. Three-phase flow may also occur in a thin-pay zone due to a higher potential of water coning or in enhanced oil recovery wells from water injection return. Under certain circumstances such as offshore wells or wells located in unconventional geological areas, three-phase flow cannot be separated until it reaches the gathering station. It is therefore important to understand and predict the behavior of three-phase flow in multiphase systems.

Flow assurance issues associated with multiphase flow are another reason why three-phase flow behavior must be comprehensively understood. These issues—which include hydrate formation, emulsion, wax deposition, and corrosion—have significant impacts on flow performance. Under specific pressures and temperatures, hydrates are formed by the chemical combination of natural gas or light hydrocarbon and water. The presence of water in three-phase flow may create conditions favorable for the formation of hydrates. Hydrate inhibitors such as methanol, glycol, and other alcohols can be injected to prevent the hydrate formation. However, the quantity of inhibitors injected should not affect the flow capacity of the lines. Corrosion is typically found in untreated gas streams. When carbon dioxide (CO_2) or hydrogen sulfide (H_2S) dissolves in water, they form corrosive carbonic acid and cause pipe corrosion. Corrosion inhibitors are the ideal way to maintain the mechanical integrity of the lines. The inhibitors are

usually oil or water-soluble, and it is essential that they come together with the phase in contact with the pipe wall. It is, therefore, extremely important to understand the flow characteristics for three-phase flow, including predicting the flow patterns to help select the appropriate inhibitors.

The addition of a third phase adds new complex flow patterns compared to the two-phase flow. Therefore, despite the practical uses of three-phase flow in the oil industry, the limited range of modeling work available in the literature is not surprising. Several incomplete modeling attempts were initiated to predict three-phase flow behavior. The drawback to these is that they do not consider all the possible three-phase flow patterns that occur, or they use two-phase flow patterns to model three-phase flow. Three-phase experimental findings show that using two-phase assumptions for three-phase flow modeling often leads to inaccurate results. Given the failure of these attempts, this study makes a major contribution to the literature by undertaking a three-phase gas-oil-water model.

Even the two-phase oil/water flow has its own complex flow behavior. Depending on the mixing forces, they can flow in separate layers or one liquid may be dispersed in the other to form an emulsion. When an emulsion is formed, either of the two phases (oil or water) may be continuous and the other dispersed in the form of droplets. In such flow, the physical properties play a crucial role and in either case they can be quite different. Therefore, an accurate determination of these properties including the viscosity of the mixture is extremely important. The mixture viscosity, and consequently the pressure gradient, also changes significantly when phase inversion takes place. Phase inversion is the phenomenon whereby the phases spontaneously exchange roles such that the dispersed phase is inverted to become the continuous phase and vice versa. Still within the stratified flow, the oil/water interface is often concave, and therefore the interfacial shear stress prediction becomes difficult.

More complicated flow characteristics are noticed when three-phase flow behaves in a transient way. Three-phase pipelines are usually planned to operate in the steady-state condition. However, changes in operational conditions, which are frequently encountered, introduce perturbations that affect the flow hydrodynamic behaviors such as pressure, holdups, and velocity distributions as functions of space and time. In this study, several transient phenomena have been simulated, predicted, and analyzed including the sudden perturbation of steady-state flow, severe slugging in pipeline-riser system, gas-lift instabilities, and severe slugging in horizontal wells.

A sudden perturbation of steady-state flow followed by a change in flow rates is the first transient phenomenon under consideration in this study. This behavior is simulated to predict the time it takes to readjust to a steady state again. As mentioned earlier, the occurrence of a three-phase flow due to the sudden inception of water is widely encountered for both the surface pipeline system and well operation. Therefore, water loading and depletion are predicted and evaluated. During the decline stages of oil fields, gas-lift instabilities such as casing heading may take place with another type of transient flow. Casing heading instability occurs when gas is overly injected due to low tubing pressure followed by a decrease or complete cessation of gas injection. These cyclic flow behaviors are simulated and the effects of two factors, including gas injection rate and port size of the gas-lift valve, are presented.

With decreasing gas and liquid flow rates, when an upward riser follows a pipeline section with a downward inclination angle, the tendency for severe slugging increases. Severe slugging, as displayed in Figure 1-1, usually occurs in four stages: slug formation, slug production, blowout, and liquid fallback. The slug formation stage occurs when the liquid begins to accumulate at the riser base due to the relatively low liquid and gas flow rates, consequently

blocking the gas passage. The liquid level in the riser then increases while the blocked gas is accumulated and compressed in the pipeline. The slug formation stage ends when the liquid level reaches the top of the riser, thus initiating the slug production stage. During this stage, the pressurized gas pushes the liquid in the pipeline and moves towards the riser base. When the compressed gas reaches the bottom of the riser, the gas will penetrate the liquid in the riser and promote the blowout. The penetrated gas will reduce the hydrostatic head by decreasing the mixture density. After the compressed gas is exhausted, the liquid film fallback. This cyclic flow behavior of single liquid flow followed by another period of high liquid and gas flow rates can considerably disrupt the surface facilities. For three-phase flow, this transient phenomenon becomes more complicated due to the distribution between the liquid phases. The understanding and prediction of this behavior is also included in this study by comprehensive comparisons with experimental results.

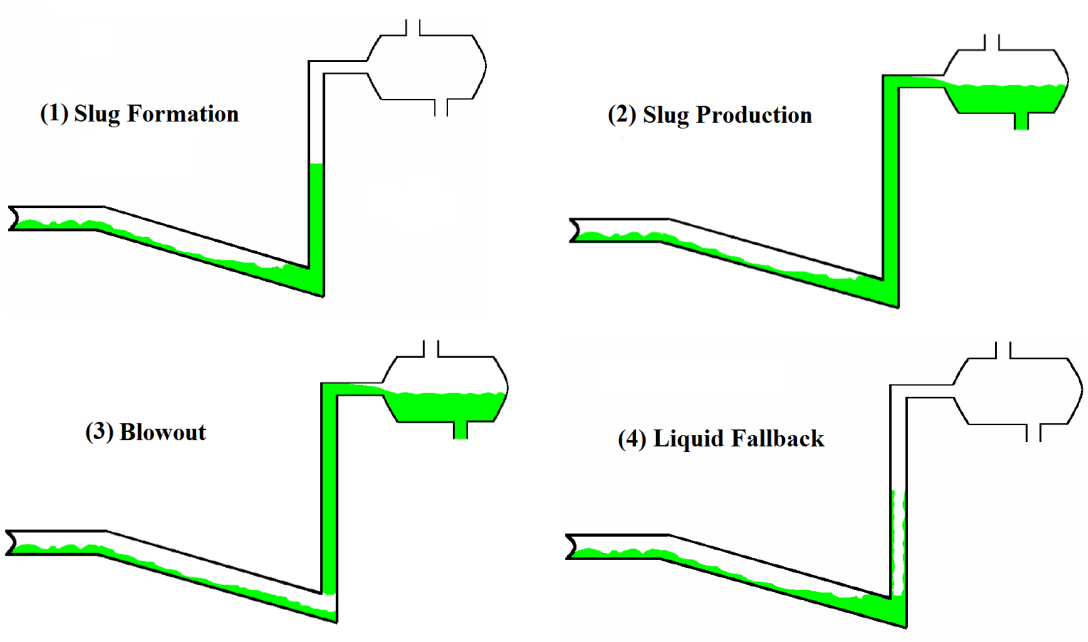

Figure 1-1: Stages for Severe Slugging in Pipeline-Riser System

A hilly-terrain pipeline, as shown in Figure 1-2, is a pipeline consisting of horizontal, upward inclined, and downward inclined sections. The hilly-terrain pipeline and some directional wells both have low spots where liquids may accumulate. The downward flow picks up liquids accumulated at the dip and causes changes in the flow characteristics such as slug initiation or slug growth. The severity of slug characteristic changes depends on pipe geometry and operational conditions. Flow assurance issues can also be induced by the hilly-terrain geometry. When water accumulates because of the downward flow and the falling back liquid from the upward section, the possibility of hydrate formation will increase. Moreover, the turbulence and high shear forces in slug flow can also disturb the corrosion inhibitors and increase damage to the pipelines. The overall flow in the hilly-terrain pipeline is considered a continuous flow. However, the pressure behaves in fluctuation form and the oscillations are primarily due to the slug evolution and flow pattern change. Moreover, the lower elbow that initiates the slugs is considered to be a transient region. Therefore, a transient solution is required to accurately model the behavior. For some unconventional wells, if the flow in the lateral section moves downward and then turns to the upward near vertical well, the flow can behave like severe slugging in pipeline-riser system but with less severity. The main difference revolves around the elimination of slug production and severe blowout stages. Therefore, this cyclic slugging behavior in unconventional wells can be used to mimic the slug evolution behavior, and in this study, it is simulated and is referred as severe slugging in horizontal wells.

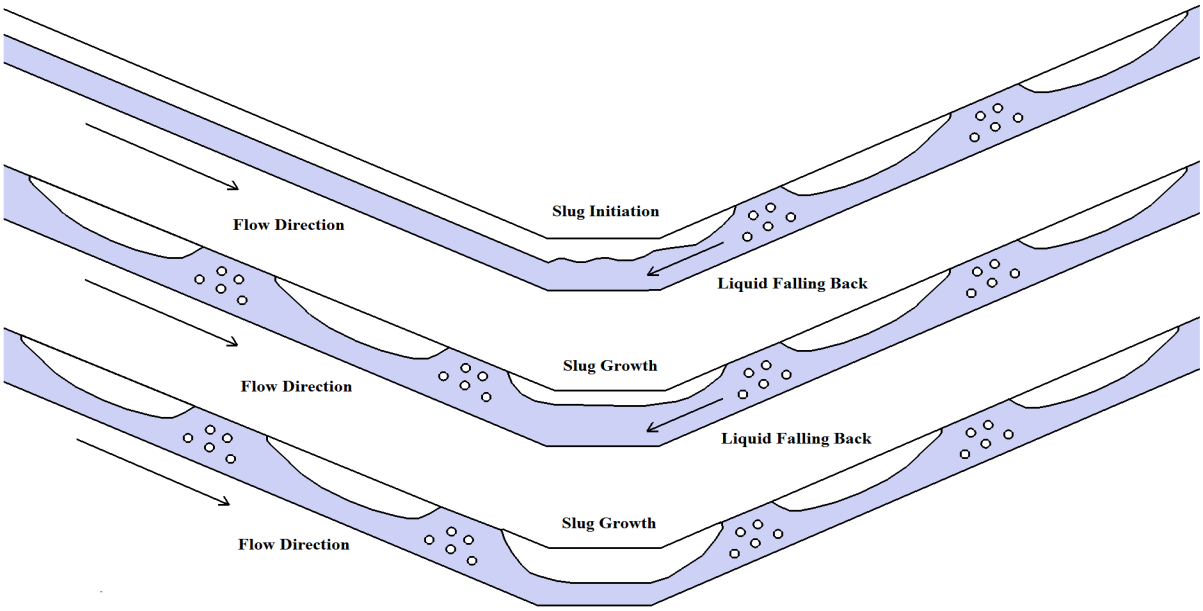

Figure 1-2: Slug Initiation and Growth in Hilly-Terrain Pipelines

Operating a well under fluctuating conditions may cause severe operational problems. The pressure changes and flow oscillations reduce the efficiency of the production system and may cause flooding of surface facilities. In artificial lift, if the parameters of the system vary with time, the production control becomes more difficult and the production target cannot be fulfilled. Therefore, these unstable operating conditions should be predicted to achieve the most productive and cost-effective production system. It is preferable to use a transient simulator to predict and investigate the general principles of unsteady-state flow. A transient simulator can help the production engineers check the stability of their designs, diagnose the instability problems, and rectify them with stabilizing measures.

In this study, a transient unified model is developed to investigate the general principles of three-phase gas-oil-water flow instability. If the two liquids are fully mixed, three-phase flow is treated as gas/liquid two-phase flow. Otherwise, three new flow patterns exist, and mass and momentum conservation equations for each phase in each flow pattern are developed. Figure 1-3

shows when to treat the three-phase flow as a two-phase mixture, and when to use the newly developed models. The set of partial differential equations is discretized using an implicit finite difference numerical scheme. A stable and fully transient model is achieved by introducing a new solution algorithm and iteration procedure. The flow patterns are predicted by combining the two-phase flow pattern transition mechanism and the liquid phases' distribution. Several closure relationships are used to calculate the additional variables in the solution procedure. The proposed model in this study not only predicts the occurrence of the flow instability but also predicts the detailed multiphase flow hydrodynamic behaviors, such as local pressure, flow pattern, liquid holdup, and fluid velocities. Furthermore, practical conditions are incorporated in the developed simulator, namely complex wellbore geometries and a wide range of operating conditions.

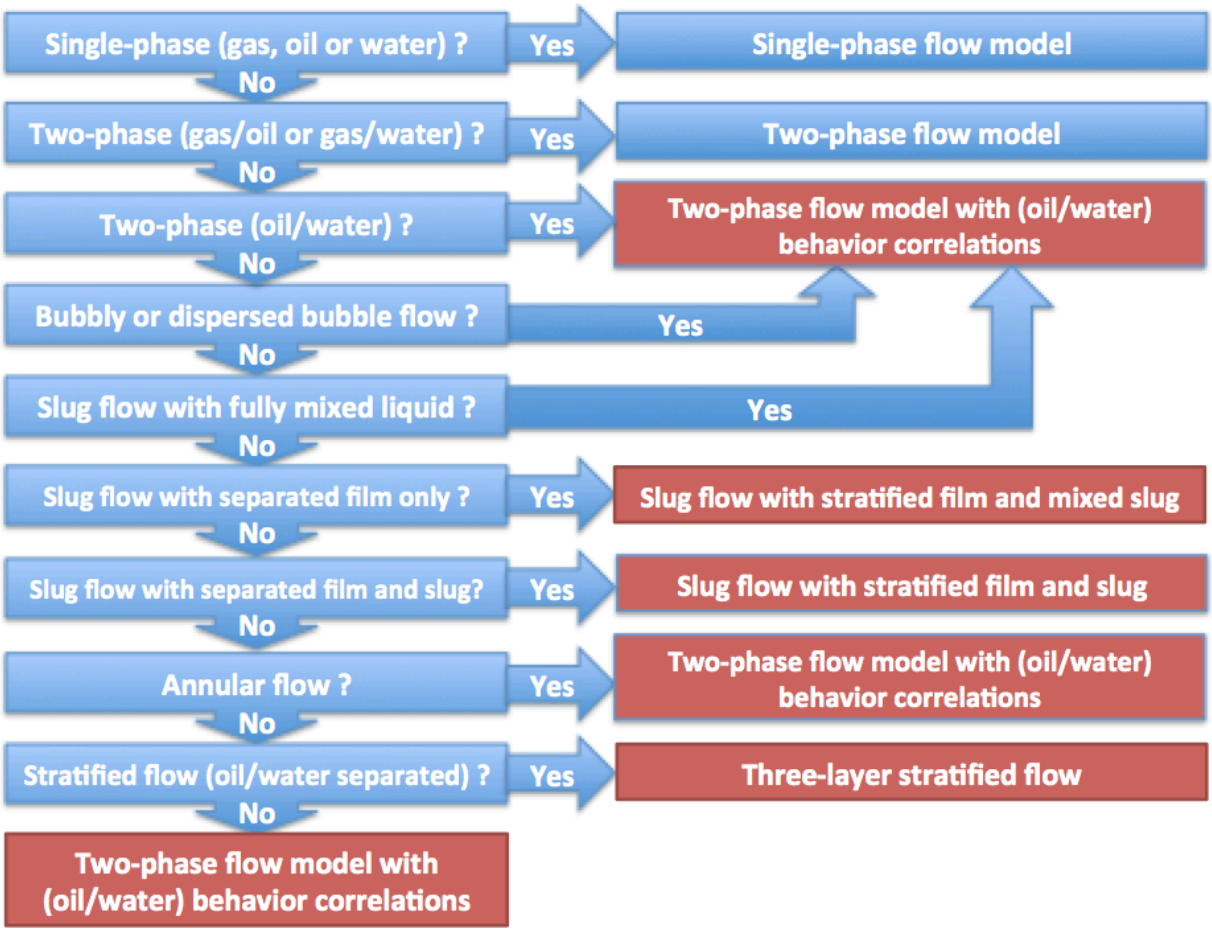

Figure 1-3: Overall Flow Chart for Transient Three-Phase Unified Model

CHAPTER 2

LITERATURE REVIEW

Several studies, including papers, theses, and dissertations, have been published since the 1950s concerning three-phase flow in petroleum production and transportation. Some studies identify the flow patterns, and others develop mechanistic models to predict the flow characteristics. The following is a comprehensive review of selected studies with their advantages and shortcomings.

2.1 Three-Phase Flow Patterns

Sobocinki (1955) was the first experimental study to investigate three-phase flow behavior. In his work, nine different three-phase flow patterns were identified. The experiments were conducted in an 11.6 m long horizontal transparent plastic tube with a 0.079 m ID (Inner Diameter). The superficial velocities ranged between 2.4–16.3 m/s for air, 0.006–0.09 m/s for oil, and 0.002–0.088 m/s for water. Based on gas-liquid and oil-water distributions, the flow patterns are classified as follows:

- Stratified-No liquid mixing
- Ripple-No liquid mixing
- Surface waves-Inception of oil and water mixing
- Light waves-Incipient emulsion
- Waves-Incipient emulsion
- Waves-Partial emulsion

- Heavy waves-Partial emulsion
- Light crests-Emulsion
- Semi annular-Emulsion

The first part of the flow pattern classifications provides the gas-liquid condition, and the second part provides the oil-water condition of the flow. It is clear that the gas-liquid conditions include only different types of stratified flow. Lack of specificity regarding the continuous phase in the oil-water condition is another drawback of this classification.

Açikgöz *et al.* (1992) performed an inclusive experimental study on horizontal three-phase flow. The experiments were conducted in a 5.78 m long horizontal Plexiglas tube with a 19 mm ID. The superficial velocities were between 0.15–50 m/s for gas, 0.043–0.24 m/s for oil, and 0.004–0.66 m/s for water. Listed below are the ten flow patterns that were identified:

- Oil based-Dispersed-Plug flow
- Oil based-Dispersed-Slug flow
- Oil based-Dispersed-Stratified wavy flow
- Oil based-Separated-Stratified wavy flow
- Oil based-Separated-Stratified annular wavy flow
- Oil based-Separated dispersed-Stratifying annular flow
- Water based-Dispersed-Slug flow
- Water based-Dispersed-Stratified wavy flow
- Water based-Separated-Incipient stratifying annular flow
- Water based-Dispersed-Stratifying annular flow

The first part of the flow pattern classifications was based on the liquid-wall relationship—whether it is oil-based or water-based. The second part was based on the liquid-

liquid relationship, and the third part was based on the gas-liquid relationship. Although the third part includes six different configurations, it covers only some of the gas-liquid flow patterns.

Pan (1996) employed an approach similar to the one used by Açikgöz *et al*. (1992), but with a different classification order. The experiments were performed in a 38 m long horizontal stainless-steel pipe with a 77.92 mm ID. Eight flow patterns were identified which are listed below:

- Separated-Stratified flow
- Separated-Slug flow
- Dispersed-Oil continuous-Stratified flow
- Dispersed-Oil continuous-Slug flow
- Dispersed-Oil continuous-Annular flow
- Dispersed-Water continuous-Stratified flow
- Dispersed-Water continuous-Slug flow
- Dispersed-Water continuous-Annular flow

The classification started with a liquid-liquid relationship instead of a liquid-wall relationship. The second part was based on a liquid-wall relationship, whether the continuous phase is oil or water, and the third part was based on a two-phase gas-liquid relationship. Pan presented fifteen flow patterns, but only eight were observed during the experiments.

Woods *et al.* (1998) carried out the first comprehensive study on three-phase vertical flow. The experiments were conducted in a 0.026 m ID vertical Perspex pipe. The flow rates were up to 0.02 m^3/s for air, 0.00015 m^3/s for water, and 0.0001 m^3/s for oil. The flow patterns were divided into two main classes: oil dominated (OD) flow (as shown in Figure 2-1) and water dominated (WD) flow (as shown in Figure 2-2).

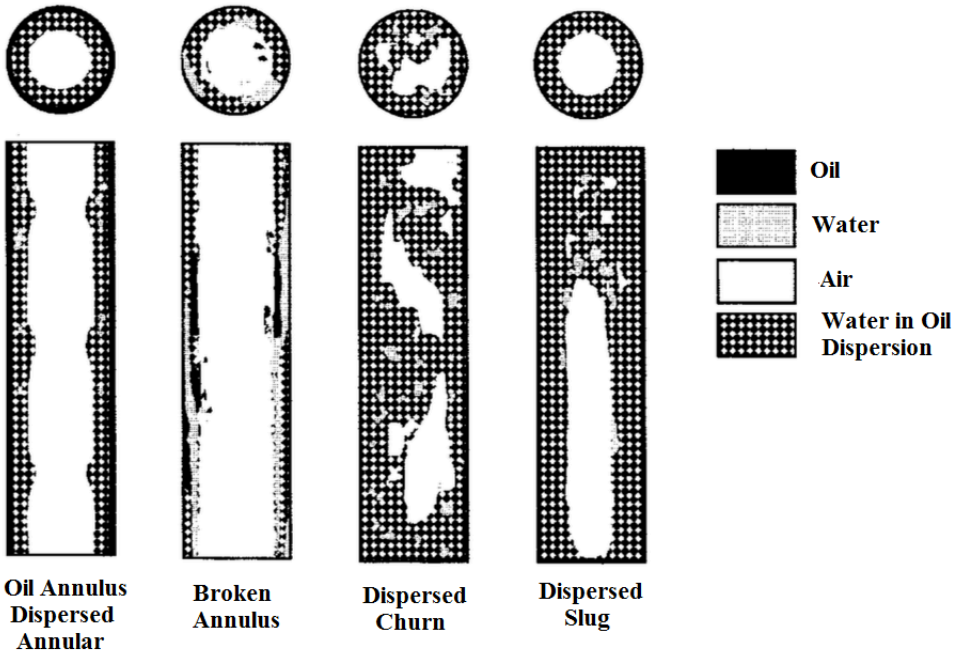

Figure 2-1: Oil Dominated Flow Regimes in Vertical Three-Phase Flow (Woods *et al.*, 1998)

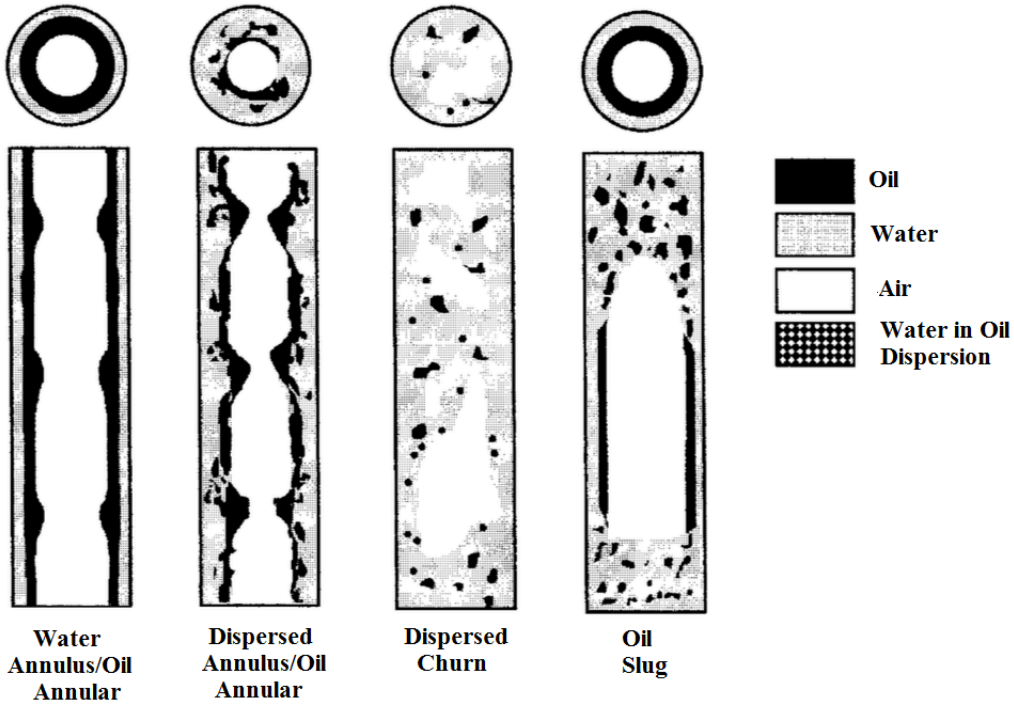

Figure 2-2: Water Dominated Flow Regimes in Vertical Three-Phase Flow (Woods *et al.*, 1998)

Oddie *et al.* (2003) conducted steady-state and transient experiments for multiphase gas-water, oil-water, and gas-oil-water flows. The pipe deviated from 0^o (upwards vertical) to 92^o (slightly downward), and the experiments were performed through a transparent 11 m long pipe with a 150 mm ID. Several flow rates for each phase were applied over wide ranges. For two-phase oil/water flows, three flow patterns were observed, as listed below:

- Dispersed/homogeneous
- Mixed/semi-mixed
- Segregated/semi-segregated flows

For gas-water and gas-oil-water, the flow patterns were:

- Bubble
- Churn
- Elongated-bubble
- Slug
- Stratified/stratified-wavy

Based on the experimental results, detailed flow pattern maps were generated over the entire range of flow rates and pipe inclinations for all the fluid systems.

Keskin *et al.* (2007) provided the most comprehensive classification of three-phase flow patterns. Three-phase gas-oil-water experiments were conducted in horizontal pipes at different water cuts. The superficial velocities ranged between 0.1–7.0 m/s for gas, 0.02–1.5 m/s for oil, and 0.01–1.0 m/s for water. Twelve flow patterns were identified and classified based on a combination of gas-liquid and oil-water distributions. The sketches of the flow patterns are displayed in Figure 2-3, Figure 2-4, and Figure 2-5.

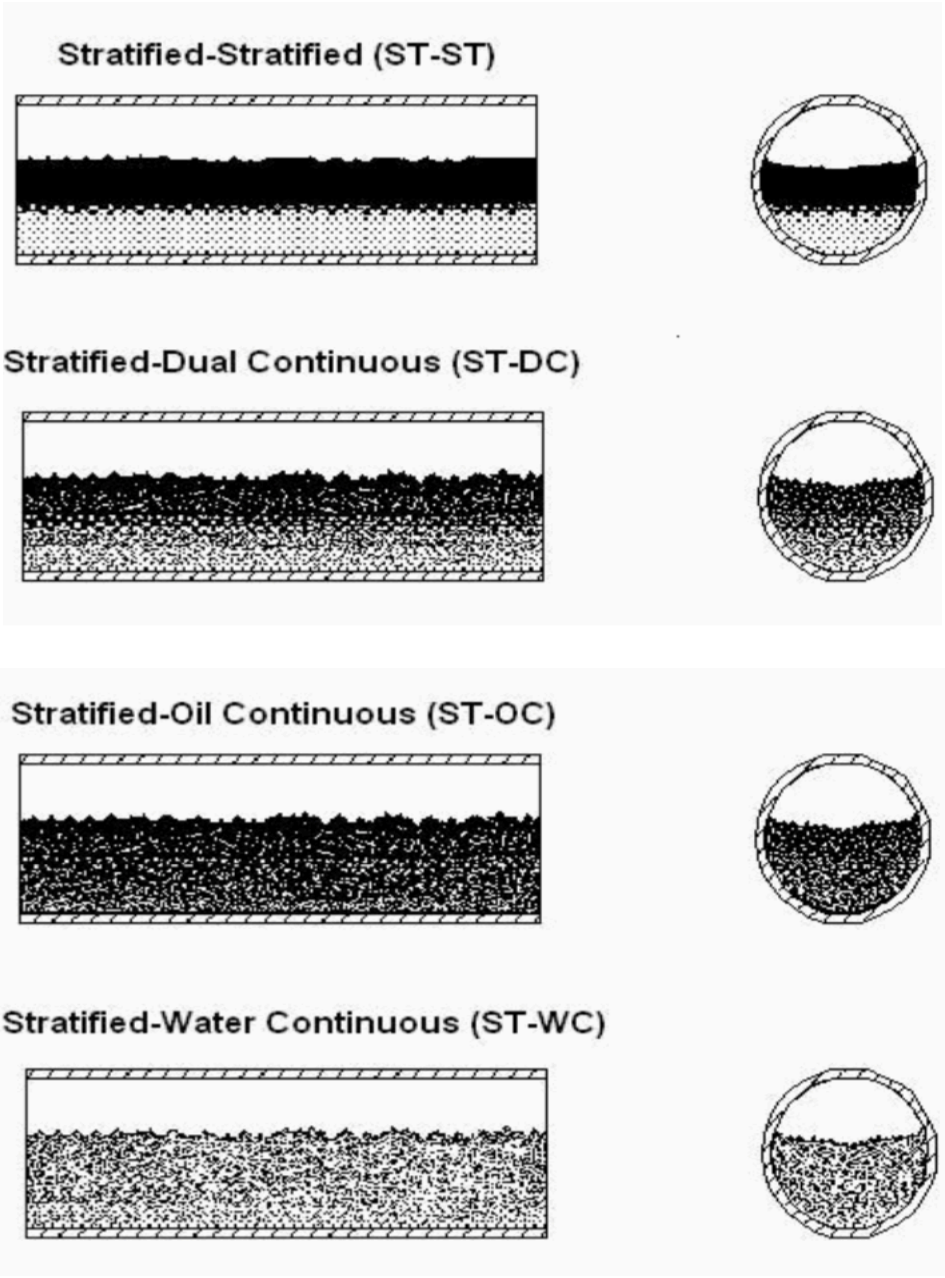

Figure 2-3: Stratified Gas-Oil-Water Flow Patterns (Keskin *et al.*, 2007)

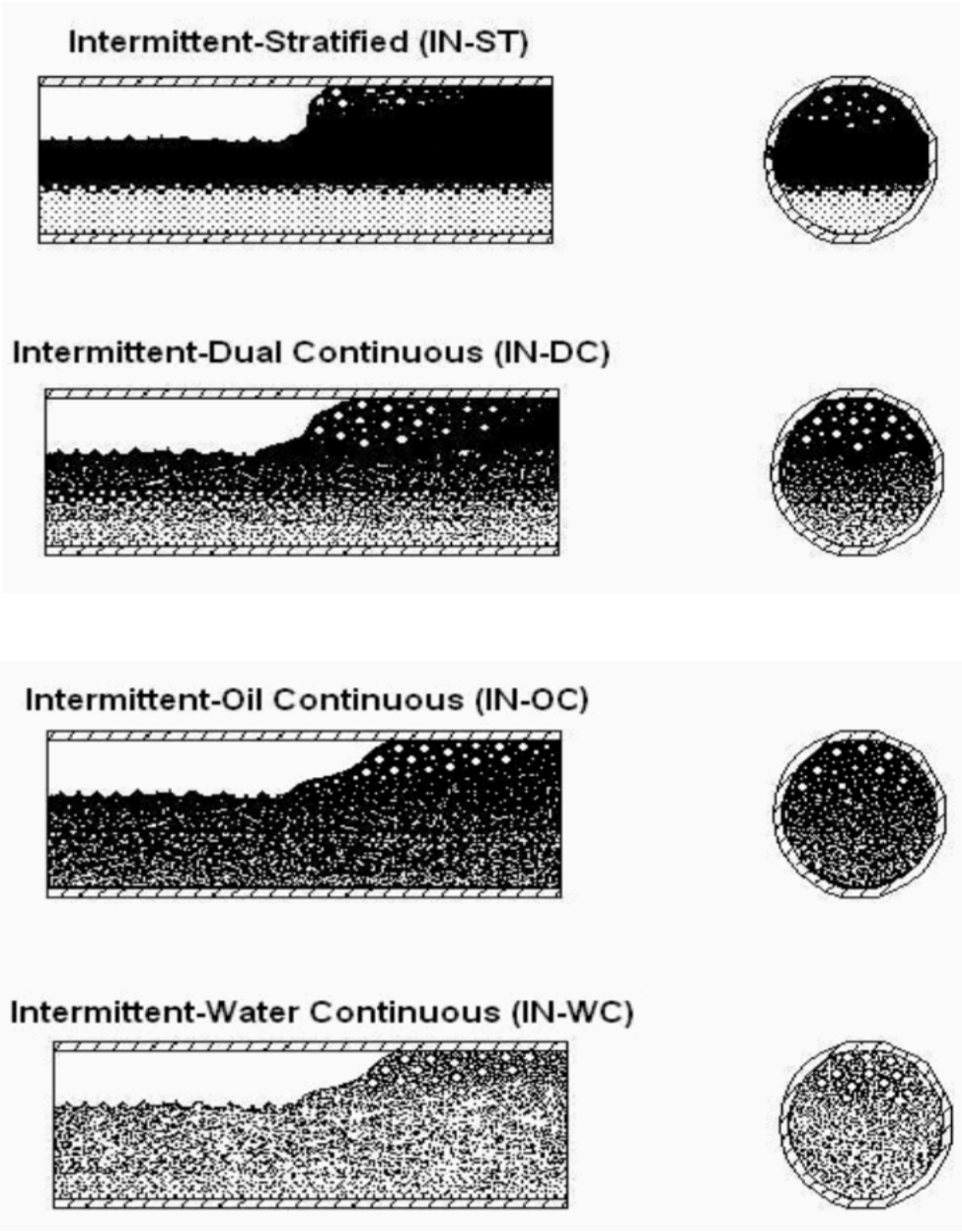

Figure 2-4: Intermittent Gas-Oil-Water Flow Patterns (Keskin *et al.*, 2007)

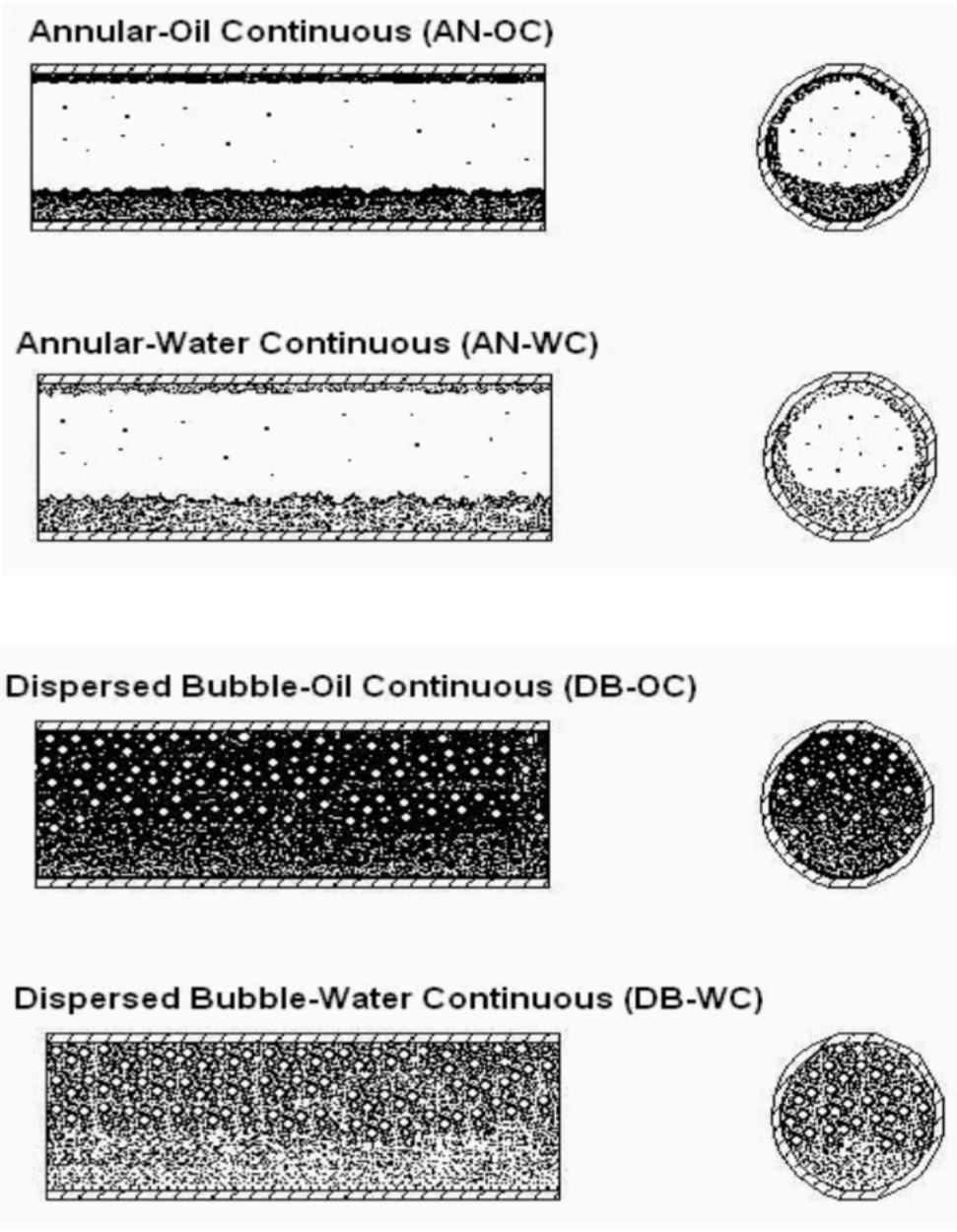

Figure 2-5: Annular and Dispersed Gas-Oil-Water Flow Patterns (Keskin *et al.*, 2007)

2.2 Three-Phase Modeling

Several studies have been conducted to model the three-phase flow behavior. Most of these studies were designed to estimate the steady-state flow characteristics. Moreover, they were developed for either a specific inclination angle or for a specific flow pattern.

Taitel *et al.*'s (1995) study was one of the first attempts to model three-phase flow. They considered three-phase stratified flow in horizontal pipes using momentum balance equations for each phase. The momentum equations for water, oil, and gas can be written as

$$-A_W\left(\frac{dp}{dx}\right)-\tau_W S_W+\tau_i S_i-\rho_W A_W g\sin\beta=0, \tag{2-1}$$

$$-A_O\left(\frac{dp}{dx}\right)-\tau_O S_O-\tau_i S_i+\tau_j S_j-\rho_O A_O g\sin\beta=0, \tag{2-2}$$

and

$$-A_G\left(\frac{dp}{dx}\right)-\tau_G S_G-\tau_j S_j-\rho_G A_G g\sin\beta=0, \tag{2-3}$$

where A is cross sectional-area, ρ is density, p is pressure, and β is the inclination angle, which is positive for upward inclination. The subscript W stands for water, O stands for oil, and G stands for gas. τ_W is the shear stress acting on the wall wetted by the water perimeter S_W, τ_O is the shear stress acting on the wall wetted by the oil perimeter S_O, τ_G is the shear stress acting on the wall wetted by the gas perimeter S_G, τ_i is the shear stress acting on the oil-water interface S_i, and τ_j is the shear stress acting on the oil-gas interface S_j.

The momentum equation for the liquid phase can be computed by summing Eq. (2-1) and Eq. (2-2) as

$$-\left(\frac{dp}{dx}\right)-\frac{\tau_L S_L}{A_L}+\frac{\tau_j S_j}{A_L}-\rho_L g\sin\beta=0, \tag{2-4}$$

where

$$\tau_L S_L = \tau_W S_W + \tau_O S_O, \tag{2-5}$$

$$\rho_L = \frac{\rho_W A_W + \rho_O A_O}{A_L}, \tag{2-6}$$

and

$$A_L = A_W + A_O. \tag{2-7}$$

The combined momentum equation for the gas and liquid streams can be obtained by eliminating the pressure drop from Eq. (2-4) and Eq. (2-3) as

$$-\frac{\tau_L S_L}{A_L} + \frac{\tau_G S_G}{A_G} + \tau_j S_j \left(\frac{1}{A_L} + \frac{1}{A_G}\right) - \left(\rho_L - \rho_G\right) g \sin\beta = 0. \tag{2-8}$$

Another combined momentum equation for oil and water streams can be obtained from the momentum equations Eq. (2-1) and Eq. (2-2) as

$$-\frac{\tau_W S_W}{A_W} + \frac{\tau_O S_O}{A_O} - \frac{\tau_j S_j}{A_O} + \tau_i S_i \left(\frac{1}{A_W} + \frac{1}{A_O}\right) - \left(\rho_W - \rho_O\right) g \sin\beta = 0. \tag{2-9}$$

Eq. (2-8) and Eq. (2-9) can be solved simultaneously to obtain the liquid level height h_L at a given set of flow rates. Three theoretical steady-state liquid level solutions for stratified flow can be estimated, but the only realistic one is the solution with the lowest liquid level. The transition from stratified flow to slug or annular flow was modeled based on liquid level instability. This model can only be applied to a specific inclination angle range and flow pattern. Additionally, the criterion for the transition from three-phase stratified flow is valid only at low gas flow rates.

Khor *et al.* (1997) extended the three-phase stratified flow model developed by Taitel *et al.* (1995) using different options for shear stresses and friction relationships. The different models vary in the choice of equations used for calculating the shear stress and hence in the method of solution. Although the fluid surfaces in three-phase stratified flow are highly

disturbed, Khor *et al.* consider this to be flat for the sake of simplicity. For gas-wall shear stress, the standard Blasius (1913) expression is recommended for smooth pipes as it requires less computational time in general with good accuracy. For turbulent flow, Blasius equation can be given by

$$f_k = 0.046\, Re_k^{-0.2}, \tag{2-10}$$

and for laminar flow,

$$f_k = 16 / Re_k, \tag{2-11}$$

where the subscript k indicates gas, oil, or water; f_k is phase friction factor; and the phase Reynolds number can be defined as

$$Re_k = \frac{u_k D_k \rho_k}{\eta_k}, \tag{2-12}$$

where ρ_k is the phase density, η_k is the phase viscosity, u_k is the phase velocity, and D_k is the hydraulic diameter of the region occupied by the phase. For rough pipes, however, the Blasius (1913) expression could not apply. For oil-wall and water-wall shear stresses, it was recommended that the Srichai (1994) relationships should be used for better predictions. The friction factor equation is given by

$$f_{oorw} = 0.765\left(\varepsilon_{oorw}\, Re_{oorw}\right)^{-0.562}, \tag{2-13}$$

where ε_{oorw} is the fraction of the relevant liquid phase and Re_{oorw} is the Reynolds number calculated from

$$Re_{oorw} = \frac{u_{oorw} D_{oorw} \rho_{oorw}}{\eta_{oorw}}. \tag{2-14}$$

For gas-oil interfacial shear stress, it is recommended that the relationship of Hart *et al.* (1989) be used. They took into account the wetted wall fraction, ϕ, to modify the gas-liquid

interfacial friction factor for three-phase flow. The wetted wall fraction as a function of Froude number, Fr_o, can be written as

$$\phi = 0.52\varepsilon_L^{0.374} + 0.26Fr_o^{0.58}, \tag{2-15}$$

where

$$Fr_o = \frac{\rho_o}{\left(\rho_o - \rho_G\right)}\frac{u_o^2}{gD} \tag{2-16}$$

and

$$\varepsilon_L = \varepsilon_w + \varepsilon_o. \tag{2-17}$$

The interfacial roughness, k_i, is calculated from

$$k_i = 2.3\frac{\varepsilon_L D}{4\phi}. \tag{2-18}$$

Finally, the interfacial friction factor, f_i, is determined from either the implicit Colebrook (1939) equation:

$$\frac{1}{\sqrt{f_k}} = 3.48 - 4.0\log_{10}\left[\frac{2k_s}{D} + \frac{9.35}{Re_k\sqrt{f_k}}\right], \tag{2-19}$$

or the explicit form developed by Eck (1973):

$$f_k = \frac{0.0625}{\left[\log_{10}\left\{15/Re_G + \frac{k_s}{D}/3.715\right\}\right]^2}. \tag{2-20}$$

The oil-water interfacial shear stress can be given with the straightforward approach recommended by Taitel *et al.* (1995), which uses a fixed value of 0.014.

Bonizzi and Issa (2003) developed a transient three-phase model to simulate stratified and slug flows in horizontal or nearly horizontal pipes. The idea was based on the two-fluid model along with a drift-flux model to combine the two sets of liquid equations into one. Using a

drift-flux approach allows the reduction of the number of transport equations from six to five. The five transport equations can be written as

- Gas continuity equation:

$$\frac{\partial\left(\rho_G \alpha_G\right)}{\partial t}+\frac{\partial\left(\rho_G \alpha_G u_G\right)}{\partial x}=0, \tag{2-21}$$

- Liquid phase (mixture) continuity equation:

$$\frac{\partial\left(\rho_M \alpha_M\right)}{\partial t}+\frac{\partial\left(\rho_M \alpha_M u_M\right)}{\partial x}=0, \tag{2-22}$$

- Water-cut transport equation:

$$\frac{\partial\left(\rho_W c_W \alpha_M\right)}{\partial t}+\frac{\partial\left(\rho_W c_W \alpha_M u_W\right)}{\partial x}=0, \tag{2-23}$$

- Gas momentum equation:

$$\frac{\partial\left(\rho_G \alpha_G u_G\right)}{\partial t}+\frac{\partial\left(\rho_G \alpha_G u_G^2\right)}{\partial x}=-\alpha_G \frac{\partial p}{dx}-\alpha_G \rho_G g \sin\beta-\frac{\tau_{GL} S_{GL}}{A}-\frac{\tau_{WG} S_G}{A}, \tag{2-24}$$

- Liquid phase (mixture) momentum equation:

$$\begin{aligned}\frac{\partial\left(\rho_M \alpha_M u_M\right)}{\partial t}+\frac{\partial\left(\rho_M \alpha_M u_M^2\right)}{\partial x}=&-\alpha_M \frac{\partial p}{dx}-\alpha_M \rho_M g \frac{\partial h}{dx}\cos\beta-\alpha_M \rho_M g \sin\beta \\ &+\frac{\tau_{GL} S_{GL}}{A}-\frac{\sum_{K=1}^{N} \tau_{WK} S_K}{A}+\Omega+\Psi,\end{aligned} \tag{2-25}$$

where the subscripts *G*, *M*, and *W* refer to the gas, mixture, and water phases respectively, the phase fraction is α, the liquid-cut is *c*, the height of the liquid-mixture is *h*, and the liquid–gas interfacial chord is S_{GL}. The index *N* in the summation represents the number of liquid phases in contact with the pipe wall. For oil and water stratified flow, it becomes 2 and for dispersed flow it becomes 1. The terms Ω and ψ in Eq. (2-25) are given by

$$\Omega = -\frac{\partial}{\partial x}\left[\frac{\alpha_M c_W \left(1-c_W\right)\rho_W \rho_O u_s^2}{\rho_M}\right] \tag{2-26}$$

and

$$\Psi = \alpha_M \left(\rho_M - \rho_O\right) g \cos\beta \frac{\partial h}{\partial x} - \alpha_W \left(\rho_W - \rho_O\right) g \cos\beta \frac{\partial h_W}{\partial x}, \tag{2-27}$$

where u_s is the slip velocity between the liquid phases. The derivatives of the liquid height in Eq. (2-27) can be given by

$$\frac{\partial h}{\partial x} = \frac{\pi D}{4\sin\left(\gamma/2\right)} \frac{\partial \alpha_M}{\partial x} \tag{2-28}$$

and

$$\frac{\partial h_W}{\partial x} = \frac{\pi D}{4\sin\left(\gamma_W/2\right)} \frac{\partial \alpha_W}{\partial x}, \tag{2-29}$$

where γ and γ_W are the stratification angles for the total liquid and water layers, respectively.

The transport equations are solved numerically using a previously developed simulator for two-phase slug flow. The model can predict whether the two liquids are segregated or fully dispersed based on the prediction of the maximum liquid droplet size that is generated under local flow conditions. They also investigated the effect of the superficial gas velocity on the phase inversion. It has been found that when gas flow rate is increased, the phase inversion would shift towards higher water-cuts.

Zhang and Sarica (2006) extended the two-phase unified model by Zhang *et al.* (2003) to a three-phase model. This model describes three-phase flow distributions based on gas-liquid flow pattern and oil-water mixing status. The three-phase continuity and momentum equations are developed for new flow patterns. For slug flow with stratified oil and water, the continuity equations for the oil, water, and gas phases in the film zone can be obtained, respectively, as

$$\left(1-H_{WGS}\right)\left(1-\alpha_{OS}\right)\left(v_T-v_{OS}\right)=H_{OF}\left(v_T-v_{OF}\right), \tag{2-30}$$

$$H_{WGS}\left(1-\alpha_{WS}\right)\left(v_T-v_{WS}\right)=H_{WF}\left(v_T-v_{WF}\right), \tag{2-31}$$

and

$$\left(1-H_{WGS}\right)\alpha_{OS}\left(v_T-v_{OS}\right)+H_{WGS}\alpha_{WS}\left(v_T-v_{WS}\right)=\left(1-H_{OF}-H_{WF}\right)\left(v_T-v_G\right). \tag{2-32}$$

The momentum equations for the oil film, water film, and the gas pocket in the gas-pocket region can be written as

$$\frac{\left(p_2-p_1\right)}{l_F}=\frac{\rho_O\left(v_T-v_{OF}\right)\left(v_{OS}-v_{OF}\right)}{l_F}+\frac{\tau_{I1}S_{I1}-\tau_{I2}S_{I2}-\tau_{OF}S_{OF}}{H_{OF}A}-\rho_O g\sin\theta, \tag{2-33}$$

$$\frac{\left(p_2-p_1\right)}{l_F}=\frac{\rho_W\left(v_T-v_{WF}\right)\left(v_{WS}-v_{WF}\right)}{l_F}+\frac{\tau_{I2}S_{I2}-\tau_{WF}S_{WF}}{H_{WF}A}-\rho_W g\sin\theta, \tag{2-34}$$

and

$$\frac{\left(p_2-p_1\right)}{l_F}=-\frac{\tau_{I1}S_{I1}+\tau_G S_G}{\left(1-H_{OF}-H_{WF}\right)A}-\rho_G g\sin\theta. \tag{2-35}$$

Because the gas density is much lower than the liquid density, the momentum exchange for the gas pocket momentum equation has been removed. Similarly, for stratified oil and water flows in the slug body, the momentum equations for oil and water respectively can be obtained as

$$\frac{\left(p_2-p_1\right)}{l_S}=\frac{\rho_O\left(v_T-v_{OS}\right)\left(v_{OF}-v_{OS}\right)}{l_S}-\frac{\tau_{I0}S_{I0}+\tau_{OS}S_{OS}}{\left(1-H_{WGS}\right)A}-\rho_O g\sin\theta \tag{2-36}$$

and

$$\frac{\left(p_2-p_1\right)}{l_S}=\frac{\rho_W\left(v_T-v_{WS}\right)\left(v_{WF}-v_{WS}\right)}{l_S}+\frac{\tau_{I0}S_{I0}-\tau_{WS}S_{WS}}{H_{WGS}A}-\rho_W g\sin\theta. \tag{2-37}$$

Two combined momentum equations can be obtained for gas and liquid streams and for oil and water streams in the gas-pocket region from Eq. (2.33), Eq. (2.34), and Eq. (2-35). They can be given, respectively, as

$$\begin{aligned}&\frac{\rho_O H_{OF}\left(v_T - v_{OF}\right)\left(v_{OS} - v_{OF}\right) + \rho_W H_{WF}\left(v_T - v_{WF}\right)\left(v_{WS} - v_{WF}\right)}{l_F\left(H_{WF} + H_{OF}\right)} \\ &- \frac{\tau_{OF} S_{OF} + \tau_{WF} S_{WF}}{\left(H_{OF} + H_{WF}\right) A} + \frac{\tau_{I1} S_{I1}}{A}\left(\frac{1}{H_{OF} + H_{WF}} + \frac{1}{1 - H_{OF} - H_{WF}}\right) \\ &+ \frac{\tau_C S_C}{\left(1 - H_{OF} - H_{WF}\right) A} - \left(\frac{\rho_O H_{OF} + \rho_W H_{WF}}{H_{OF} + H_{WF}} - \rho_G\right) g \sin\theta = 0\end{aligned} \tag{2-38}$$

and

$$\begin{aligned}&\frac{\rho_W\left(v_T - v_{WF}\right)\left(v_{WS} - v_{WF}\right) - \rho_O\left(v_T - v_{OF}\right)\left(v_{OS} - v_{OF}\right)}{l_F} \\ &- \frac{\tau_{WF} S_{WF}}{H_{WF} A} + \frac{\tau_{OF} S_{OF} - \tau_{I1} S_{I1}}{H_{OF} A} + \frac{\tau_{I2} S_{I2}}{A}\left(\frac{1}{H_{WF}} + \frac{1}{H_{OF}}\right) - \left(\rho_W - \rho_O\right) g \sin\theta = 0.\end{aligned} \tag{2-39}$$

One more combined momentum equation can be obtained for the slug body from Eq. (2-36) and Eq. (2-37) as

$$\begin{aligned}&\frac{\rho_W\left(v_T - v_{WS}\right)\left(v_{WF} - v_{WS}\right) - \rho_O\left(v_T - v_{OS}\right)\left(v_{OF} - v_{OS}\right)}{l_S} \\ &- \frac{\tau_{WS} S_{WS}}{H_{WGS} A} + \frac{\tau_{OS} S_{OS}}{\left(1 - H_{WGS}\right) A} + \frac{\tau_{I0} S_{I0}}{A}\left[\frac{1}{H_{WGS}} + \frac{1}{\left(1 - H_{WGS}\right)}\right] - \left(\rho_W - \rho_O\right) g \sin\theta = 0.\end{aligned} \tag{2-40}$$

In the above equations, the unknowns are calculated using both the continuity and combined momentum equations. For three-layer stratified flow, the combined momentum equations for gas and liquid streams and for oil and water streams can be obtained if the momentum-exchange terms are removed from Eq. (2-38) and Eq. (2-39). The two-phase oil-water stratified flow has one combined momentum equation for oil and water streams and is obtained if the momentum-exchange term is removed from Eq. (2-40). The slug flow with fully mixed oil and water is considered the simplest three-phase slug flow scenario. The two-phase

gas-liquid continuity and momentum equations can be followed, but the effective physical properties of the liquid mixture are calculated using empirical correlations. They can also be used in annular flow, because the oil and water are assumed to be fully mixed due to high turbulence. For bubbly flow with fully mixed oil and water, the gas and liquid are assumed to be homogeneously mixed and the bubble-rise velocity relative to the liquid is considered. The authors proposed that one liquid is dispersed in the other when the total turbulence energy is greater than the total surface-free energy. However, a gradual transition from stratified layers to partial dispersion and then to full dispersion should be provided with more realistic criterion.

2.3 Transient Modeling

For decades, several attempts have been made to develop a transient model for simulation and analysis. The complexity of solving the transient conservation equations forced several simplifications and assumptions in these development attempts. For example, Taitel *et al.* (1989) used a simplified transient approach by assuming a quasi-steady-state gas flow and a transient liquid flow. This can lead to inaccurate results in many applications. The previous transient studies are presented and arranged below based on the type of simplification.

Many studies proposed models for a particular transient phenomenon. Pothapragada (1996) and Tang (1998) presented transient dynamic models and simulators to predict the gas-lift unloading process. The developed transient partial differential equations are solved using an explicit finite difference scheme, and different types of empirical correlations for slug and bubble flow are used in their development. They coupled the two transient mass conservation equations with the steady-state empirical correlations for the liquid holdup and superficial velocities and then used the transient momentum equation for pressure estimation. Although they obtained

satisfactory results, it is inadequate to determine a major variable such as the holdup using a steady-state correlation. Sarica and Shoham (1991) developed a simplified, transient two-phase approach for severe slugging phenomenon in a pipeline-riser system. They assumed a quasi-equilibrium process and a one-dimensional gravity-dominant flow in both the pipeline and the riser. Beltran (2005) extended the two-phase model developed by Sarica and Shoham (1991) into a three-phase gas-oil-water model. In his model, a homogeneous pseudo-liquid phase is considered by assuming that the oil and water phases are always fully mixed.

Designing a transient model for a specific flow pattern is another common practice. Sharma (1985) developed a transient two-phase flow model for slug flow. The simulator is based on a mathematical two-fluid model coupled with a hydrodynamic slug flow model and can be used to predict the slug characteristics as a function of space and time. Hanich and Thompson (2001) developed a transient three-phase model for three-layer stratified flow. They presented a new numerical algorithm solution for solving the system of partial differential equations and showed a wide range of stability.

The majority of the transient three-phase models are developed based on a two-fluid model between liquid and gas and a drift-flux model between oil and water in the liquid phase. Shirdel and Sepehrnoori (2016) tested and solved the partial differential equations using two different numerical approaches—the semi-implicit and nearly implicit algorithms. Bonizzi and Issa (2003) used the same drift-flux model to represent the oil and water behavior. However, they solved the transient equations with Euler-implicit discretization in time and first order upwind in space. Using the drift-flux model overcomes the limitation of the homogeneous non-slip assumption for oil and water. Nevertheless, it cannot be used to cover the entire three-phase flow patterns. In the previous studies, the oil and water in the slug body are assumed to be fully

mixed, whereas the flow pattern changes to stratified flow when they are separated. However, there is another flow pattern created during the transition from stratified flow to fully mixed slug flow. This flow pattern is slug flow with stratified film and slug, and in this study, a mechanistic model has been developed to cover it.

An analytical solution for the set of partial differential mass and momentum conservation equations is almost impossible. Therefore, another substantial difference between the previously developed models is the numerical approach they used to solve the partial differential equations. Different numerical solution procedures including the method of characteristics, implicit finite differences, or explicit finite differences have been used and tested. The method of characteristics can be eliminated due to a stability restriction. Scoggins (1977) used a fully implicit finite difference numerical scheme to solve the partial differential equations. The solution algorithm for solving the non-linear system of equations was based on Newton-Raphson iteration scheme. The implicit finite difference methods usually guarantee stability. However, they require solving a large and complex matrix of equations for every time step. The explicit finite difference solutions impose a stability restriction on the ratio of the maximum time step to the length step. However, most of the transient processes in the production systems are rather short and a small time step is quite satisfactory. They also require much simpler computer programs that can be designed and used for different transient petroleum applications. The semi-implicit and nearly implicit solution algorithms are simplified approaches of the fully implicit scheme. Their numerical formulation is based on using both explicit and implicit terms during the solution procedure. Many multiphase flow simulators, including OLGA, use a semi-implicit approach to solve the finite difference equations and have been promising with regard to stability.

In this study, the mechanistic models have been built based on fewer assumptions compared with the previous models. Moreover, the development of unique and complex flow patterns, such as transient slug flow with stratified film and slug, increases the number of partial differential equations to be solved for each time step. Therefore, the stability of the fully implicit formulation makes it the ideal candidate for solving the transient conservation equations in the current work. The length of the implicit finite difference solving mechanism is simplified by using an innovative solution procedure. Throughout the calculations, several variables are used in their previous time step and updated during the iterations to ensure implicit implementation.

CHAPTER 3

MODEL DEVELOPMENT

At the TUALP 2014 Fall Advisory Board Meeting (ABM), Zhang (2014) first presented a unified model for transient gas-liquid pipe flow. The transient model is an extension of the steady-state unified model Zhang *et al.* (2003) developed over a decade ago. Almudairis (2014) in his thesis extended Zhang's (2014) theoretical model into practical applications. The thesis presents a model for the simulation and analysis of various steady and unsteady-state gas-lift processes. The model is comprehensive and can be used as a tool to predict different transient multiphase flow phenomena in petroleum production and transportation through wells and pipelines. In this study, Almudairis' (2014) two-phase model is extended further to a three-phase gas-oil-water model. Three-phase mass and momentum conservation equations are developed for new flow patterns and will be presented below. Some simplifications and assumptions are made in the development. The black oil or compositional models can be used for calculating the fluid physical properties such as density and viscosity. Finally, closure relationships for determining the remaining terms in the conservation equations are provided.

3.1 Transient Hydrodynamic Model

For low to intermediate liquid flow rates, the oil and water usually separate, and three different three-phase flow patterns may prevail. The two-phase models assume fully mixed oil and water and therefore the prediction is usually inaccurate. The three-phase flow patterns are the three-layer stratified flow, the slug flow with stratified film and slug, and the slug flow with

stratified film and mixed slug. In the following sections, three different mechanistic models will be presented for each of the flow patterns based on the physical behavior of the phases.

3.1.1 Three-Layer Stratified Flow

The two-phase oil-water stratified flow is considered a simpler version of the three-layer stratified flow. The presence of gas will increase the number of conservation equations. Based on the control volume diagram in Figure 3-1, the mass balance equations for the incompressible oil and water phases respectively can be formulated as

$$\frac{\partial}{\partial t}\left(H_{OF}\right) = -\frac{\partial}{\partial z}\left(H_{OF} v_{OF}\right) \tag{3-1}$$

and

$$\frac{\partial}{\partial t}\left(H_{WF}\right) = -\frac{\partial}{\partial z}\left(H_{WF} v_{WF}\right), \tag{3-2}$$

while the mass balance equation for the gas phase is

$$\frac{\partial}{\partial t}\left(\rho_C H_C\right) = -\frac{\partial}{\partial z}\left(\rho_C H_C v_C\right), \tag{3-3}$$

where t and z represent time and position respectively, v_{OF}, $v_{WF,}$ and v_C respectively represent the velocities of oil film, water film, and gas core , H_{OF}, H_{WF}, and H_C represent oil film holdup, water film holdup, and gas core holdup, respectively. In these formulae, the phase change between liquid and gas is neglected.

All the forces acting on the oil film control volume are shown in Figure 3-2. The momentum conservation equation for oil film can be written as

$$\frac{\partial v_{OF}}{\partial t} = -\frac{1}{\rho_O}\frac{\partial p}{\partial z} - v_{OF}\frac{\partial v_{OF}}{\partial z} + \frac{\tau_{I1} S_{I1} - \tau_{I2} S_{I2} - \tau_{OF} S_{OF}}{\rho_O A H_{OF}} - g\sin\theta. \tag{3-4}$$

Similarly, for water film and gas core, respectively,

$$\frac{\partial v_{WF}}{\partial t} = -\frac{1}{\rho_W}\frac{\partial p}{\partial z} - v_{WF}\frac{\partial v_{WF}}{\partial z} + \frac{\tau_{I2}S_{I2} - \tau_{WF}S_{WF}}{\rho_W A H_{WF}} - g\sin\theta \tag{3-5}$$

and

$$\frac{\partial v_C}{\partial t} = -\frac{1}{\rho_C}\frac{\partial p}{\partial z} - v_C\frac{\partial v_C}{\partial z} - \frac{\tau_C S_C + \tau_{I1}S_{I1}}{\rho_C A\left(1 - H_{OF} - H_{WF}\right)} - g\sin\theta, \tag{3-6}$$

where S_{I1} and S_{I2} are the interfacial perimeters for gas/oil interface and oil/water interface respectively, S_{OF}, S_{WF}, and S_C are the pipe perimeters wetted by oil film, water film, and gas core respectively, and τ_{I1} and τ_{I2} are the shear stresses for gas/oil interface and oil/water interface respectively, and τ_{OF} , τ_{WF}, and τ_C are the shear stresses for oil film, water film, and gas core, respectively.

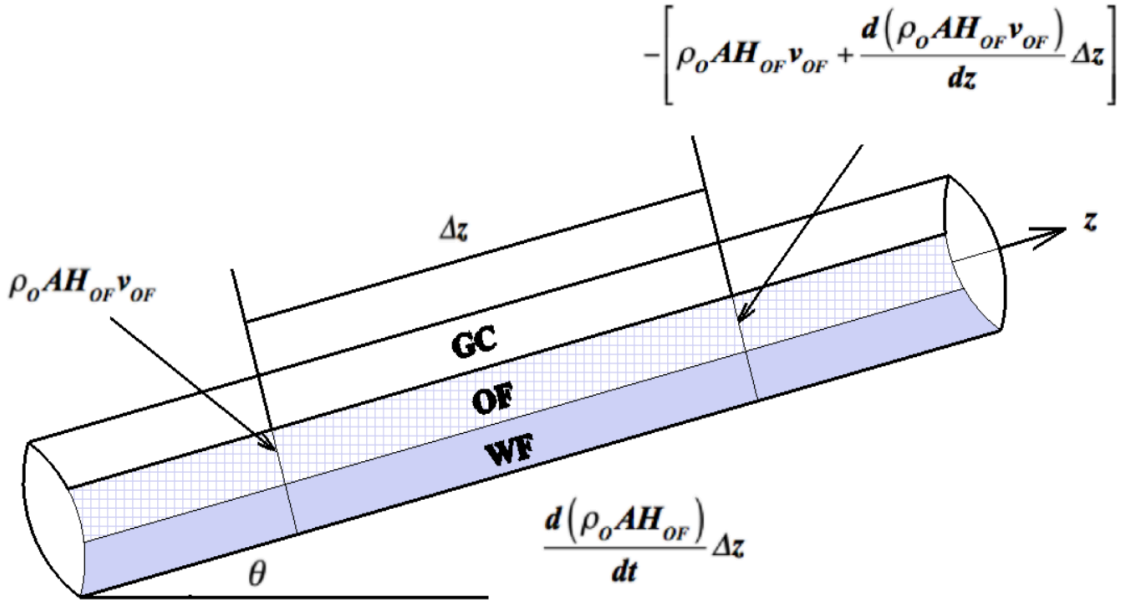

Figure 3-1: Mass Conservation Control Volume for Oil Film in Three-Phase Stratified Flow

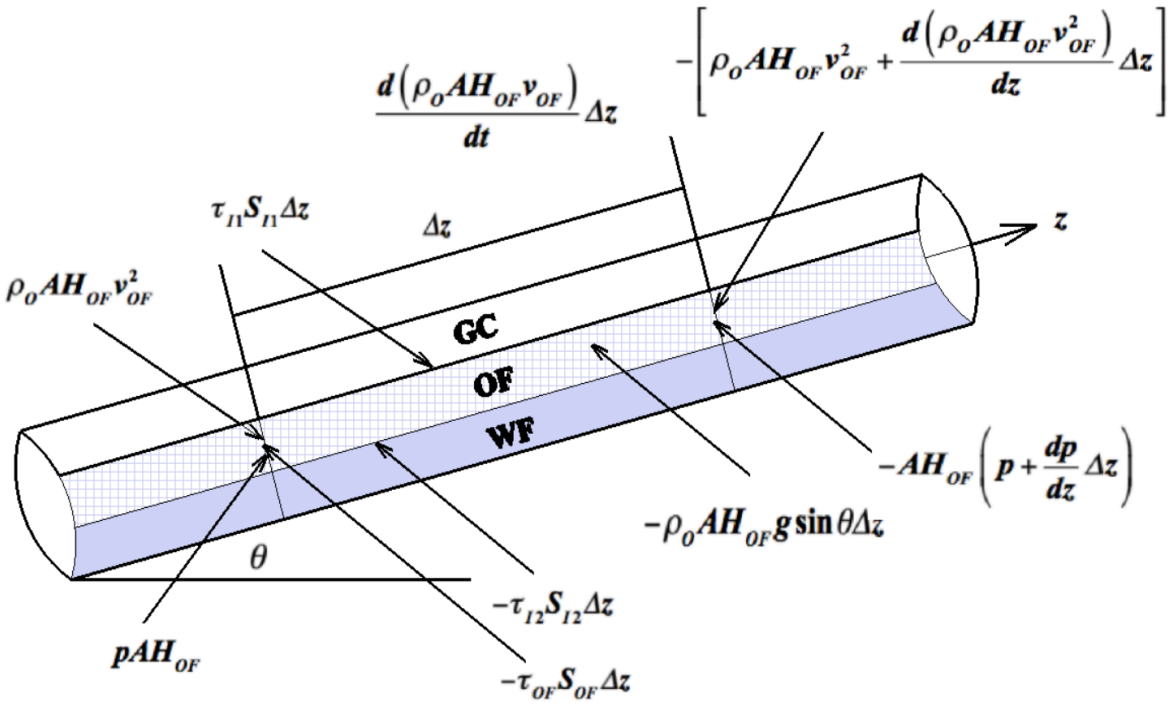

Figure 3-2: Momentum Conservation Control Volume for Oil Film in Three-Phase Stratified Flow

The holdups and local velocities are calculated using the following basic relationships. The gas core velocity is

$$v_C = \frac{v_{SG} + v_{SL} F_E}{1 - H_{LF}}, \tag{3-7}$$

where F_E is the liquid entrainment fraction and can be estimated using a steady-state correlation. The oil and water film holdups in gas core are obtained by

$$H_{OC} = \frac{v_{SO} F_E}{v_C} \tag{3-8}$$

and

$$H_{WC} = \frac{v_{SW} F_E}{v_C}. \tag{3-9}$$

The oil and water film holdups are calculated as

$$H_{OF} = H_O - H_{OC} \tag{3-10}$$

and

$$H_{WF} = H_W - H_{WC}. \tag{3-11}$$

The local oil and water velocities are obtained by

$$v_{OF} = \frac{v_{SO}\left(1 - F_E\right)}{H_{OF}} \tag{3-12}$$

and

$$v_{WF} = \frac{v_{SW}\left(1 - F_E\right)}{H_{WF}}. \tag{3-13}$$

The gravitational, accelerational, and transient pressure gradients can be calculated for different flow patterns using the same principle of average holdups and velocities once the primary variables are determined. They are given, respectively, by

$$\left.\frac{\partial p}{\partial z}\right|_G = -\left[\rho_W H_W + \rho_O H_O + \rho_G H_G\right] g \sin\theta, \tag{3-14}$$

$$\left.\frac{\partial p}{\partial z}\right|_A = -\left[\rho_O H_O v_O \frac{\partial v_O}{\partial z} + \rho_W H_W v_W \frac{\partial v_W}{\partial z} + \rho_G H_G v_G \frac{\partial v_G}{\partial z}\right], \tag{3-15}$$

and

$$\left.\frac{\partial p}{\partial z}\right|_T = -\left[\rho_O H_O \frac{\partial v_O}{\partial t} + \rho_W H_W \frac{\partial v_W}{\partial t} + \rho_G H_G \frac{\partial v_G}{\partial t}\right]. \tag{3-16}$$

The frictional pressure gradient, however, is different for each flow pattern. For three-layer stratified flow it is given by

$$\left.\frac{\partial p}{\partial z}\right|_F = -\left(S_{OF} f_{OF} \rho_O v_{OF}^2 + S_{WF} f_{WF} \rho_W v_{WF}^2 + S_C f_C \rho_C v_C^2\right) / \left(2A\right). \tag{3-17}$$

3.1.2 Slug Flow with Stratified Film and Slug

For slug flow in the two-phase flow system, the liquid and gas are fully mixed in the slug body and the slug liquid holdup is the only variable to be provided. In this flow pattern, the oil and water are fully separated in the slug body region. Consequently, five new variables (H_{WGS}, α_{OS}, α_{WS}, v_{OS}, v_{WS},) are introduced to express the distribution between the oil, water, and gas in the slug region. The mass and momentum conservation equations are developed for each region separately, and the interaction between them is presented in the form of momentum exchange. As illustrated in Figure 3-3, assuming no liquid entrainment in the gas core, the mass conservation equations for incompressible oil and water in the film region can be written, respectively, as

$$\frac{\partial}{\partial t}\left(H_{OF}\right)=-\frac{\partial}{\partial z}\left(H_{OF}v_{OF}\right)+\frac{\left[\left(1-H_{WGS}\right)\left(1-\alpha_{OS}\right)\left(v_T-v_{OS}\right)-H_{OF}\left(v_T-v_{OF}\right)\right]}{l_F} \tag{3-18}$$

and

$$\frac{\partial}{\partial t}\left(H_{WF}\right)=-\frac{\partial}{\partial z}\left(H_{WF}v_{WF}\right)+\frac{\left[H_{WGS}\left(1-\alpha_{WS}\right)\left(v_T-v_{WS}\right)-H_{WF}\left(v_T-v_{WF}\right)\right]}{l_F}, \tag{3-19}$$

while the gas core in the film region can be obtained by

$$\begin{aligned}\frac{\partial}{\partial t}\left[\rho_C H_C\right]=&-\frac{\partial}{\partial z}\left(\rho_C H_C v_C\right)\\&+\frac{\rho_C\left[\left(1-H_{WGS}\right)\alpha_{OS}\left(v_T-v_{OS}\right)-H_C\left(v_T-v_C\right)\right]}{l_F}\\&+\frac{\rho_C\left[H_{WGS}\alpha_{WS}\left(v_T-v_{WS}\right)-H_C\left(v_T-v_C\right)\right]}{l_F},\end{aligned} \tag{3-20}$$

where v_T is the slug translational velocity, v_{OS} and v_{WS} are the oil and water slug velocities respectively, l_F is the liquid film length, H_{WGS} is the water holdup with entrapped gas in slug

body, α_{OS} and α_{WS} are the gas-volume fraction in oil of slug body and gas-volume fraction in water of slug body.

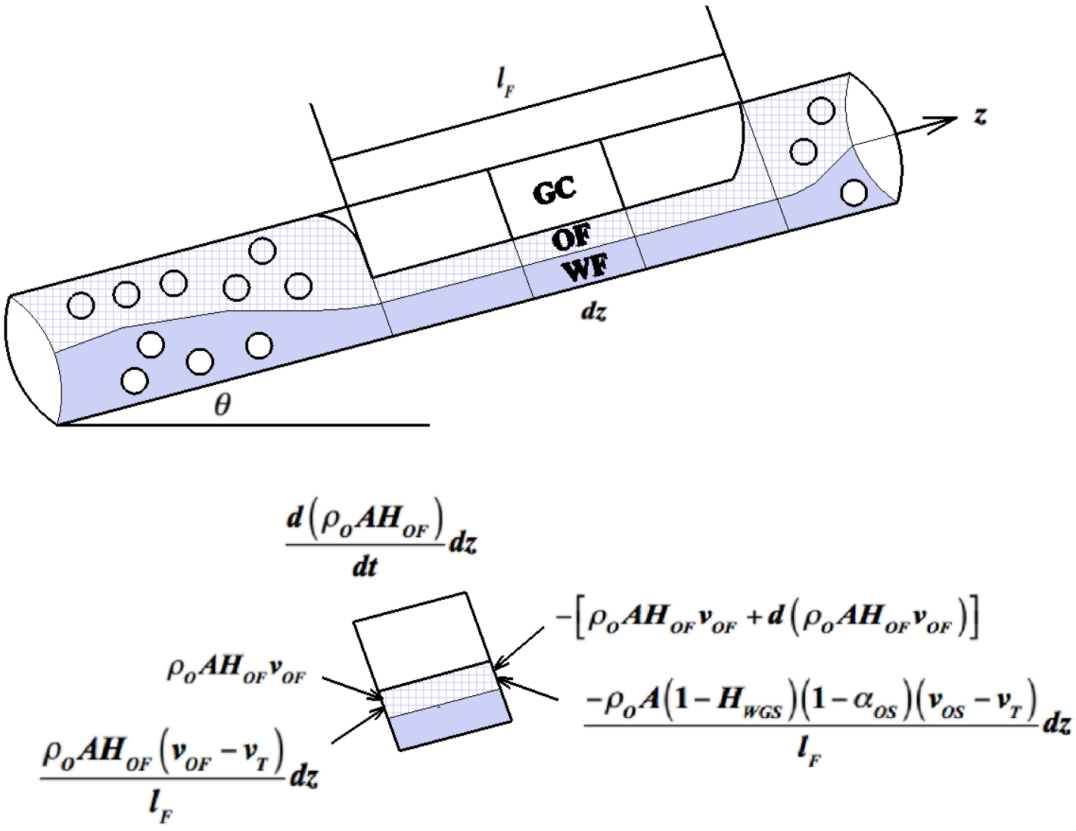

Figure 3-3: Mass Conservation Control Volume for Oil Film in Slug Flow with Stratified Film and Slug

For slug body as shown in Figure 3-4, the mass conservation equations for oil, water, and gas can be written as

$$\frac{\partial}{\partial t}\left[\left(1-H_{WGS}\right)\left(1-\alpha_{OS}\right)\right] = -\frac{\partial}{\partial z}\left[\left(1-H_{WGS}\right)\left(1-\alpha_{OS}\right)v_{OS}\right] - \frac{\left[\left(1-H_{WGS}\right)\left(1-\alpha_{OS}\right)\left(v_T-v_{OS}\right)-H_{OF}\left(v_T-v_{OF}\right)\right]}{l_S}, \tag{3-21}$$

$$\frac{\partial}{\partial t}\left[H_{WGS}\left(1-\alpha_{WS}\right)\right]=-\frac{\partial}{\partial z}\left[H_{WGS}\left(1-\alpha_{WS}\right)v_{WS}\right] - \frac{\left[H_{WGS}\left(1-\alpha_{WS}\right)\left(v_T-v_{WS}\right)-H_{WF}\left(v_T-v_{WF}\right)\right]}{l_S}, \tag{3-22}$$

and

$$\frac{\partial}{\partial t}\left[\rho_G\left\{\left(1-H_{WGS}\right)\alpha_{OS}+H_{WGS}\alpha_{WS}\right\}\right]= -\frac{\partial}{\partial z}\left(\rho_G\left(1-H_{WGS}\right)\alpha_{OS}v_{OS}\right)-\frac{\partial}{\partial z}\left(\rho_G H_{WGS}\alpha_{WS}v_{WS}\right) - \frac{\rho_G\left[\left(1-H_{WGS}\right)\alpha_{OS}\left(v_T-v_{OS}\right)-H_C\left(v_T-v_C\right)\right]}{l_S} - \frac{\rho_G\left[H_{WGS}\alpha_{WS}\left(v_T-v_{WS}\right)-H_C\left(v_T-v_C\right)\right]}{l_S}. \tag{3-23}$$

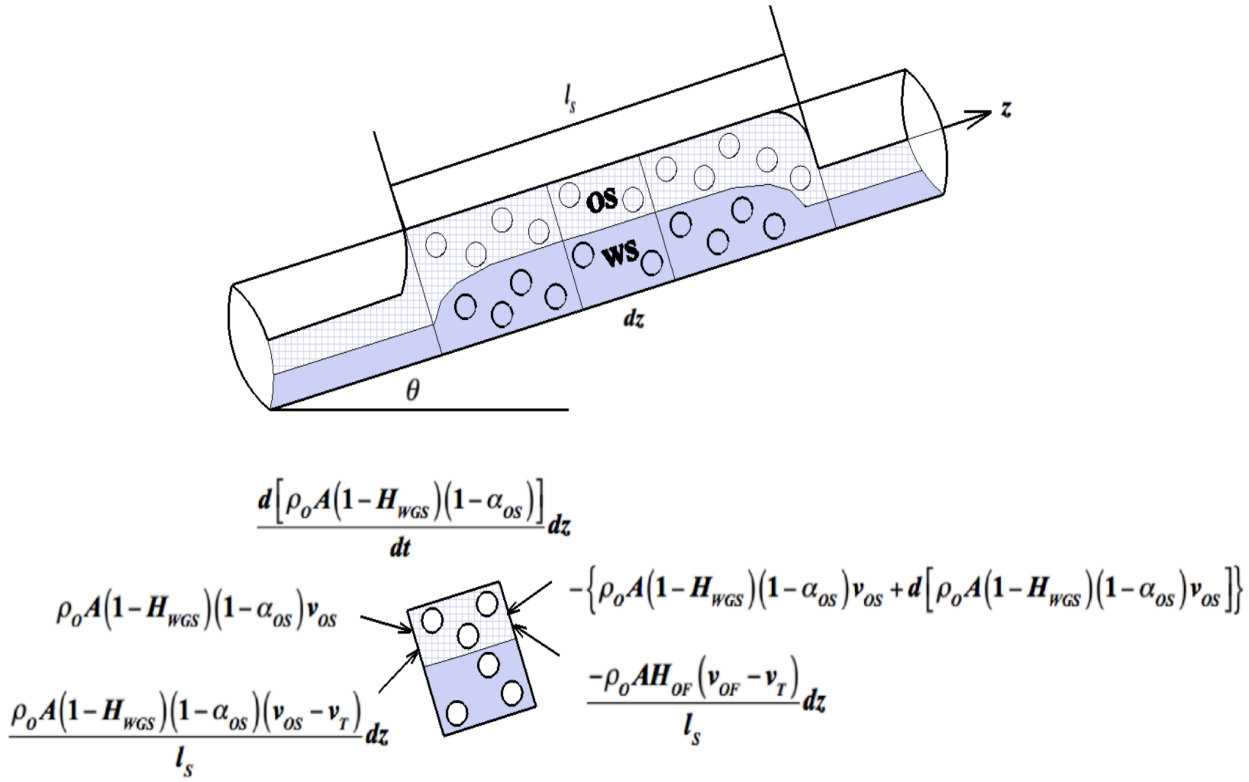

Figure 3-4: Mass Conservation Control Volume for Oil Slug in Slug Flow with Stratified Film and Slug

The forces acting on the oil film in the film region of slug flow are shown in Figure 3-5. The momentum conservation equations for the oil, water, and gas in the film region can be written, respectively, as

$$\frac{\partial v_{OF}}{\partial t} = -\frac{1}{\rho_O}\frac{\partial p}{\partial z} - v_{OF}\frac{\partial v_{OF}}{\partial z} + \frac{\left(v_T - v_{OF}\right)\left(v_{OS} - v_{OF}\right)}{l_F} + \frac{\tau_{I1}S_{I1} - \tau_{I2}S_{I2} - \tau_{OF}S_{OF}}{\rho_O A H_{OF}} - g\sin\theta, \tag{3-24}$$

$$\frac{\partial v_{WF}}{\partial t} = -\frac{1}{\rho_W}\frac{\partial p}{\partial z} - v_{WF}\frac{\partial v_{WF}}{\partial z} + \frac{\left(v_T - v_{WF}\right)\left(v_{WS} - v_{WF}\right)}{l_F} + \frac{\tau_{I2}S_{I2} - \tau_{WF}S_{WF}}{\rho_W A H_{WF}} - g\sin\theta, \tag{3-25}$$

and

$$\frac{\partial v_C}{\partial t} = -\frac{1}{\rho_C}\frac{\partial p}{\partial z} - v_C\frac{\partial v_C}{\partial z} + \frac{\left(v_T - v_C\right)\left(v_{OS} - v_C\right)}{l_F} + \frac{\left(v_T - v_C\right)\left(v_{WS} - v_C\right)}{l_F} - \frac{\tau_C S_C + \tau_{I1}S_{I1}}{\rho_C A H_C} - g\sin\theta. \tag{3-26}$$

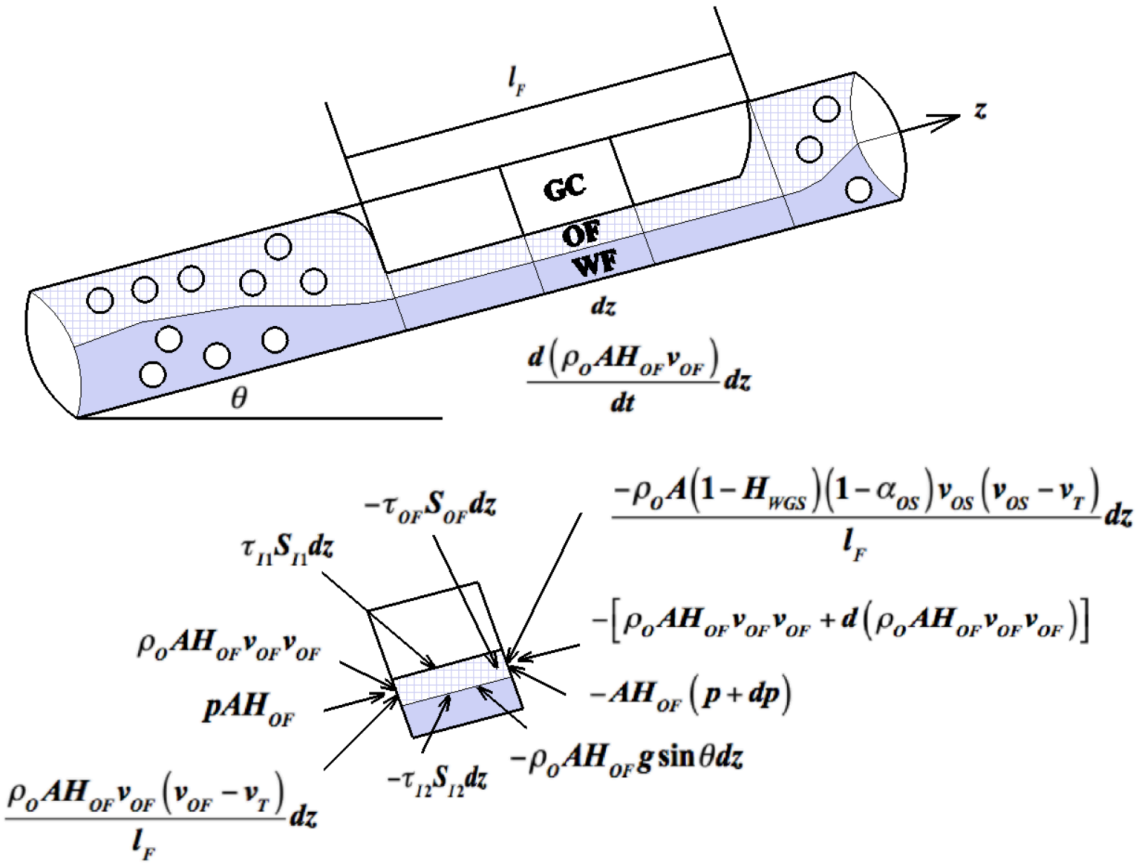

Figure 3-5: Momentum Conservation Control Volume for Oil Film in Slug Flow with Stratified Film and Slug

For stratified oil and water flows in the slug body, as shown in Figure 3-6, the momentum equations can be obtained as

$$\frac{\partial v_{OS}}{\partial t} = -\frac{1}{\rho_{OS}}\frac{\partial p}{\partial z} - v_{OS}\frac{\partial v_{OS}}{\partial z} + \frac{\left(v_T - v_{OS}\right)\left(v_{OF} - v_{OS}\right)}{l_S} - \frac{\tau_{I0} S_{I0} + \tau_{OS} S_{OS}}{\rho_{OS} A\left(1 - H_{WGS}\right)} - g\sin\theta \tag{3-27}$$

and

$$\frac{\partial v_{WS}}{\partial t} = -\frac{1}{\rho_{WS}}\frac{\partial p}{\partial z} - v_{WS}\frac{\partial v_{WS}}{\partial z} + \frac{\left(v_T - v_{WS}\right)\left(v_{WF} - v_{WS}\right)}{l_S} + \frac{\tau_{I0} S_{I0} - \tau_{WS} S_{WS}}{\rho_{WS} A H_{WGS}} - g\sin\theta. \tag{3-28}$$

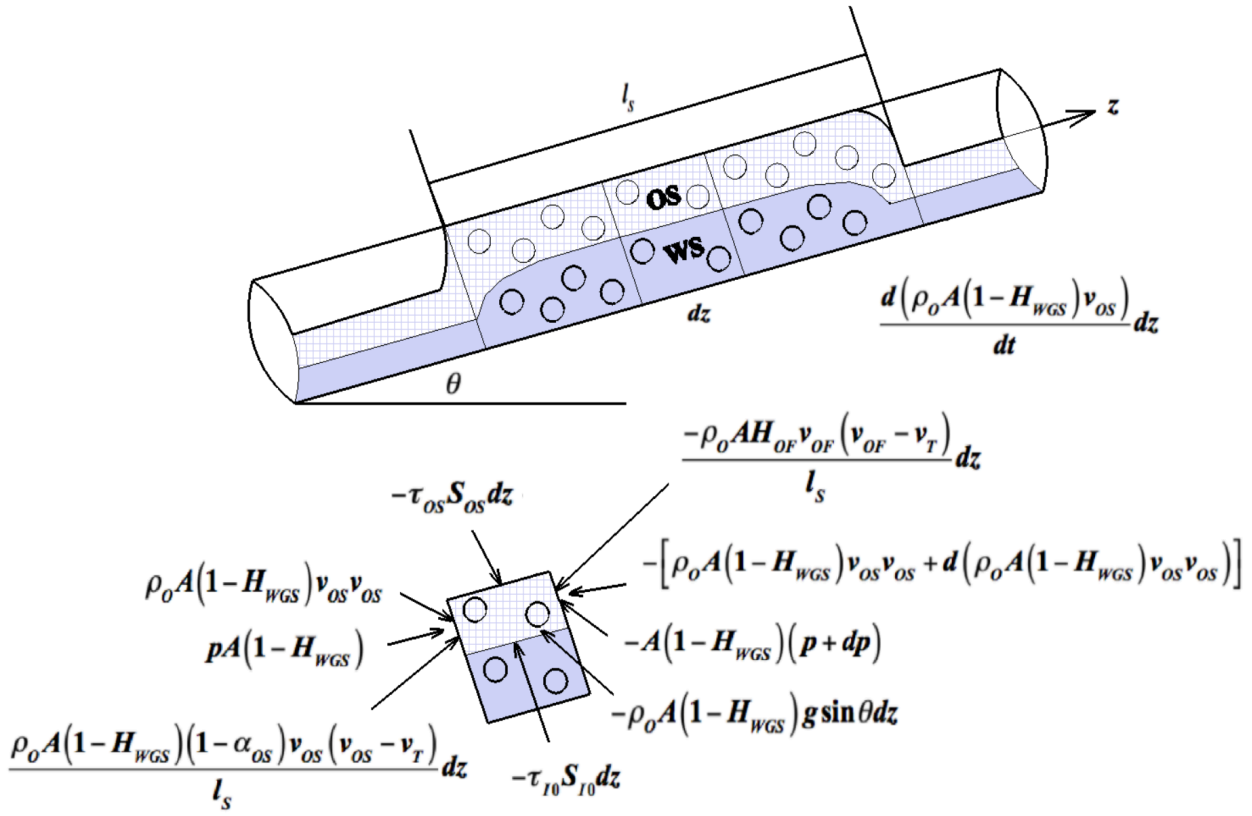

Figure 3-6: Momentum Conservation Control Volume for Oil Slug in Slug Flow with Stratified Film and Slug

In order to solve the mass and momentum conservation equations, all the physical variables that are presented should be determined first. The slug length and the translational velocity can be determined using closure relationships. Considering the passage of a slug unit at an observation point, the following relationships hold for oil, water, and gas:

$$l_U v_{SO} = l_S\left(1-H_{WGS}\right)\left(1-\alpha_{OS}\right)v_{OS} + l_F H_{OF} v_{OF}, \tag{3-29}$$

$$l_U v_{SW} = l_S H_{WGS}\left(1-\alpha_{WS}\right)v_{WS} + l_F H_{WF} v_{WF}, \tag{3-30}$$

and

$$l_U v_{SG} = l_S\left[\left(1-H_{WGS}\right)\alpha_{OS}v_{OS} + H_{WGS}\alpha_{WS}v_{WS}\right] + l_F H_C v_C. \tag{3-31}$$

The mixture velocity based on the local velocities in the slug body and the film zone can be given as

$$v_M = \left(1 - H_{WGS}\right) v_{OS} + H_{WGS} v_{WS} \tag{3-32}$$

and

$$v_M = H_{OF} v_{OF} + H_{WF} v_{WF} + \left(1 - H_{OF} - H_{WF}\right) v_C . \tag{3-33}$$

The average oil and water holdups in a slug unit are expressed as

$$H_O = \left[\left(1 - H_{WGS}\right)\left(1 - \alpha_{OS}\right) l_S + H_{OF} l_F\right] / l_U \tag{3-34}$$

and

$$H_W = \left[H_{WGS}\left(1 - \alpha_{WS}\right) l_S + H_{WF} l_F\right] / l_U . \tag{3-35}$$

Zhang *et al.* (2003) developed a mechanistic model for slug liquid holdup based on a balance between the turbulent kinetic energy of the liquid phase and the surface free energy of dispersed gas bubbles in a slug body. The model is developed for two-phase gas-liquid flow, and because the oil and water are completely separated in this flow pattern, the model can be used also to predict the gas-volume fraction in each of the oil and water layers separately. The main model equation is expressed by

$$\alpha_{LS} = 1 - \frac{1}{1 + \dfrac{T_{sm}}{3.16\left[\left(\rho_L - \rho_G\right) g \sigma_{GL}\right]^{1/2}}} . \tag{3-36}$$

The above equation can be used between the gas-oil and gas-water by replacing the L with the actual phase. The T_{sm} for gas-oil and gas-water can be given, respectively, by

$$T_{sm}^{GO} = \frac{1}{C_e}\left[\begin{array}{l} \dfrac{f_{SO}}{2}\rho_{OS} v_{OS}^2 + \dfrac{d}{4}\dfrac{\rho_O (v_T - v_{OF})(v_{OS} - v_{OF}) H_{OF}}{l_S} \\ + \dfrac{d}{4}\dfrac{\rho_C (v_T - v_C)(v_{OS} - v_C)(1 - H_{LF})\left(v_{SO} / v_{SL}\right)}{l_S} \end{array}\right], \tag{3-37}$$

and

$$T_{sm}^{GW} = \frac{1}{C_e}\left[\begin{array}{l} \dfrac{f_{SW}}{2}\rho_{WS}v_{WS}^2 + \dfrac{d}{4}\dfrac{\rho_W(v_T - v_{WF})(v_{WS} - v_{WF})H_{WF}}{l_S} \\ + \dfrac{d}{4}\dfrac{\rho_C(v_T - v_C)(v_{WS} - v_C)(1 - H_{LF})\left(v_{SW}/v_{SL}\right)}{l_S} \end{array}\right], \tag{3-38}$$

where

$$C_e = \frac{2.5 - \left|\sin(\theta)\right|}{2}. \tag{3-39}$$

The solution procedure is based on an iteration method, which will be discussed in detail in Chapter 4. As explained initially, the frictional pressure gradient is different for each flow pattern. For slug flow with stratified oil and water, the frictional pressure gradient is calculated with

$$\begin{aligned} \left.\frac{\partial p}{\partial z}\right|_F = &-R_{FU}\left(S_{OF}f_{OF}\rho_O v_{OF}^2 + S_{WF}f_{WF}\rho_W v_{WF}^2 + S_C f_C \rho_C v_C^2\right)/\left(2A\right) \\ &- \left(1 - R_{FU}\right)\left(S_{OS}f_{OS}\rho_{OS}v_{OS}^2 + S_{WS}f_{WS}\rho_{WS}v_{WS}^2\right)/\left(2A\right), \end{aligned} \tag{3-40}$$

where R_{FU} is the film to slug unit length ratio.

3.1.3 Slug Flow with Stratified Film and Mixed Slug

The film region is the same as the slug flow with stratified film and slug. In the slug region, however, the three-phases are fully mixed with one of the liquid phases as the continuous phase. As a result, the slug body holdup fractions (α_{OS}, α_{WS}, H_{WGS}) are replaced with simple no-slip holdup (f_O and f_W). Moreover, the previous slug velocities (v_{OS} and v_{WS}) disappear, to be replaced with a mixture velocity that can be given by

$$v_M = v_{SO} + v_{SW} + v_{SG}. \tag{3-41}$$

Based on the new modifications, the mass conservation equations for incompressible oil and water respectively in the film region can be written as

$$\frac{\partial}{\partial t}\left(H_{OF}\right)=-\frac{\partial}{\partial z}\left(H_{OF}v_{OF}\right)+\frac{\left[f_{O}H_{LS}\left(v_{T}-v_{M}\right)-H_{OF}\left(v_{T}-v_{OF}\right)\right]}{l_{F}} \tag{3-42}$$

and

$$\frac{\partial}{\partial t}\left(H_{WF}\right)=-\frac{\partial}{\partial z}\left(H_{WF}v_{WF}\right)+\frac{\left[f_{W}H_{LS}\left(v_{T}-v_{M}\right)-H_{WF}\left(v_{T}-v_{WF}\right)\right]}{l_{F}}, \tag{3-43}$$

while the gas core in the film region can be obtained by

$$\frac{\partial}{\partial t}\left[\rho_{C}H_{C}\right]=-\frac{\partial}{\partial z}\left(\rho_{C}H_{C}v_{C}\right)+\frac{\rho_{C}\left[\left(1-H_{LS}\right)\left(v_{T}-v_{M}\right)-H_{C}\left(v_{T}-v_{C}\right)\right]}{l_{F}}. \tag{3-44}$$

For slug body, the mass conservation equations for oil, water, and gas respectively can be written as

$$\frac{\partial}{\partial t}\left(f_{O}H_{LS}\right)=-\frac{\partial}{\partial z}\left(f_{O}H_{LS}v_{M}\right)-\frac{\left[f_{O}H_{LS}\left(v_{T}-v_{M}\right)-H_{OF}\left(v_{T}-v_{OF}\right)\right]}{l_{S}}, \tag{3-45}$$

$$\frac{\partial}{\partial t}\left(f_{W}H_{LS}\right)=-\frac{\partial}{\partial z}\left(f_{W}H_{LS}v_{M}\right)-\frac{\left[f_{W}H_{LS}\left(v_{T}-v_{M}\right)-H_{WF}\left(v_{T}-v_{WF}\right)\right]}{l_{S}}, \tag{3-46}$$

and

$$\begin{aligned}\frac{\partial}{\partial t}\left[\rho_{G}\left(1-H_{LS}\right)\right]=&-\frac{\partial}{\partial z}\left[\rho_{G}\left(1-H_{LS}\right)v_{M}\right]\\&-\frac{\rho_{G}\left[\left(1-H_{LS}\right)\left(v_{T}-v_{M}\right)-H_{C}\left(v_{T}-v_{C}\right)\right]}{l_{S}}.\end{aligned} \tag{3-47}$$

The momentum conservation equations for the oil, water, and gas in the film region can be written as

$$\frac{\partial v_{OF}}{\partial t} = -\frac{1}{\rho_O}\frac{\partial p}{\partial z} - v_{OF}\frac{\partial v_{OF}}{\partial z} + \frac{\left(v_T - v_{OF}\right)\left(v_M - v_{OF}\right)}{l_F} + \frac{\tau_{I1}S_{I1} - \tau_{I2}S_{I2} - \tau_{OF}S_{OF}}{\rho_O A H_{OF}} - g\sin\theta, \tag{3-48}$$

$$\frac{\partial v_{WF}}{\partial t} = -\frac{1}{\rho_W}\frac{\partial p}{\partial z} - v_{WF}\frac{\partial v_{WF}}{\partial z} + \frac{\left(v_T - v_{WF}\right)\left(v_M - v_{WF}\right)}{l_F} + \frac{\tau_{I2}S_{I2} - \tau_{WF}S_{WF}}{\rho_W A H_{WF}} - g\sin\theta, \tag{3-49}$$

and

$$\frac{\partial v_C}{\partial t} = -\frac{1}{\rho_C}\frac{\partial p}{\partial z} - v_C\frac{\partial v_C}{\partial z} + \frac{\left(v_T - v_C\right)\left(v_M - v_C\right)}{l_F} - \frac{\tau_C S_C + \tau_{I1}S_{I1}}{\rho_C A H_C} - g\sin\theta. \tag{3-50}$$

The variables in the mass and momentum conservation equations can be solved using the following relationships. Considering the passage of a slug unit at an observation point, the following relationships hold for oil, water, and gas:

$$l_U v_{SO} = l_S f_O H_{LS} v_M + l_F H_{OF} v_{OF}, \tag{3-51}$$

$$l_U v_{SW} = l_S f_W H_{LS} v_M + l_F H_{WF} v_{WF}, \tag{3-52}$$

and

$$l_U v_{SG} = l_S\left(1 - H_{LS}\right)v_M + l_F H_C v_C. \tag{3-53}$$

The average oil and water holdups in a slug unit are expressed by

$$H_O = \left[f_O H_{LS} l_S + H_{OF} l_F\right] / l_U \tag{3-54}$$

and

$$H_W = \left[f_W H_{LS} l_S + H_{WF} l_F\right] / l_U. \tag{3-55}$$

Zhang *et al.*'s (2003) model for slug liquid holdup can be also used here, but both the oil and the water films in the gas-pocket region should be considered. The model then becomes

$$H_{LS} = \frac{1}{1 + \dfrac{T_{sm}}{3.16\left[\left(\rho_L - \rho_G\right) g \sigma_{GL}\right]^{1/2}}}, \tag{3-56}$$

where

$$T_{SM} = \frac{1}{C_e}\left[\begin{array}{l} \dfrac{f_S}{2}\rho_S v_M^2 + \dfrac{d}{4}\dfrac{\rho_O (v_T - v_{OF})(v_M - v_{OF}) H_{OF}}{l_S} \\ + \dfrac{d}{4}\dfrac{\rho_W (v_T - v_{WF})(v_M - v_{WF}) H_{WF}}{l_S} \\ + \dfrac{d}{4}\dfrac{\rho_C (v_T - v_C)(v_M - v_C)(1 - H_{LF})}{l_S} \end{array}\right], \tag{3-57}$$

where f_S is the friction factor of slug body and ρ_S is the density of slug body. The solution procedure of the above relationships is explained in detail in Chapter 4. The slug body mixture properties can be calculated using the same equations for oil/water dispersed flow. The frictional pressure gradient is updated with

$$\begin{aligned} \left.\frac{\partial p}{\partial z}\right|_F = & -R_{FU}\left(S_{OF} f_{OF} \rho_O v_{OF}^2 + S_{WF} f_{WF} \rho_W v_{WF}^2 + S_C f_C \rho_C v_C^2\right) / \left(2A\right) \\ & -\left(1 - R_{FU}\right)\left(\pi d f_S \rho_S v_M^2\right) / \left(2A\right). \end{aligned} \tag{3-58}$$

3.2 Oil-Water Flow Behavior

As opposed to the case of two-phase gas-liquid flow, the phenomena that drive the two-phase oil-water are more complicated. The physical relationships of interfacial shear stress and volumetric averaging are often inaccurate. In three-layer stratified flow and slug flow with stratified film and slug, the liquid phases are separated everywhere, and an accurate

determination of the interfacial shear stress is crucial. However, in slug flow with fully mixed oil and water and dispersed or bubbly flow, the mixture properties and inversion are more significant. In the following sections, the two-phase oil-water models will be presented for both separated and mixed cases and the same closure relationships to describe the distribution between the liquid phases can be used later for the three-phase models. To determine whether the oil and water are mixed or separated, a previous flow pattern transition criterion based on the droplet diameter is proposed with slight modification in case of gas presence.

3.2.1 Closure Relationships

Stratified flow with complete separation of the liquids may prevail for low flow rates, where the stabilizing gravity force due to a finite density difference is dominant. Unlike the two-phase gas-liquid flow, the oil-water interfacial tension exhibits a unique behavior, and a special closure relationship should be used. According to Zhang *et al.* (2011), the oil-water interface is often concave, and the interfacial shear stress can be given by

$$\tau_I = \sqrt{\frac{f_W \Theta_W + f_O\left(1-\Theta_W\right)}{2}} \sqrt{\rho_M \left[\Theta_W \tau_{WF} + \left(1-\Theta_W\right)\tau_{OF}\right]} \times \left(v_{OF} - v_{WF}\right), \tag{3-59}$$

where f_O and f_W are the friction factors for oil and water, respectively, Θ_O and Θ_W are the oil and water wetted wall fractions, respectively, and ρ_M is the mixture density.

With increasing flow rates, when the water layer moves faster than the oil layer, oil drops get entrained into the water. Vice versa, with a faster oil layer, water drops are entrained into the oil layer. The rate of droplet entrainment at the interface increases with increasing liquid flow rates. For sufficiently high liquid flow rate, the entire dispersed phase becomes discontinuous in another continuous liquid phase, resulting in an oil-in-water or water-in-oil dispersion. The

system of two immiscible liquids, such as oil and water, could become even more complex, since the resulting mixed fluid can turn into an emulsion. The emulsion is a quasi-stable suspension of fine droplets of one liquid dispersed in another liquid. The behavior is different from that in gas-liquid mixture, especially the fluid physical properties. If the oil and water are fully mixed, Brinkman's (1952) correlation can be used to calculate the apparent viscosity of the mixture. The correlation is a function of the phase fraction and the viscosity of the continuous phase. It can be given as

$$\frac{\mu_{LM}}{\mu_C} = \left(1 - \phi_{Int}\right)^{-2.5}, \tag{3-60}$$

where μ_C and μ_{LM} are the viscosities of the continuous phase and the liquid mixture, respectively. In order to predict the continuous phase, Brauner and Ullmann (2002) combined the criterion of minimum system-free energy with Brauner (2001) model for droplet size in dense dispersions to predict the critical conditions for phase inversion. The correlation is given by

$$\phi_{OI} = \frac{\tilde{\rho}^{0.6}\tilde{\mu}^{0.4}}{1 + \tilde{\rho}^{0.6}\tilde{\mu}^{0.4}}, \tag{3-61}$$

where

$$\tilde{\rho} = \frac{\rho_O}{\rho_W}, \tag{3-62}$$

and

$$\tilde{\mu} = \frac{\mu_O}{\mu_W}, \tag{3-63}$$

where ϕ_{OI} is the critical-oil holdup in the oil/water mixture, corresponding to the inversion from oil continuous to water continuous or vice versa.

3.2.2 Flow Pattern Transition

The transition to dispersed flow pattern occurs when the continuous liquid phase turbulence is sufficiently intense to break the other liquid phase into small droplets and disperse them. In gas-liquid two-phase flows, the mixing status of the gas and liquid is determined based on the balance between the total turbulent energy of the liquid and the total free-surface energy of the gas bubbles. The same concept can be used to model the mixing status of the oil and water in two-phase and three-phase pipe flows. The high turbulence forces usually occur when one or both liquid flow rates are increased. Therefore, a criterion can be derived that one liquid becomes dispersed in the other when liquid-mixture velocity is higher than a certain value. In order to establish the dispersion criterion, the maximum liquid droplet size d_{max} that can be generated under the specific flow conditions is smaller than a critical diameter value d_{CRIT}. The methods used to estimate these diameters will be presented below with and without the presence of gas.

3.2.2.1 Two-Phase Oil-Water Liquid Droplets Size: Hinze (1955) studied the breakup process and discovered that the maximum stable diameter of the dispersed-phase results from a balance between surface tension forces and turbulent forces. The droplet behaviors are studied for dilute and dense dispersion regimes. When the droplets are fully suspended and transported at low pressure and high velocity, the droplets float in a dilute dispersion. In order to confirm the Hinze (1955) equation, a dimensionless analysis was performed in this study in terms of density, droplet diameter, surface tension, and energy dissipation per unit mass and the resultant equation can be written as

$$C_1 = \frac{\rho \varepsilon^{\frac{2}{3}} d_{MAX}^{\frac{5}{3}}}{\sigma_{OW}}, \tag{3-64}$$

where the energy dissipation per unit mass is expressed as

$$\varepsilon = \frac{2}{d} f_M v_M^3, \tag{3-65}$$

and

$$f_M = 0.046 \left(\frac{d \rho_M v_M}{\mu_M} \right)^{-0.2}. \tag{3-66}$$

By rearranging in terms of the maximum droplet diameter,

$$d_{MAX} = C_2 \frac{\sigma^{0.6} d^{0.4}}{1.32 f_M^{0.4} v_M^{1.2} \rho_M^{0.6}}. \tag{3-67}$$

Hinze (1955) suggested a constant value of 0.725 for parameter C_2, and by applying the value in Eq. (3-67), the maximum droplet diameter for dilute dispersion regime can be obtained as

$$d_{MAX}^{Dilute} = 0.549 \frac{\sigma^{0.6} d^{0.4}}{f_M^{0.4} v_M^{1.2} \rho_M^{0.6}}. \tag{3-68}$$

The resulting equation mentioned above matches the one provided by Hinze (1955) for dilute dispersion regime. On the other hand, the droplets are floating in a dense dispersion when they are not suspended and transported at high pressure and low velocity. Under such conditions, the droplets coalesce, requiring higher turbulent energy to disrupt the process and promote the dispersion. Brauner (2001) provided a correction factor for the maximum bubble size in dense flow dispersions, which is based on the gas void fraction. He proposed the following value for the parameter C_2,

$$C_2 = 2.93 \left(\frac{\alpha_D}{1 - \alpha_D} \right)^{0.6}. \tag{3-69}$$

By applying this C_2 relation in Eq. (3-67), the maximum droplet diameter for dense

dispersion regime becomes

$$d_{MAX}^{Dense} = 2.221\left(\frac{\alpha_D}{1-\alpha_D}\right)^{0.6} \frac{\sigma^{0.6} d^{0.4}}{f_M^{0.4} v_M^{1.2} \rho_M^{0.6}}. \tag{3-70}$$

It is recommended that for a liquid-liquid flow the maximum droplet size diameter be the largest obtained from the dilute and dense dispersion expressions as

$$d_{MAX} = Max\left(d_{MAX}^{Dilute}, d_{MAX}^{Dense}\right). \tag{3-71}$$

The bubbles resulting from the breakup process can exhibit different types of behavior. For stable and sustained droplets with a low rate of coalescence, the continuous phase turbulent forces should be sufficiently high to overcome the bubble agglomeration and creaming mechanisms. The bubble agglomeration tends to lead to coalescence when the resulting bubble size is larger than a critical value. An expression for the critical bubble diameter which is a strong function of the surface tension was proposed by Brodkey (1967) and modified by Barnea *et al.* (1982) as

$$d_{CD} = 2\left[\frac{0.4\sigma}{\left|\rho_C - \rho_D\right| g \cos\theta}\right]^{1/2}. \tag{3-72}$$

The migration of the dispersed phase of an emulsion under the influence of buoyancy is called the creaming effect. This mechanism takes place when the turbulent forces of the continuous phase overcome the buoyancy force of the droplets. Unlike the agglomeration mechanism which is a function of the constant value of surface tension, the creaming effect is a strong function of a continuous phase turbulent force—namely mixture velocity. Taitel and Duckler (1976) suggested the following relation by equating the buoyancy and turbulent forces and solved for the diameter,

$$d_{CB} = \frac{3}{8}\frac{\rho_C}{\left(\rho_W - \rho_O\right)}\frac{f_M v_M^2}{g\cos\theta}. \tag{3-73}$$

For oil and water emulsion to occur, the maximum droplet diameter should be less than both the critical droplet diameters due to agglomeration and creaming mechanisms,

$$d_{MAX} \le d_{CD} \quad and \quad d_{MAX} \le d_{CB} \quad . \tag{3-74}$$

3.2.2.2 Three-Phase Gas-Oil-Water Liquid Droplets Size: The previous section discussed the case when the oil and water are fully distributed in the pipe. When there is gas layer present at the top of the pipe, the liquid film holdup and velocity will be altered and create conditions favorable for liquid dispersion. This can be seen in three-layer stratified flow and in the film region of slug flow. The previous criteria can be similarly used, but by replacing the mixture velocity with local film velocity and the pipe diameter with liquid hydraulic diameter. First, the two-phase gas-liquid model is used by assuming that the oil-water are fully mixed. The gas-liquid model is used to estimate the liquid film characteristics such as liquid velocity, wetted perimeters, and corresponding liquid hydraulic diameter. The calculated liquid phase characteristics are used to calculate the maximum and critical droplet diameters. When superficial gas velocity is increased, the liquid holdup will decrease, and the liquid film velocity will increase, which in turn will promote the dispersion. The maximum droplet diameter for dilute and dense flows then become

$$d_{MAX}^{Dilute} = 0.549\frac{\sigma^{0.6} d_L^{0.4}}{f_M^{0.4} v_F^{1.2} \rho_M^{0.6}} \tag{3-75}$$

and

$$d_{MAX}^{Dense} = 2.221\left(\frac{\alpha_D}{1-\alpha_D}\right)^{0.6} \frac{\sigma^{0.6} d_L^{0.4}}{f_M^{0.4} v_F^{1.2} \rho_M^{0.6}}. \tag{3-76}$$

The mixture friction factor becomes

$$f_M = 0.046\left(\frac{d_L \rho_M v_F}{\mu_M}\right)^{-0.2}. \tag{3-77}$$

The critical diameter in Eq. (3-72) stays the same, as it is not a function of either the diameter or the flow rate. However, the critical diameter due to the creaming effect becomes

$$d_{CB} = \frac{3}{8}\frac{\rho_C}{\left(\rho_W - \rho_O\right) g\cos\theta}\frac{f_M v_F^2}{}. \tag{3-78}$$

CHAPTER 4

NUMERICAL SCHEME AND SOLUTION ALGORITHM

The set of conservation equations developed in the previous chapter are non-linear and one-dimensional partial differential equations. Those equations are impossible to be solved analytically, and require the application of numerical methods. In this chapter, two different solution algorithms are proposed and tested—the fully transient and semi-transient calculations. The fully transient procedure requires several iterations, and therefore more simulation time is required. The semi-transient one is simpler and faster and has good accuracy. Both methods require converging the main variables, which are holdups, velocities, and pressures. For both the fully transient and semi-transient methods and for all the flow patterns, the procedure for the pressure calculation is as follows. Given the local pressure (from previous time step), the physical properties for each cell can be calculated. After following the procedures proposed below for the velocities and holdups, the pressure drop between every two adjacent cells can be obtained. Assuming that the outlet pressure is given, the pressure drops are used to calculate the pressure at the jth increment using the pressure at the $(j+1)$th increment. The fluid properties can then be modified to the new pressure and a new iteration for the other variables is performed. The solution algorithm that will be presented below is started after the calculation of the pressure and fluid properties to converge the mass and momentum conservation equations for the holdups, velocities, and pressure drops.

4.1 Fully-Transient Solution

The three primary flow patterns in this study are the three-layer stratified flow, slug flow with stratified film and slug, and slug flow with stratified film and mixed slug. Each flow pattern has different unknowns, which requires different solution algorithms, and they will be presented below individually.

4.1.1 Three-Layer Stratified Flow

For three-layer stratified flow, there are fourteen hydrodynamic variables *(H_O, H_W, H_G, H_{OF}, H_{WF}, H_C, H_{OC}, H_{WC}, v_{SO}, v_{SW}, v_{SG}, v_{OF}, v_{WF}, v_C)*, which require fourteen equations to predict them. Since the water, oil, and gas must fill the pipe ($H_O+H_W+H_G=1$ and $H_{OF}+H_{WF}+H_C=1$), the variables are reduced to twelve. These hydrodynamic variables can then be estimated directly using the six mass and momentum conservation equations for the three phases and other six basic relationships. However, the mass and momentum conservation equations are implicit equations for the velocities and holdups and should be coupled and solved simultaneously and thus allow a stepwise integration. Moreover, the conservation equations are partial differentials and need to be discretized and solved numerically using finite difference schemes. As described in the literature review, the complexity of the new model requires using the fully implicit finite difference scheme to avoid the instability associated with the explicit and semi-implicit schemes. The numerical solution demands that the pipe be divided into discrete finite cells Δz. At each cell, the point *(n, j)* is used to express the n-th time and j-th node in the pipe. To link the cells together, the known variables *U(n, j), U(n, j-1)*, and *U(n+1, j-1)* are used to obtain the new time step at the current cell *U(n+1, j)*. Using this terminology, the space and time derivatives in the mass and momentum differential equations are discretized as follows:

(i) Space derivative (backward Euler differencing):

$$\frac{\left(U\right)_j^{n+1}-\left(U\right)_{j-1}^{n+1}}{\Delta z}. \tag{4-1}$$

(ii) Time derivative (forward time differencing):

$$\frac{\left(U\right)_j^{n+1}-\left(U\right)_j^{n}}{\Delta t}. \tag{4-2}$$

Using the above differencing, the mass conservation equations for oil, water, and gas can be respectively written as

$$\frac{\left(H_O\right)_j^{n+1}-\left(H_O\right)_j^{n}}{\Delta t}=-\frac{\left[\left(v_{SO}\right)_j^{n+1}-\left(v_{SO}\right)_{j-1}^{n+1}\right]}{\Delta z}, \tag{4-3}$$

$$\frac{\left(H_W\right)_j^{n+1}-\left(H_W\right)_j^{n}}{\Delta t}=-\frac{\left[\left(v_{SW}\right)_j^{n+1}-\left(v_{SW}\right)_{j-1}^{n+1}\right]}{\Delta z}, \tag{4-4}$$

and

$$\frac{\left[\left(\rho_G\right)_j^{n+1}\left(H_G\right)_j^{n+1}-\left(\rho_G\right)_j^{n}\left(H_G\right)_j^{n}\right]}{\Delta t}=-\frac{\left[\left(\rho_G\right)_j^{n+1}\left(v_{SG}\right)_j^{n+1}-\left(\rho_G\right)_{j-1}^{n+1}\left(v_{SG}\right)_{j-1}^{n+1}\right]}{\Delta z}. \tag{4-5}$$

The three momentum equations in three-layer stratified flow are used to confirm the water and liquid holdups and to calculate the pressure gradients. Since the solution of the momentum equations for these variables is in principle an implicit solution, direct calculation is not possible, and a new formulation must be used. The proposed method is obtained by creating two combined momentum equations and one pressure equation. The two combined momentum equations are achieved by eliminating the pressure gradient, while the pressure equation is

reached by direct summation. This allows the calculation of water and liquid holdups without prior knowledge of pressure gradient which in turn reduce the implicitness of the momentum equations. The combined momentum equations for gas and liquid streams and for oil and water streams can be respectively written as

$$\begin{aligned}
&\rho_C\left(\frac{\partial v_C}{\partial t}+v_C\frac{\partial v_C}{\partial z}\right)-\frac{\rho_O\left(\frac{\partial v_{OF}}{\partial t}+v_{OF}\frac{\partial v_{OF}}{\partial z}\right)}{\left(H_{WF}+H_{OF}\right)}-\frac{\rho_W\left(\frac{\partial v_{WF}}{\partial t}+v_{WF}\frac{\partial v_{WF}}{\partial z}\right)}{\left(H_{WF}+H_{OF}\right)}\\
&-\frac{\tau_{OF}S_{OF}+\tau_{WF}S_{WF}}{\left(H_{WF}+H_{OF}\right)A}+\frac{\tau_{I1}S_{I1}}{A}\left(\frac{1}{H_{OF}+H_{WF}}+\frac{1}{1-H_{OF}-H_{WF}}\right)\\
&+\frac{\tau_C S_C}{\left(1-H_{OF}-H_{WF}\right)A}-\left(\frac{\rho_O H_{OF}+\rho_W H_{WF}}{H_{OF}+H_{WF}}-\rho_C\right)g\sin\theta=0.
\end{aligned}\tag{4-6}$$

and

$$\begin{aligned}
&\rho_O\left(\frac{\partial v_{OF}}{\partial t}+v_{OF}\frac{\partial v_{OF}}{\partial z}\right)-\rho_W\left(\frac{\partial v_{WF}}{\partial t}+v_{WF}\frac{\partial v_{WF}}{\partial z}\right)\\
&-\frac{\tau_{WF}S_{WF}}{H_{WF}A}+\frac{\tau_{OF}S_{OF}-\tau_{I1}S_{I1}}{H_{OF}A}+\frac{\tau_{I2}S_{I2}}{A}\left(\frac{1}{H_{WF}}+\frac{1}{H_{OF}}\right)-\left(\rho_W-\rho_O\right)g\sin\theta=0.
\end{aligned}\tag{4-7}$$

Following the fully implicit numerical scheme, the combined momentum equations for gas and liquid streams and for oil and water streams can be respectively discretized as

$$
\begin{aligned}
&\left(\rho_C\right)_j^{n+1}\left(\frac{\left(v_C\right)_j^{n+1}-\left(v_C\right)_j^{n}}{\Delta t}+\left(v_C\right)_j^{n+1}\frac{\left(v_C\right)_j^{n+1}-\left(v_C\right)_{j-1}^{n+1}}{\Delta z}\right)\\
&-\frac{\left(\rho_W\right)_j^{n+1}\left(\frac{\left(v_{WF}\right)_j^{n+1}-\left(v_{WF}\right)_j^{n}}{\Delta t}+\left(v_{WF}\right)_j^{n+1}\frac{\left(v_{WF}\right)_j^{n+1}-\left(v_{WF}\right)_{j-1}^{n+1}}{\Delta z}\right)}{\left(H_{OF}+H_{WF}\right)_j^{n+1}}\\
&-\frac{\left(\rho_O\right)_j^{n+1}\left(\frac{\left(v_{OF}\right)_j^{n+1}-\left(v_{OF}\right)_j^{n}}{\Delta t}+\left(v_{OF}\right)_j^{n+1}\frac{\left(v_{OF}\right)_j^{n+1}-\left(v_{OF}\right)_{j-1}^{n+1}}{\Delta z}\right)}{\left(H_{OF}+H_{WF}\right)_j^{n+1}}\\
&\left[-\frac{\tau_{OF}S_{OF}+\tau_{WF}S_{WF}}{\left(H_{OF}+H_{WF}\right)A}+\frac{\tau_{I1}S_{I1}}{A}\left(\frac{1}{H_{OF}+H_{WF}}+\frac{1}{1-H_{OF}-H_{WF}}\right)\right.\\
&\left.+\frac{\tau_C S_C}{\left(1-H_{OF}-H_{WF}\right)A}-\left(\frac{\rho_O H_{OF}+\rho_W H_{WF}}{H_{OF}+H_{WF}}-\rho_C\right)g\sin\theta\right]_j^{n+1}=0
\end{aligned}
\tag{4-8}
$$

and

$$
\begin{aligned}
&\left(\rho_O\right)_j^{n+1}\left(\frac{\left(v_{OF}\right)_j^{n+1}-\left(v_{OF}\right)_j^{n}}{\Delta t}+\left(v_{OF}\right)_j^{n+1}\frac{\left(v_{OF}\right)_j^{n+1}-\left(v_{OF}\right)_{j-1}^{n+1}}{\Delta z}\right)\\
&-\left(\rho_W\right)_j^{n+1}\left(\frac{\left(v_{WF}\right)_j^{n+1}-\left(v_{WF}\right)_j^{n}}{\Delta t}+\left(v_{WF}\right)_j^{n+1}\frac{\left(v_{WF}\right)_j^{n+1}-\left(v_{WF}\right)_{j-1}^{n+1}}{\Delta z}\right)\\
&\left[-\frac{\tau_{WF}S_{WF}}{H_{WF}A}+\frac{\tau_{OF}S_{OF}-\tau_{I1}S_{I1}}{H_{OF}A}+\frac{\tau_{I2}S_{I2}}{A}\left(\frac{1}{H_{WF}}+\frac{1}{H_{OF}}\right)-\left(\rho_W-\rho_O\right)g\sin\theta\right]_j^{n+1}=0.
\end{aligned}
\tag{4-9}
$$

The calculation steps for every cell in order to confirm the water and liquid holdups are as follows:

1. Start by assuming the values of H_W^{n+1} and H_L^{n+1}.
2. Calculate v_{SO}^{n+1} from the mass balance equation, Eq. (4-3).
3. Calculate v_{SW}^{n+1} from the mass balance equation, Eq. (4-4).

4. Calculate v_{SG}^{n+1} from the mass balance equation, Eq. (4-5).
5. Calculate the liquid entrainment fraction F_E using the selected closure relationship.
6. Calculate the gas core velocity v_C^{n+1} from Eq. (3-7).
7. Calculate the oil film holdup in gas core H_{OC}^{n+1} from Eq. (3-8).
8. Calculate the water film holdup in gas core H_{WC}^{n+1} from Eq. (3-9).
9. Calculate the oil film holdup H_{OF}^{n+1} from Eq. (3-10).
10. Calculate the water film holdup H_{WF}^{n+1} from Eq. (3-11).
11. Calculate the local oil velocity v_{OF}^{n+1} from Eq. (3-12).
12. Calculate the local water velocity v_{WF}^{n+1} from Eq. (3-13).
13. The combined momentum equations Eq. (4-8) and Eq. (4-9) are used to confirm the assumed next step water and liquid holdups in step 1, and a new iteration should be performed until convergence.

4.1.2 Slug Flow with Stratified Film and Slug

For slug flow with stratified film and slug, due to momentum exchange between the film and slug regions, extra variables are introduced and consequently more complexity exists. By eliminating the void fraction H_G and gas core holdup H_C due to the holdup restriction, sixteen hydrodynamic variables (H_O, H_W, H_{OF}, H_{WF}, H_{WGS}, α_{OS}, α_{WS}, v_{SO}, v_{SW}, v_{SG}, v_{OF}, v_{WF}, v_C, v_{OS}, v_{WS}, l_f) emerge. The mass conservation equations from the three-layer stratified flow Eq. (4-3), Eq. (4-4), and Eq. (4-5) can be used for the average holdup and superficial velocities of the slug unit. The mass conservation equations for the oil and water films in the gas-pocket region Eq. (3-18) and Eq. (3-19) can be discretized using the same approach described for three-layer stratified flow continuity equations as

$$\frac{\left(H_{OF}\right)_j^{n+1}-\left(H_{OF}\right)_j^{n}}{\Delta t}=-\frac{\left[\left(H_{OF}\right)_j^{n+1}\left(v_{OF}\right)_j^{n+1}-\left(H_{OF}\right)_{j-1}^{n+1}\left(v_{OF}\right)_{j-1}^{n+1}\right]}{\Delta z}+\left[\frac{\left(1-H_{WGS}\right)\left(1-\alpha_{OS}\right)\left(v_T-v_{OS}\right)-H_{OF}\left(v_T-v_{OF}\right)}{l_F}\right]_j^{n+1} \tag{4-10}$$

and

$$\frac{\left(H_{WF}\right)_j^{n+1}-\left(H_{WF}\right)_j^{n}}{\Delta t}=-\frac{\left[\left(H_{WF}\right)_j^{n+1}\left(v_{WF}\right)_j^{n+1}-\left(H_{WF}\right)_{j-1}^{n+1}\left(v_{WF}\right)_{j-1}^{n+1}\right]}{\Delta z}+\left[\frac{H_{WGS}\left(1-\alpha_{WS}\right)\left(v_T-v_{WS}\right)-H_{WF}\left(v_T-v_{WF}\right)}{l_F}\right]_j^{n+1}. \tag{4-11}$$

For slug flow with stratified film and slug, five momentum conservation equations are present, three for the gas-pocket region and two for the slug body. In the gas pocket region, the three momentum equations follow the same formulation for the three-layer stratified flow in producing two combined momentum equations. They can also be used to confirm the estimation of water and liquid holdups. The combined momentum equations for gas and liquid streams and for oil and water streams can be respectively written as

$$\begin{aligned}&\rho_C\left(\frac{\partial v_C}{\partial t}+v_C\frac{\partial v_C}{\partial z}\right)-\frac{\rho_O\left(\frac{\partial v_{OF}}{\partial t}+v_{OF}\frac{\partial v_{OF}}{\partial z}\right)}{\left(H_{OF}+H_{WF}\right)}-\frac{\rho_W\left(\frac{\partial v_{WF}}{\partial t}+v_{WF}\frac{\partial v_{WF}}{\partial z}\right)}{\left(H_{OF}+H_{WF}\right)}\\&+\frac{\rho_O H_{OF}\left(v_T-v_{OF}\right)\left(v_{OS}-v_{OF}\right)+\rho_W H_{WF}\left(v_T-v_{WF}\right)\left(v_{WS}-v_{WF}\right)}{l_F\left(H_{OF}+H_{WF}\right)}\\&-\frac{\tau_{OF}S_{OF}+\tau_{WF}S_{WF}}{\left(H_{OF}+H_{WF}\right)A}+\frac{\tau_{I1}S_{I1}}{A}\left(\frac{1}{H_{OF}+H_{WF}}+\frac{1}{1-H_{OF}-H_{WF}}\right)\\&+\frac{\tau_C S_C}{\left(1-H_{OF}-H_{WF}\right)A}-\left(\frac{\rho_O H_{OF}+\rho_W H_{WF}}{H_{OF}+H_{WF}}-\rho_C\right)g\sin\theta=0\end{aligned} \tag{4-12}$$

and

$$\rho_O\left(\frac{\partial v_{OF}}{\partial t}+v_{OF}\frac{\partial v_{OF}}{\partial z}\right)-\rho_W\left(\frac{\partial v_{WF}}{\partial t}+v_{WF}\frac{\partial v_{WF}}{\partial z}\right)$$
$$+\frac{\rho_W\left(v_T-v_{WF}\right)\left(v_{WS}-v_{WF}\right)-\rho_O\left(v_T-v_{OF}\right)\left(v_{OS}-v_{OF}\right)}{l_F} \tag{4-13}$$
$$-\frac{\tau_{WF}S_{WF}}{H_{WF}A}+\frac{\tau_{OF}S_{OF}-\tau_{I1}S_{I1}}{H_{OF}A}+\frac{\tau_{I2}S_{I2}}{A}\left(\frac{1}{H_{WF}}+\frac{1}{H_{OF}}\right)-\left(\rho_W-\rho_O\right)g\sin\theta=0.$$

In the slug body region, the gas is dispersed in both oil and water layers and therefore, only two momentum equations are present. These two equations are used to produce the third combined momentum equation, which is used to estimate the water holdup with entrapped gas in the slug body H_{WGS}. The combined momentum equation for the slug body can be obtained as

$$\rho_{OS}\left(\frac{\partial v_{OS}}{\partial t}+v_{OS}\frac{\partial v_{OS}}{\partial z}\right)-\rho_{WS}\left(\frac{\partial v_{WS}}{\partial t}+v_{WS}\frac{\partial v_{WS}}{\partial z}\right)$$
$$+\frac{\rho_{WS}\left(v_T-v_{WS}\right)\left(v_{WF}-v_{WS}\right)-\rho_{OS}\left(v_T-v_{OS}\right)\left(v_{OF}-v_{OS}\right)}{l_S} \tag{4-14}$$
$$-\frac{\tau_{WS}S_{WS}}{H_{WGS}A}+\frac{\tau_{OS}S_{OS}}{\left(1-H_{WGS}\right)A}+\frac{\tau_{I0}S_{I0}}{A}\left[\frac{1}{H_{WGS}}+\frac{1}{\left(1-H_{WGS}\right)}\right]-\left(\rho_{WS}-\rho_{OS}\right)g\sin\theta=0.$$

The discretized combined momentum conservation equations for gas and liquid streams and for oil and water streams in the gas-pocket region can be respectively written as

$$
\begin{aligned}
&\left(\rho_C\right)_j^{n+1}\left(\frac{\left(v_C\right)_j^{n+1}-\left(v_C\right)_j^{n}}{\Delta t}+\left(v_C\right)_j^{n+1}\frac{\left(v_C\right)_j^{n+1}-\left(v_C\right)_{j-1}^{n+1}}{\Delta z}\right)\\
&-\frac{\left(\rho_W\right)_j^{n+1}\left(\frac{\left(v_{WF}\right)_j^{n+1}-\left(v_{WF}\right)_j^{n}}{\Delta t}+\left(v_{WF}\right)_j^{n+1}\frac{\left(v_{WF}\right)_j^{n+1}-\left(v_{WF}\right)_{j-1}^{n+1}}{\Delta z}\right)}{\left(H_{OF}+H_{WF}\right)_j^{n+1}}\\
&-\frac{\left(\rho_O\right)_j^{n+1}\left(\frac{\left(v_{OF}\right)_j^{n+1}-\left(v_{OF}\right)_j^{n}}{\Delta t}+\left(v_{OF}\right)_j^{n+1}\frac{\left(v_{OF}\right)_j^{n+1}-\left(v_{OF}\right)_{j-1}^{n+1}}{\Delta z}\right)}{\left(H_{OF}+H_{WF}\right)_j^{n+1}}\\
&\left[\begin{array}{l}
\dfrac{\rho_O H_{OF}\left(v_T-v_{OF}\right)\left(v_{OS}-v_{OF}\right)+\rho_W H_{WF}\left(v_T-v_{WF}\right)\left(v_{WS}-v_{WF}\right)+}{l_F\left(H_{OF}+H_{WF}\right)}\\
-\dfrac{\tau_{OF}S_{OF}+\tau_{WF}S_{WF}}{\left(H_{OF}+H_{WF}\right)A}+\dfrac{\tau_{I1}S_{I1}}{A}\left(\dfrac{1}{H_{OF}+H_{WF}}+\dfrac{1}{1-H_{OF}-H_{WF}}\right)\\
+\dfrac{\tau_C S_C}{\left(1-H_{OF}-H_{WF}\right)A}-\left(\dfrac{\rho_O H_{OF}+\rho_W H_{WF}}{H_{OF}+H_{WF}}-\rho_C\right)g\sin\theta
\end{array}\right]_j^{n+1}=0
\end{aligned}
\tag{4-15}
$$

and

$$
\begin{aligned}
&\left(\rho_O\right)_j^{n+1}\left(\frac{\left(v_{OF}\right)_j^{n+1}-\left(v_{OF}\right)_j^{n}}{\Delta t}+\left(v_{OF}\right)_j^{n+1}\frac{\left(v_{OF}\right)_j^{n+1}-\left(v_{OF}\right)_{j-1}^{n+1}}{\Delta z}\right)\\
&-\left(\rho_W\right)_j^{n+1}\left(\frac{\left(v_{WF}\right)_j^{n+1}-\left(v_{WF}\right)_j^{n}}{\Delta t}+\left(v_{WF}\right)_j^{n+1}\frac{\left(v_{WF}\right)_j^{n+1}-\left(v_{WF}\right)_{j-1}^{n+1}}{\Delta z}\right)\\
&\left[\begin{array}{l}
\dfrac{\rho_W\left(v_T-v_{WF}\right)\left(v_{WS}-v_{WF}\right)-\rho_O\left(v_T-v_{OF}\right)\left(v_{OS}-v_{OF}\right)}{l_F}\\
-\dfrac{\tau_{WF}S_{WF}}{H_{WF}A}+\dfrac{\tau_{OF}S_{OF}-\tau_{I1}S_{I1}}{H_{OF}A}+\dfrac{\tau_{I2}S_{I2}}{A}\left(\dfrac{1}{H_{WF}}+\dfrac{1}{H_{OF}}\right)-\left(\rho_W-\rho_O\right)g\sin\theta
\end{array}\right]_j^{n+1}=0.
\end{aligned}
\tag{4-16}
$$

The discretized combined momentum equation for the slug body can be written as

$$
\begin{aligned}
&\left(\rho_{OS}\right)_j^{n+1}\left(\frac{\left(v_{OS}\right)_j^{n+1}-\left(v_{OS}\right)_j^{n}}{\Delta t}+\left(v_{OS}\right)_j^{n+1}\frac{\left(v_{OS}\right)_j^{n+1}-\left(v_{OS}\right)_{j-1}^{n+1}}{\Delta z}\right)\\
&-\left(\rho_{WS}\right)_j^{n+1}\left(\frac{\left(v_{WS}\right)_j^{n+1}-\left(v_{WS}\right)_j^{n}}{\Delta t}+\left(v_{WS}\right)_j^{n+1}\frac{\left(v_{WS}\right)_j^{n+1}-\left(v_{WS}\right)_{j-1}^{n+1}}{\Delta z}\right)\\
&\left[\begin{array}{l}\dfrac{\rho_{WS}\left(v_T-v_{WS}\right)\left(v_{WF}-v_{WS}\right)-\rho_{OS}\left(v_T-v_{OS}\right)\left(v_{OF}-v_{OS}\right)}{l_S}\\[2ex] -\dfrac{\tau_{WS}S_{WS}}{H_{WGS}A}+\dfrac{\tau_{OS}S_{OS}}{\left(1-H_{WGS}\right)A}+\dfrac{\tau_{I0}S_{I0}}{A}\left(\dfrac{1}{H_{WGS}}+\dfrac{1}{\left(1-H_{WGS}\right)}\right)-\left(\rho_{WS}-\rho_{OS}\right)g\sin\theta\end{array}\right]_j^{n+1}=0.
\end{aligned}
\tag{4-17}
$$

The calculation steps are as follows:

1. Start by assuming the values of H_W^{n+1}, H_L^{n+1}, and H_{WGS}^{n+1}.
2. Calculate v_{SO}^{n+1} from the mass balance equation, Eq. (4-3).
3. Calculate v_{SW}^{n+1} from the mass balance equation, Eq. (4-4).
4. Calculate v_{SG}^{n+1} from the mass balance equation, Eq. (4-5).
5. Calculate the slug length l_s and the translational velocity v_T from steady state correlations.
6. Calculate H_{OF}^{n+1} from the mass balance equation, Eq. (4-10).
7. Calculate H_{WF}^{n+1} from the mass balance equation, Eq. (4-11).
8. Calculate l_F^{n+1} by combining Eq. (3-34) and Eq. (3-35).
9. The five relationships Eq. (3-29), Eq. (3-30), Eq. (3-31), Eq. (3-32), Eq. (3-33) are used to determine the five velocities v_{OF}^{n+1}, v_{WF}^{n+1}, v_C^{n+1}, v_{OS}^{n+1}, v_{WS}^{n+1} in an iterative procedure.
10. Update α_{OS}^{n+1} and α_{WS}^{n+1} from Eq. (3-36).
11. The three combined momentum equations Eq. (4-15), Eq. (4-16), and Eq. (4-17) are used to confirm the three assumed holdups in step 1, and a new iteration should be performed until convergence.

It should be noted that the gas-volume fraction in oil of the slug body α_{OS} and the gas-volume fraction in water of the slug body α_{WS} are used initially from the previous time step and updated in step 10.

4.1.3 Slug Flow with Stratified Film and Mixed Slug

For slug flow with stratified film and mixed slug, the oil, water, and gas are all fully mixed in the slug body. The oil and water holdups in the slug body can be calculated using the no-slip concept (f_O and f_W) and the oil and water slug velocities can be calculated using the mixture velocity v_m. Because the mixture velocity and the no-slip holdups are direct functions of superficial velocities, the hydrodynamic variables are reduced to twelve (H_O, H_W, H_{OF}, H_{WF}, H_{LS}, v_{SO}, v_{SW}, v_{SG}, v_{OF}, v_{WF}, v_C, l_f). The discretized mass conservation equations for the oil and water streams in the gas-pocket region can be written as

$$\frac{\left(H_{OF}\right)_j^{n+1}-\left(H_{OF}\right)_j^{n}}{\Delta t}=-\frac{\left[\left(H_{OF}\right)_j^{n+1}\left(v_{OF}\right)_j^{n+1}-\left(H_{OF}\right)_{j-1}^{n+1}\left(v_{OF}\right)_{j-1}^{n+1}\right]}{\Delta z}+\left[\frac{f_O H_{LS}\left(v_T-v_M\right)-H_{OF}\left(v_T-v_{OF}\right)}{l_F}\right]_j^{n+1} \tag{4-18}$$

and

$$\frac{\left(H_{WF}\right)_j^{n+1}-\left(H_{WF}\right)_j^{n}}{\Delta t}=-\frac{\left[\left(H_{WF}\right)_j^{n+1}\left(v_{WF}\right)_j^{n+1}-\left(H_{WF}\right)_{j-1}^{n+1}\left(v_{WF}\right)_{j-1}^{n+1}\right]}{\Delta z}+\left[\frac{f_W H_{LS}\left(v_T-v_M\right)-H_{WF}\left(v_T-v_{WF}\right)}{l_F}\right]_j^{n+1}. \tag{4-19}$$

Because in this flow pattern the fluids are fully mixed in the slug body, the momentum equation for the slug body is neglected. In the gas pocket region, the gas, oil, and water are fully

separated and three momentum equations emerge. The same criteria for the slug flow with stratified film and slug of creating two-combined momentum equations can be followed but with replacing the slug velocities with mixture velocity. The combined momentum equations for gas and liquid streams and for oil and water streams can be respectively written as

$$\begin{aligned}
&\rho_C\left(\frac{\partial v_C}{\partial t}+v_C\frac{\partial v_C}{\partial z}\right)-\frac{\rho_W\left(\frac{\partial v_{WF}}{\partial t}+v_{WF}\frac{\partial v_{WF}}{\partial z}\right)}{\left(H_{OF}+H_{WF}\right)}-\frac{\rho_O\left(\frac{\partial v_{OF}}{\partial t}+v_{OF}\frac{\partial v_{OF}}{\partial z}\right)}{\left(H_{OF}+H_{WF}\right)}\\
&+\frac{\rho_O H_{OF}\left(v_T-v_{OF}\right)\left(v_M-v_{OF}\right)+\rho_W H_{WF}\left(v_T-v_{WF}\right)\left(v_M-v_{WF}\right)}{l_F\left(H_{OF}+H_{WF}\right)}\\
&-\frac{\tau_{OF}S_{OF}+\tau_{WF}S_{WF}}{\left(H_{OF}+H_{WF}\right)A}+\frac{\tau_{I1}S_{I1}}{A}\left(\frac{1}{H_{OF}+H_{WF}}+\frac{1}{1-H_{OF}-H_{WF}}\right)\\
&+\frac{\tau_C S_C}{\left(1-H_{OF}-H_{WF}\right)A}-\left(\frac{\rho_O H_{OF}+\rho_W H_{WF}}{H_{OF}+H_{WF}}-\rho_C\right)g\sin\theta=0.
\end{aligned}\tag{4-20}$$

and

$$\begin{aligned}
&\rho_O\left(\frac{\partial v_{OF}}{\partial t}+v_{OF}\frac{\partial v_{OF}}{\partial z}\right)-\rho_W\left(\frac{\partial v_{WF}}{\partial t}+v_{WF}\frac{\partial v_{WF}}{\partial z}\right)\\
&+\frac{\rho_W\left(v_T-v_{WF}\right)\left(v_M-v_{WF}\right)-\rho_O\left(v_T-v_{OF}\right)\left(v_M-v_{OF}\right)}{l_F}\\
&-\frac{\tau_{WF}S_{WF}}{H_{WF}A}+\frac{\tau_{OF}S_{OF}-\tau_{I1}S_{I1}}{H_{OF}A}+\frac{\tau_{I2}S_{I2}}{A}\left(\frac{1}{H_{WF}}+\frac{1}{H_{OF}}\right)-\left(\rho_W-\rho_O\right)g\sin\theta=0.
\end{aligned}\tag{4-21}$$

The discretized combined momentum conservation equations for gas and liquid streams and for oil and water streams in the gas-pocket region can be respectively written as

$$
\begin{aligned}
&\left(\rho_C\right)_j^{n+1}\left(\frac{\left(v_C\right)_j^{n+1}-\left(v_C\right)_j^{n}}{\Delta t}+\left(v_C\right)_j^{n+1}\frac{\left(v_C\right)_j^{n+1}-\left(v_C\right)_{j-1}^{n+1}}{\Delta z}\right)\\
&-\frac{\left(\rho_W\right)_j^{n+1}\left(\frac{\left(v_{WF}\right)_j^{n+1}-\left(v_{WF}\right)_j^{n}}{\Delta t}+\left(v_{WF}\right)_j^{n+1}\frac{\left(v_{WF}\right)_j^{n+1}-\left(v_{WF}\right)_{j-1}^{n+1}}{\Delta z}\right)}{\left(H_{OF}+H_{WF}\right)_j^{n+1}}\\
&-\frac{\left(\rho_O\right)_j^{n+1}\left(\frac{\left(v_{OF}\right)_j^{n+1}-\left(v_{OF}\right)_j^{n}}{\Delta t}+\left(v_{OF}\right)_j^{n+1}\frac{\left(v_{OF}\right)_j^{n+1}-\left(v_{OF}\right)_{j-1}^{n+1}}{\Delta z}\right)}{\left(H_{OF}+H_{WF}\right)_j^{n+1}}\\
&\left[\begin{array}{l}
\dfrac{\rho_O H_{OF}\left(v_T-v_{OF}\right)\left(v_M-v_{OF}\right)+\rho_W H_{WF}\left(v_T-v_{WF}\right)\left(v_M-v_{WF}\right)}{l_F\left(H_{OF}+H_{WF}\right)}\\
-\dfrac{\tau_{OF}S_{OF}+\tau_{WF}S_{WF}}{\left(H_{OF}+H_{WF}\right)A}+\dfrac{\tau_{I1}S_{I1}}{A}\left(\dfrac{1}{H_{OF}+H_{WF}}+\dfrac{1}{1-H_{OF}-H_{WF}}\right)\\
+\dfrac{\tau_C S_C}{\left(1-H_{OF}-H_{WF}\right)A}-\left(\dfrac{\rho_O H_{OF}+\rho_W H_{WF}+}{H_{OF}+H_{WF}}-\rho_C\right)g\sin\theta
\end{array}\right]_j^{n+1}=0
\end{aligned}
\tag{4-22}
$$

and

$$
\begin{aligned}
&\left(\rho_O\right)_j^{n+1}\left(\frac{\left(v_{OF}\right)_j^{n+1}-\left(v_{OF}\right)_j^{n}}{\Delta t}+\left(v_{OF}\right)_j^{n+1}\frac{\left(v_{OF}\right)_j^{n+1}-\left(v_{OF}\right)_{j-1}^{n+1}}{\Delta z}\right)\\
&-\left(\rho_W\right)_j^{n+1}\left(\frac{\left(v_{WF}\right)_j^{n+1}-\left(v_{WF}\right)_j^{n}}{\Delta t}+\left(v_{WF}\right)_j^{n+1}\frac{\left(v_{WF}\right)_j^{n+1}-\left(v_{WF}\right)_{j-1}^{n+1}}{\Delta z}\right)\\
&\left[\begin{array}{l}
\dfrac{\rho_W\left(v_T-v_{WF}\right)\left(v_M-v_{WF}\right)-\rho_O\left(v_T-v_{OF}\right)\left(v_M-v_{OF}\right)}{l_F}\\
-\dfrac{\tau_{WF}S_{WF}}{H_{WF}A}+\dfrac{\tau_{OF}S_{OF}-\tau_{I1}S_{I1}}{H_{OF}A}+\dfrac{\tau_{I2}S_{I2}}{A}\left(\dfrac{1}{H_{WF}}+\dfrac{1}{H_{OF}}\right)-\left(\rho_W-\rho_O\right)g\sin\theta
\end{array}\right]_j^{n+1}=0.
\end{aligned}
\tag{4-23}
$$

The calculation steps are as follows:

1. Start by assuming the values of H_W^{n+1} and H_L^{n+1}.
2. Calculate v_{SO}^{n+1} from the mass balance equation, Eq. (4-3).
3. Calculate v_{SW}^{n+1} from the mass balance equation, Eq. (4-4).
4. Calculate v_{SG}^{n+1} from the mass balance equation, Eq. (4-5).
5. Calculate v_M^{n+1} from Eq. (3-41).
6. Calculate the slug length l_s and the translational velocity v_T from steady state correlations.
7. Calculate H_{OF}^{n+1} from the mass balance equation, Eq. (4-18).
8. Calculate H_{WF}^{n+1} from the mass balance equation, Eq. (4-19).
9. Calculate l_F^{n+1} by combining Eq. (3-54) and Eq. (3-55).
10. Calculate v_{OF}^{n+1} from Eq. (3-51).
11. Calculate v_{WF}^{n+1} from Eq. (3-52).
12. Calculate v_C^{n+1} from Eq. (3-53).
13. Update H_{LS}^{n+1} from Eq. (3-56).
14. The two combined momentum equations Eq. (4-22) and Eq. (4-23) are used to confirm the two assumed holdups in step 1, and a new iteration should be performed until convergence.

It should also be noted that the slug liquid holdup H_{LS} is used initially from the previous time step and updated in step 13.

4.2. Semi-Transient Solution

This solution method is considered semi-transient because the holdups are converged by using the transient mass conservation equations, while the combined momentum equations are used in their steady-state forms. The simplicity of these types of conservation equations allows

them to be solved also using implicit finite difference schemes. The solution starts with a guess of the next step holdups (H_O^{n+1} *and* H_W^{n+1}). The next step superficial velocities can be subsequently calculated from the mass conservation equations. The discretized transient mass conservation equations for oil, water, and gas can be given, respectively, as

$$\frac{\left(H_O\right)_j^{n+1}-\left(H_O\right)_j^n+\left(H_O\right)_{j-1}^{n+1}-\left(H_O\right)_{j-1}^n}{2\Delta t}=-\frac{\left[\left(v_{SO}\right)_j^{n+1}-\left(v_{SO}\right)_{j-1}^{n+1}\right]}{\Delta z}, \tag{4-24}$$

$$\frac{\left(H_W\right)_j^{n+1}-\left(H_W\right)_j^n+\left(H_W\right)_{j-1}^{n+1}-\left(H_W\right)_{j-1}^n}{2\Delta t}=-\frac{\left[\left(v_{SW}\right)_j^{n+1}-\left(v_{SW}\right)_{j-1}^{n+1}\right]}{\Delta z}, \tag{4-25}$$

and

$$\frac{\left(\rho_G H_G\right)_j^{n+1}-\left(\rho_G H_G\right)_j^n+\left(\rho_G H_G\right)_{j-1}^{n+1}-\left(\rho_G H_G\right)_{j-1}^n}{2\Delta t}= -\frac{\left[\left(\rho_G v_{SG}\right)_j^{n+1}-\left(\rho_G v_{SG}\right)_{j-1}^{n+1}\right]}{\Delta z}. \tag{4-26}$$

The space derivative is solved using backward Euler differencing, while the time derivative is solved using centered space and forward time differencing. The solutions of the momentum equations for the local velocities are in principle implicit solutions. However, in this method, the transient and acceleration terms are removed from the momentum equations, which allows them to be solved explicitly for the local velocities. The local velocities are distributed in the interfacial shear stress τ_i, friction factor f, and the wall shear stress τ_W. Because the interfacial shear stress and friction factor are very weak functions of local velocity, the convergence is performed explicitly by using the one in the wall shear stress. All the local velocity values are then updated in the next iteration. This explicit convergence allows faster simulation without sacrificing result accuracy. Although the momentum conservation equations are solved

explicitly, the numerical scheme can be considered implicit, in the sense that all the hydrodynamic variables are calculated based on the next time step holdups and superficial velocities. During the combined momentum equations' convergence, the holdups for each flow pattern can be determined from the following relations:

- Three-layer stratified flow:

$$H_W = \frac{v_{SW}}{v_{WF}} \tag{4-27}$$

$$H_O = \frac{v_{SO}}{v_{OF}} \tag{4-28}$$

- Slug flow with stratified film and slug:

$$H_O = \left[\left(1 - H_{WGS}\right)\left(1 - \alpha_{OS}\right)\left(v_T - v_{OS}\right) + v_{SO}\right] / v_T \tag{4-29}$$

$$H_W = \left[\left(1 - H_{WGS}\right)\left(1 - \alpha_{WS}\right)\left(v_T - v_{WS}\right) + v_{SW}\right] / v_T \tag{4-30}$$

- Slug flow with stratified film and mixed slug:

$$H_O = \left[f_O H_{LS}\left(v_T - v_M\right) + v_{SO}\right] / v_T \tag{4-31}$$

$$H_W = \left[f_W H_{LS}\left(v_T - v_M\right) + v_{SW}\right] / v_T \tag{4-32}$$

Finally, compare the assumed and calculated values of holdups, and if no convergence is reached, update them and repeat the previous steps. It should be noted that the solution algorithm is based on a double iteration method. The assumed values of holdups are used only to estimate the next time step superficial velocities in outer loop iteration. The inner loop iteration is used to solve the combined momentum equations based on the estimated superficial velocities, whereas the holdups are modified internally using the above relationships.

CHAPTER 5

MODEL VERIFICATIONS

In this chapter, the newly developed three-phase models are tested with different production setups. Large-scale validations have been performed to ensure the accuracy and stability of the new simulator. Two different three-phase flow patterns and a special case of low liquid loading are used to verify the steady-state part of the code. Three-phase flow pattern maps are used to confirm the smoothness and accuracy of the flow pattern transitions. Four different transient phenomena including steady-state perturbation, severe slugging in pipeline-riser system, gas-lift instabilities, and severe slugging in horizontal wells are used to validate the transient calculations of the new model. Validating the results against experimental or field data as a benchmark is essential but in the absence of such data, results from widely used simulators such as OLGA can be considered as a good touchstone. The new simulator predictions are compared with OLGA for the three-phase steady-state flow, the transient behavior of steady-state perturbation, gas-lift instabilities, and severe slugging in horizontal wells. Experimental results by Karami (2015) were used for the verifications of three-phase flow low liquid loading. Three-phase flow pattern maps for different water cuts were generated and compared with the experimental results of Keskin *et al.* (2007). Full analyses for three-phase severe slugging in pipeline-riser system have been conducted and the results were compared with Beltran (2005).

5.1 Steady-State Flow

The new transient hydrodynamic model for gas-oil-water pipe flow is first tested for the new flow patterns in which the flows are expected to be stable and in a steady state. The results are compared with the commercial simulator OLGA. The liquid holdups and pressure drops are calculated for different flow conditions and water cuts. The input data used to define the flows are listed in Tables A-1 and A-2 for three-layer stratified flow and slug flow with stratified film and slug, respectively.

For three-layer stratified flow in a straight horizontal pipe, the superficial liquid velocity is set as 0.01 m/s with water cut 40% and the superficial gas velocities range from 0.1 to 2.5 m/s. In Figure 5-1, the pressure drops from the new model match the prediction of the OLGA simulator. At constant liquid velocity, when the gas velocity increases, the pressure drop increases due to increasing of the wall shear stresses. However, the liquid and water holdups decrease with increasing gas velocity. They are plotted in Figure 5-2 and agree with the predictions of the OLGA simulator. The increase in gas flow rate creates stronger wave structure at the interface and increases the interfacial shear stress, which leads to a drop in the liquid level, accelerating the liquid phase velocity, and thereby decreasing the water and liquid holdups. In the new simulator, the holdups are converged, and the pressures are calculated afterwards. Therefore, if the holdup calculations between the newly developed models and the OLGA simulator are identical and the deviation exists only in the pressures, this means that the difference arises from using different closure relationships for calculating the shear stresses.

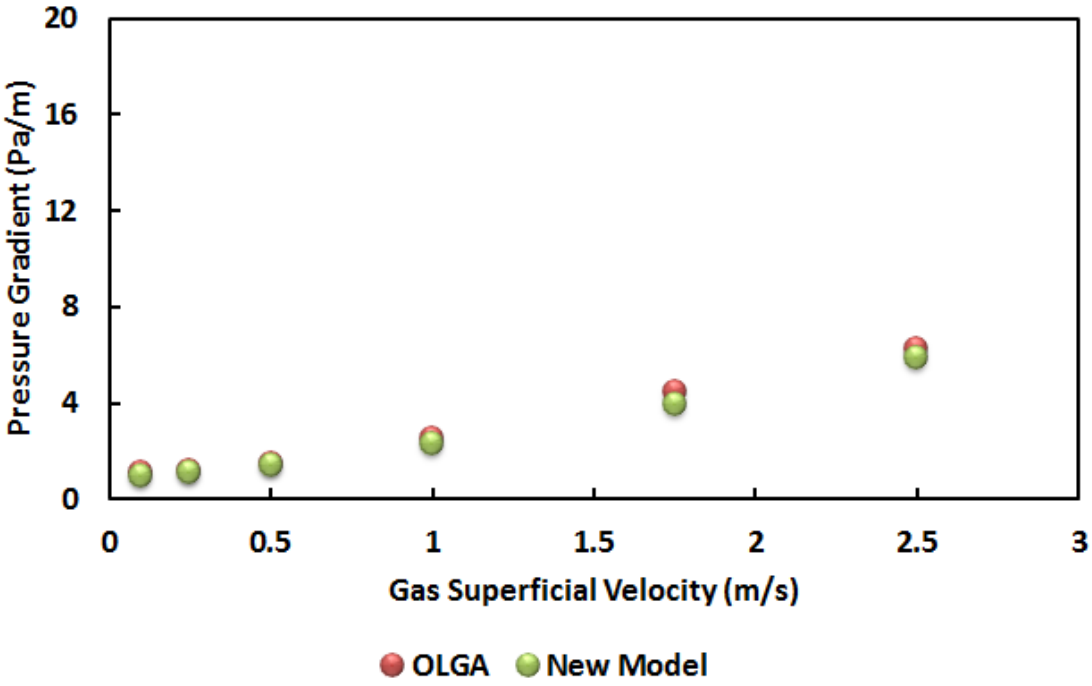

Figure 5-1: Pressure Drop Comparison with OLGA for Three-Layer Stratified Flow (WC = 40%)

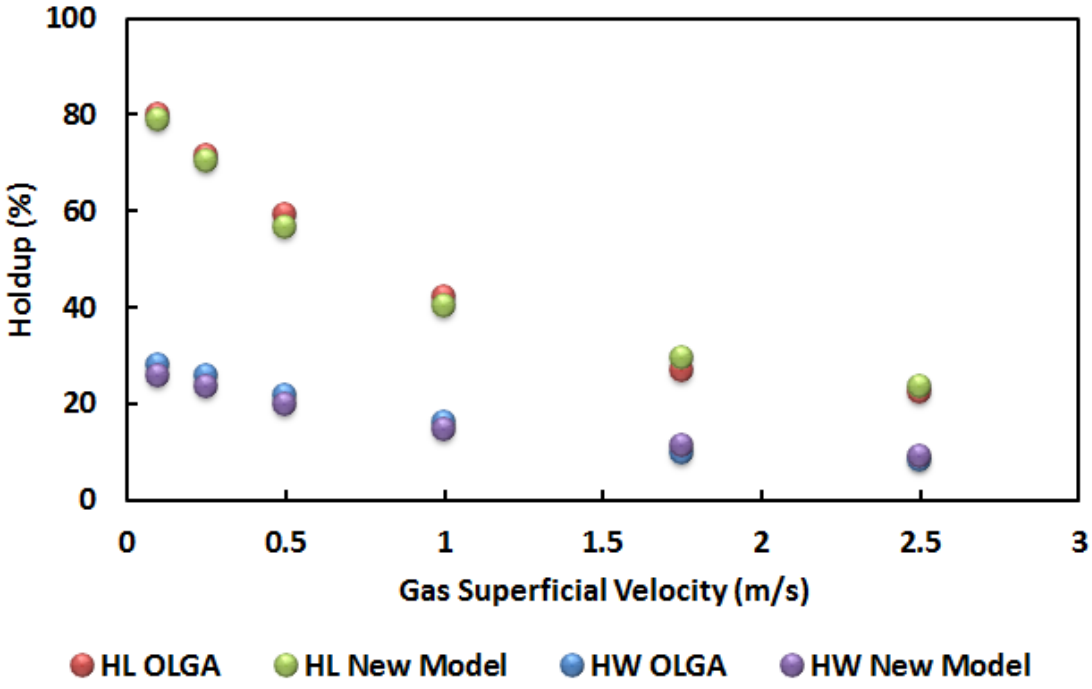

Figure 5-2: Holdups Comparison with OLGA for Three-Layer Stratified Flow (WC = 40%)

The second comparison is made by increasing the water cut to 80%. The pressure drops and water and liquid holdups are plotted in Figure 5-3 and Figure 5-4, respectively. The pressure gradients corresponding to 40% and 80% water cuts are close but the liquid holdups decrease with the increase in water cut. The three-layer stratified flow corresponds to relatively low gas and liquid flow rates. Therefore, the three phases are fully separated and no liquid is entrained in the gas layer. When the liquids are completely separated, the mixture viscosity has a linear effect. For this simulation setup, the viscosity of oil is much higher than that of water. Therefore, when the water cut increases, the mixture viscosity decreases. The increase in fluid viscosity increases the frictional pressure gradient, which is the dominant force in the horizontal pipeline, and leads to increased liquid holdup in the pipe.

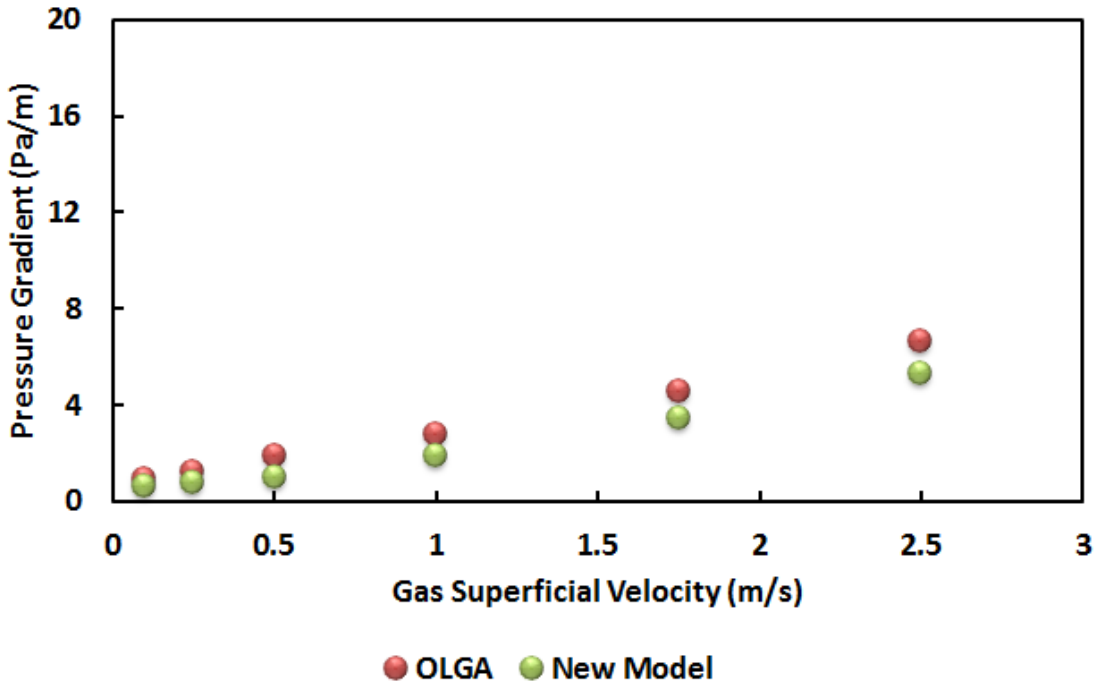

Figure 5-3: Pressure Drop Comparison with OLGA for Three-Layer Stratified Flow (WC = 80%)

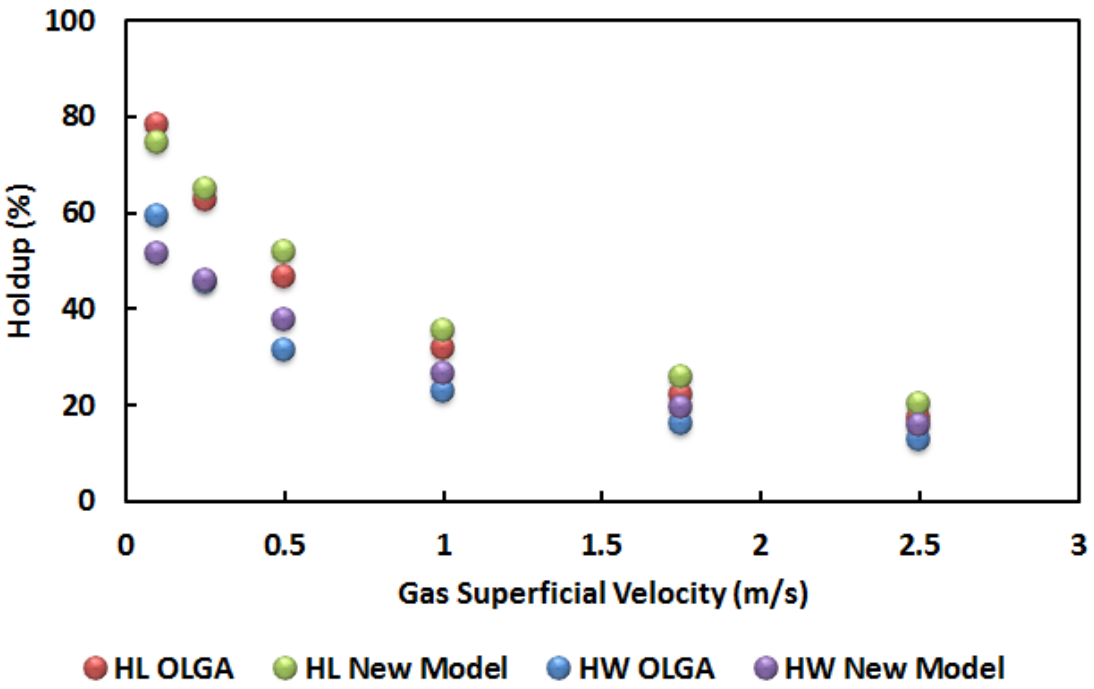

Figure 5-4: Holdups Comparison with OLGA for Three-Layer Stratified Flow (WC = 80%)

The slug flow with stratified film and slug is the transitional flow pattern between the three-layer stratified flow and the slug flow with fully mixed oil and water. This flow pattern is divided into two regions: film region and slug region. The film region is similar to the three-layer stratified flow, while the slug region contains two stratified layers of oil and water with dispersion of gas. In order to achieve this flow pattern, the liquid superficial velocity is increased from 0.01 m/s to 0.2 m/s. The gas superficial velocities range from 0.1 to 0.5 m/s. The pressure drop and liquid holdup results for the 40% and 60% water cuts are compared with the OLGA simulation results. The pressure drops and holdups for 40% water cut are plotted in Figure 5-5 and Figure 5-6 respectively, while Figure 5-7 and Figure 5-8 display the same variables for the 60% water cut. The increase in liquid flow rate for this flow pattern increases the pressure gradient significantly from maximum 8 Pa/m for three-layer stratified flow to 50 Pa/m for slug flow with stratified film and slug. A similar decrease in liquid holdup with increase in water cut

is also noticed for this flow pattern. For slug flow with stratified film and slug, the oil and water are fully separated in the gas pocket region and slug body region. Therefore, the linear mixture viscosity effect is still valid and explains the similar water cut and holdup relationships.

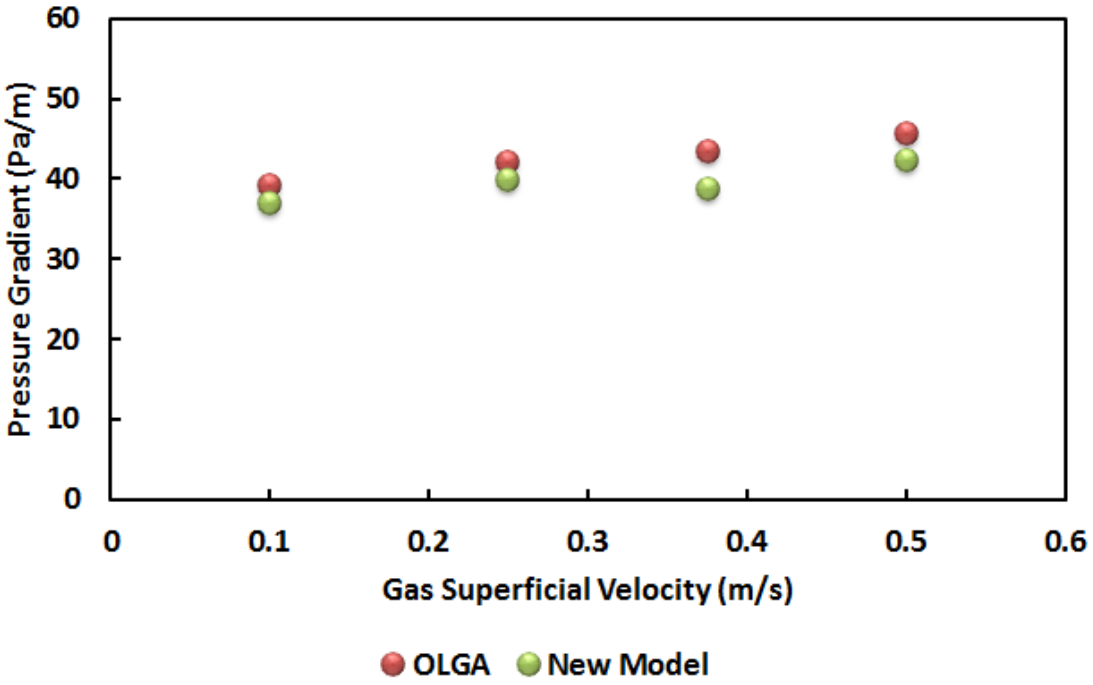

Figure 5-5: Pressure Drop Comparison with OLGA for Slug Flow with Stratified Film and Slug (WC = 40%)

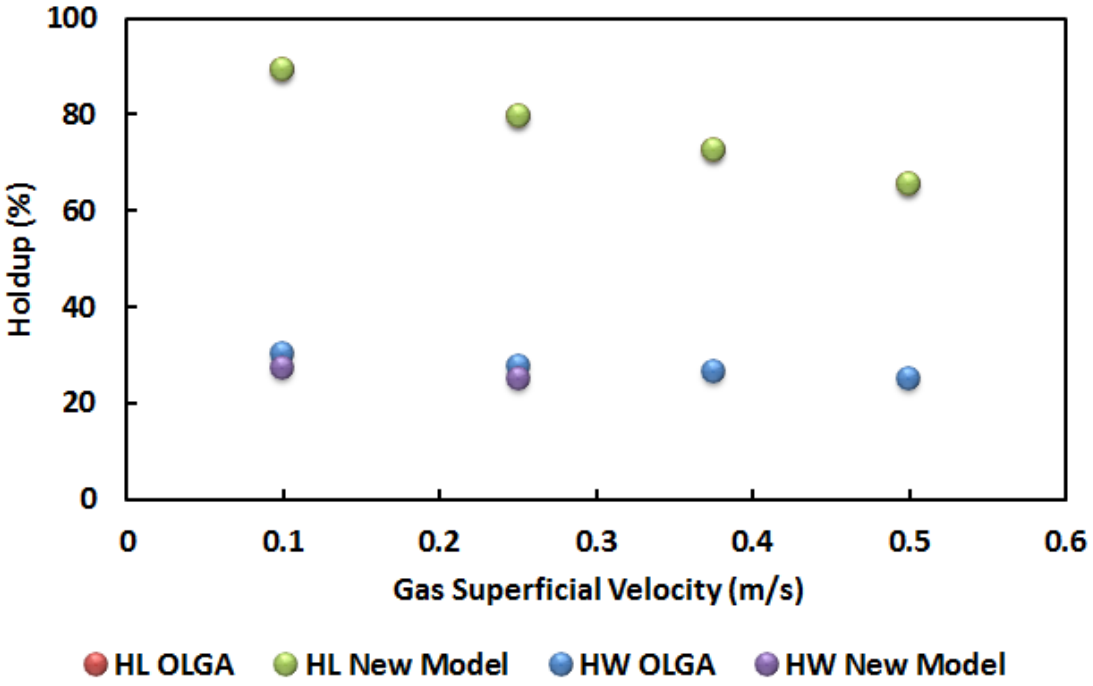

Figure 5-6: Holdups Comparison with OLGA for Slug Flow with Stratified Film and Slug (WC = 40%)

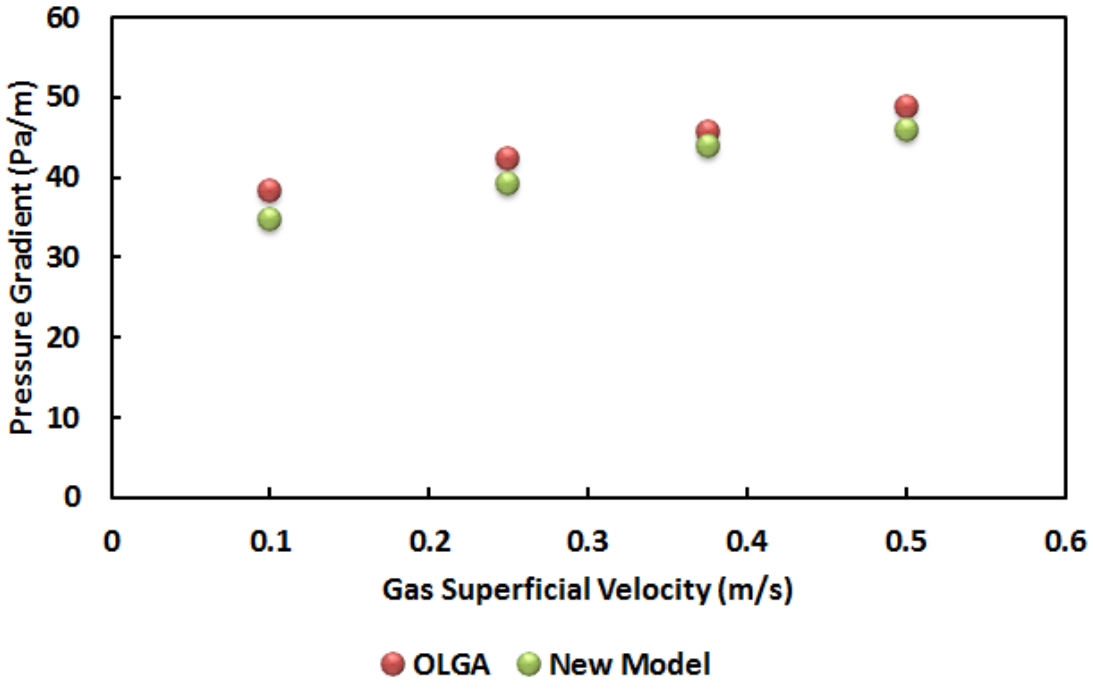

Figure 5-7: Pressure Drop Comparison with OLGA for Slug Flow with Stratified Film and Slug (WC = 60%)

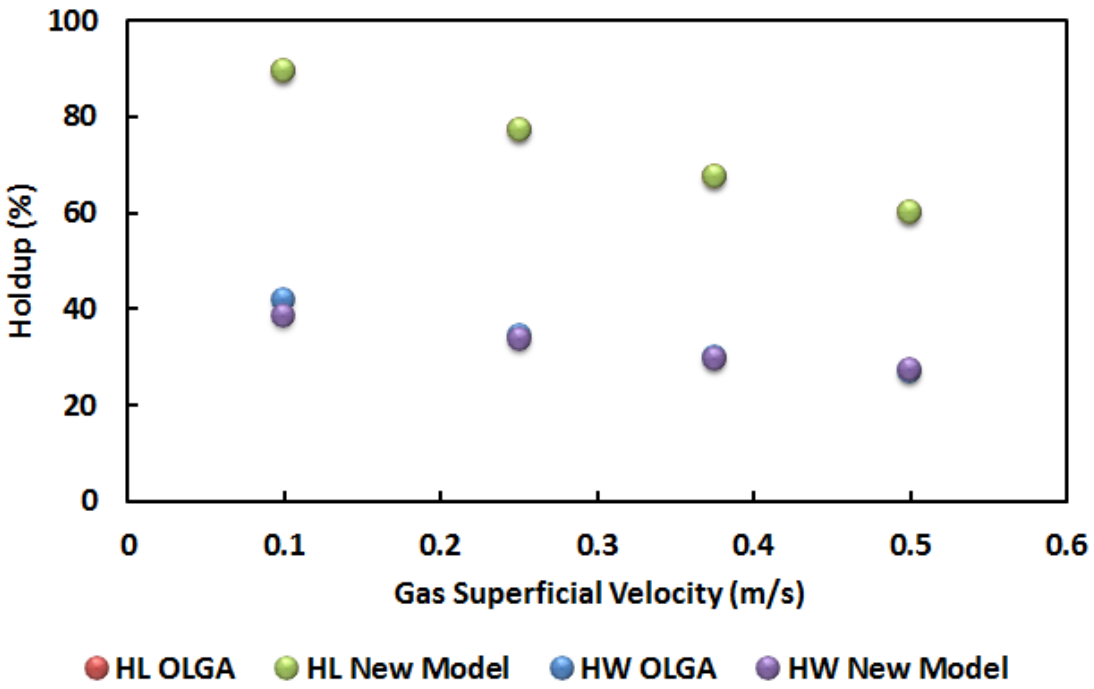

Figure 5-8: Holdups Comparison with OLGA for Slug Flow with Stratified Film and Slug (WC = 60%)

5.2 Low Liquid Loading

Low liquid loading flow is classified with high gas and low liquid flow rates. The small amount of liquid may have significant impact on the liquid holdups and pressure drops as well as flow issuance issues. Karami (2015) performed extensive experiments on three-phase low liquid loading in horizontal pipelines. The flow conditions have been used in the new model validation and they are listed in Table A-3. The liquid superficial velocity is set as 1 m/s, while the superficial gas velocity ranges from 9.5 to 22.5 m/s. The pressure drop results for the water cuts at 20%, 40%, 60%, and 80% are plotted in Figures 5-9, 5-10, 5-11, and 5-12, respectively. When the gas flow rate increases, the liquid film thickness decreases, and therefore the liquid film velocity increases. Both of these high velocities tend to increase the wall shear stress leading to an increase in the pressure gradient. Both liquid and water holdups are decreased and the results

for the water cuts at 20%, 40%, 60%, and 80% are plotted in Figures 5-13, 5-14, 5-15, and 5-16, respectively.

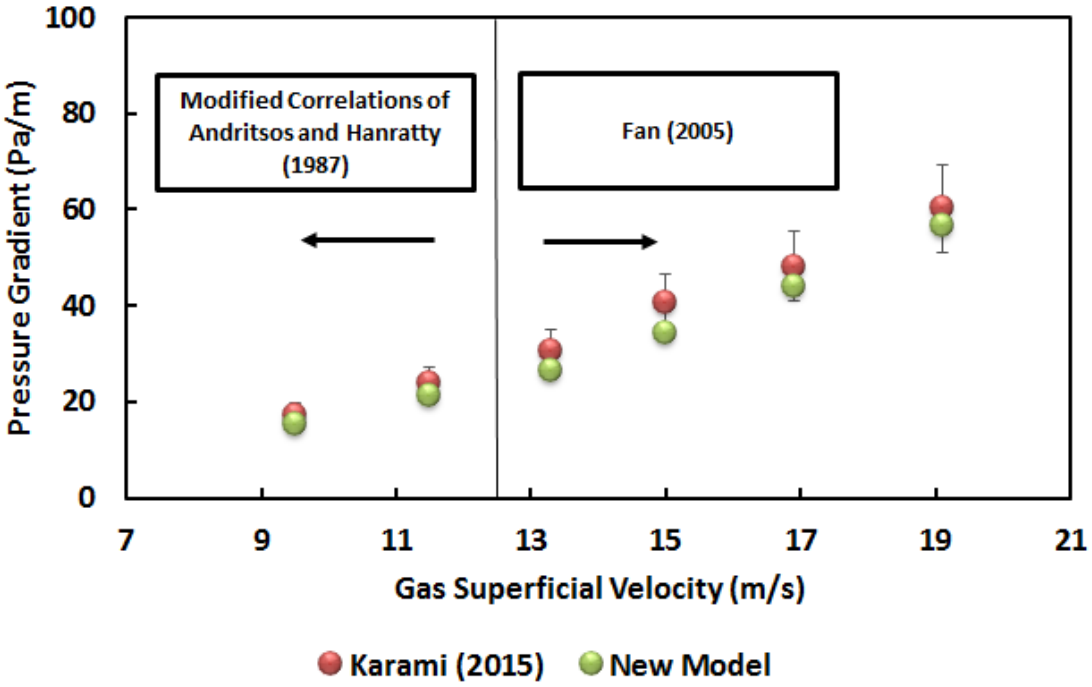

Figure 5-9: Pressure Drop Comparison with Karami (2015) for Low Liquid Loading (WC = 20%)

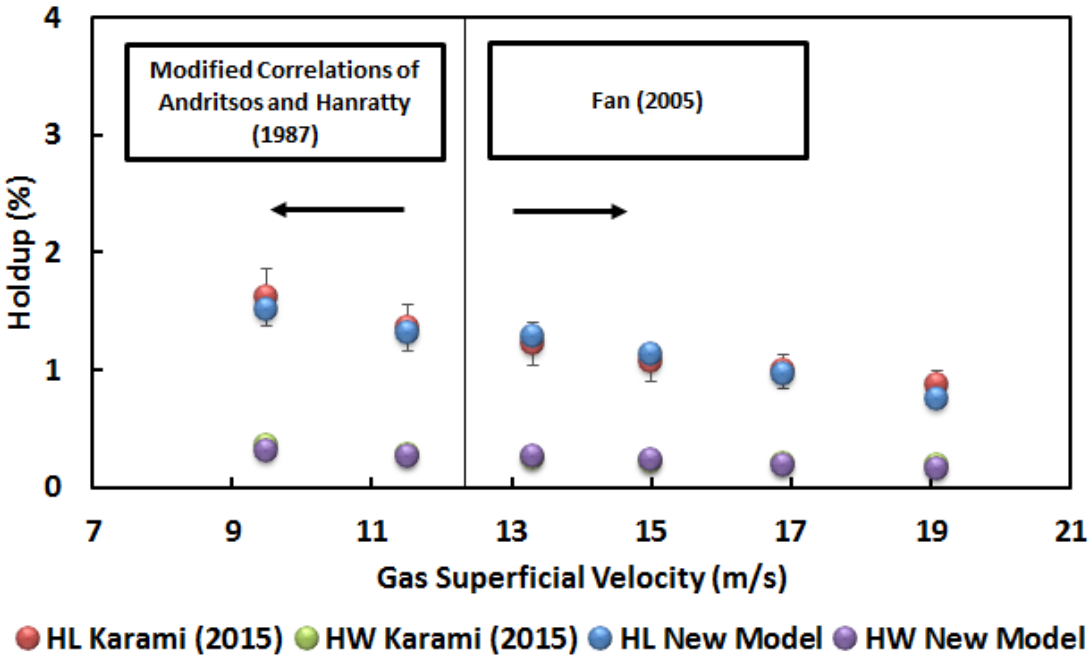

Figure 5-10: Holdups Comparison with Karami (2015) for Low Liquid Loading (WC = 20%)

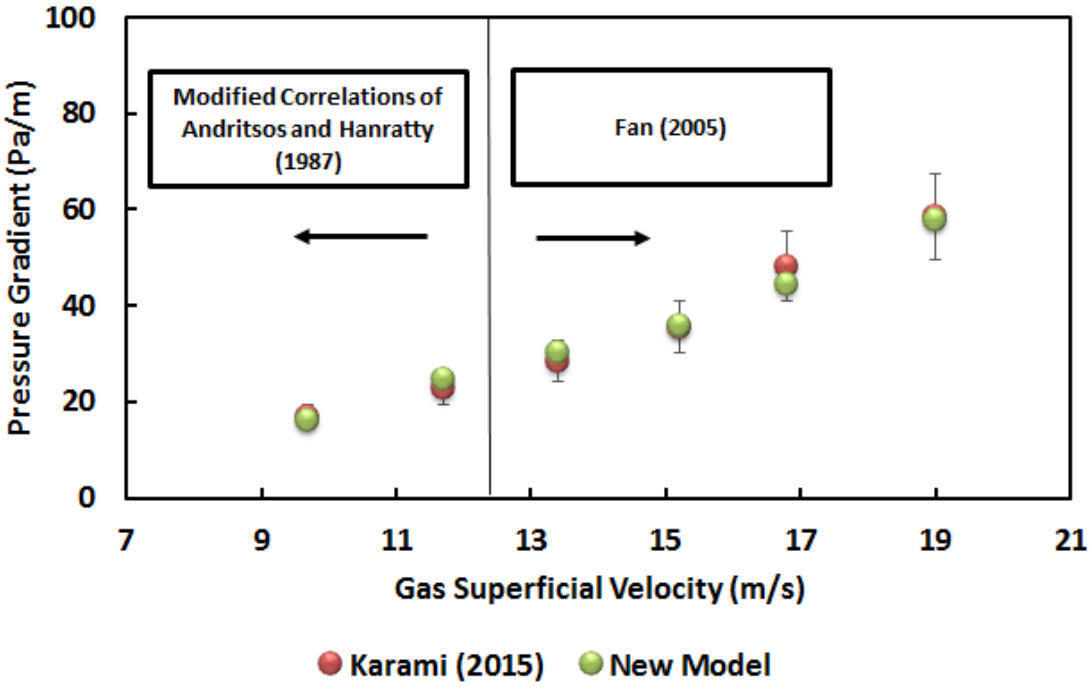

Figure 5-11: Pressure Drop Comparison with Karami (2015) for Low Liquid Loading (WC = 40%)

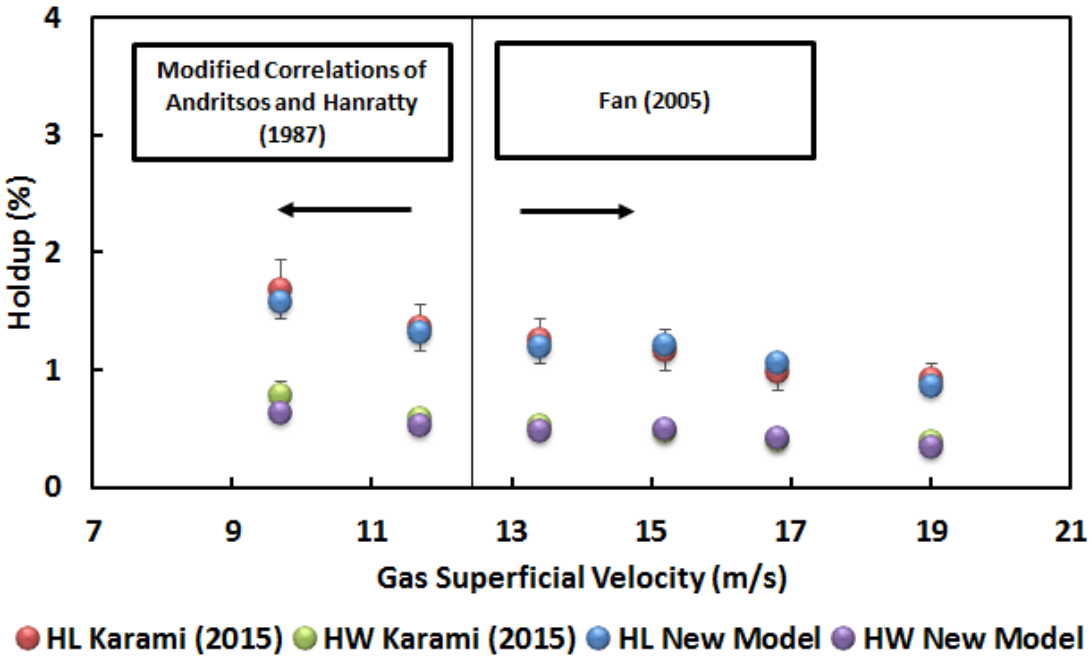

Figure 5-12: Holdups Comparison with Karami (2015) for Low Liquid Loading (WC = 40%)

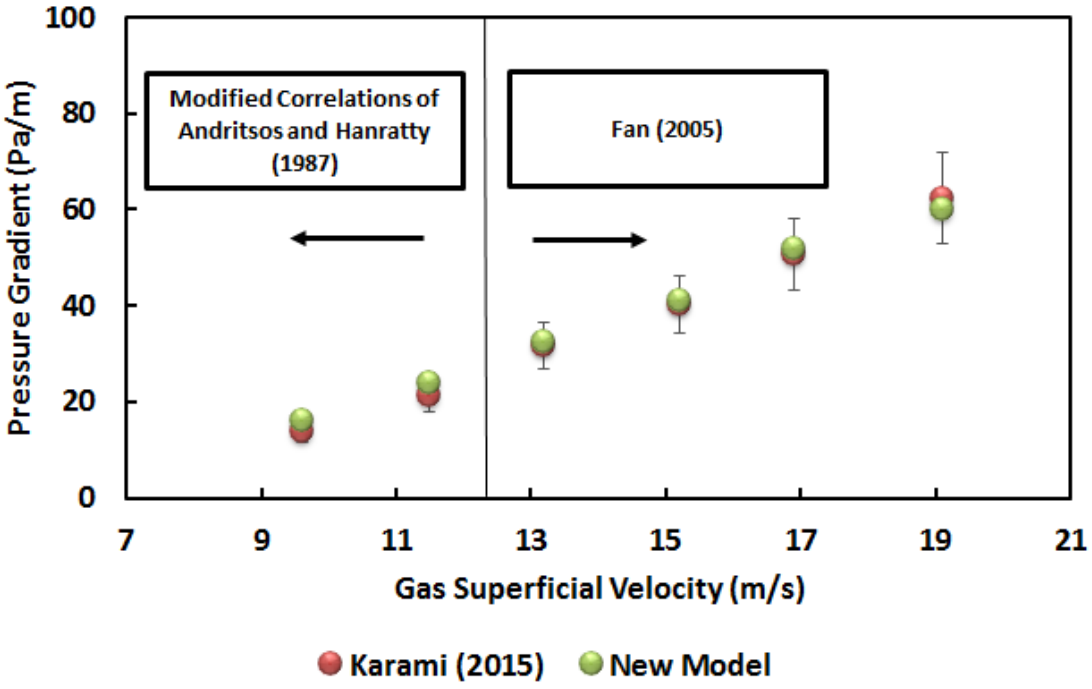

Figure 5-13: Pressure Drop Comparison with Karami (2015) for Low Liquid Loading (WC = 60%)

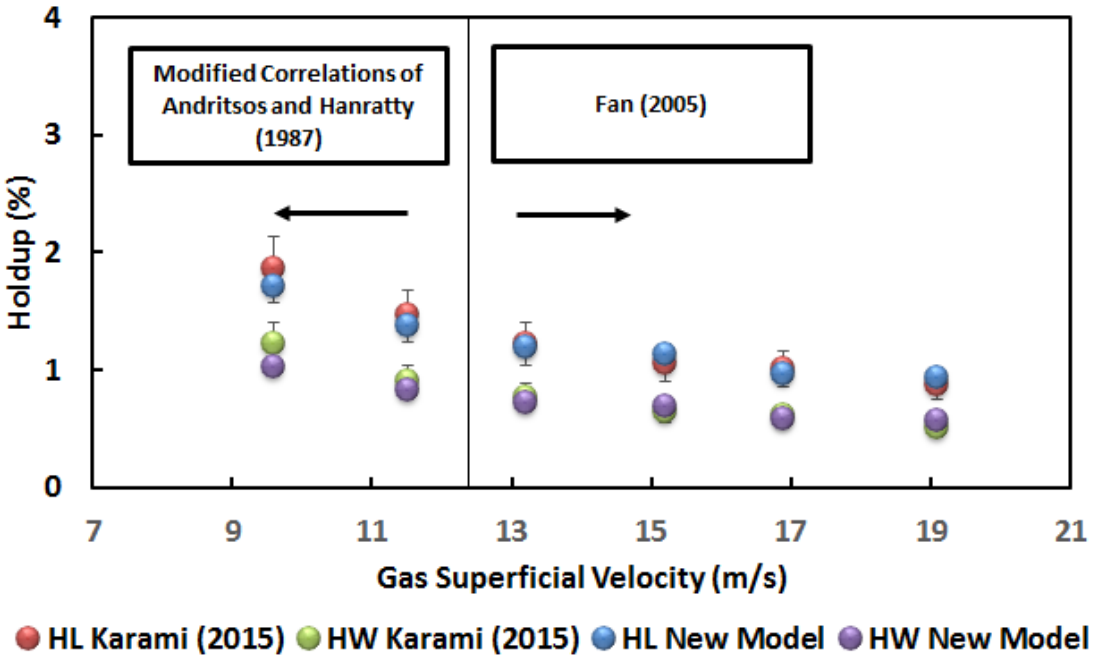

Figure 5-14: Holdups Comparison with Karami (2015) for Low Liquid Loading (WC = 60%)

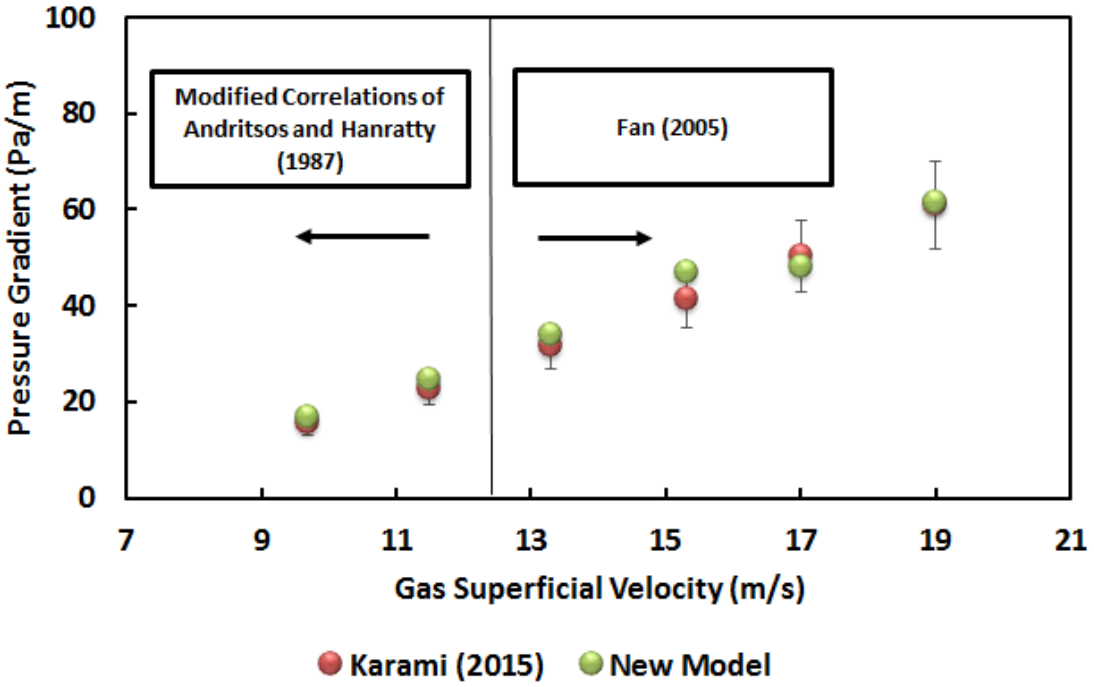

Figure 5-15: Pressure Drop Comparison with Karami (2015) for Low Liquid Loading (WC = 80%)

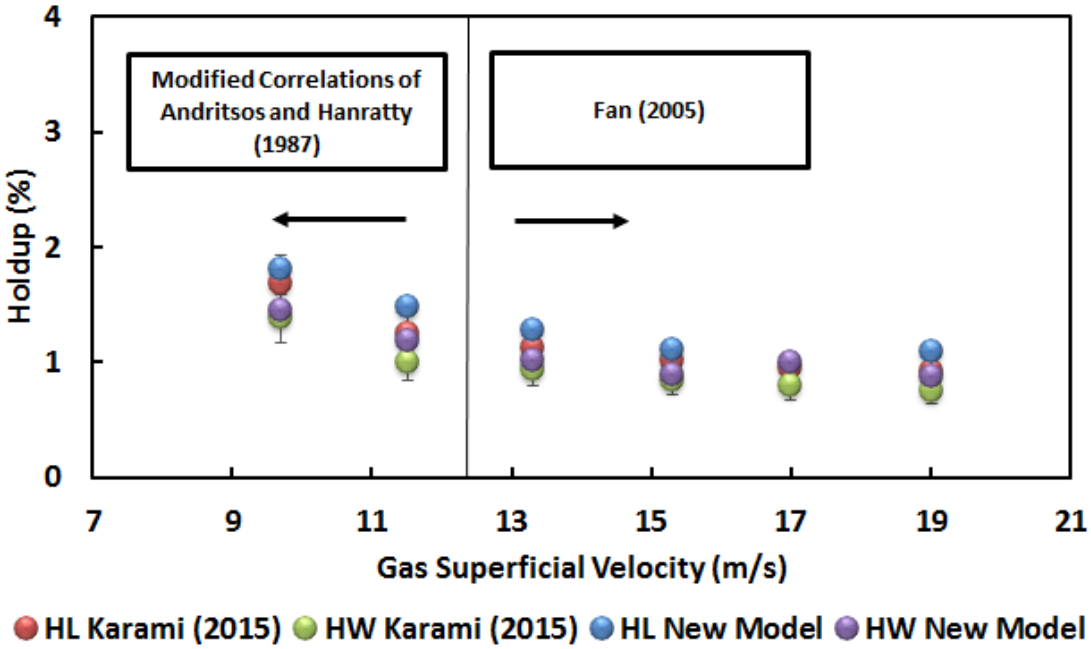

Figure 5-16: Holdups Comparison with Karami (2015) for Low Liquid Loading (WC = 80%)

Initially, the pressure drop and holdup simulation results agree well with the experimental results only for gas superficial velocity less than 12.5 m/s. At higher gas superficial velocity, the new model always over-predicts the pressure gradient and underestimates the water and liquid holdups. With the increase in gas flow rates, the interfacial wave structure becomes stronger and the effect of interfacial shear stress becomes more important. The Andritsos and Hanratty (1987) correlation for interfacial friction factor was developed for stratified flow assuming flat interface. Zhang (2001) modified the correlation for concave interface to be applicable at high gas flow rates or high inclination angles. The modified correlation is used in the new model for the three-layer stratified flow and the film region of the slug flow with stratified film and slug and shows positive results. For low liquid loading, the correlation provides very good predictions up to 12.5 m/s superficial gas velocity and overestimates after that. The modified correlation is replaced by Fan (2005) correlation developed for low liquid loading at high superficial gas velocity and the

predictions are improved significantly. This shows the importance of selecting the proper steady-state correlation to be used in the model particularly in special cases like low liquid loading.

Unlike the three-layer stratified flow, the high gas flow rate in the low liquid loading increases the liquid film velocity and promotes the dispersion between the oil and water. When the liquids flow in the dispersed phase, the mixture viscosity is not linear anymore and the water cut effect on the liquid holdup is different from the previous case. For fully dispersed oil and water, the effective viscosity is calculated using Brinkman's (1952) correlation given in Eq. (3-64). The approximate trends of the Brinkman (1952) equation are shown in Figure 5-17.

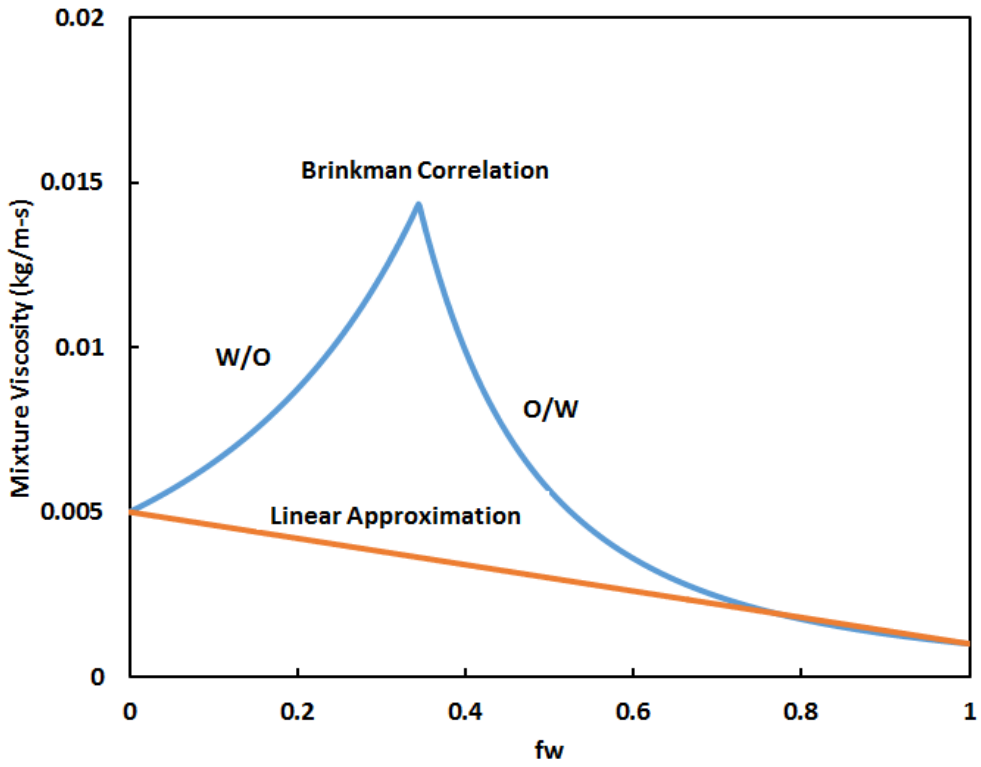

Figure 5-17: Estimated Effective Viscosity for Water/Oil Emulsion

In case of higher oil viscosity than water, the effective viscosity increases with an increase in the water cut until it reaches the inversion point with the maximum value. The effective viscosity then decreases until it reaches the water viscosity as the minimum viscosity in

the system. Because in horizontal pipeline, the mixture viscosity is a primary contributing factor to the pressure drop and holdup, the liquid holdup in the system follows the trend of increasing effective viscosity until the inversion point and then changes trend with decreasing effective viscosity until 100% water cut. The new liquid holdup trend can be seen clearly in the results of the new model and Karami (2015) measurement.

5.3 Flow Pattern Maps

In horizontal pipeline, the four significant flow patterns observed are the three-layer stratified flow, stratified (or annular) flow with fully mixed oil and water, slug flow with stratified film and slug, and slug flow with fully mixed oil and water. Keskin *et al.* (2007) conducted experiments and created flow pattern maps for different water cuts. These four flow patterns were observed and identified widely throughout the experiments. In this section, flow pattern maps are developed using the new model and compared with the experimental maps. The pipeline setup and flow conditions are listed in Table A-4. The flow pattern map for 20% water cut is shown in Figure 5-18. A good comparison has been obtained between the experimental map and the simulation results. For low liquid and gas flow rates, the flow pattern is three-layer stratified flow. If the gas flow rate increases at low liquid flow rate, the high gas rate will accelerate the liquid film and therefore promote a mixing of the liquids. The flow pattern subsequently becomes stratified flow with fully mixed oil and water. At low gas flow rate, if the liquid flow rate increases, the liquid will have the tendency to disperse some gases and the flow pattern becomes slug flow with stratified film and slug. If the liquid flow rate increases further, the liquid in the film and slug regions mix fully and the flow pattern becomes slug flow with fully mixed oil and water.

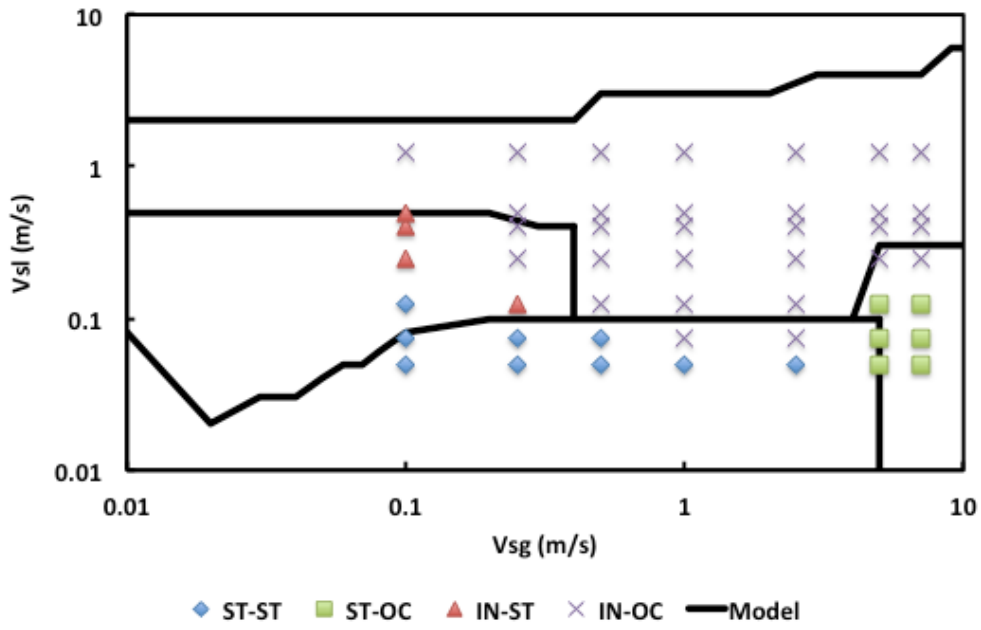

Figure 5-18: Model Predicted Flow Patterns Compared with Keskin *et al.* (2007) (WC = 20%)

The flow pattern map comparison for water cut 40% is shown in Figure 5-19. With higher water cut, a greater flow rate is required to disperse the heavier water layer. Therefore, the three-layer stratified flow and the slug flow with stratified film and slug margins are extended in the expanse of the slug flow with fully mixed oil and water and stratified flow with fully mixed oil and water. Furthermore, a new flow pattern, slug flow with stratified film and mixed slug, appears in a small margin. In the slug body, liquid dispersion occurs earlier than in the film region due to higher turbulence. Therefore, the appearance of this transitional flow pattern due to the increase in water cut is not surprising.

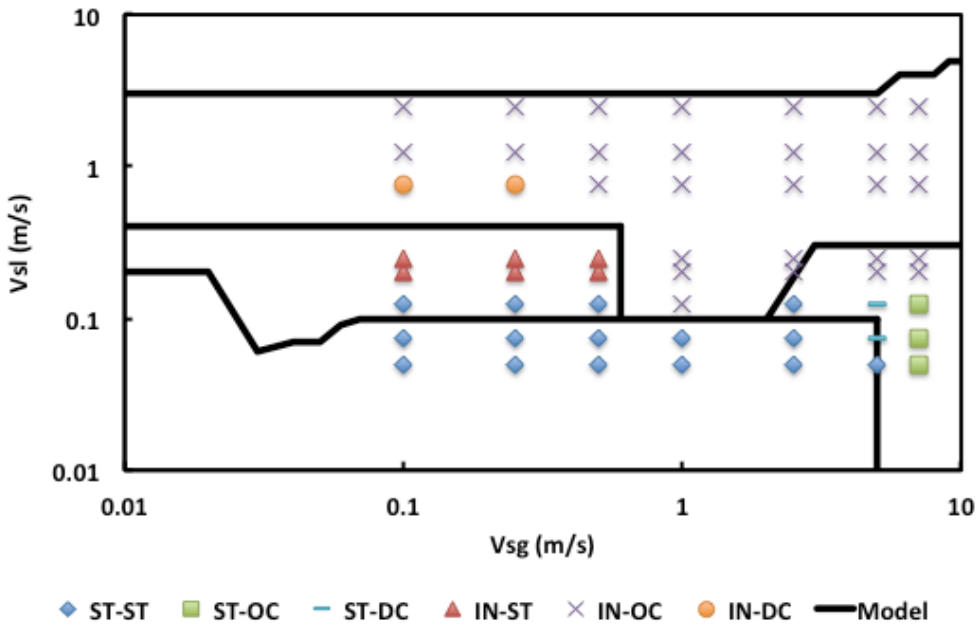

Figure 5-19: Model Predicted Flow Patterns Compared with Keskin *et al.* (2007) (WC = 40%)

Then, the water cut is increased to 60% and the flow pattern comparison is shown in Figure 5-20. The stratified flow with fully mixed oil and water region is expanded. This is because water can disperse oil easier than the alternative. Moreover, the tendency for the liquid to disperse the gas reduces the stratified margin and increases the tendency of the slug flow with stratified film and slug and slug flow with fully mixed oil and water.

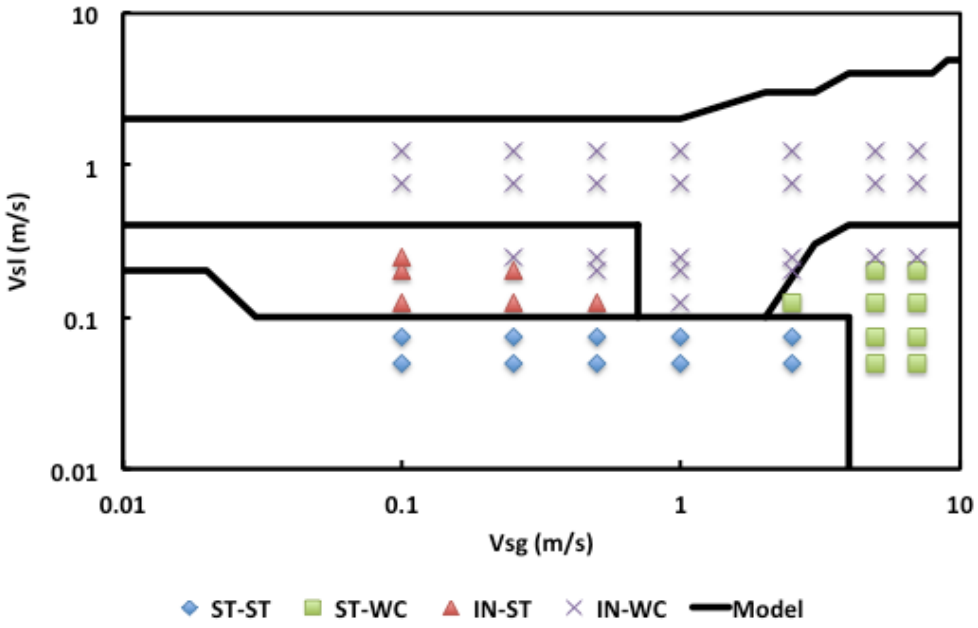

Figure 5-20: Model Predicted Flow Patterns Compared with Keskin *et al.* (2007) (WC = 60%)

5.4 Steady-State Perturbation

A sudden perturbation of steady-state flow by a change in flow rates is the most common transient phenomenon in the oil industry. This change can affect the pressure and liquid holdup distribution as functions of space and time and can introduce a transient flow. The transient flow simulation results from OLGA are used to verify the calculations with the newly developed transient model. Two types of transient flow conditions are used with different boundary conditions. A sensitivity analysis on the effect of cell length and time steps on the simulation results is also performed. The validations are based on a single pipeline with a 0.0508 m inner diameter and a length of 15 m. The outlet or separator pressure is set to 2 bara and different inclination angles are used.

5.4.1 Water Buildup

The first transient case commences with a water buildup by sudden increase in water flow rate. This change in water flow rate occurs frequently in pipelines and wellbores. The rapid increase in water flow rate to a flow that is already in a steady-state condition can induce temporary slugging with an increase in pressure drop. The initial condition for the steady-state flow is set as 1.0 m/s gas superficial velocity, 0.01 m/s oil superficial velocity, and 0.01 m/s water superficial velocity. The transient phenomena are induced at t = 1 sec by increasing the inlet water superficial velocity suddenly to 1 m/s and by keeping the inlet gas and oil superficial velocities and the separator pressure unchanged.

The results of the current model simulations and OLGA simulations for the inclinations 0^o, 30^o, 60^o, and 90^o are shown in Figures 5-21, 5-22, 5-23, and 5-24 respectively. The comparison is for the outlet superficial velocities, which clearly indicates a high fluctuation due to the intense slugging following the sudden increase in water flow rate. The gas, oil, and water outlet superficial velocities all increased following the sudden increase in the inlet water flow rate into the system. The effect on gas is much more than on oil and water due to the high compressibility of gas. After the initial increase, gas and oil then decrease to their original values and water keeps increasing until they all finally stabilize. The simulation predictions for the inclinations 30^o, 60^o, and 90^o agree well with the OLGA results in terms of the increase in the velocities and the stabilization time. For horizontal flow, the new model underestimates the initial increase of the gas flow rate while agreeing very well with the stabilization time. Due to the higher gravitational forces, the pressure gradient is increased with the increase of the inclination angle. Therefore, it should take more time to stabilize the flow. However, other factors also play important roles throughout the stabilization process. For example, due to the diminishing effect of gravitational forces for the horizontal pipeline, the water buildup

perturbation meets less resistance and hence creates higher tendency for the gas flow rate initial increase. Therefore, the flow pattern changes from slug to stratified flow and return to slug shortly after. These transitions in flow patterns slow down the overall process by taking longer time for the new flow pattern to be fully developed and, henceforth, overcome the inclination effect. The flow pattern for upward 30^{o} remains as slug flow during and after the transient process. For upward 60^{o} and vertical flows, the flow pattern starts as slug flow for the entire pipeline. After the buildup, the local pressure in the lower section increases and hence decreases the gas velocity. Consequently, the flow pattern in the lower section becomes a dispersed bubble flow while the upper section remains as slug flow. This transition does not noticeably affect the stabilization time and, therefore, the horizontal flow still stabilizes within the same time range of the upward inclined and vertical flows.

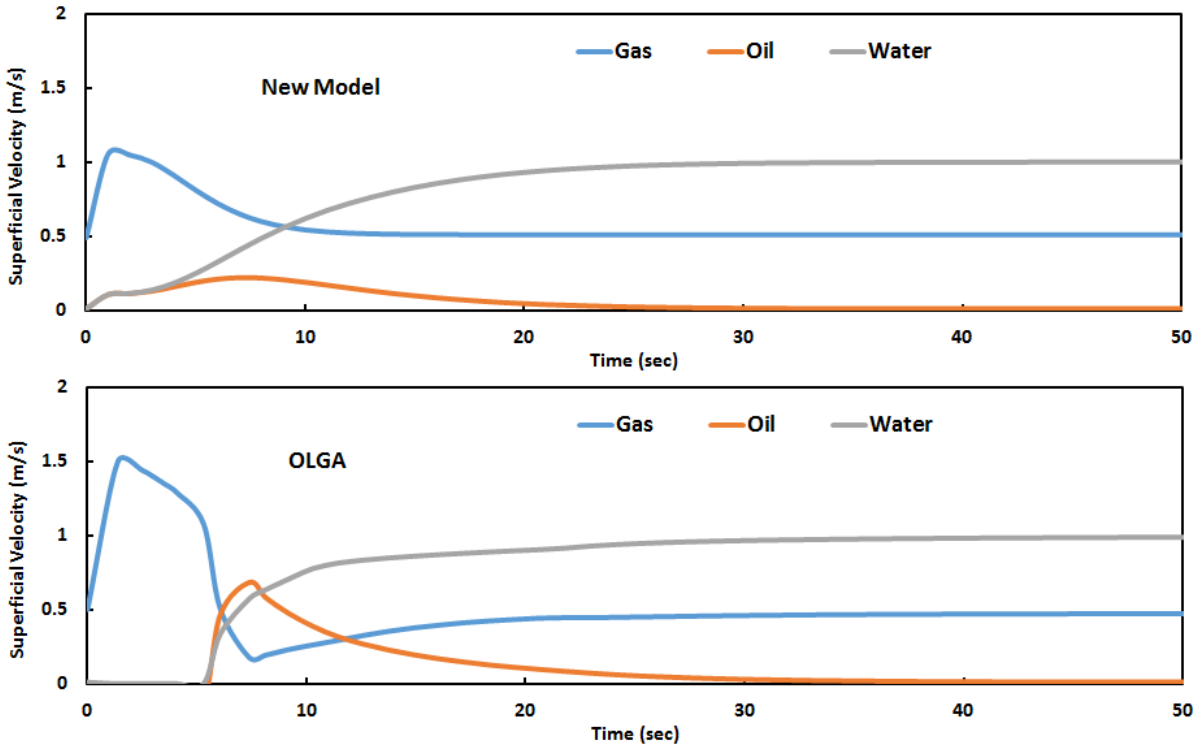

Figure 5-21: Water Buildup Comparison with OLGA for 0^{o} Inclination

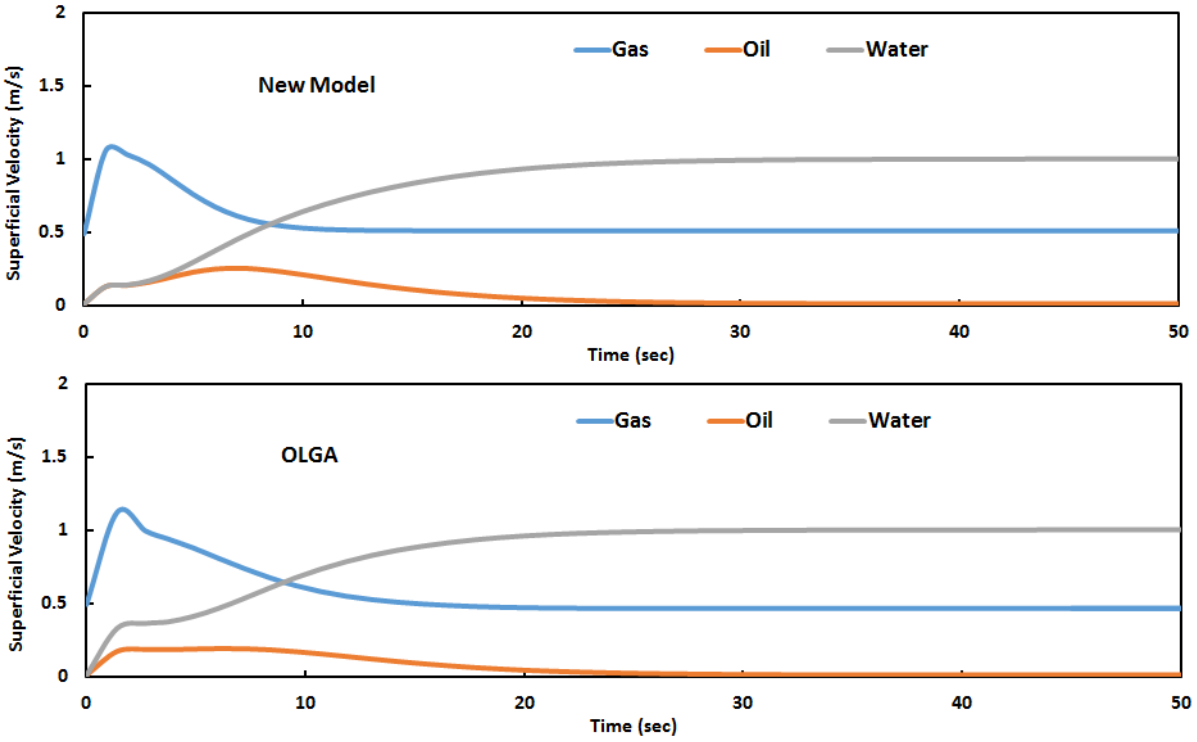

Figure 5-22: Water Buildup Comparison with OLGA for 30^{o} Inclination

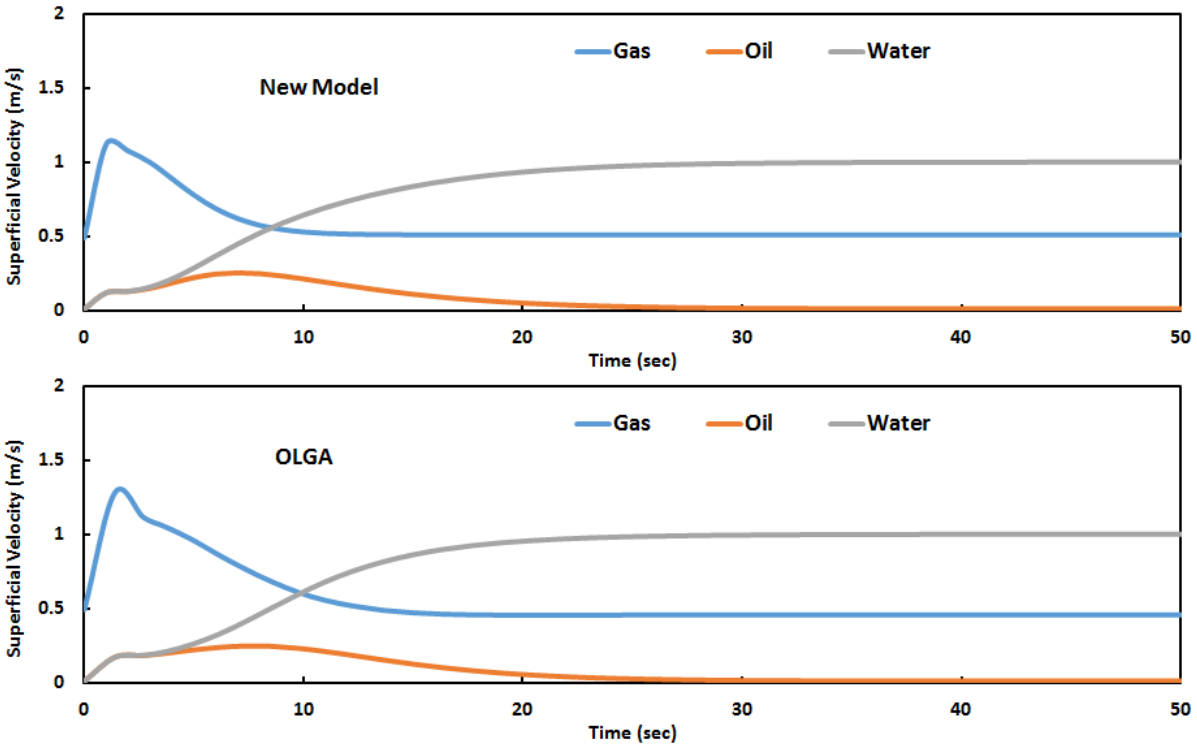

Figure 5-23: Water Buildup Comparison with OLGA for 60^{o} Inclination

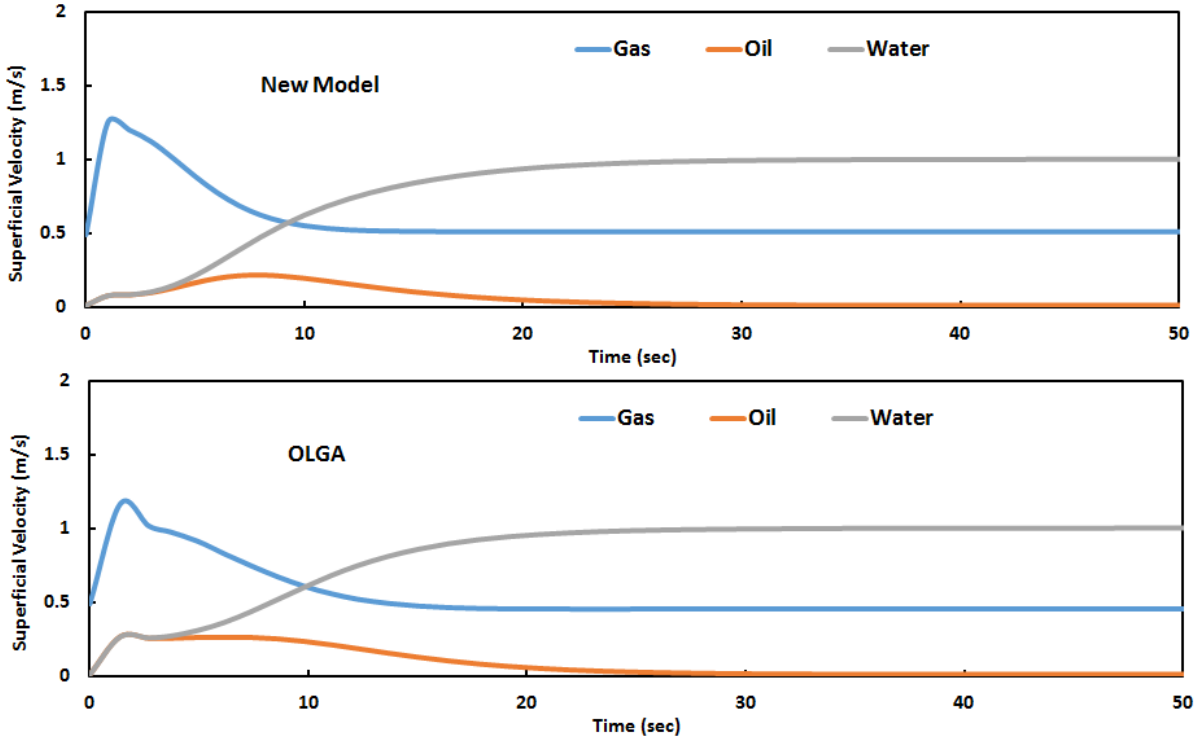

Figure 5-24: Water Buildup Comparison with OLGA for 90^{o} Inclination

5.4.2 Water Depletion

Water decrease or depletion occurs when a three-phase flow reduces to a nearly two-phase flow by decreasing the water flow rate. The initial steady-state three-phase flow condition is given by 1.0 m/s gas superficial velocity, 0.01 m/s oil superficial velocity, and 1.0 m/s water superficial velocity. The water depletion process is initiated at t = 1 sec by simply decreasing the inlet water superficial velocity to 0.01 m/s, while the gas and oil superficial velocities are kept constant.

The outlet superficial velocities from the transient model simulations and OLGA simulations for inclination angles 0^{o}, 30^{o}, 60^{o}, and 90^{o} are presented in Figures 5-25, 5-26, 5-27, and 5-28, respectively. From these curves, the time it takes for the water to be completely displaced from the pipeline can be determined. The OLGA simulations and the new transient

model results are in agreement for the upward and vertical cases. However, OLGA predicts that the gas reaches negative values during the reduction period, which is physically not possible for the horizontal pipeline flow. This is primarily due to numerical error and will be explained in detail in the sensitivity analysis section. Following the decrease in water superficial velocity, steep gas, oil, and water velocity reductions are observed before they readjust to their new values. The flow pattern effect also slowed down the stabilization process for the water depletion case in horizontal flow. Due to the sudden decrease in gas and oil flow rates, the flow pattern changes from slug to stratified flow and ultimately returns to slug after the complete readjustments. For 30^{o} upward flow, the flow pattern starts and remains slug flow throughout the transient process. For both 60^{o} upward and the vertical flows, the flow patterns change from slug flow with dispersed bubble in the lower section of the pipe to fully slug flow with minor effect on the stabilization time.

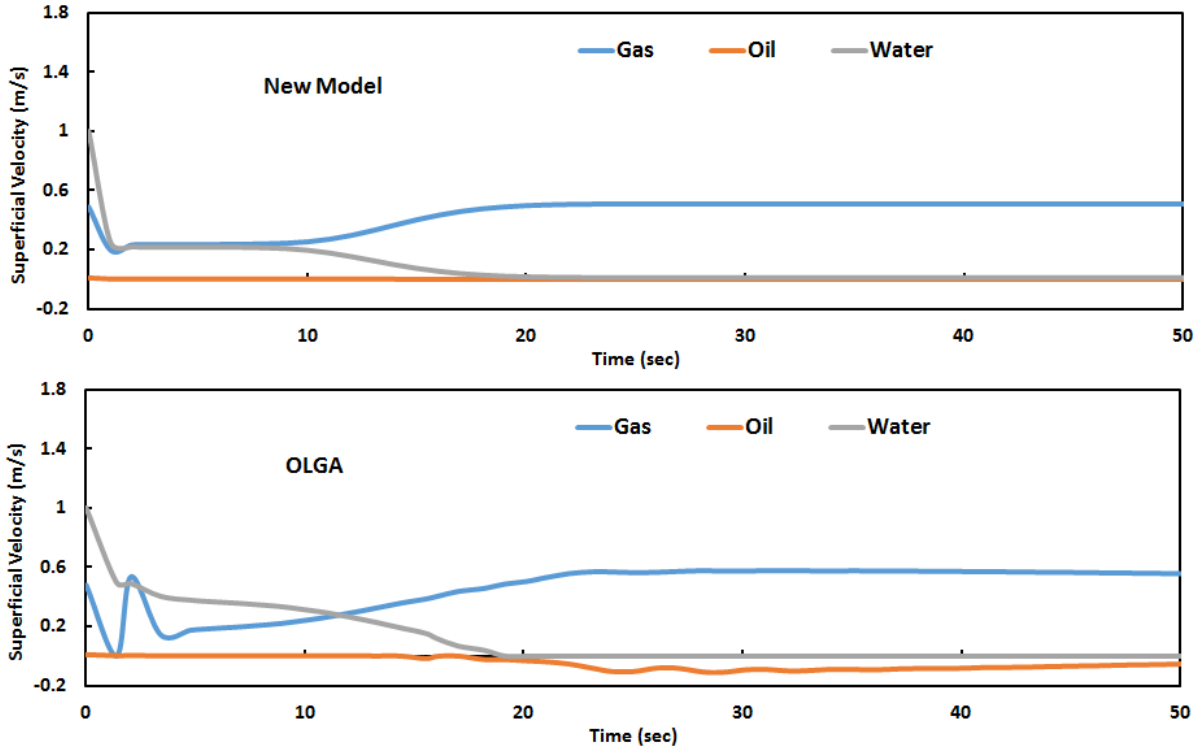

Figure 5-25: Water Depletion Comparison with OLGA for 0^{o} Inclination

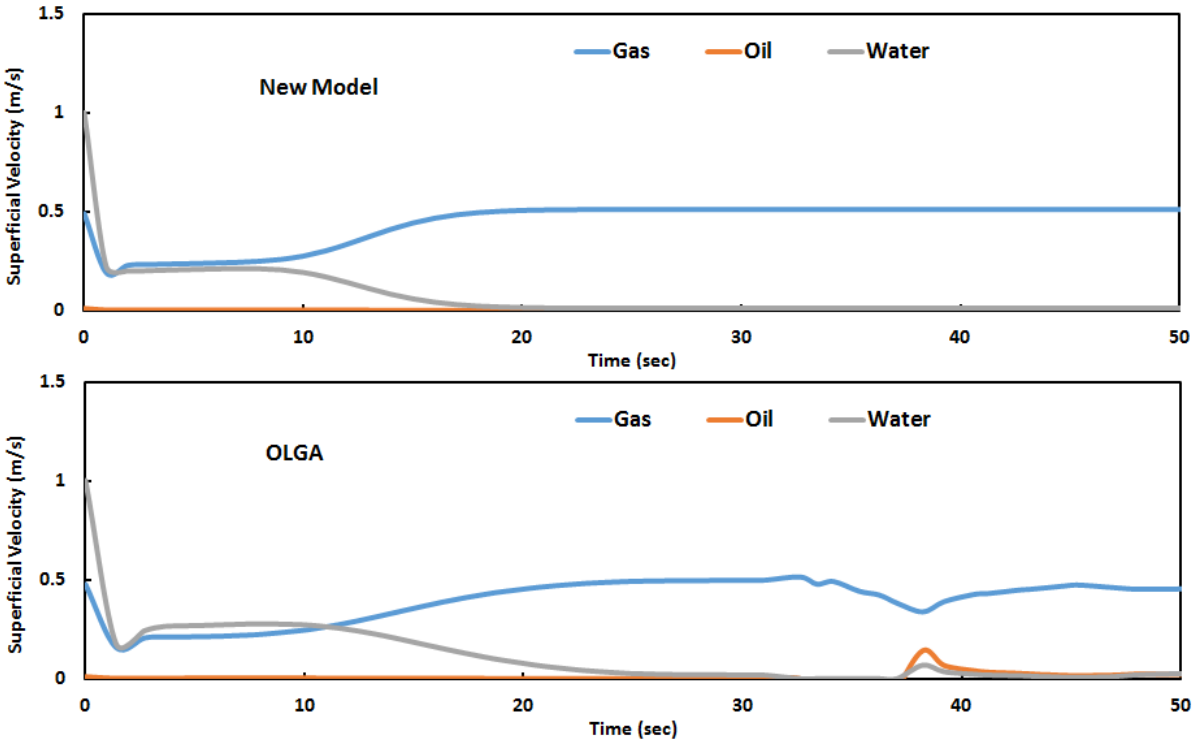

Figure 5-26: Water Depletion Comparison with OLGA for 30^{o} Inclination

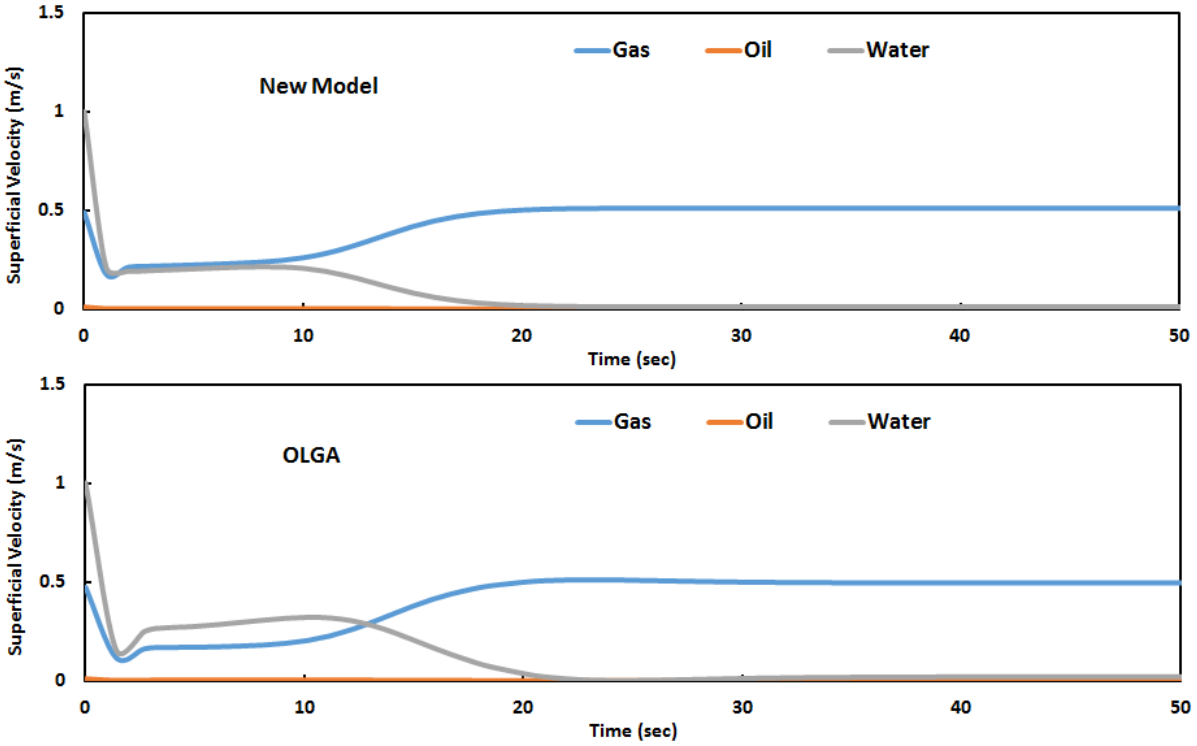

Figure 5-27: Water Depletion Comparison with OLGA for 60^{o} Inclination

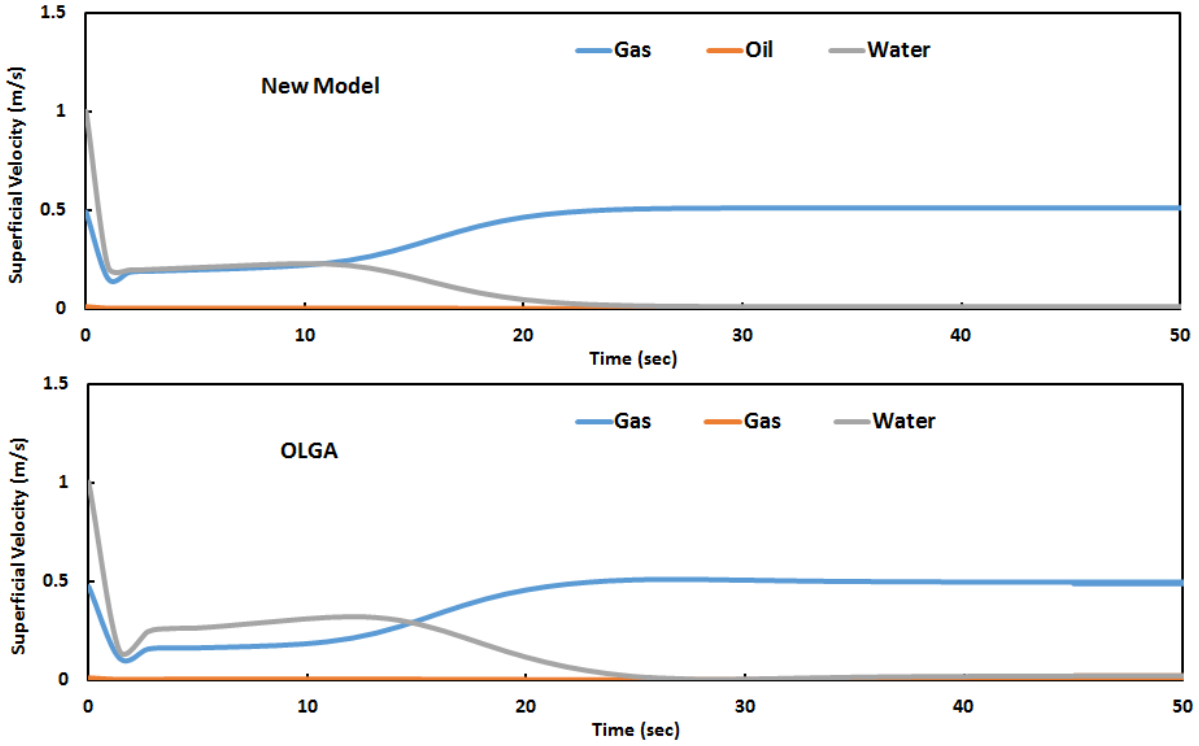

Figure 5-28: Water Depletion Comparison with OLGA for 90^{o} Inclination

5.4.3 Sensitivity Analysis of Spatial and Time Discretization

The choices of cell length and time steps are extremely important for better numerical convergence and accuracy. Most of the multiphase transient simulators are restricted by the Courant-Friedrichs-Lewy (CFL) stability criterion. For implicit finite difference scheme, it can be expressed mathematically as

$$\Delta t \le \min \forall j \left\{ \Delta z / \left| v_j \right| \right\}, \tag{5-1}$$

where v_j is the velocity across each cell. To verify the spatial discretization effect, three different cell lengths are tried (Δz = 1 m, Δz = 3 m, and Δz = 5 m) while fixing the time steps to 0.5 seconds. The effect of cell length appears to be the same for all the inclination angles. Therefore, only the 30^{o} inclination angle is displayed for the water buildup case to avoid redundancy. The

outlet superficial velocities from the new model and OLGA simulations for water buildup, 30° inclination angle, and cell lengths of 1 m, 3 m, and 5 m are presented in Figures 5-29, 5-30, and 5-31, respectively.

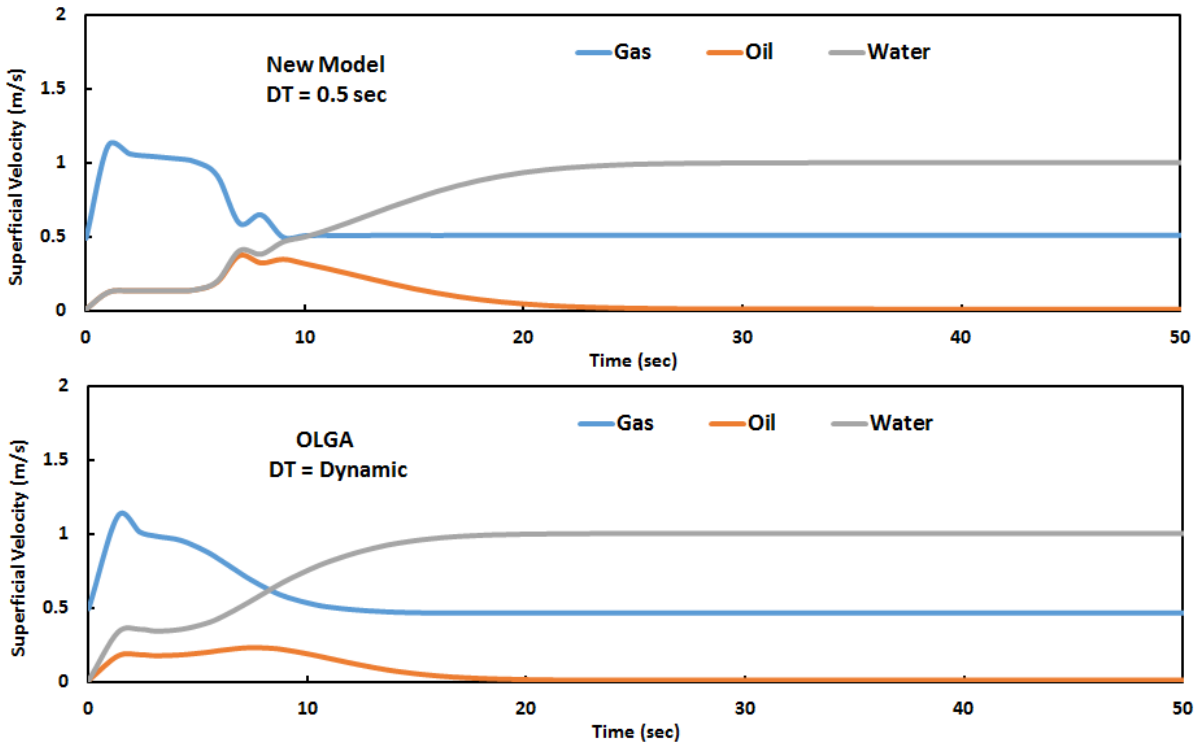

Figure 5-29: Water Buildup Comparison with OLGA for 30° Inclination and Δz = 1 m

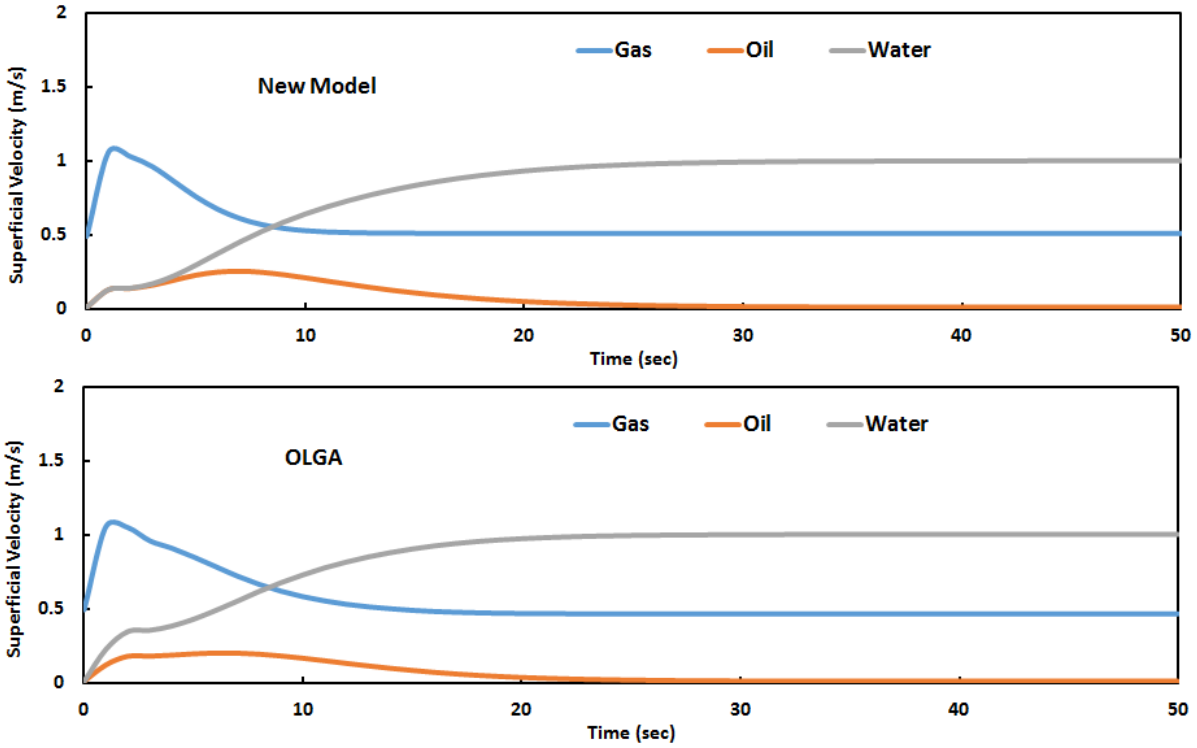

Figure 5-30: Water Buildup Comparison with OLGA for 30^o Inclination and Δz = 3 m

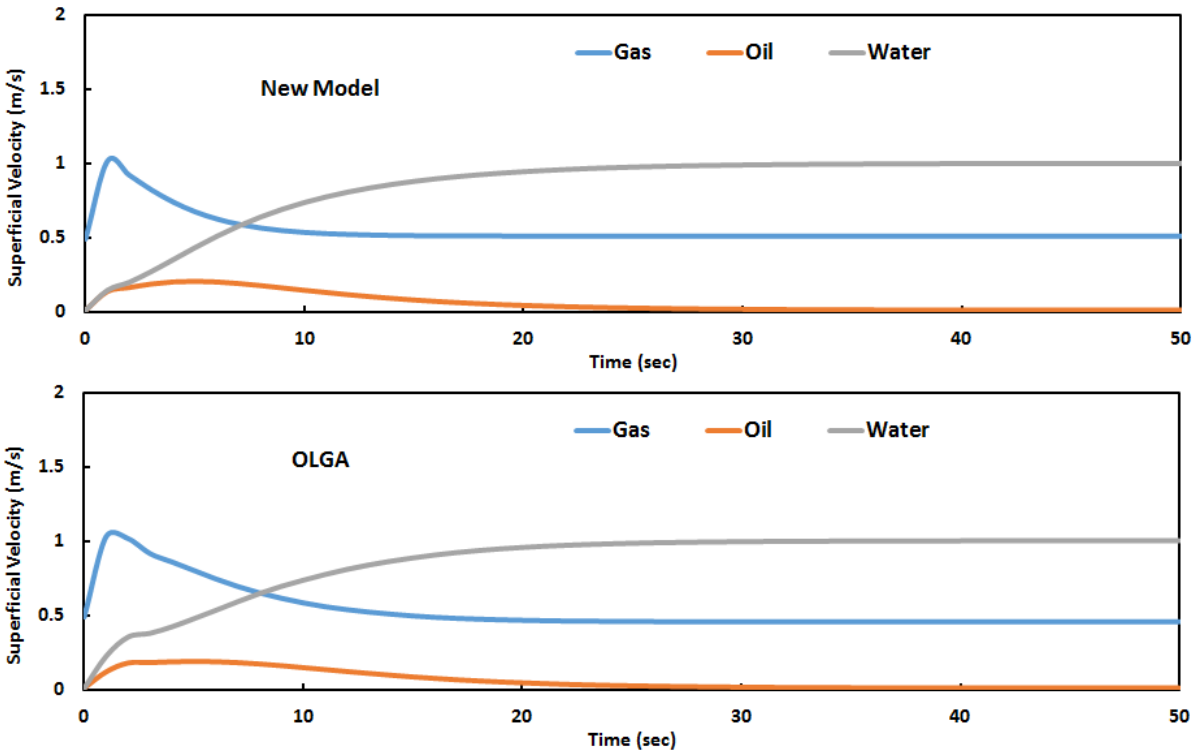

Figure 5-31: Water Buildup Comparison with OLGA for 30^o Inclination and Δz = 5 m

In OLGA simulations with longer spacing, it takes longer for the flow to readjust to a steady state again while the new model shows less effect. For the smallest cell length (Δz = 1 m), the CFL condition is not met and the new model shows different behavior than the other bigger spacing while OLGA does not converge. Due to the failure of achieving a stable flow using the initially specified length and time steps in OLGA, dynamic time steps were used for OLGA predictions in Figure 5-29. For bigger cell lengths (Δz = 3 m and Δz = 5 m), the CFL condition is met and both the new model and OLGA predict stable and similar results.

Then, the cell length effect is evaluated for the water depletion case. In this instance, the 90^o inclination angle is chosen for the test and comparison. The outlet superficial velocities from the new model and OLGA simulations for cell lengths of 1 m, 3 m, and 5 m are presented in Figures 5-32, 5-33, and 5-34, respectively.

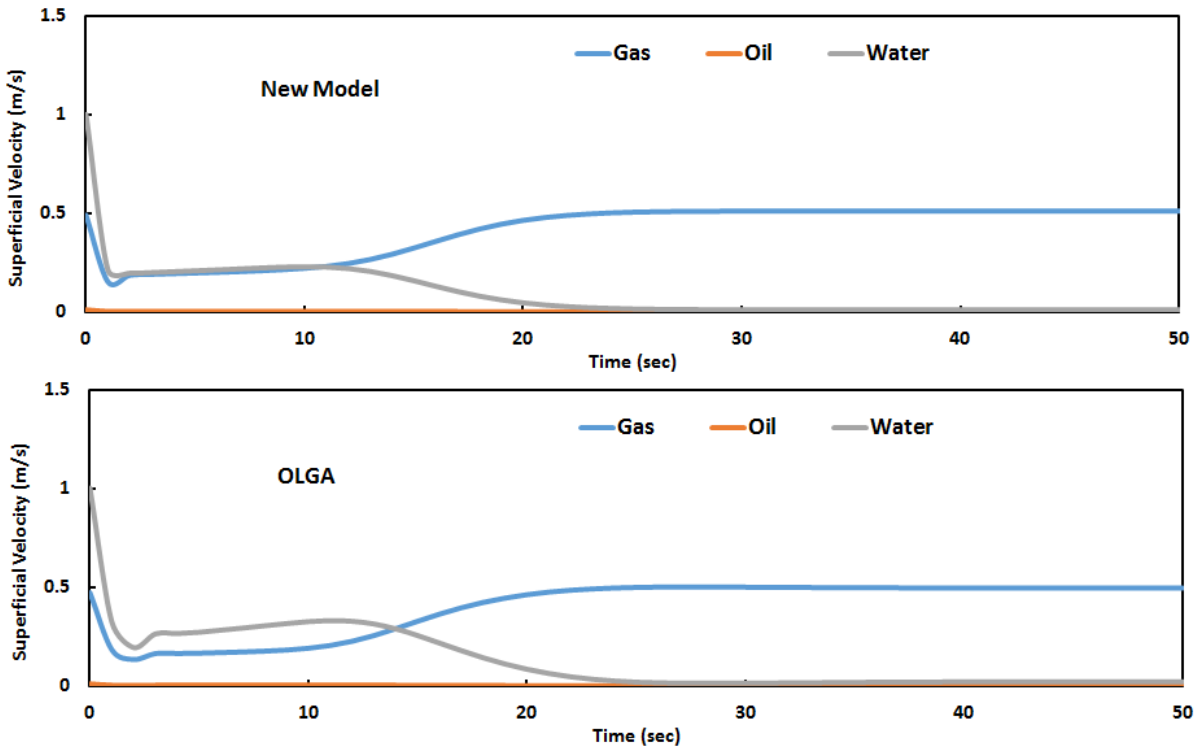

Figure 5-32: Water Depletion Comparison with OLGA for 90^o Inclination and Δz = 1 m

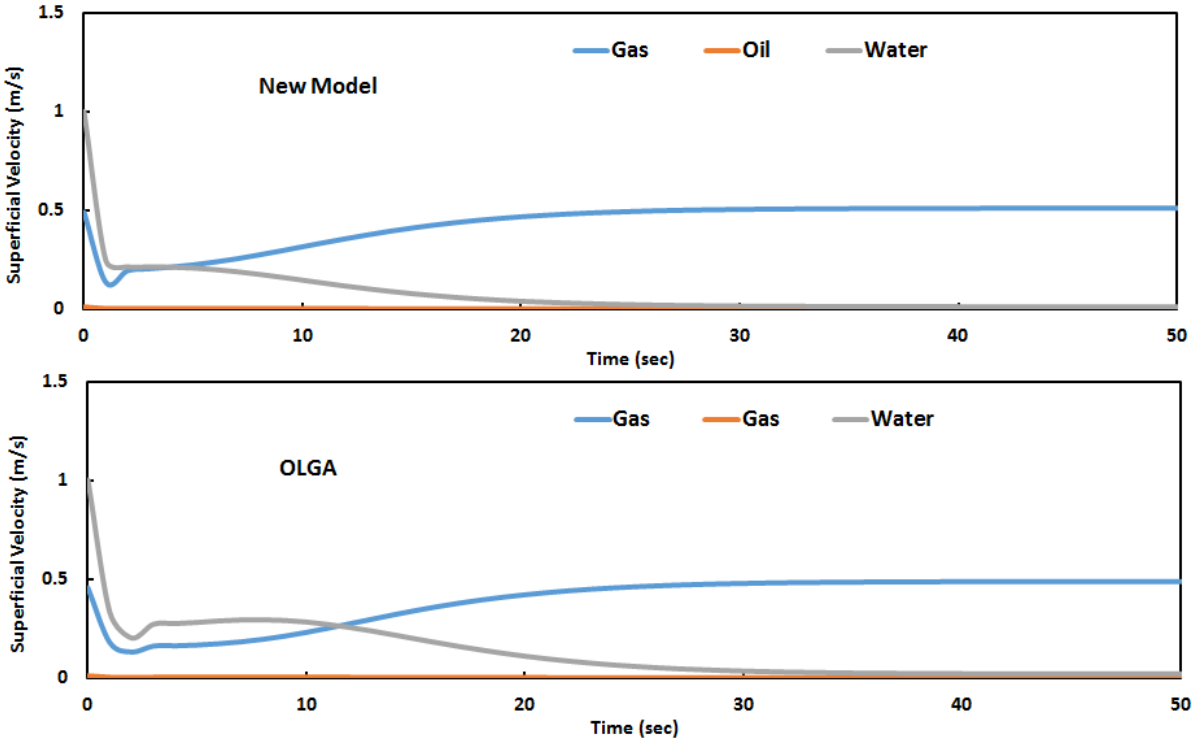

Figure 5-33: Water Depletion Comparison with OLGA for 90^{o} Inclination and Δz = 3 m

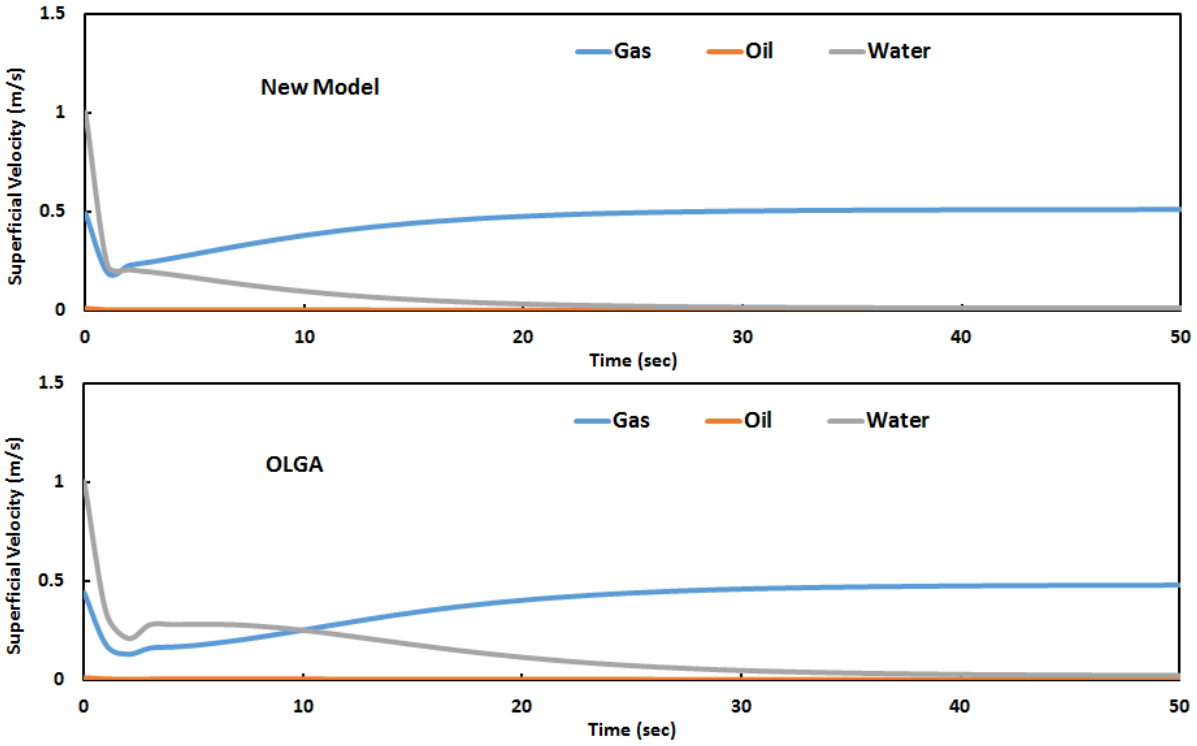

Figure 5-34: Water Depletion Comparison with OLGA for 90^{o} Inclination and Δz = 5 m

The results for the water buildup case are similar to that of the water depletion. The time it takes for the flow to stabilize in OLGA simulations increases with increasing cell length. The CFL condition is met for all the cases and both the new model and OLGA display the most stable and realistic results when the minimum cell length (Δz = 1 m) is used.

Time discretization represented by time steps also play a very important role during the transient process. According to the CFL criterion, for the water buildup case with 30^o inclination angle and 3 m cell length, the time step should be less than 2.5 seconds. For all the previous OLGA simulations, dynamic time steps were used ranging from 0.1 to 5.0 seconds while a fixed time step of 0.5 seconds is used in the new model. The time step range used by OLGA for the water buildup case with 30^o inclination angle is shown in Figure 5-35.

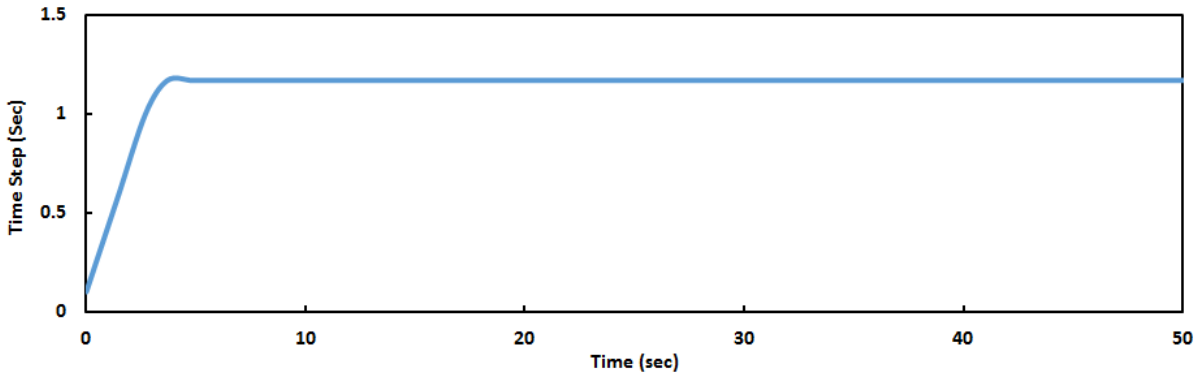

Figure 5-35: OLGA Time Step Change for Water Buildup, 30^o Inclination and Δz = 3 m

In the water buildup OLGA simulation, the time step is dynamically changed from 0.1 seconds to 1.16 seconds. In order to compare with the new model, the time step in OLGA simulation is changed from dynamic to static and three different time steps are chosen (Δt = 0.2 sec, Δt = 0.5 sec, and Δt = 1.0 sec) to cover the range used by OLGA during the transient process. The outlet superficial velocities from the new model and OLGA simulations for water

buildup, 30^{o} inclination angle, and time steps 0.2 sec, 0.5 sec, and 1 sec are presented in Figures 5-36, 5-37, and 5-38, respectively.

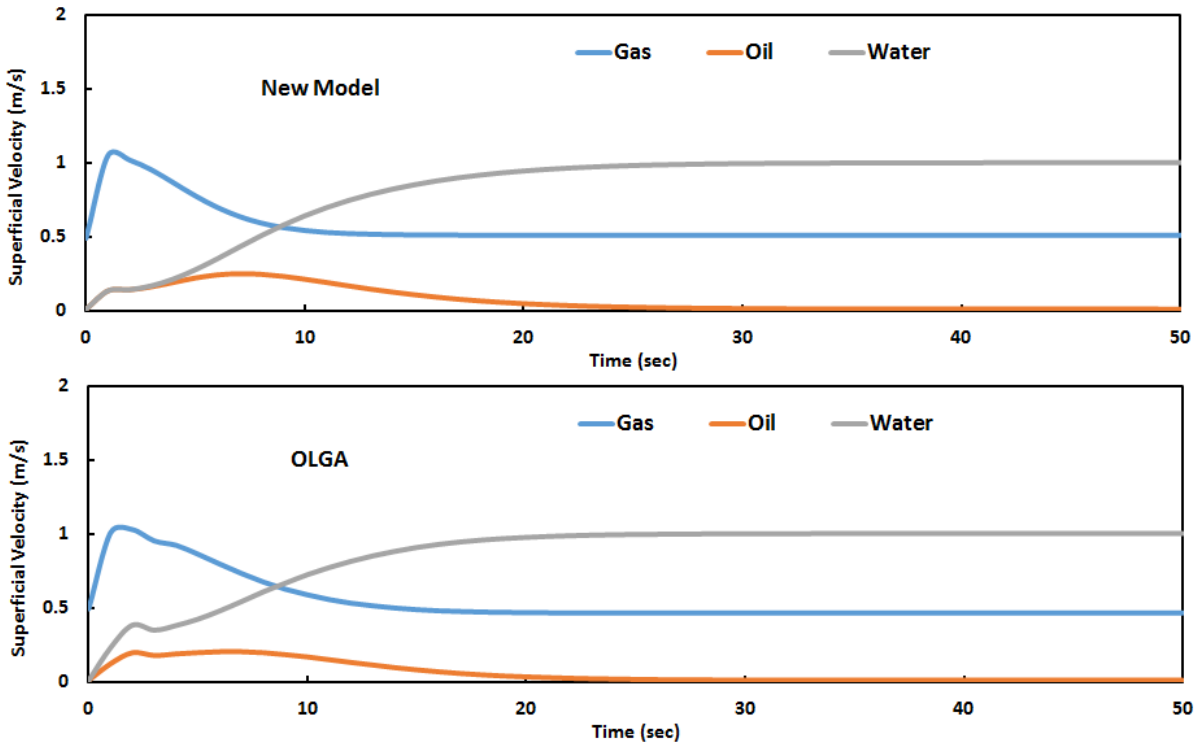

Figure 5-36: Water Buildup Comparison with OLGA for 30^{o} Inclination and Δt = 0.2 sec

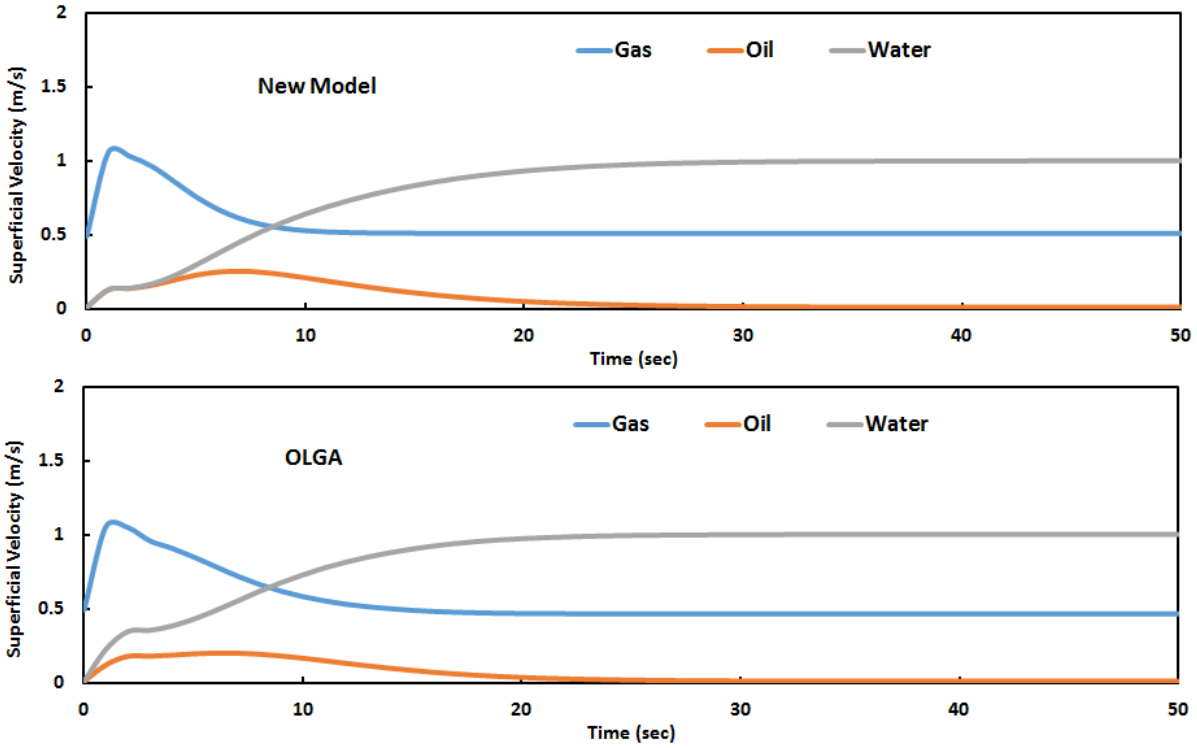

Figure 5-37: Water Buildup Comparison with OLGA for 30^o Inclination and Δt = 0.5 sec

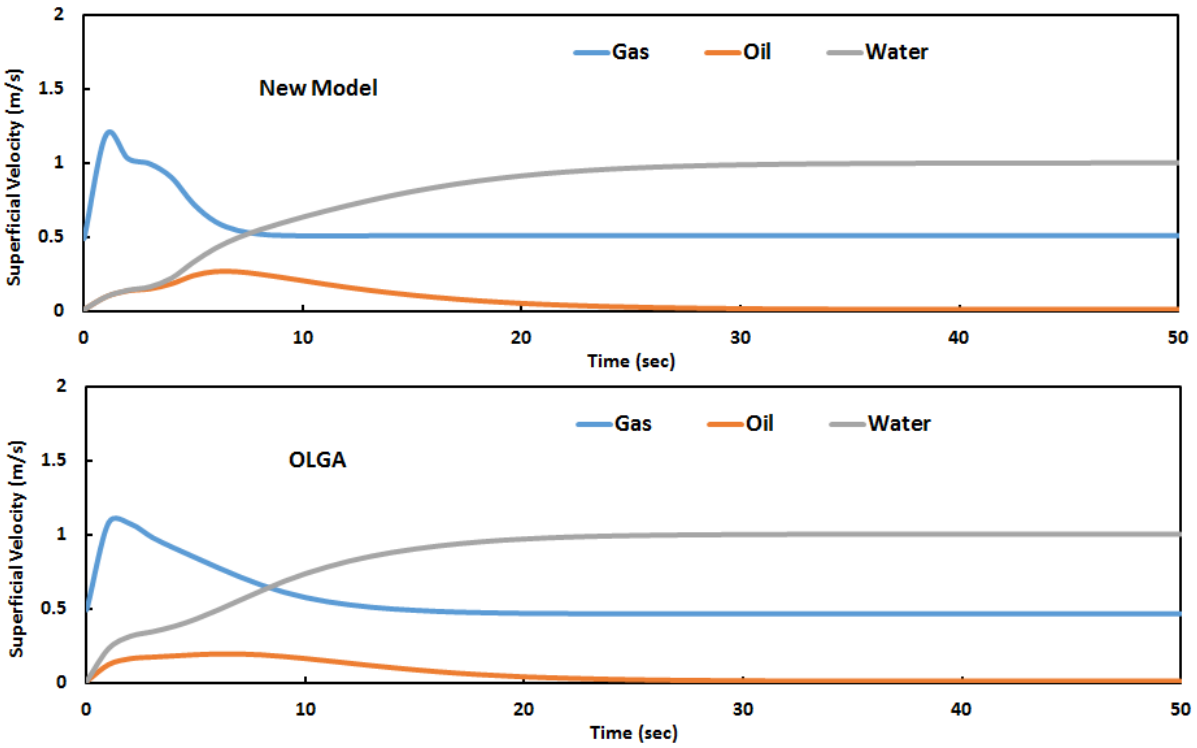

Figure 5-38: Water Buildup Comparison with OLGA for 30^o Inclination and Δt = 1.0 sec

The new model and OLGA simulation results are not significantly affected by the change in time steps for the water buildup case. The time steps used are far below the CFL restriction and therefore they have no major effect on the numerical integrity.

The time step change in OLGA simulation for water depletion and 90° inclination angle is displayed in Figure 5-39.

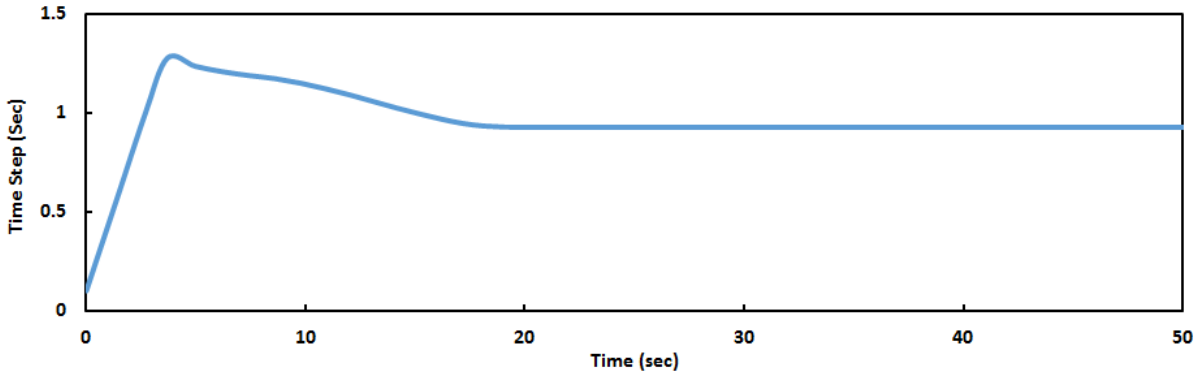

Figure 5-39: OLGA Time Step Change for Water Depletion, 90° Inclination and Δz = 1 m

OLGA used longer time steps for the water depletion case with a minimum 0.1 of seconds and maximum of 1.28 seconds. The CFL condition shows that the maximum time step to be used for the water depletion with 90° inclination angle is 1 second. It is fair then to use the same previous time steps in the water buildup case to investigate the water depletion one (Δt = 0.2 sec, Δt = 0.5 sec, and Δt = 1.0 sec). The outlet superficial velocities from the new model and OLGA simulations for water depletion, 90° inclination angle, and time steps of 0.2 sec, 0.5 sec, and 1 sec are presented in Figures 5-40, 5-41, and 5-42, respectively.

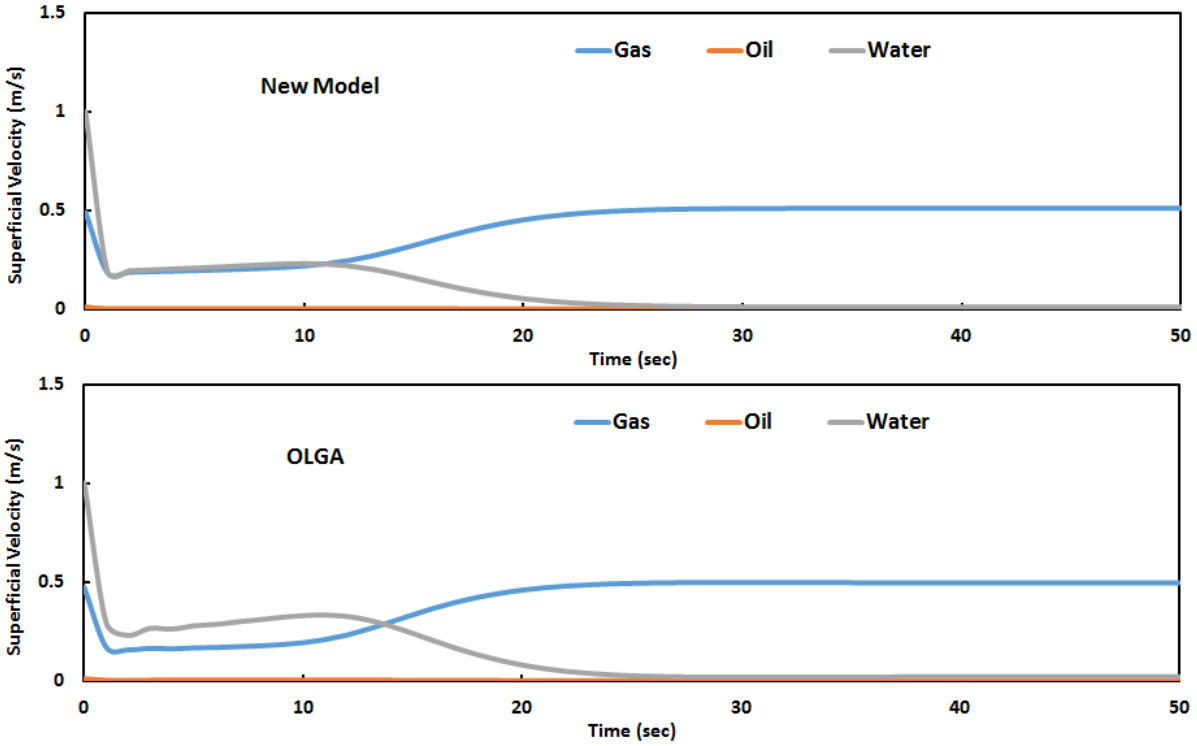

Figure 5-40: Water Depletion Comparison with OLGA for 90^{o} Inclination and Δt = 0.2 sec

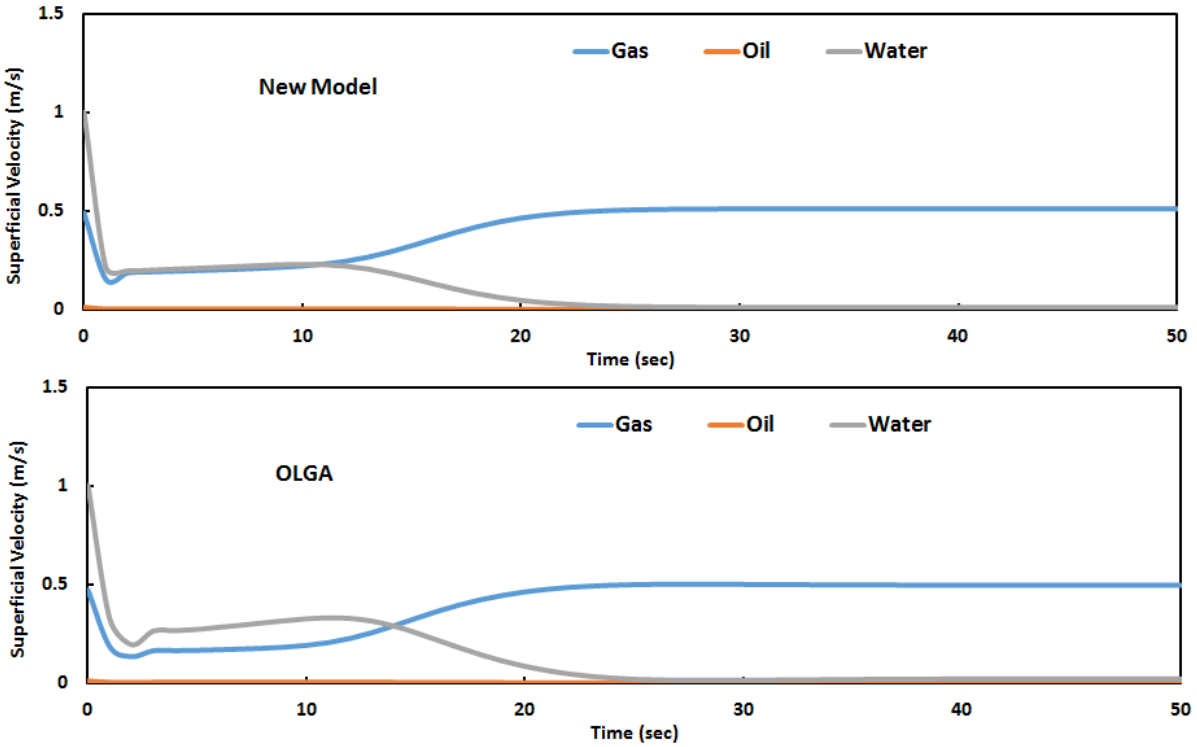

Figure 5-41: Water Depletion Comparison with OLGA for 90^{o} Inclination and Δt = 0.5 sec

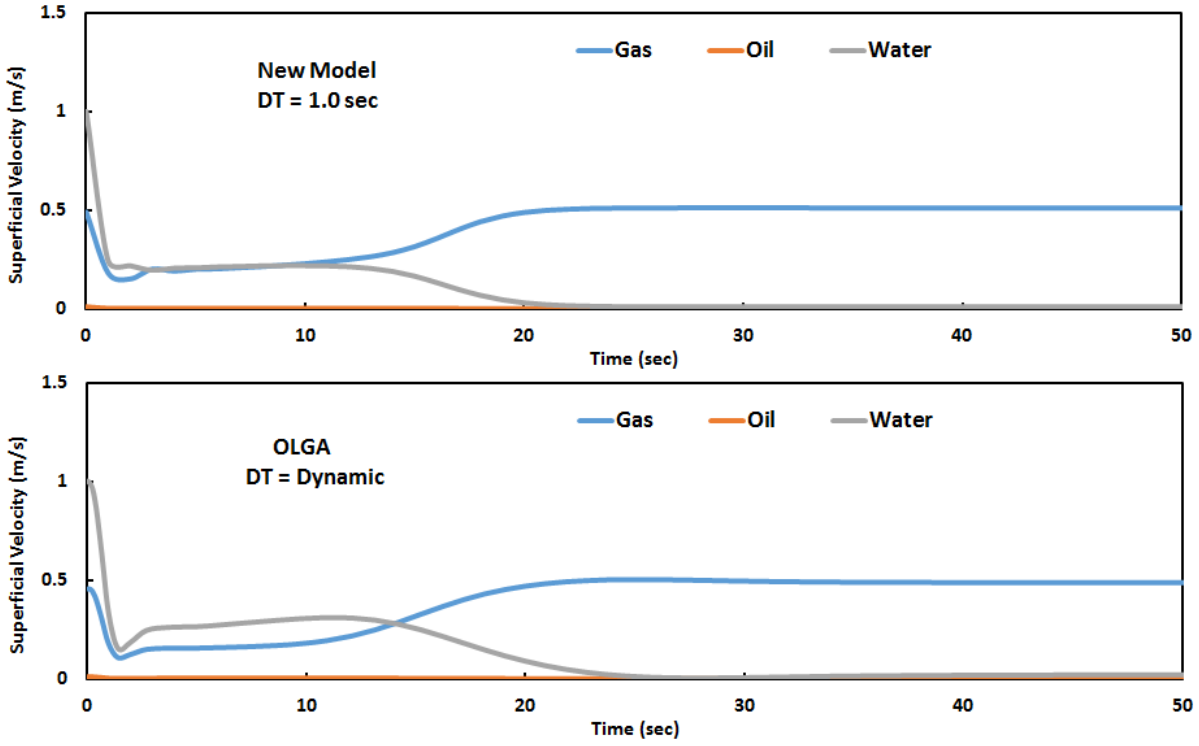

Figure 5-42: Water Depletion Comparison with OLGA for 90^{o} Inclination and Δt = 1.0 sec

The new model results agree well with OLGA when small time steps are used (Δt = 0.2 sec and Δt = 0.5). When time step increased to 1 second, the CFL condition is not met and OLGA failed to converge. The new model, however, converged well and produced stable results with good accuracy. Unlike OLGA semi-implicit formulation, the implicit discretization and solution of the new model allows the use of large time step.

5.5 Severe Slugging in Pipeline-Riser System

Severe slugging is a terrain-dominated phenomenon, characterized by the formation and cyclical production of long liquid slugs and fast gas blowout. As described in the introduction, each cycle of severe slugging contains four stages: slug formation, slug production, blowout, and liquid fallback. For better understanding of the phenomenon, the new model is used to analyze detailed transient responses of several variables. These variables are the pressure at the bottom of

the riser and the reverse liquid penetration length at the pipeline end (Figure 5-43), the void fraction at the bottom and top of the riser (Figure 5-44), gas superficial velocity at the bottom and top of the riser (Figure 5-45), and the liquid superficial velocity at the bottom and top of the riser (Figure 5-46).

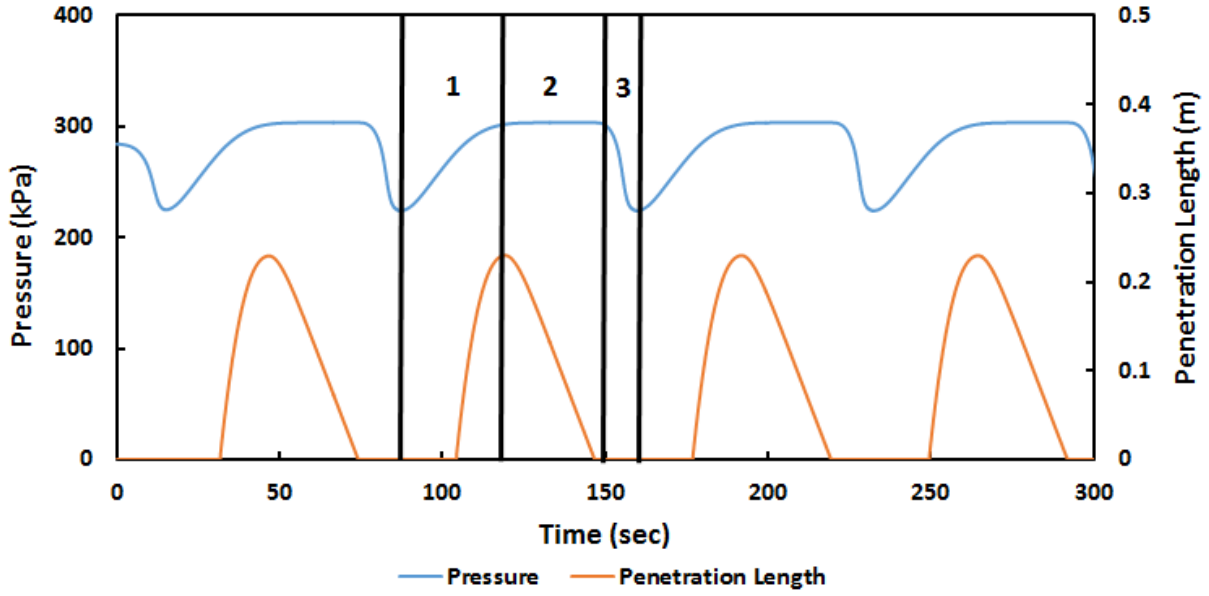

Figure 5-43: Transient Responses of Pressure at the Bottom of the Riser and Liquid Penetration Length at Pipeline End during Severe Slugging

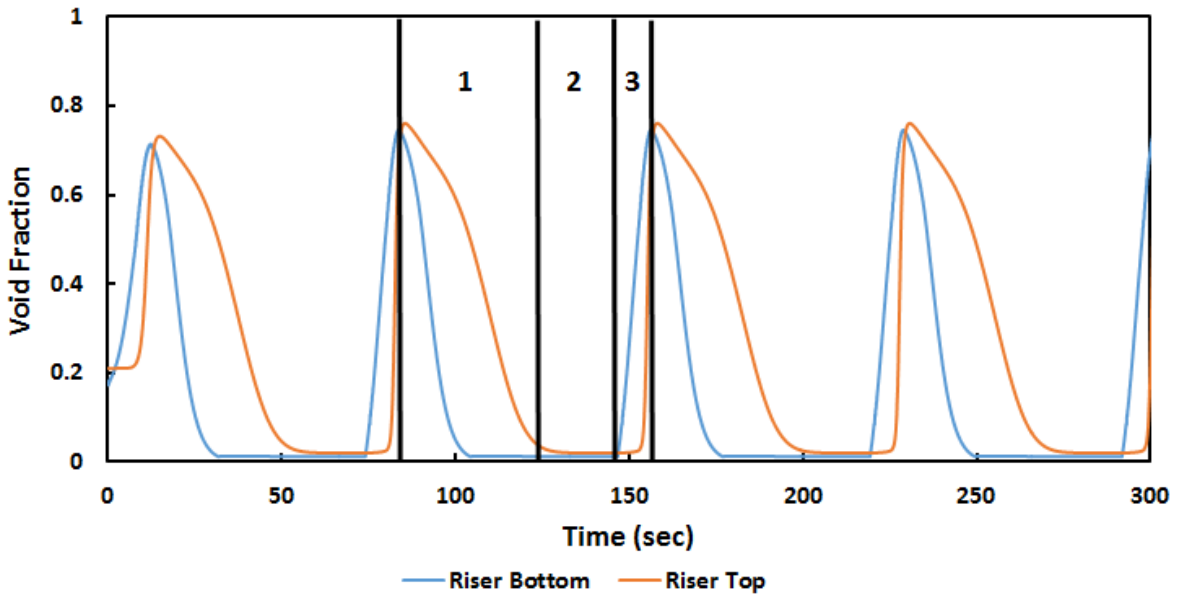

Figure 5-44: Transient Responses of Void Fractions at the Bottom and Top of the Riser during Severe Slugging

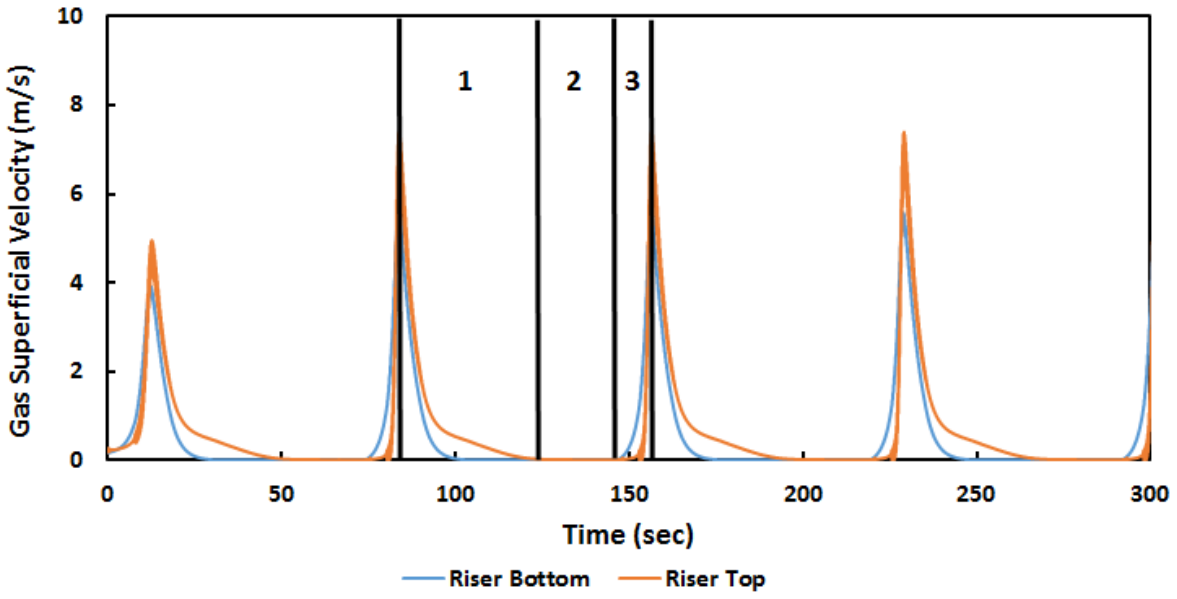

Figure 5-45: Transient Responses of Gas Superficial Velocities at the Bottom and Top of the Riser during Severe Slugging

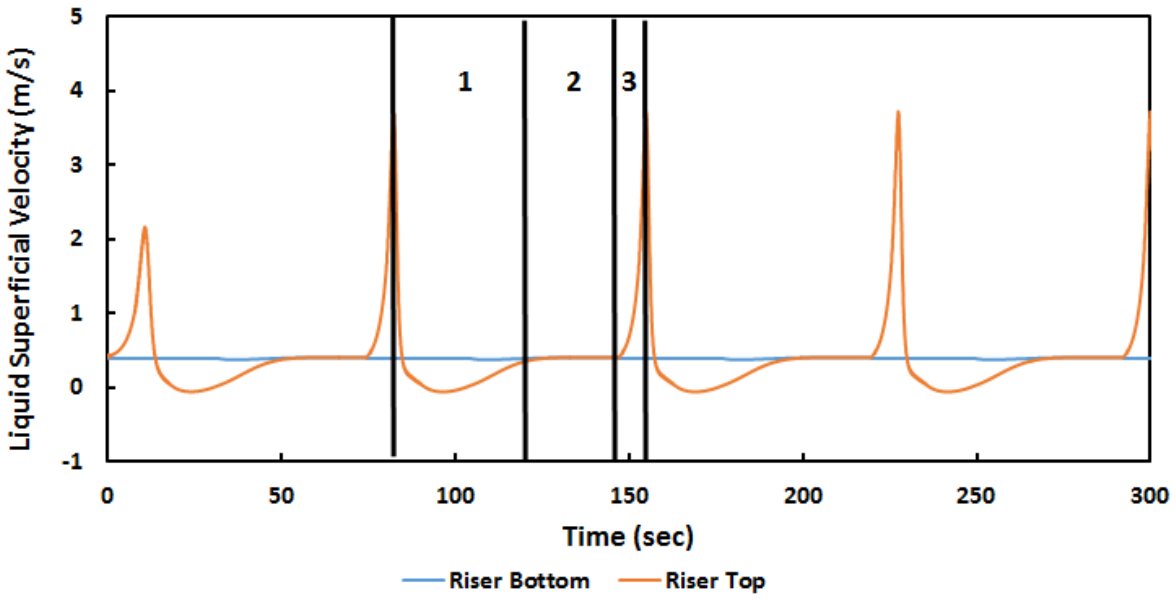

Figure 5-46: Transient Responses of Liquid Superficial Velocities at the Bottom and Top of the Riser during Severe Slugging

Prior to the slug formation stage, the intense blowout of gas into the riser rapidly depletes the pressured gas in the pipeline. Therefore, the slug formation stage starts with liquid blockage at the bottom of the riser, which leads to a sharp decrease in gas superficial velocity and void fraction at the bottom of the riser. Due to the incompressibility of liquid and the blockage at the bottom elbow, the superficial liquid velocity remains almost the same at the bottom of the riser and close to the inlet rate. At the top of the riser, because the blowout stage dissipates and produces most of the buildup liquid in the riser, the liquid decreases sharply to the point of falling back which reflects a negative value as indicated in Figure 5-46. As there is liquid supply at the bottom of the riser, the liquid level further increases and the liquid column in the riser becomes higher. The pressure at the riser base increases until it reaches the maximum value when the riser is filled with liquid. The liquid penetration back in the pipeline helps balance the pressure increase due to the liquid column buildup in the riser.

The riser now is filled with liquid and the liquid penetration fills a portion of the pipeline. As gas keeps flowing into the pipeline, the compressed gas pressure increases. The slug production stage starts when the liquid in the pipeline is pushed and only liquid is produced from the riser. The gas superficial velocity and void fraction at the riser stay at their minimum values, zero in most cases, while the pressure at the riser base remains constant corresponding to the static head of the liquid.

When the liquid front in the pipeline reaches the bottom of the riser, the blowout stage starts. The gas bubbles penetrate the riser, and the column becomes lighter which promotes gas flow. During this stage, the liquid and gas superficial velocities sharply increase and the void fraction distribution in the riser becomes very high, making the pressure at the bottom of the riser reach to its minimum. Due to the compressibility effect, the gas superficial velocity at the top of the riser is higher than that at the bottom. Because the gas is penetrating the riser, the liquid penetration length is zero. These behaviors can be clearly observed in the above figures numbered as the third stage. The blowout and fallback stages are combined into one stage.

Beltran (2005) investigated the three-phase gas-oil-water severe slugging phenomenon and presented a wide range of experimental results. In his study, an extensive range of gas and liquid superficial velocities are used for three different downward inclination angles for the pipeline and multiple water cuts. The new model in this study is validated using these sets of data. The experimental facility schematic used by Beltran (2005) is shown in Figure 5-47.

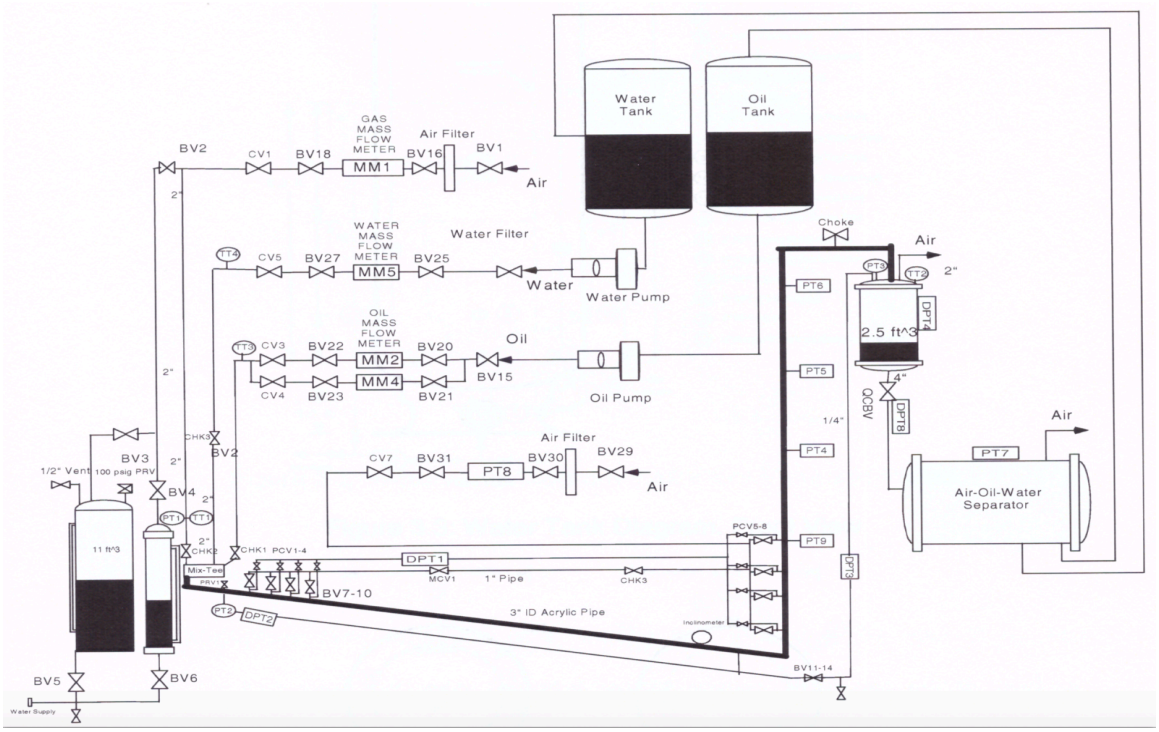

Figure 5-47: Beltran (2005) Experimental Facility Schematic

The facility consists of a 65-ft pipeline followed by a 48-ft riser, and the inner diameter of the pipe is 3 in. In order to achieve a full severe slugging cycle, the pipeline should be long for the gas to be pressurized and decompressed. Therefore, an additional expansion volume tank is added to increase the effective pipeline length to 290 ft. This extra length is used only for the gas stream and therefore, increases the time to gain pressure significantly. The option of an additional effective length is incorporated into the code for future uses. The fluids used in the experiments were air, mineral oil, and water. The API gravity of the mineral oil is 33.7^{o} and the viscosity is 14.6 cP. The gas and liquid superficial velocities varied from 0.1 to 3.0 m/s and 0.1 to 2.0 m/s respectively. The separator pressure was set at 12 psig for all cases. Three inclination angles for the pipeline were studied: -1^{o}, -3^{o}, and -5^{o} with the -1^{o} as the base angle with more detailed experimental results. The water cuts used were 0%, 20%, 40%, 60%, 80%, and 100%. The flow pattern in the pipeline was maintained as stratified flow for the entire experiment to

ensure the existence of severe slugging. The pressure at the bottom of the riser and the severe slugging cycle time are used primarily throughout the comparisons.

5.5.1 Effect of Water Cut on Severe Slugging

The comparison of the transient model against the experimental tests for superficial gas and liquid velocities of 0.4 m/s and -1° inclination angle at water cuts of 20%, 40%, 60%, and 100% are shown in Figures 5-48, 5-49, 5-50, and 5-51, respectively.

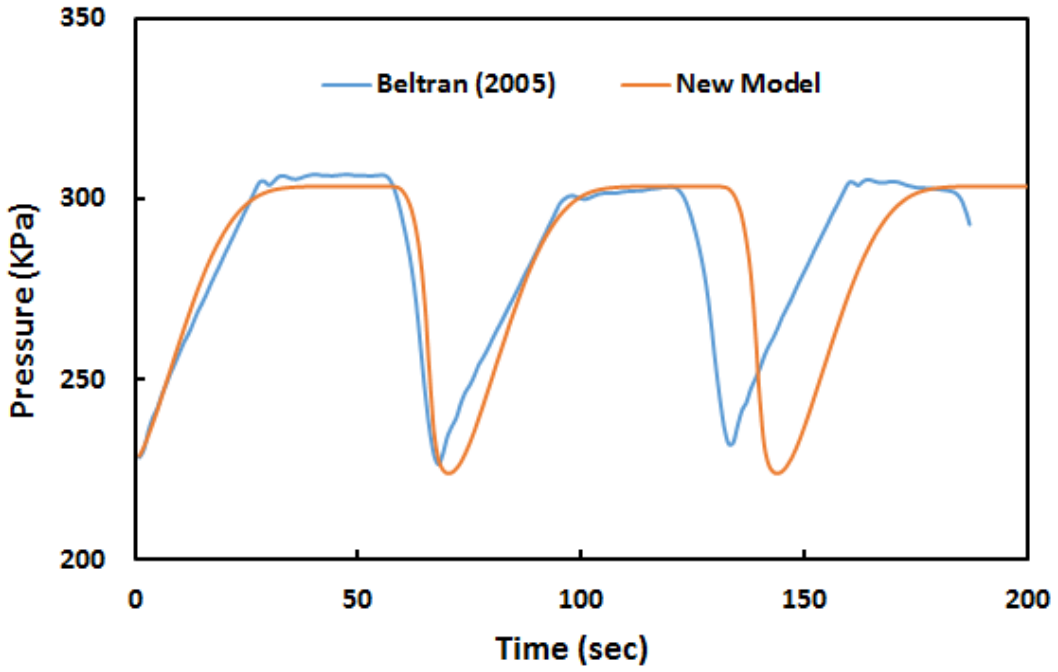

Figure 5-48: Severe Slugging Comparison with Beltran (2005) for v_{SG} = 0.4 m/s, v_{SL} = 0.4 m/s, θ = -1°, and WC = 20%

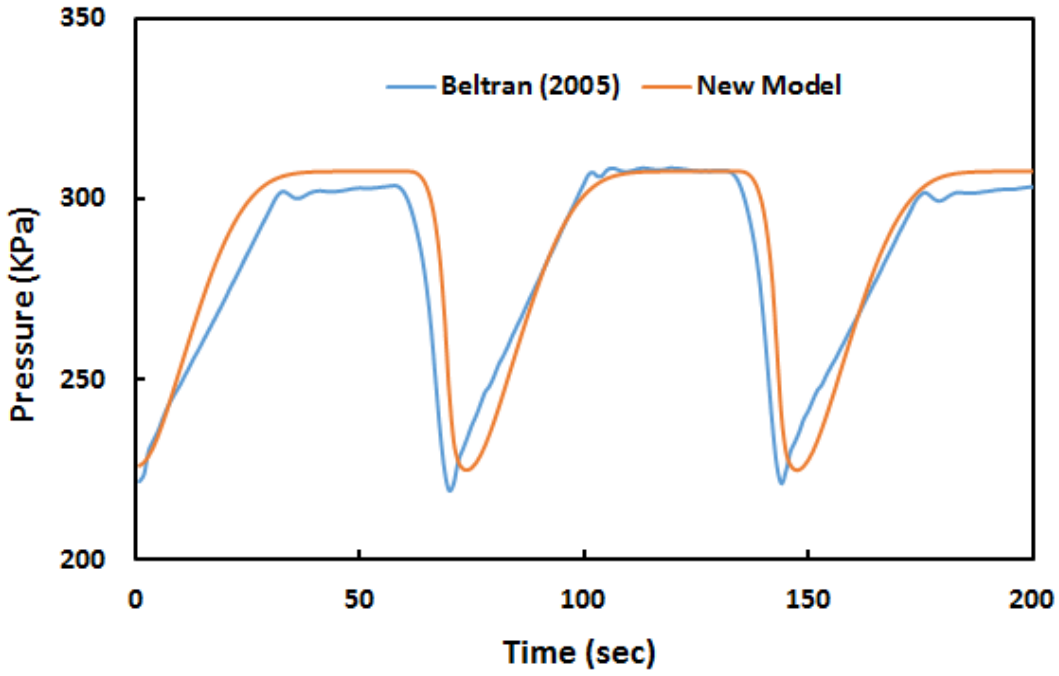

Figure 5-49: Severe Slugging Comparison with Beltran (2005) for v_{SG} = 0.4 m/s, v_{SL} = 0.4 m/s, θ = -1°, and WC = 40%

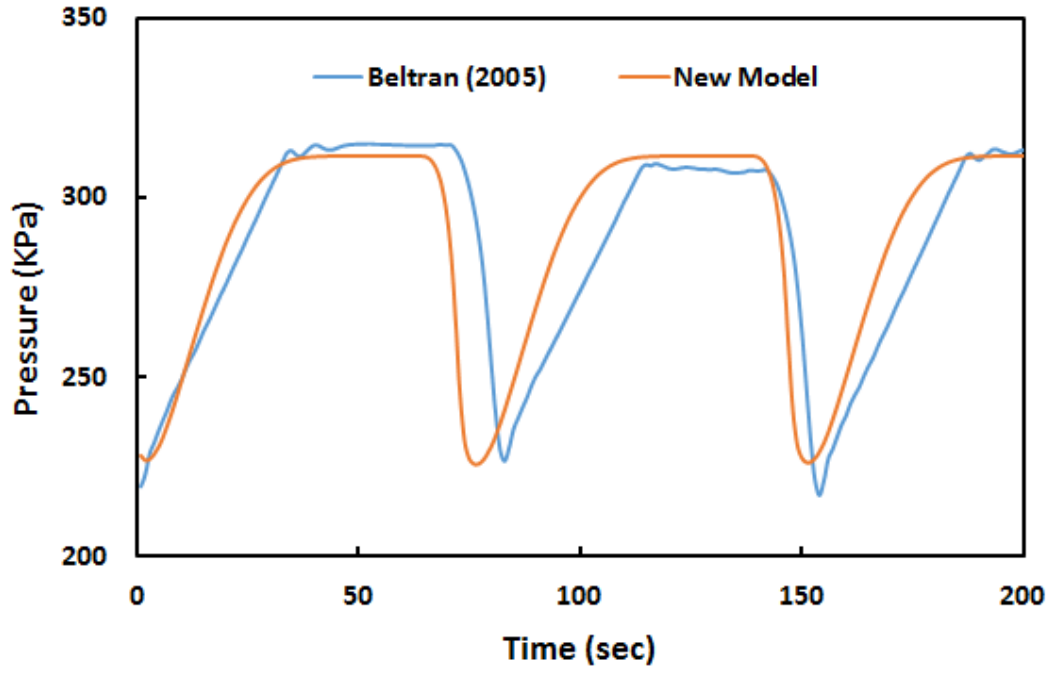

Figure 5-50: Severe Slugging Comparison with Beltran (2005) for v_{SG} = 0.4 m/s, v_{SL} = 0.4 m/s, θ = -1°, and WC = 60%

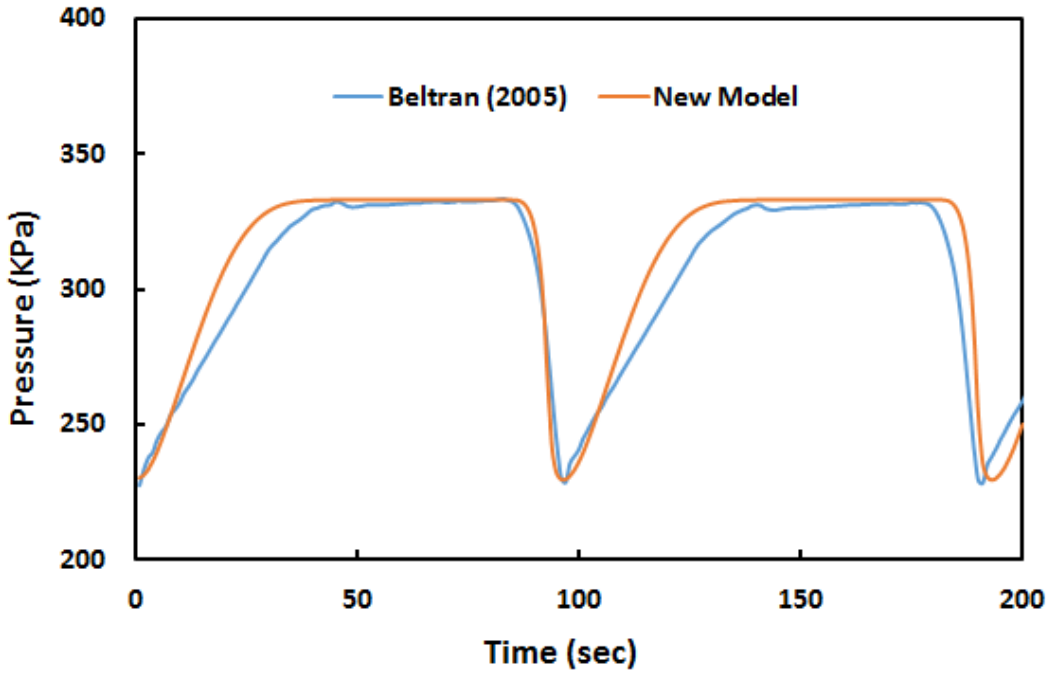

Figure 5-51: Severe Slugging Comparison with Beltran (2005) for v_{SG} = 0.4 m/s, v_{SL} = 0.4 m/s, θ = -1°, and WC = 100%

The transient model agrees well with the experimental results for the pressure difference between the minimum and maximum pipeline pressure. Moreover, the predicted severe slugging periods match the experimental results. Several previous studies developed their slugging models based on one-dimensional gravity-dominant flow. This study considers the frictional components of the momentum equation and most importantly captures efficiently the fallback of the liquid after the blowout stage which significantly supports the accurate predictions illustrated above. From the previous figures, it can be concluded that the severe slugging period is highly affected by the water cut. When the water cut increases, the mixture density of the liquid increases and therefore, higher mass flow rate is required to overcome the heavier column. The low mass flow rate needs longer time to create the required pressurized gas for the heavier liquid column and this results in a longer severe slugging cycle. A detailed demonstration of this behavior is achieved using the new model and is displayed in Figure 5-52. With a fixed superficial liquid

velocity, it can be seen clearly that the period increases as the water cut increases at any superficial gas velocity. It can also be observed that the severe slugging period declines exponentially with the increase in the superficial gas velocity.

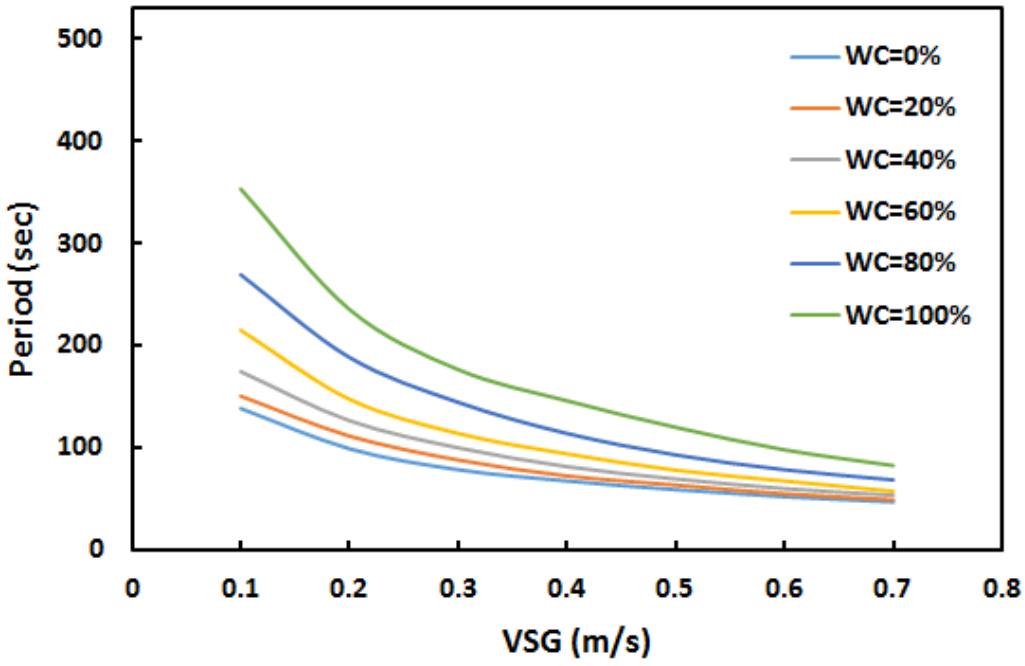

Figure 5-52: Severe Slugging Period for v_{SL} = 0.2 m/s, θ = -1°, and Different Water Cuts

5.5.2 Effect of Inclination Angle on Severe Slugging

The comparison of the transient model against the experimental tests for superficial gas and liquid velocities of 0.4 m/s and 20% water cut at inclination angles -3° and -5° are shown in Figures 5-53 and 5-54, respectively.

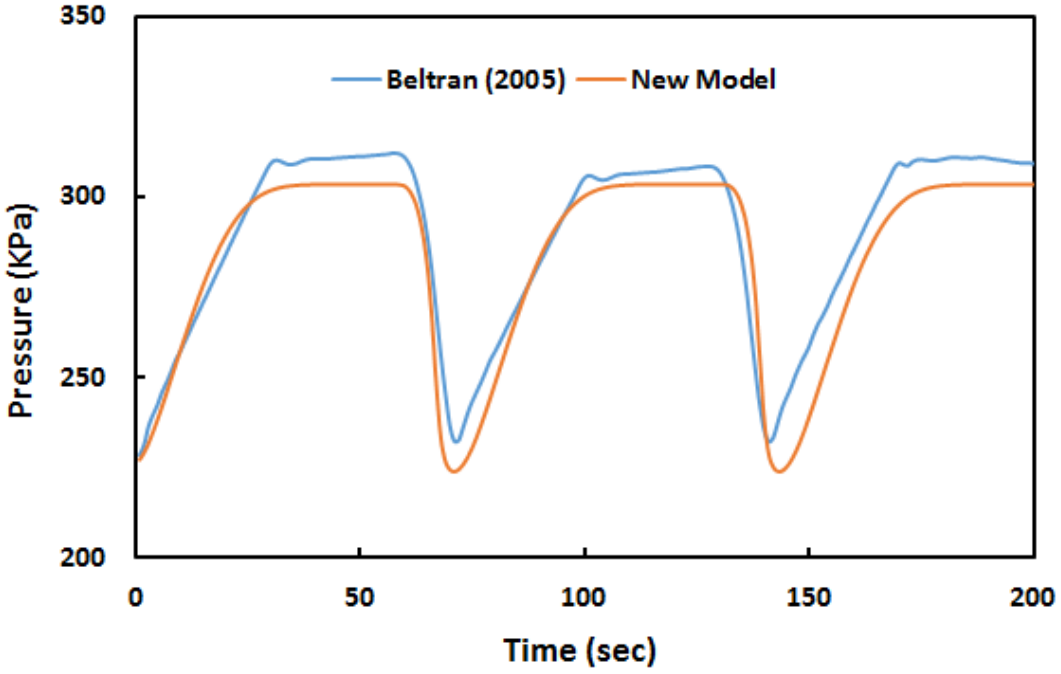

Figure 5-53: Severe Slugging Comparison with Beltran (2005) for v_{SG} = 0.4 m/s, v_{SL} = 0.4 m/s, θ = -3°, and WC = 20%

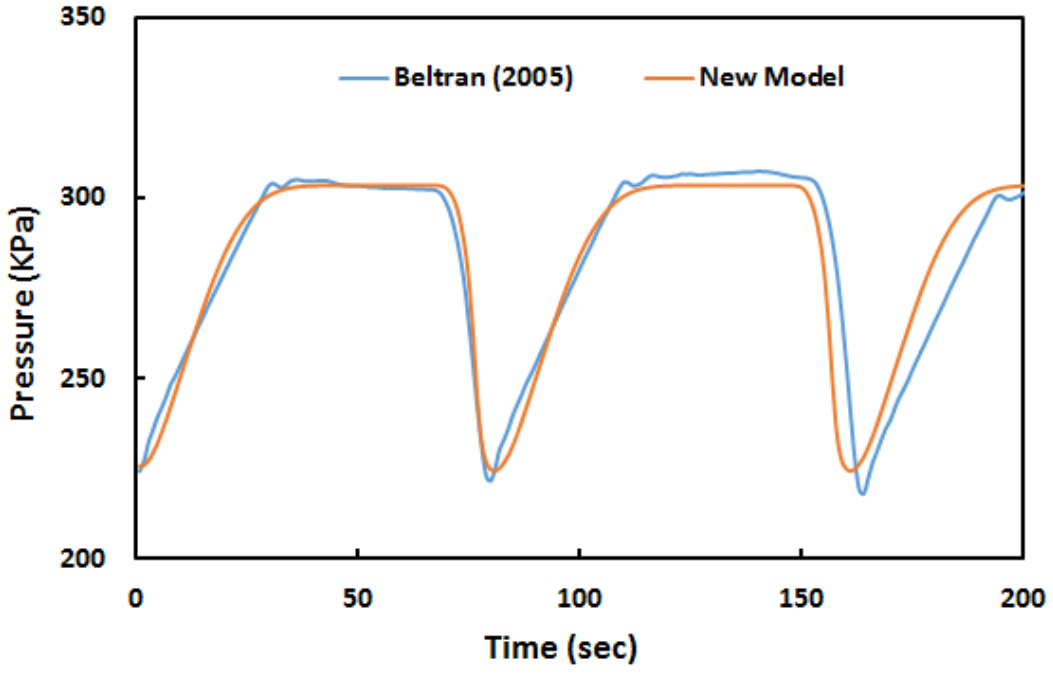

Figure 5-54: Severe Slugging Comparison with Beltran (2005) for v_{SG} = 0.4 m/s, v_{SL} = 0.4 m/s, θ = -5°, and WC = 20%

The severe slugging cycle time increases with the increase of the downward angle and the transient model adjusts well with this effect. In two-phase flow, when the downward inclination angle increases, the liquid tends to accumulate at the elbow and penetrate into the pipeline. The compressed gas in turn needs longer time to overcome the higher buildup pressure and the longer liquid in the pipeline. For three-phase flow, another unique behavior is observed and increases the severe slugging period even further. During the slug formation stage, the increase of downward angle promotes water penetration into the pipeline while blocking the oil from entering the riser. Hence, the water fraction in the riser increases which requires higher pipeline pressure buildup and therefore a longer cycle. Another reason is that when the accumulated oil starts to penetrate the accumulated water in the riser during the slug production and blowout stages, the oil fraction may even become higher than the inlet oil fraction. This oil blowout tends to dissipate a higher amount of oil and increases the tendency of higher water fraction in the riser at a later stage.

5.5.3 Effect of Three-Phase on Severe Slugging

During the blowout stage, the oil penetrates the column of water in the riser first in the forms of droplets, followed by the gas blowout. Therefore, the use of two-phase gas-liquid modeling approximation of the fully mixed liquid in the riser during this stage is reasonable. However, during the slug formation stage, the oil and water are separated in the riser and therefore the use of the mixture approximation approach may lead to inaccurate results. Moreover, the downward stratified flow in the pipeline needs special consideration. The condition of creating a stratified flow with mixed liquids requires either high liquid or high gas flow rate. Because severe slugging occurs only with low inlet flow rates, the three-layer stratified

flow becomes the dominant flow regime in the downward pipeline. The three-layer stratified flow model developed in this study is used for the downward calculations and the results are compared with the two-phase flow model approximation. The pressure behavior for severe slugging using the two-phase modeling approximation for superficial gas and liquid velocities of 0.4 m/s and 60% water cut at inclination angles of -1° is shown in Figures 5-55.

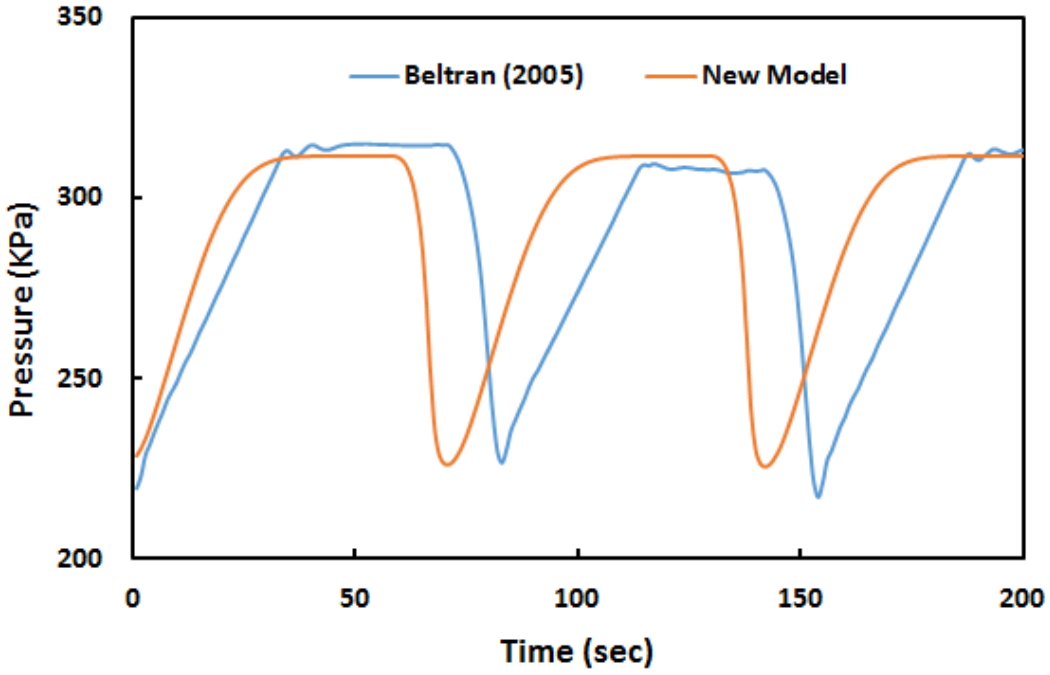

Figure 5-55: Severe Slugging Comparison with Beltran (2005) for v_{SG} = 0.4 m/s, v_{SL} = 0.4 m/s, θ = -1°, WC = 20%, and Using Two-Phase Flow Modeling

In comparison with Figure 5-48 developed using the three-phase modeling, the two-phase approximation predicts a shorter severe slugging period. The fully mixed approximation between the oil and water decreases the overall slippage in the system. This results in lower liquid holdup in the pipeline and lower liquid accumulation in the elbow, which in return requires less time for the gas to overcome the liquid buildup pressure in the riser. The three-layer stratified flow model considers two slippages, between the gas and oil layers and between the oil and water layers, and

therefore, leads to a higher holdup in the pipeline. This obviously impacts the severe slugging cycle with a longer period.

5.5.4 Severe Slugging Stability

In order to achieve a fully stable flow in the geometry of downward pipeline followed by an upward riser, the gas should penetrate the riser continuously and a stable pressure in the pipeline should be achieved. The flow is considered a partially stable when the gas is continuously penetrating the riser but is not sufficient to maintain a stable pressure in the pipeline. In this scenario, there is still some gas accumulation in the pipeline, which in return creates less severe cyclic behavior. Using the new model, the inlet gas flow rate is increased gradually and the pressure behavior in the pipeline is analyzed. For this severe slugging case, the results from the new model and Beltran (2005) are also compared with the predictions from the OLGA simulator. Using the same inputs of Figure 5-34 with 20% water cut and -1^{o} inclination angle, the superficial gas velocity is increased from 0.4 m/s to 0.8 m/s and the results are displayed in Figure 5-56.

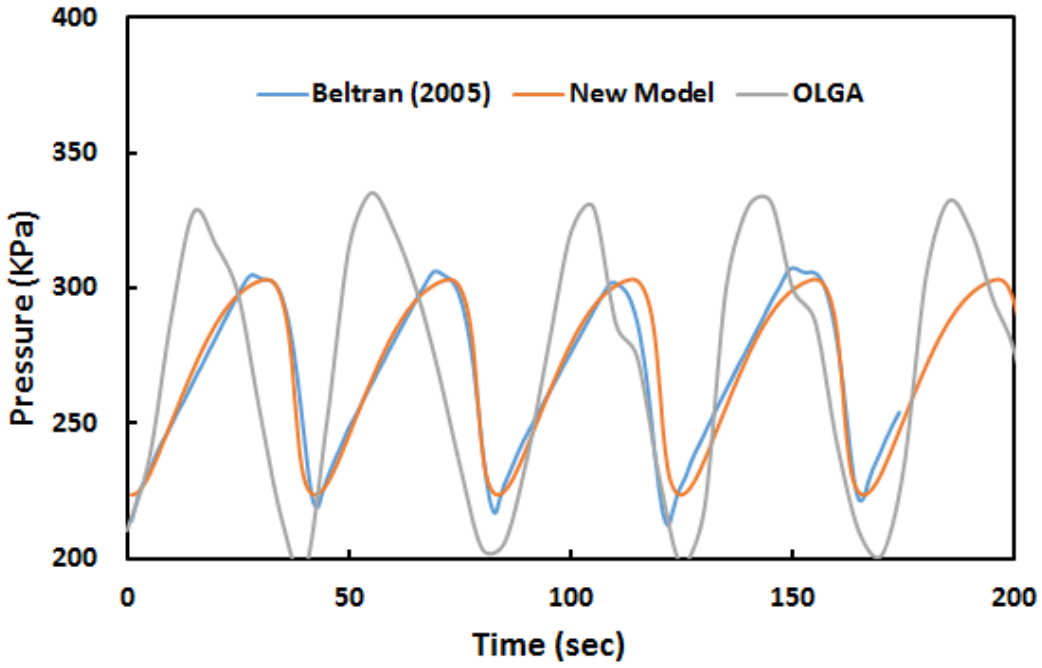

Figure 5-56: Severe Slugging Comparison with Beltran (2005) for v_{SG} = 0.8 m/s, v_{SL} = 0.4 m/s, θ = -1°, and WC = 20%

The severe slugging cycle time decreased dramatically, and the major difference revolves around the disappearance of the reverse liquid penetration into the pipeline. This slugging behavior is less severe. The simulation predictions agree well with the experimental results in terms of the maximum and minimum pressures and the cyclic time. The OLGA simulator, however, overestimates the pressure fluctuation with higher maximum pressure and lower minimum pressure. OLGA also gives a different shape while agreeing only on the severe slugging frequency. The gas is then gradually increased further until the flow becomes completely stable. The pipeline pressure behaviors for several gas superficial values with the same previous inputs are displayed in Figure 5-57.

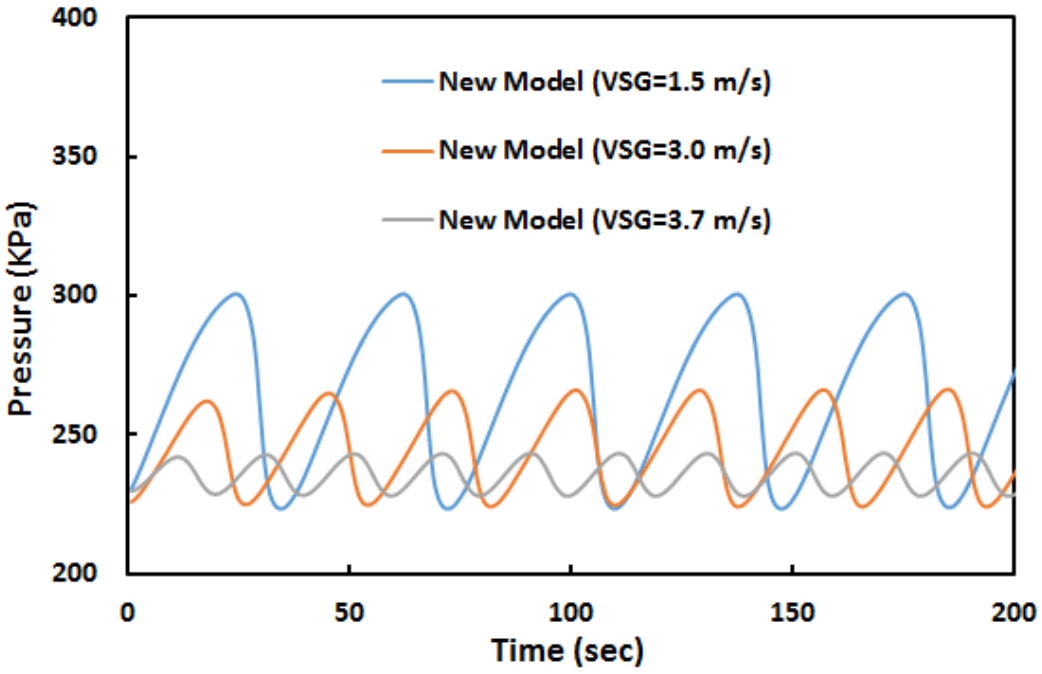

Figure 5-57: Severe Slugging Comparison with Beltran (2005) for Different v_{SG}, v_{SL} = 0.4 m/s, θ = -1°, and WC = 20%

With the increase in the gas flow rate, the gas penetrating the riser immediately after the liquid reaches the top of the riser and therefore the slug production stage disappears. It can be also observed that the higher the superficial gas velocity increases, the shorter the severe slugging cycle becomes, and therefore, the more stable the flow will be. For the previous inputs, the flow becomes fully stable when the v_{SG} reaches 3.7 m/s.

5.6 Gas-Lift Instability Analysis

Gas-lift is accomplished by injecting gas into the lower part of the production string from the casing-tubing annulus through one or more gas-lift valves. This process aims to increase the gas fraction and reduce the average density of the mixture and thereby decrease the hydrostatic pressure gradient. However, due to a decrease in mixture density, the gas injection subsequently becomes even higher than required due to the low tubing pressure, causing depletion of the gas

in the annulus. If the surface gas injection is not high enough to compensate for the gas depletion, the annulus pressure is then decreased followed by a drop or complete cessation of gas injection, which causes the tubing pressure to build up. After the annulus pressure recovers, gas injection restarts and a new cycle begins.

The transient behavior in gas-lift wells described above is called casing heading, and it is simulated using the newly developed transient model. The gas-lift instability predictions are compared with the commercial simulator OLGA using a hypothetical vertical well model. Optimization techniques to avoid the unsteady state behaviors in gas-lift wells are proposed. The effect of water cut on the gas-lift casing heading and on the optimization techniques are also presented. The detailed well setup information for the base case is presented in Figure 5-58.

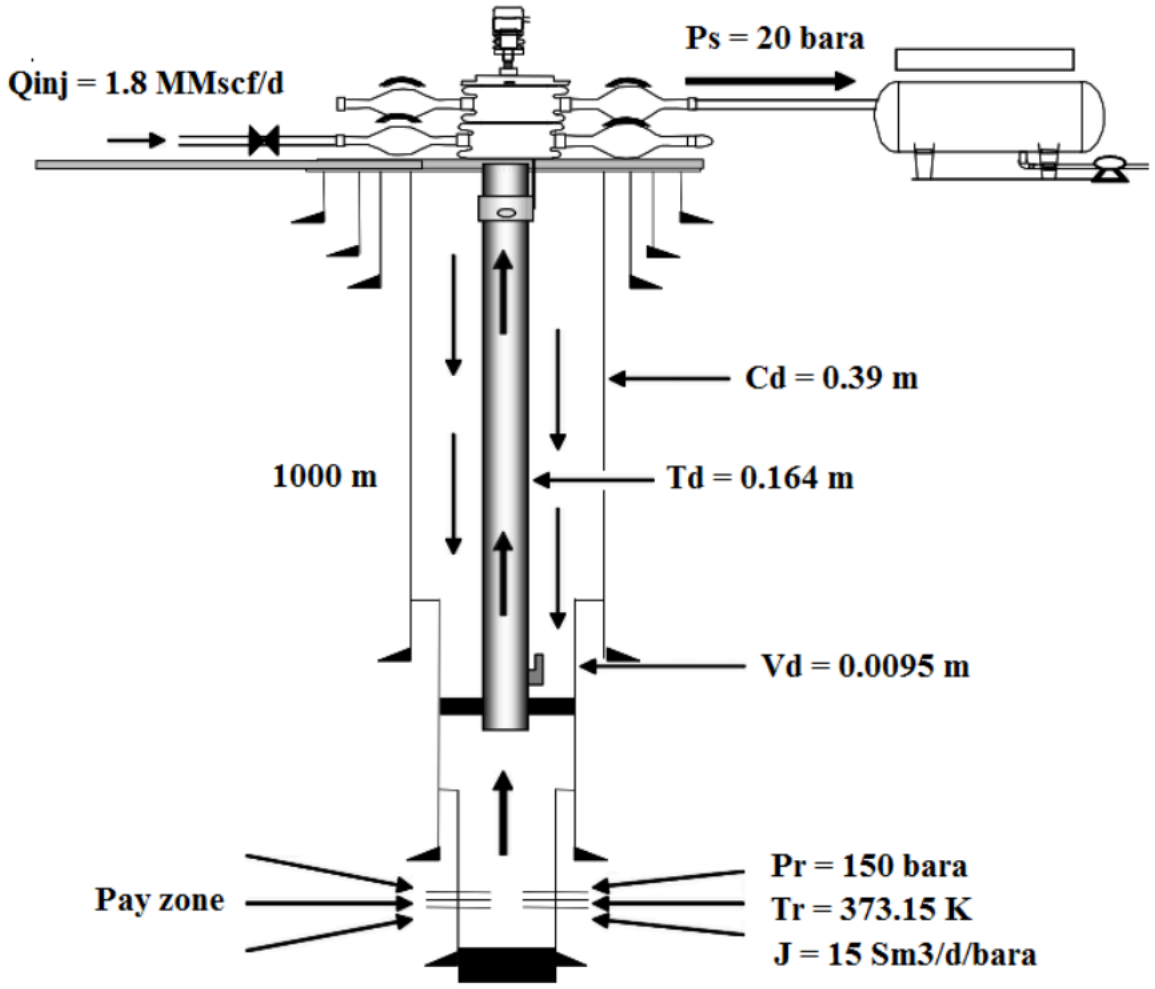

Figure 5-58: Base Case Inputs for Casing Heading Hypothetical Well

The simulation results for the base case using the newly developed transient model and the OLGA simulator at water cuts of 0%, 20%, 40%, 60%, 80%, and 100% are shown in Figures 5-59, 5-60, 5-61, 5-62, 5-63, and 5-64, respectively.

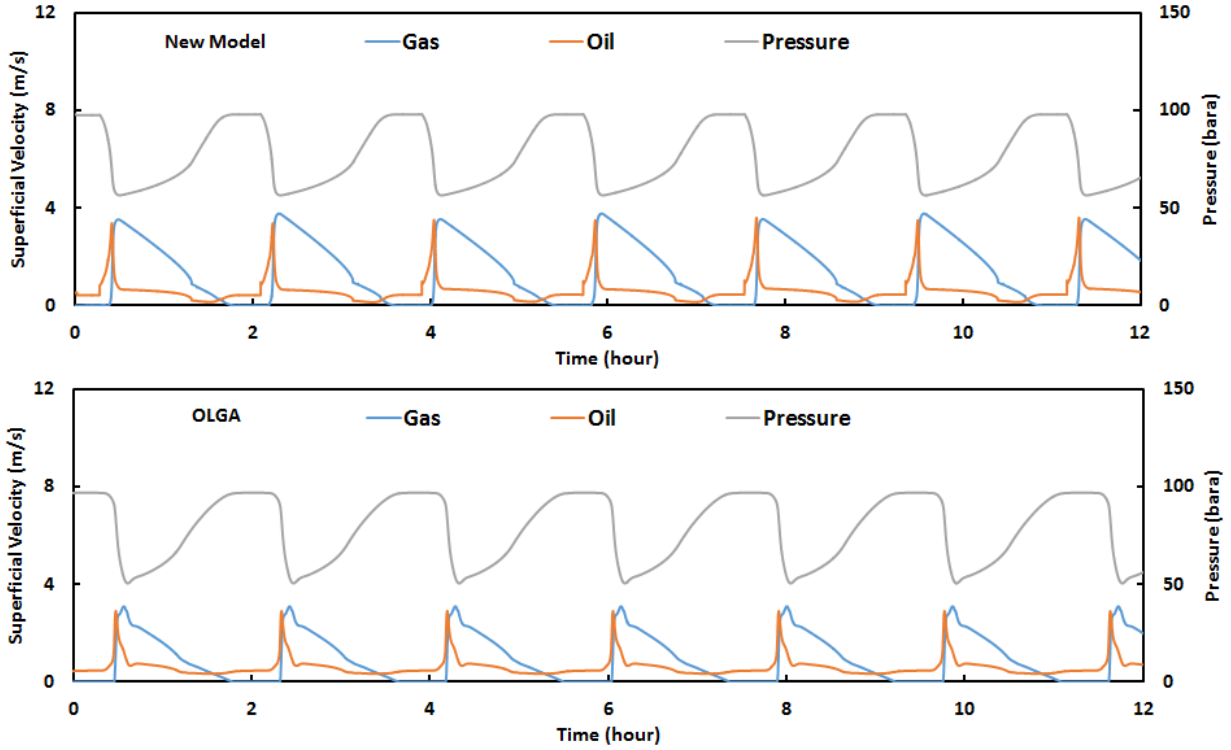

Figure 5-59: Casing Heading Comparison with OLGA for Base Case and 0% WC

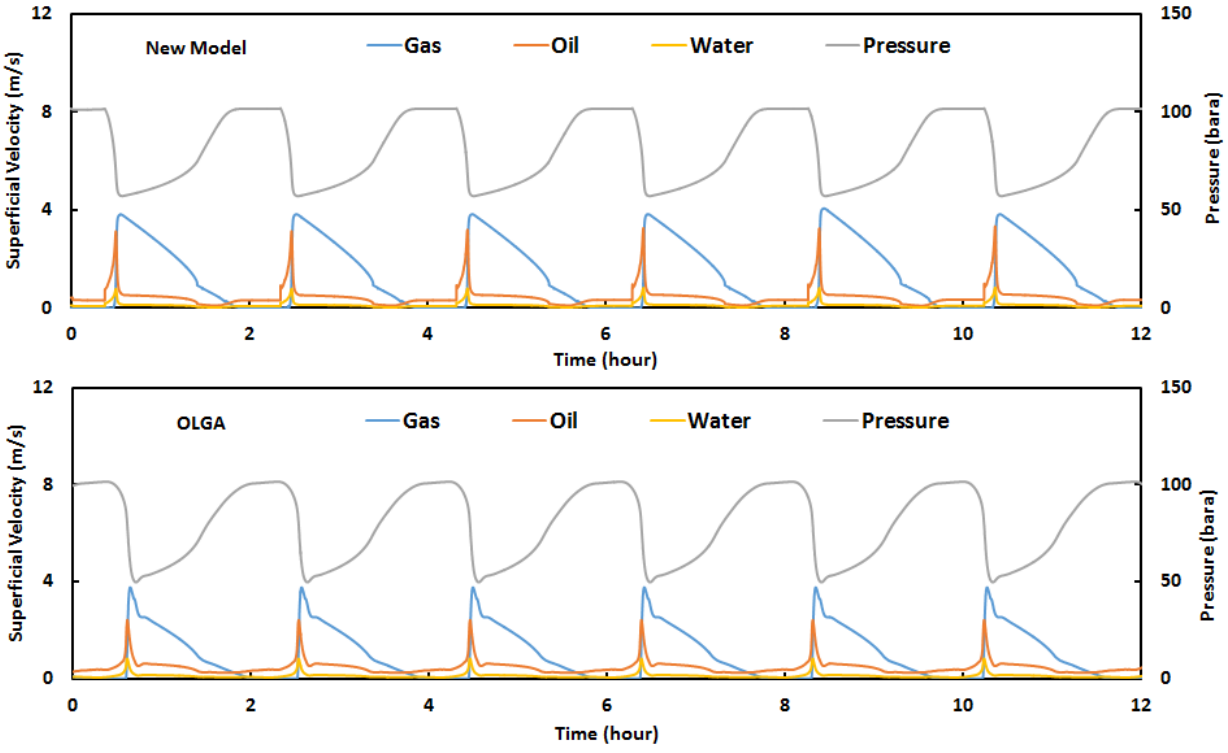

Figure 5-60: Casing Heading Comparison with OLGA for Base Case and 20% WC

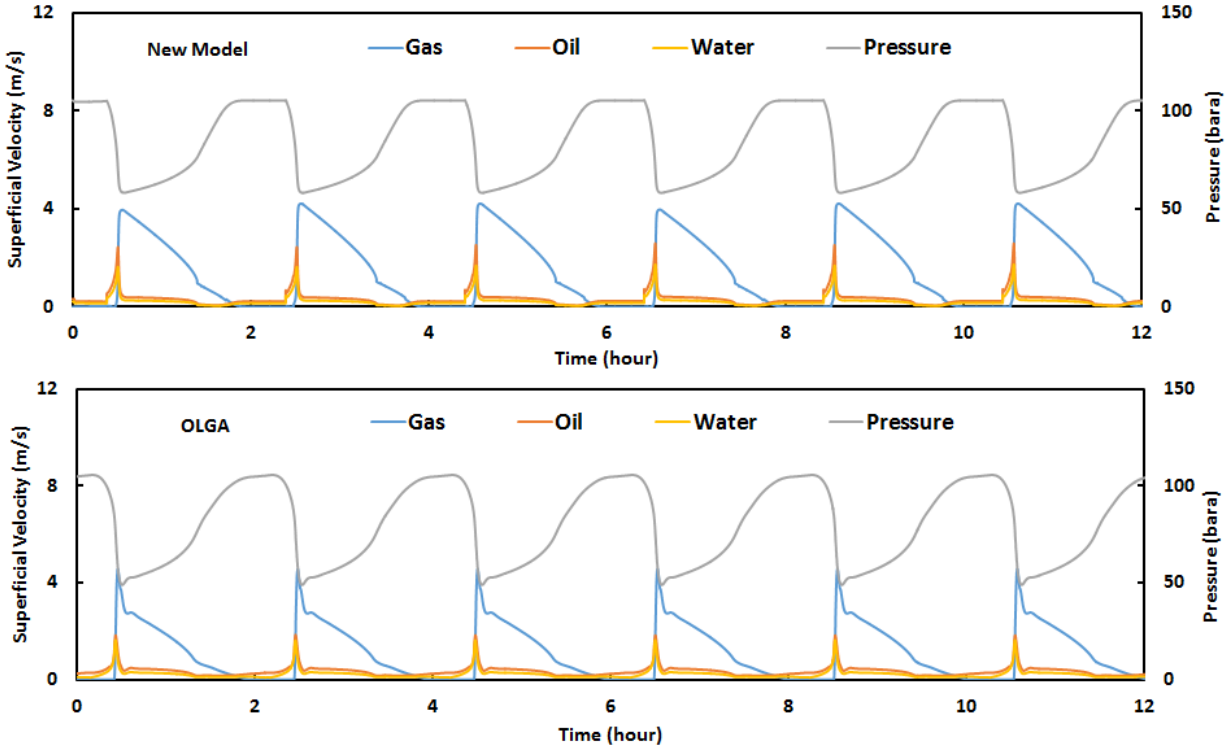

Figure 5-61: Casing Heading Comparison with OLGA for Base Case and 40% WC

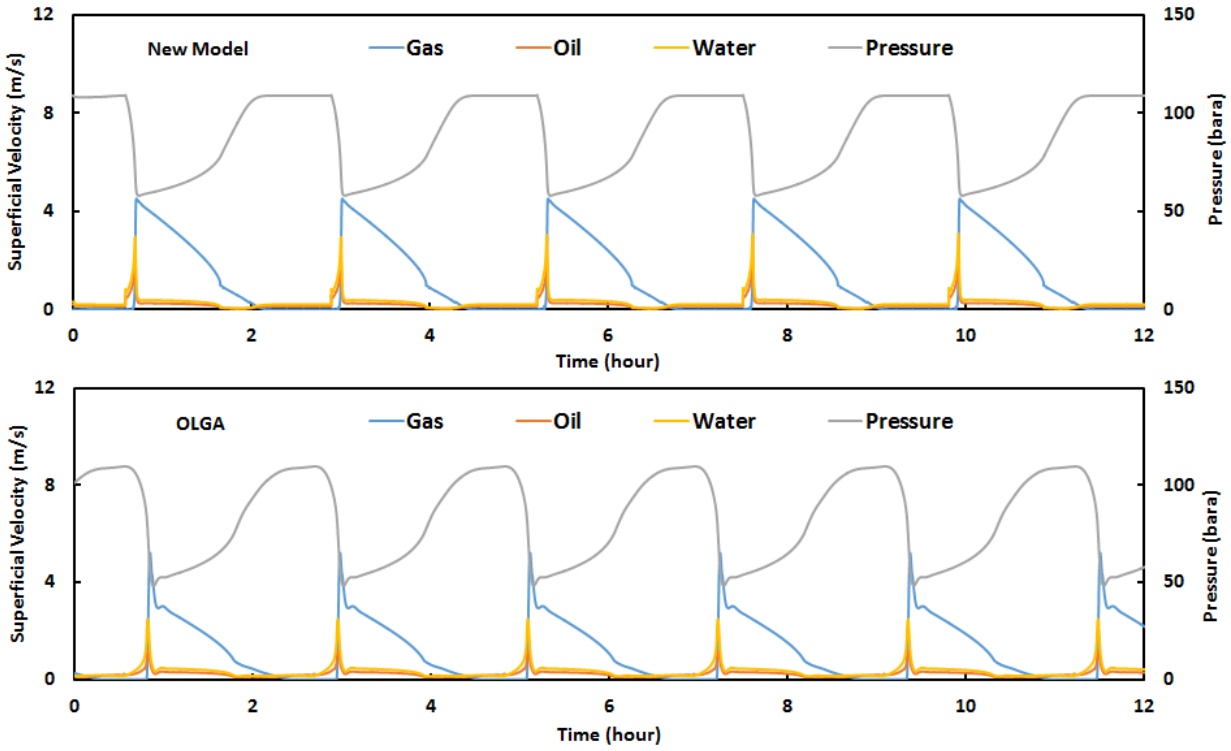

Figure 5-62: Casing Heading Comparison with OLGA for Base Case and 60% WC

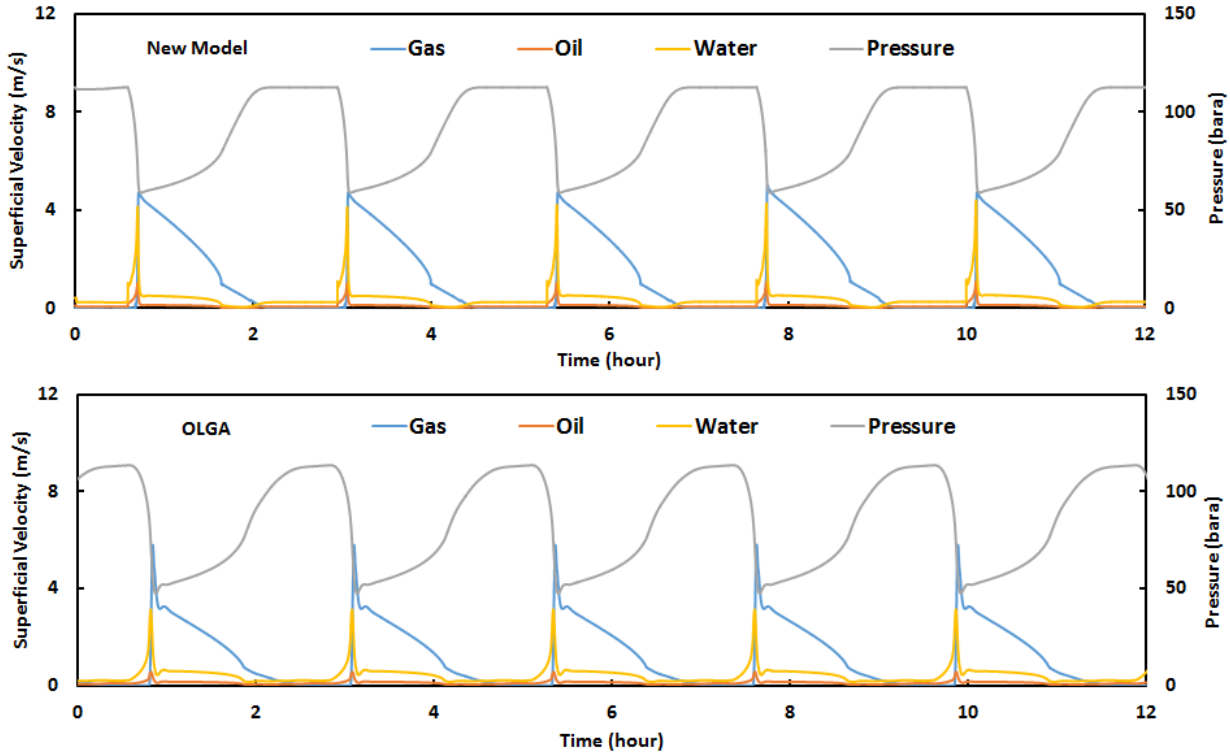

Figure 5-63: Casing Heading Comparison with OLGA for Base Case and 80% WC

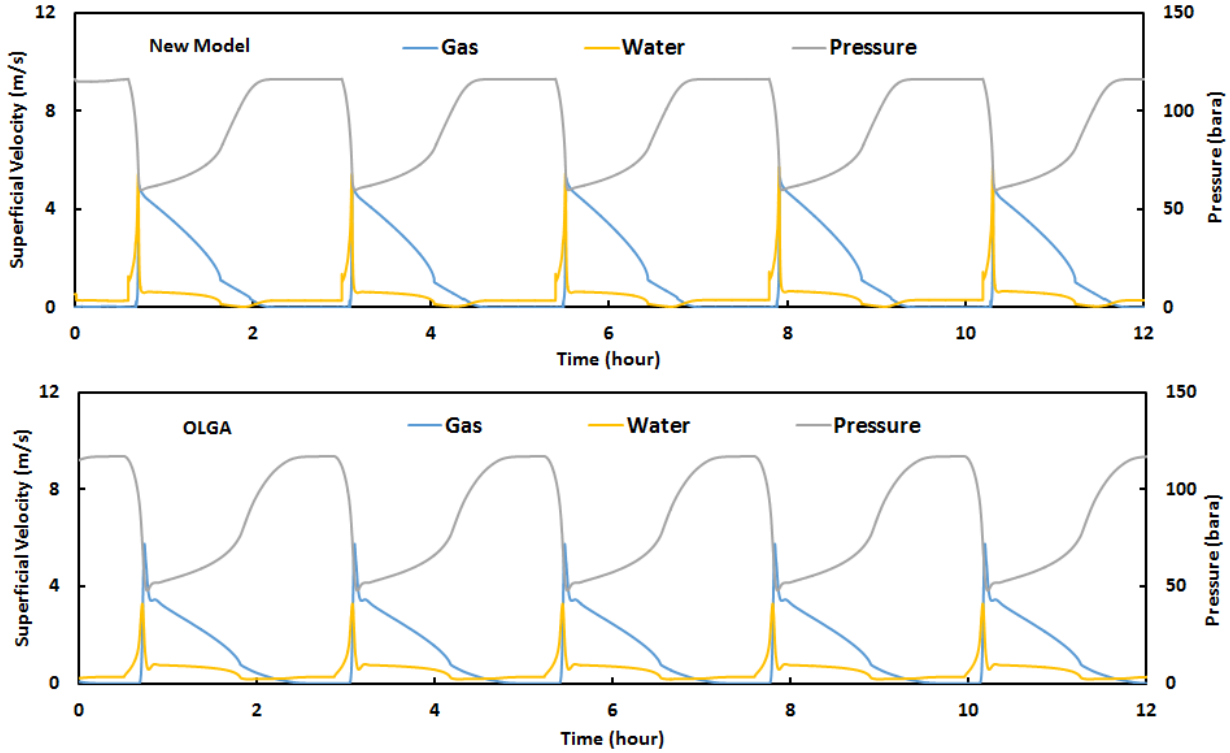

Figure 5-64: Casing Heading Comparison with OLGA for Base Case and 100% WC

It is clear that casing heading occurs for all water cuts as displayed by the oscillations of the outlet liquid and gas superficial velocities and bottom hole pressure. The maximum pressure and outlet superficial velocities agree very well with the OLGA simulations. However, the minimum pressure is higher than that from OLGA simulations for all the water cuts. In severe slugging, the gas in the pipeline penetrates the liquid column in the riser whenever the compressed gas pressure becomes higher than the hydrostatic head of the liquid. However, the gas-lift valve operating principle requires that the pressure in the casing to be at least 100 psia higher than the tubing pressure, which in return creates a different type of severity. With the same surface gas injection flow rate, when the water cut increases, the compressed gas in the annulus requires longer time to reach the required pressure and, consequently, a longer cycle. Moreover, the outlet flow rates become high for higher water cut and this does not reflect the actual behavior which can be observed only when the flow becomes stable. For stable flow, a higher water cut increases the mixture density and in return reduces the outlet flow rates. Increasing the surface gas injection is the first optimization technique for achieving a stable flow. In the following figures, the surface gas injection flow rate increases with small increments from the base case (1.8 MMscf/d) until the flow becomes stable. The outlet superficial velocities for different surface gas injections at water cuts of 0%, 20%, 40%, 60%, 80%, 100% are shown in Figures 5-65, 5-66, 5-67, 5-68, 5-69, and 5-70, respectively.

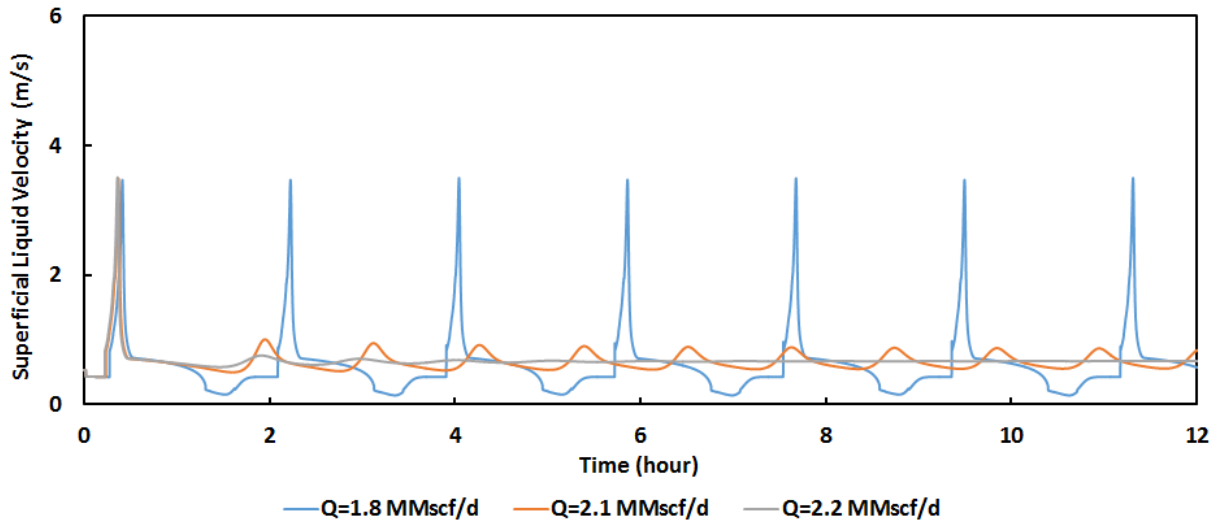

Figure 5-65: Effect of Gas Injection Rate on Casing Heading Predicted by New Model for 0% WC

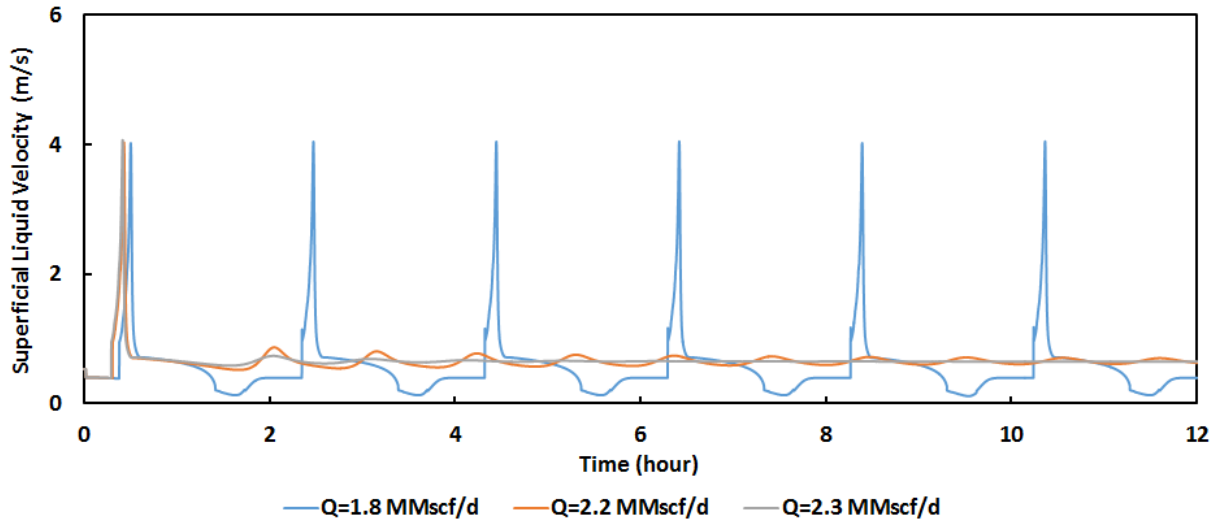

Figure 5-66: Effect of Gas Injection Rate on Casing Heading Predicted by New Model for 20% WC

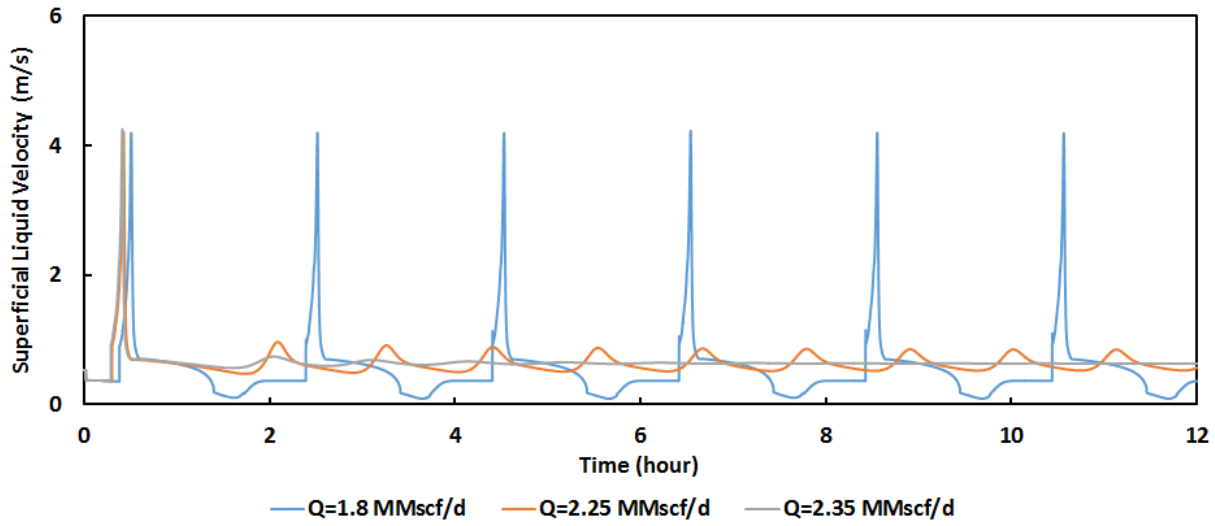

Figure 5-67: Effect of Gas Injection Rate on Casing Heading Predicted by New Model for 40% WC

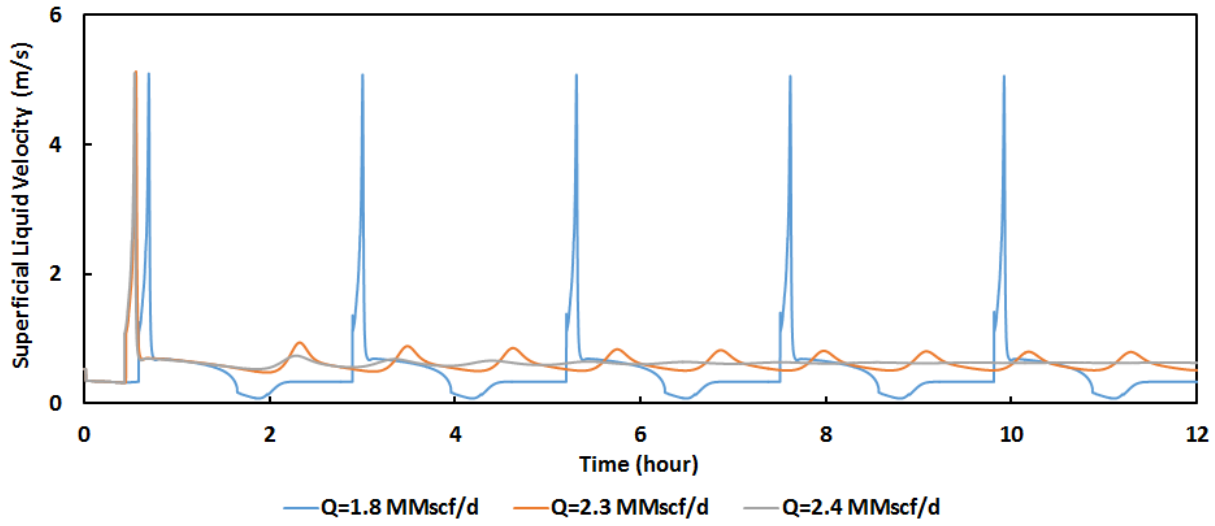

Figure 5-68: Effect of Gas Injection Rate on Casing Heading Predicted by New Model for 60% WC

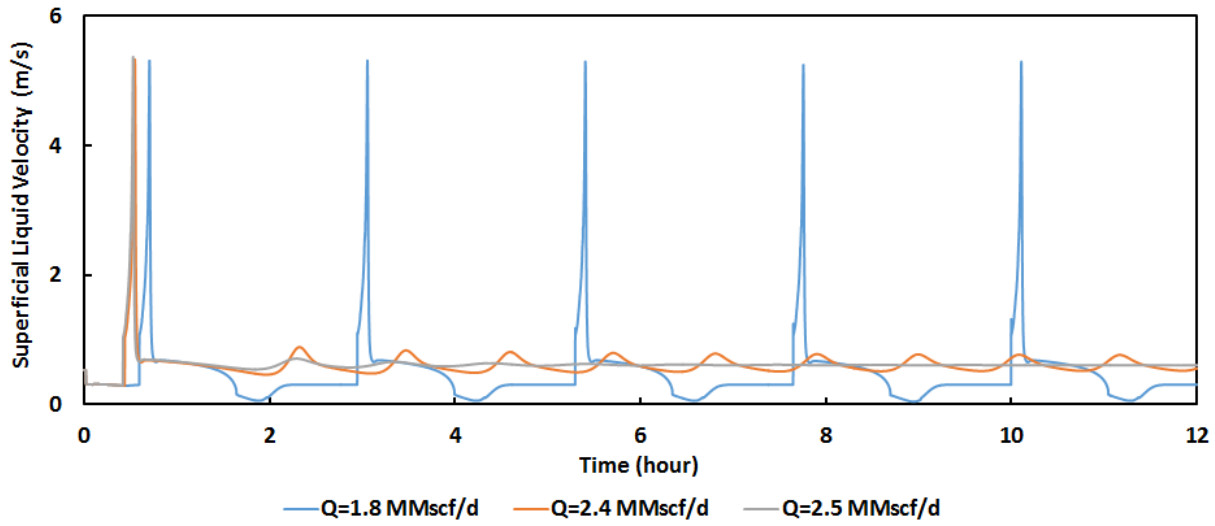

Figure 5-69: Effect of Gas Injection Rate on Casing Heading Predicted by New Model for 80% WC

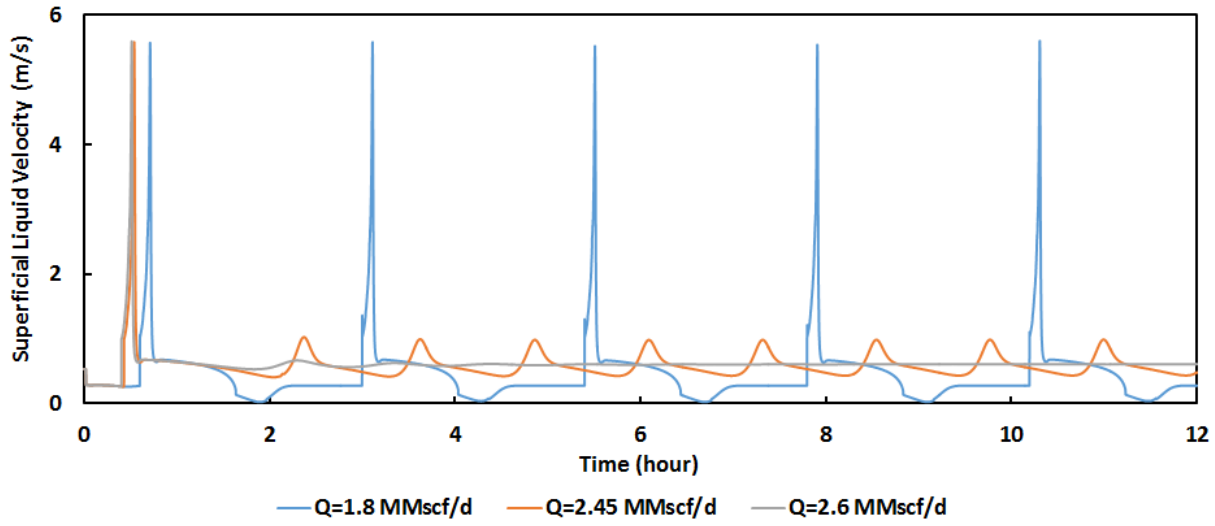

Figure 5-70: Effect of Gas Injection Rate on Casing Heading Predicted by New Model for 100% WC

When gas is injected, the bottom hole pressure decreases until it reaches a minimum value which leads to an excessive gas flow rate through the gas-lift valve. Therefore, a stable flow can be achieved if the surface gas injection is high enough to compensate for the gas depletion in the casing-tubing annulus. From the above figures, when the water cut increases, the

required gas injection rate for stable flow increases as well to overcome the heavier liquid in the tubing. For 0% WC, the required gas injection is 2.2 MMscf/d while it increases to 2.6 MMscf/d for 100% WC. Although for low water cut the surface gas injection is less, the outlet flow rates are higher than high water cut due to lighter fluid in the tubing which contradicts the behavior of the unstable flow.

Decreasing the gas-lift valve port diameter is another useful way to achieve a stable flow. The gas-lift valves come with standard sizes and in the following figures the gas-lift valve diameter is decreased from the base case of 0.375 inch to the first available one which is 0.3125 inch. The outlet superficial velocity for 0.3125 inch valve diameter at water cuts 0%, 20%, 40%, 60%, 80%, 100% are shown in Figures 5-71, 5-72, 5-73, 5-74, 5-75, and 5-76, respectively.

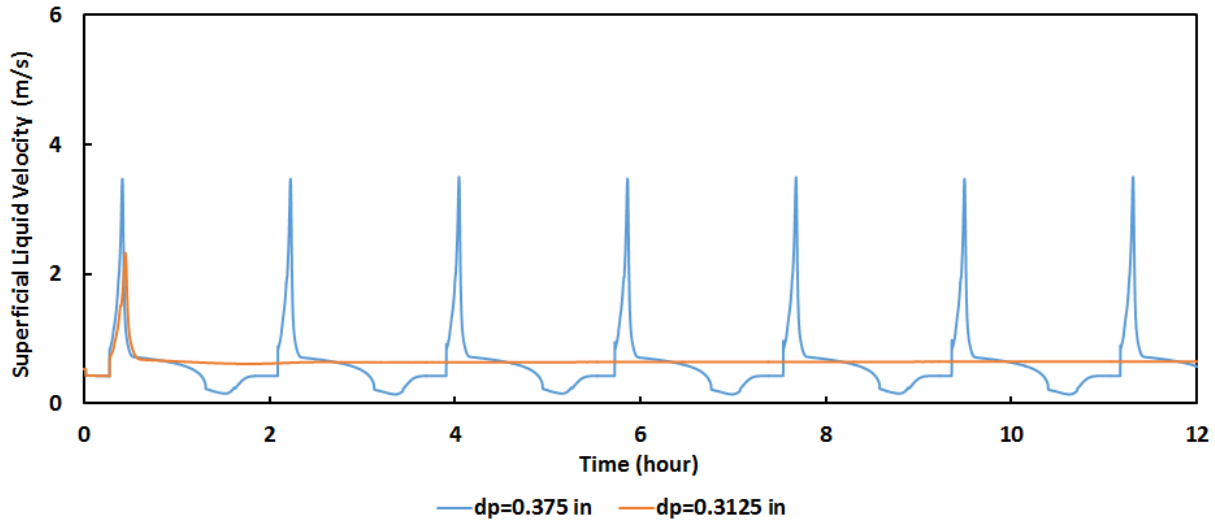

Figure 5-71: Effect of Gas-Lift Valve Port Size on Casing Heading Predicted by New Model for 0% WC

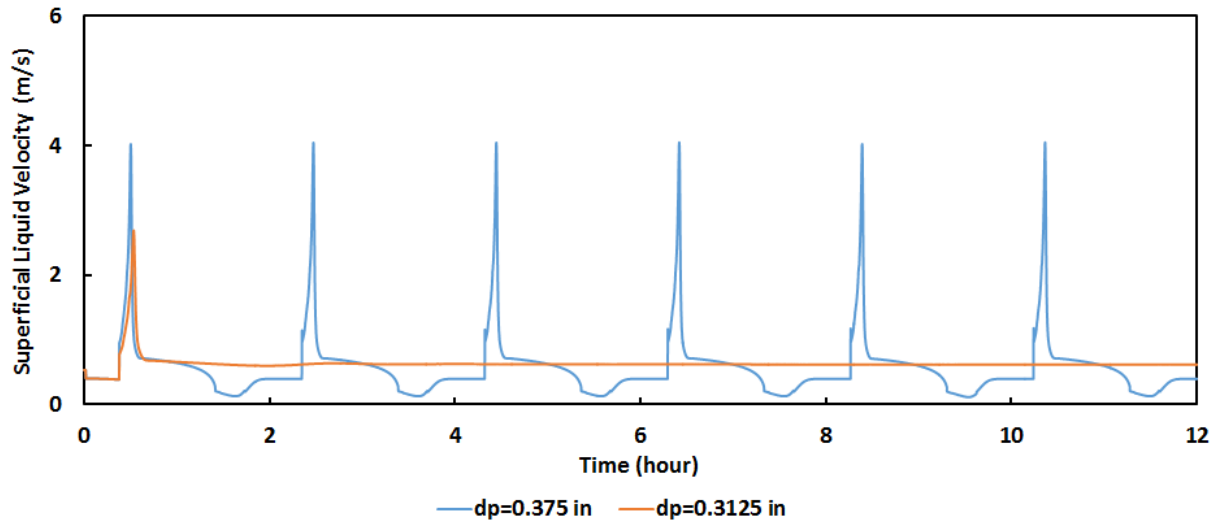

Figure 5-72: Effect of Gas-Lift Valve Port Size on Casing Heading Predicted by New Model for 20% WC

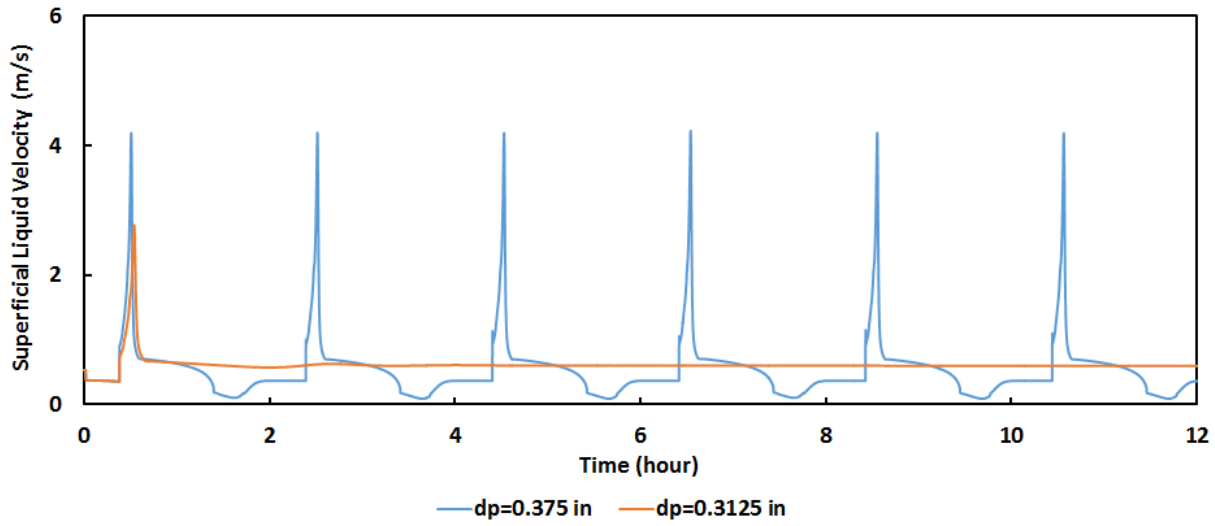

Figure 5-73: Effect of Gas-Lift Valve Port Size on Casing Heading Predicted by New Model for 40% WC

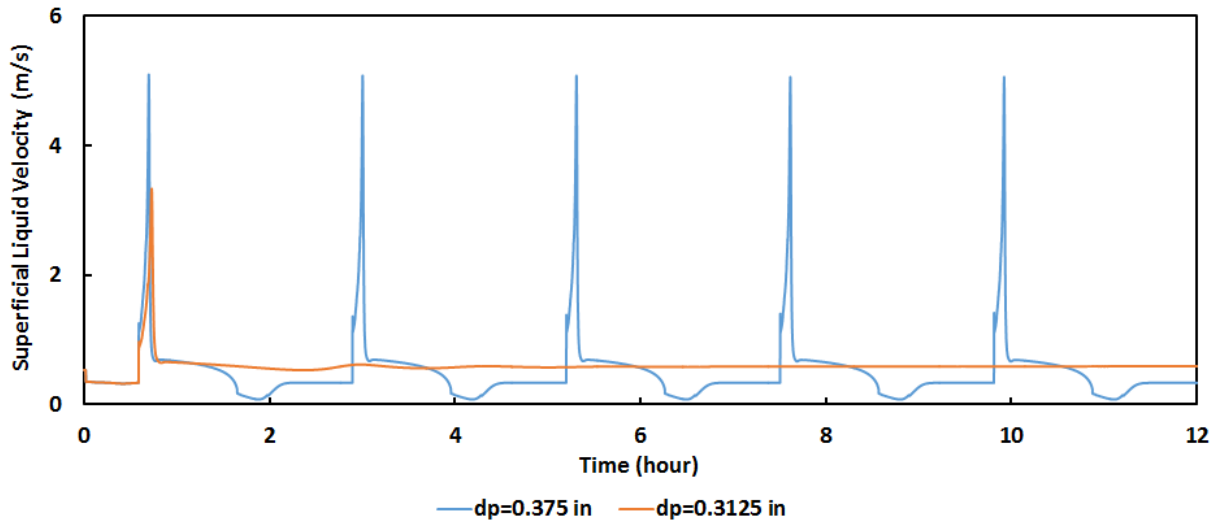

Figure 5-74: Effect of Gas-Lift Valve Port Size on Casing Heading Predicted by New Model for 60% WC

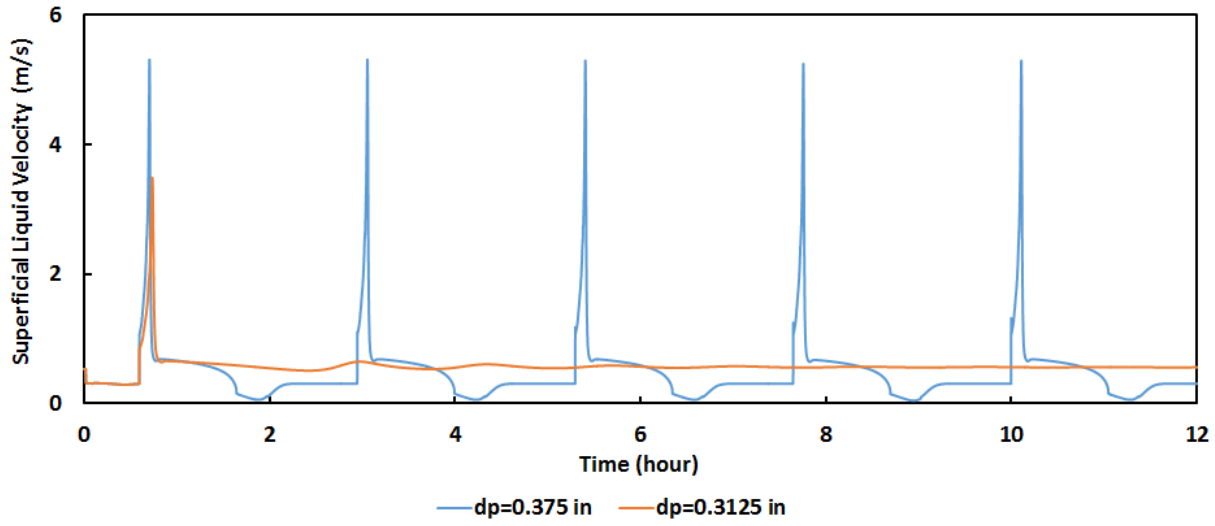

Figure 5-75: Effect of Gas-Lift Valve Port Size on Casing Heading Predicted by New Model for 80% WC

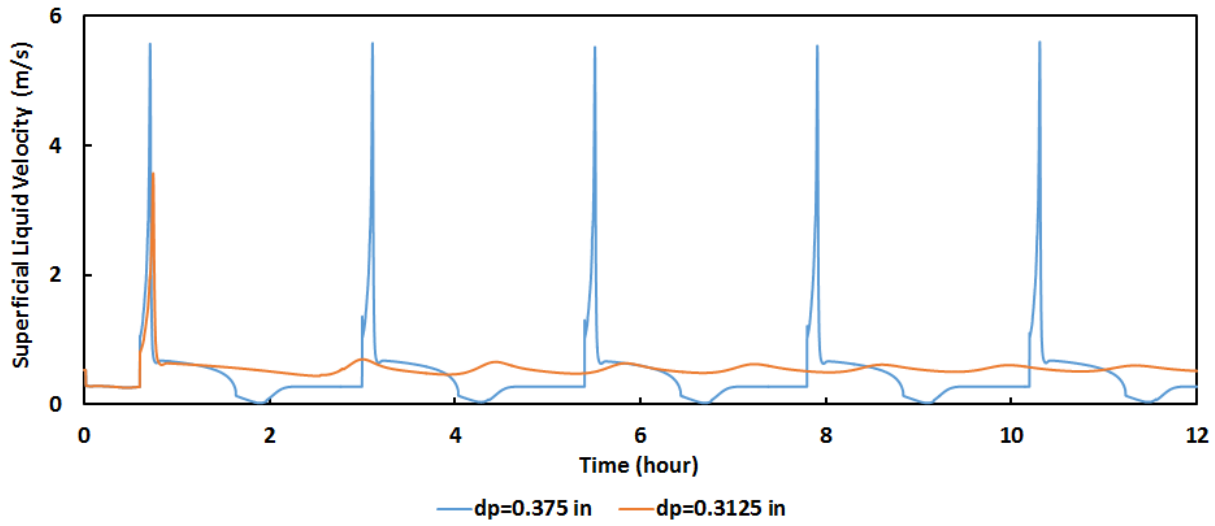

Figure 5-76: Effect of Gas-Lift Valve Port Size on Casing Heading Predicted by New Model for 100% WC

Smaller port size can slow down the high gas depletion in the annulus by limiting the flow through the gas-lift valve. However, a small port size also causes a high pressure-drop and increases operational cost due to the additional energy consumption. It can be observed that the flow becomes stable for all the water cuts with the smaller port diameter. This shows the significant effect of gas-lift valve size on gas-lift flow stability. Due to the flow restriction the decrease of gas-lift valve creates, the outlet flow rate decreases substantially for all the water cut cases. Although changing the gas-lift valve to achieve stable flow is one of the easiest approaches, one should still consider the loss in production as a determining factor.

5.7 Severe Slugging in Horizontal Wells

Severe slugging usually occurs in an offshore downward pipeline followed by an upward vertical riser system. The same geometry can be also found in an unconventional long horizontal well with downward inclined lateral. Horizontal wells are useful for thin-layered reservoirs and for scattered and isolated hydrocarbon pockets. The downward lateral, which is responsible for

the occurrence of severe slugging, could be designed on purpose or as in many cases due to the lack of sufficient drilling control. In the offshore pipeline-riser system, the large diameter of the pipeline over the sea floor and the relatively low pressure in the pipeline are the two primary conditions for severe slugging to happen. In horizontal wells, fast decline of production rate and the extended lateral length may lead to full or partial severe slugging. Partial severe slugging presents shorter slugs and cyclic duration in comparison to severe slugging. This makes the horizontal well a good option to mimic the slug evolution behavior. The objective of this section is to investigate physically the possibility of flow instabilities in unconventional wells and to test the new model for simulating slug evolution behavior.

5.7.1 Well Profile

A hypothetical extended reach horizontal well is used to demonstrate the occurrence of severe slugging. The well is simulated with both the new model and the OLGA simulator, and the results are compared. The source of the accumulated gas in the lateral during the severe slugging cycle is based solely on the solution gas, which comes out of the solution when the pressure drops below the bubble point pressure. The oil is chosen based on a high bubble point pressure to ensure that the gas starts to emerge out of the solution before entering the lateral to maximize the available length for the free gas to accumulate and expand. Based on this assumption, Vogel IPR is chosen to represent the two-phase flow model instead of linear IPR. The Vogel IPR is expressed by the form

$$\frac{q_o}{q_{o,\max}} = 1 - 0.2\left(\frac{p_{wf}}{\bar{p}_r}\right) - 0.8\left(\frac{p_{wf}}{\bar{p}_r}\right)^2, \tag{5-2}$$

where q_o is the oil flow rate in STB/D, $q_{o,max}$ is the maximum oil flow rate a well could

theoretically deliver at zero p_{wf} in STB/D, p_{wf} is the flowing pressure at the bottom of the wellbore in psia, and p_r is the average reservoir pressure in psia. The flow instabilities caused by severe slugging is relatively small and the reservoir only feels the time-average of the instabilities. Therefore, the reservoir transient effect is ignored. The geometry schematic of the well used in OLGA simulation is shown in Figure 5-77.

Figure 5-77: Geometry Schematic of the Unconventional Horizontal Well

As a base case, the vertical section of the well is 2000 m long. The downward-inclined section is 2500 m long with -3.8^o inclination angle. For simplicity, it is assumed that the tubing is lowered all the way to a few meters below the perforation instead of setting it in the vertical section. The remaining well data and reservoir characteristics are listed in Table 5-1.

Table 5-1: Well Data and Reservoir Characteristics of the Unconventional Horizontal Well

Vertical length (m)	2000	Average reservoir pressure (bara)	251
Lateral length (m)	2500	Gas-oil ratio (Sm^3/Sm^3)	150
Lateral Inclination (Deg)	-3.8	Maximum oil flow rate (m^3/d)	605
Vertical tubing inner diameter (m)	0.089	Reservoir temperature (K)	338.15
Lateral tubing inner diameter (m)	0.089	Gas specific gravity	0.65
Wellhead pressure (bara)	20	Oil specific gravity	0.85

5.7.2 Base Case Results

The results are presented first for the base case followed by different production setups in order to achieve the optimal scenario. The comparison between the new model and OLGA simulator are based on the outlet liquid and gas superficial velocities and the pressure at the bottom of the vertical section. The pressure behavior at the bottom of the vertical section, the outlet liquid superficial velocity, and the outlet gas superficial velocity for the base case are shown in Figures 5-78, 5-79, 5-80, respectively.

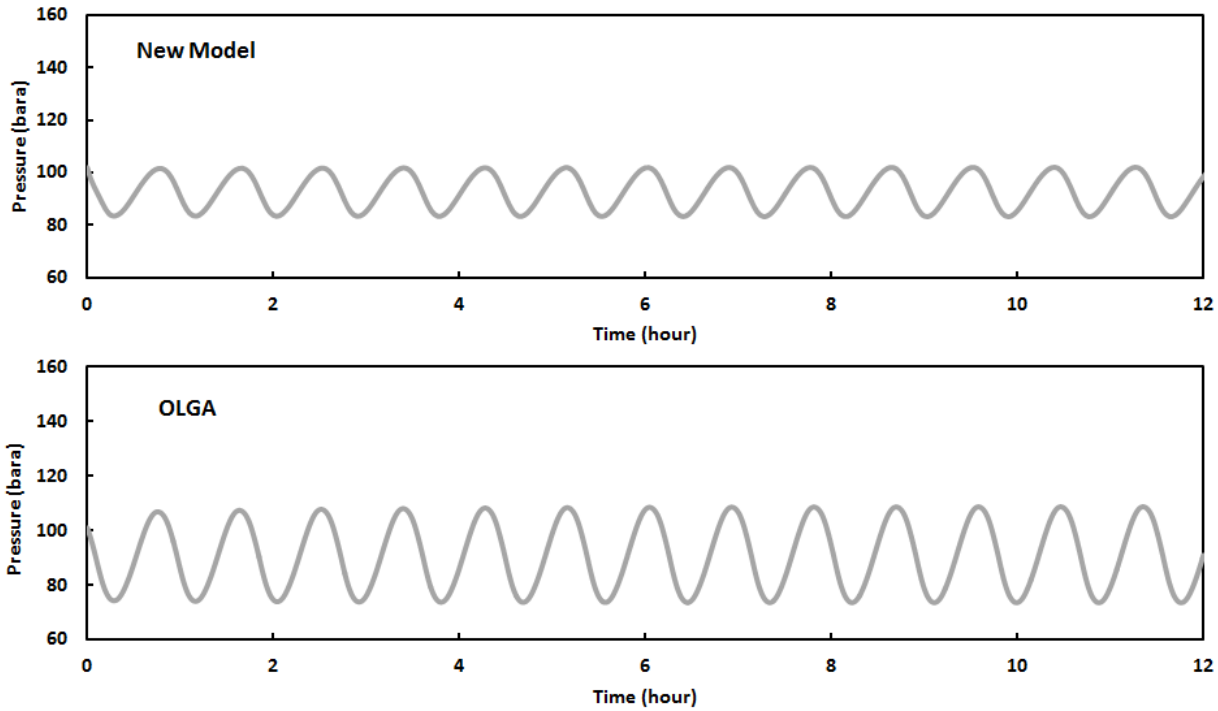

Figure 5-78: Severe Slugging in Horizontal Well, Bottom Pressure Behavior Comparison with OLGA for the Base Case

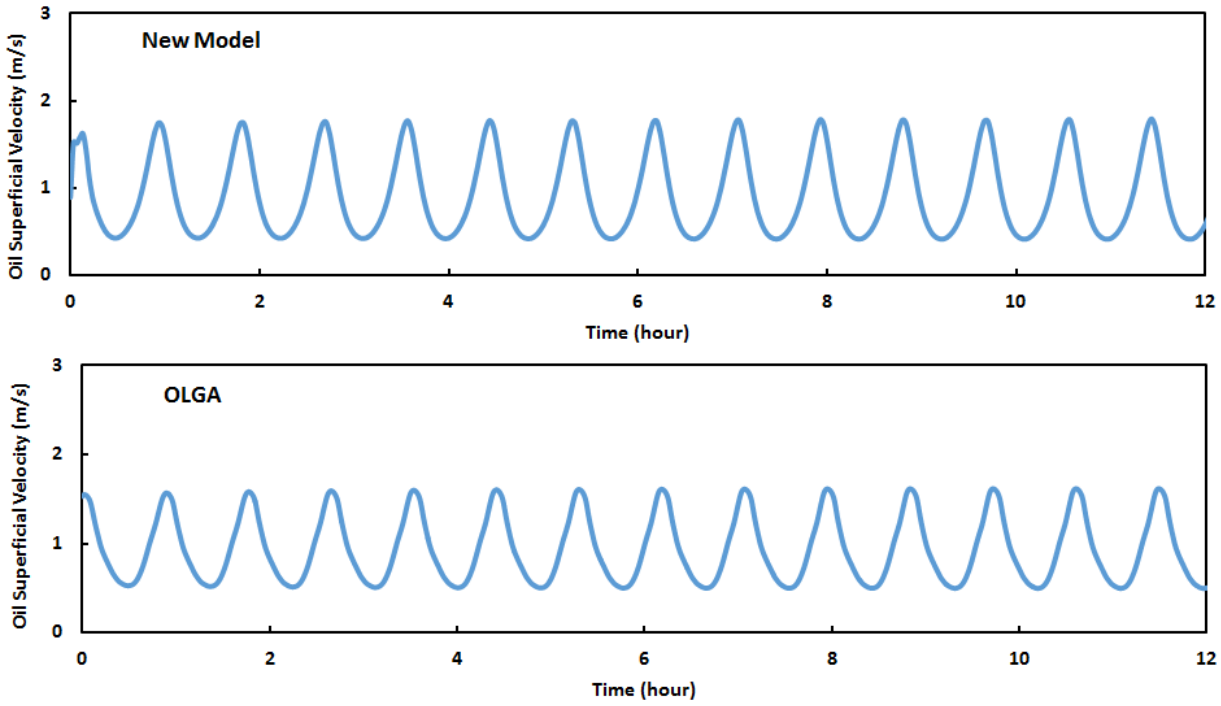

Figure 5-79: Severe Slugging in Horizontal Well, Outlet Oil Superficial Velocity Comparison with OLGA for the Base Case

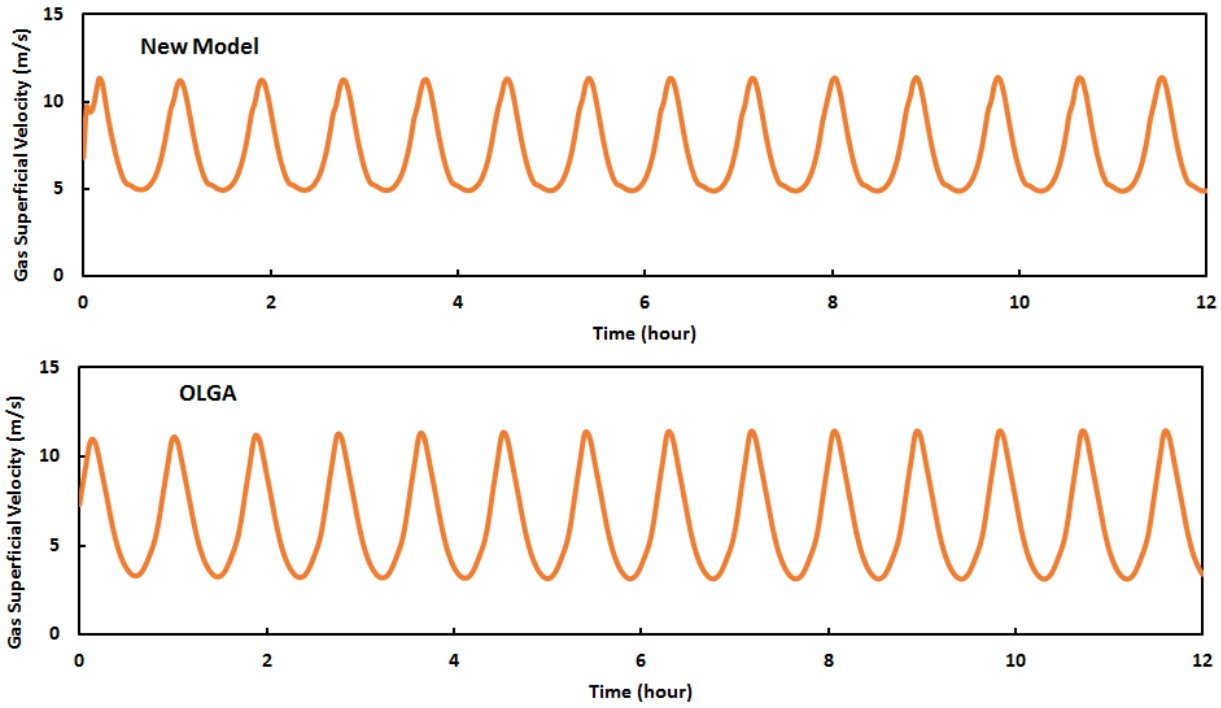

Figure 5-80: Severe Slugging in Horizontal Well, Outlet Gas Superficial Velocity Comparison with OLGA for the Base Case

Both the new model and OLGA display unsteady behavior. They agree well on the slugging frequency and the outlet superficial velocities. However, the pressure fluctuation amplitude predicted by the new model is considerably lower than that obtained from OLGA simulation. Figure 5-78 shows the pressure changes at the lowest point in the wellbore. The fluctuation is corresponding to the accumulation of the liquid after the elbow and the evolution of slug flow confirming the partial severe slugging behavior. The liquid and gas at the wellhead also exhibit significant oscillations associated with the long slug length. Due to the long vertical section and inclined lateral, the period of the severe slugging takes approximately 54 minutes while the pressure amplitude is about 20 bara (from the new model). This large and slow slugging can reduce the efficiency of the surface facility and cause severe operational problems. Moreover, for downhole pumps such as ESP, the high amount of gas during the severe slugging cycle may create a gas lock and lead to pump failure. In a small experimental facility, such as the one explained earlier, the liquid penetrates the pipeline during the slug formation stage while rising in the upward section. The slug production stage plays an important role in controlling the severe slugging cycle. In horizontal well with severe slugging, the liquid falls back, accumulates at the lower point, and is picked up by gas in the form of a slug. The compressed gas penetrates the liquid continuously and therefore the slug production and gas blowout stages are skipped. The severe slugging in horizontal wells is relatively new to the petroleum industry. In the following section, various production setups are tested in order to analyze and understand the phenomenon.

5.7.3 Stability Analysis

The well behavior predictions are useful during the design stage to avoid the undesirable instability. If the well is already drilled, interferences sometimes are economically unfeasible. However, if the severity of the flow leads to well abandonment, expensive adjustment to the well design becomes justifiable. Different scenarios are simulated in this section which may be used to rectify the problem and revive the well. If the diameter of the tubing is decreased, the velocities of the gas and liquid increase, which in turn reduces the tendency of liquid accumulation. The flow pattern in the well lateral may also change from stratified to slug flow making the severe slugging less pronounced. First, the tubing ID is decreased from 0.089 m (3.5 in) to 0.06 m (2.375 in) in both the new model and OLGA simulations and the results are compared. The pressure behavior, the outlet liquid superficial velocity, and the outlet gas superficial velocity for the decreased diameter are expressed in Figures 5-81, 5-82 and 5-83, respectively.

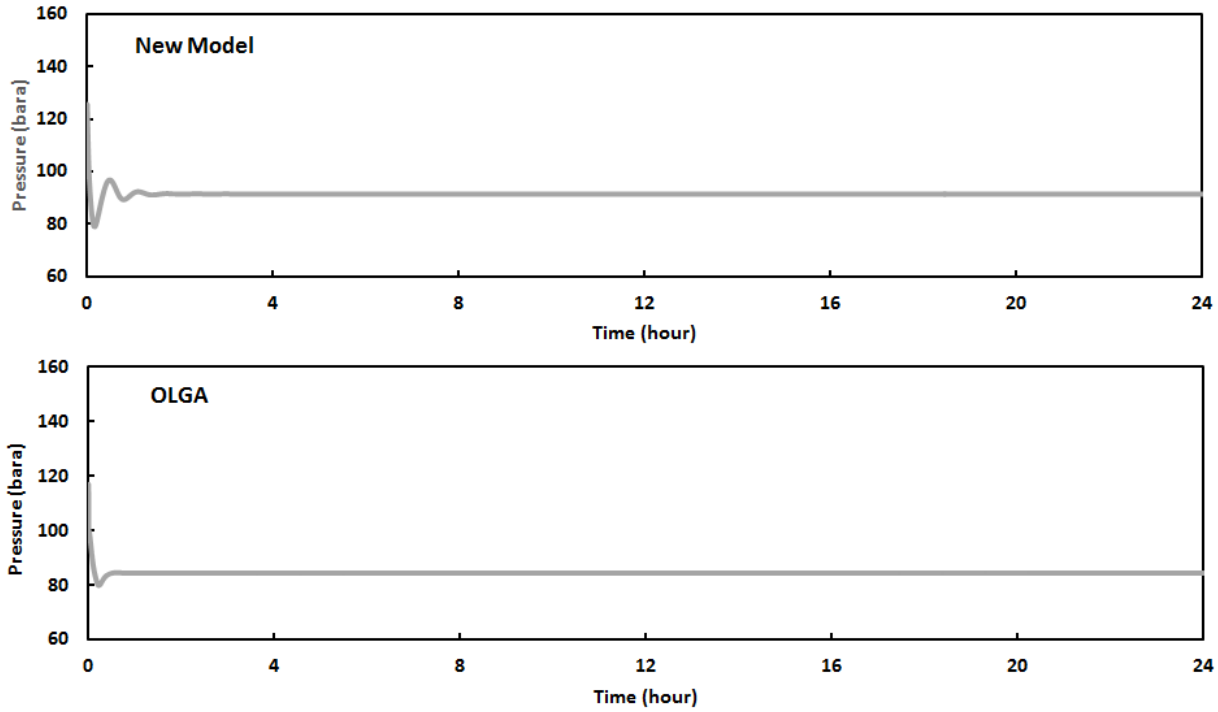

Figure 5-81: Severe Slugging in Horizontal Well, Bottom Pressure Behavior Comparison with OLGA for 0.06 m Tubing Diameter

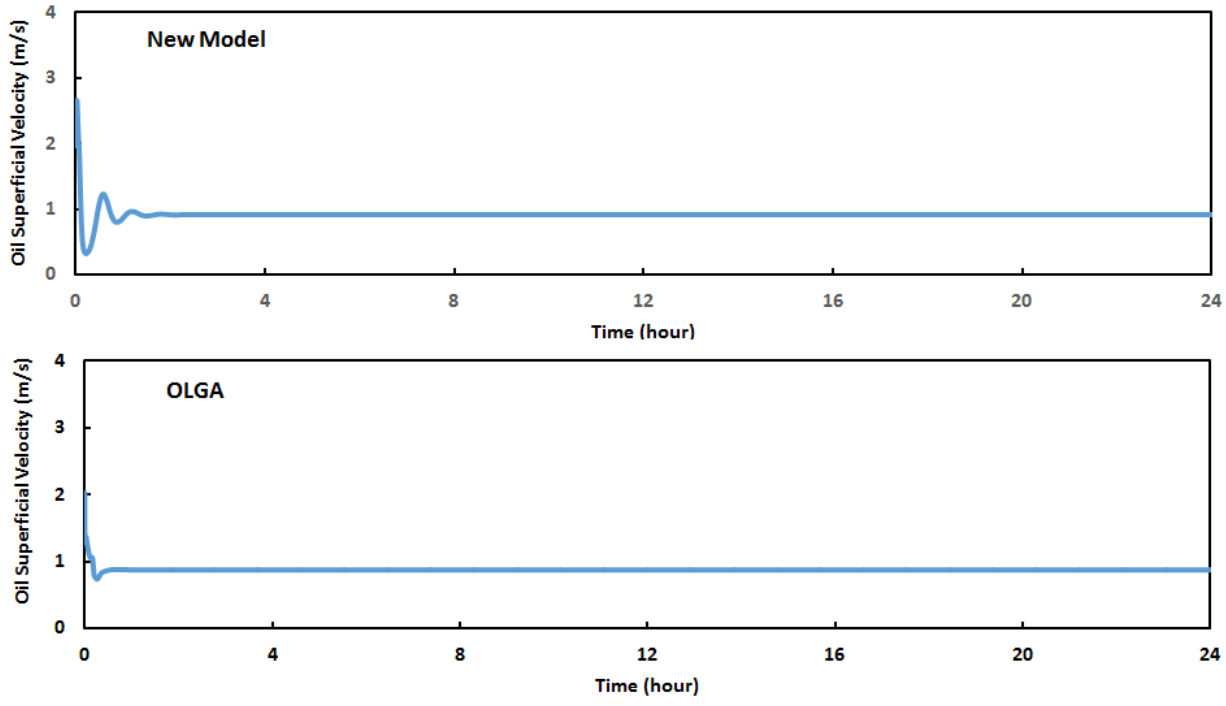

Figure 5-82: Severe Slugging in Horizontal Well, Outlet Oil Superficial Velocity Comparison with OLGA for 0.06 m Tubing Diameter

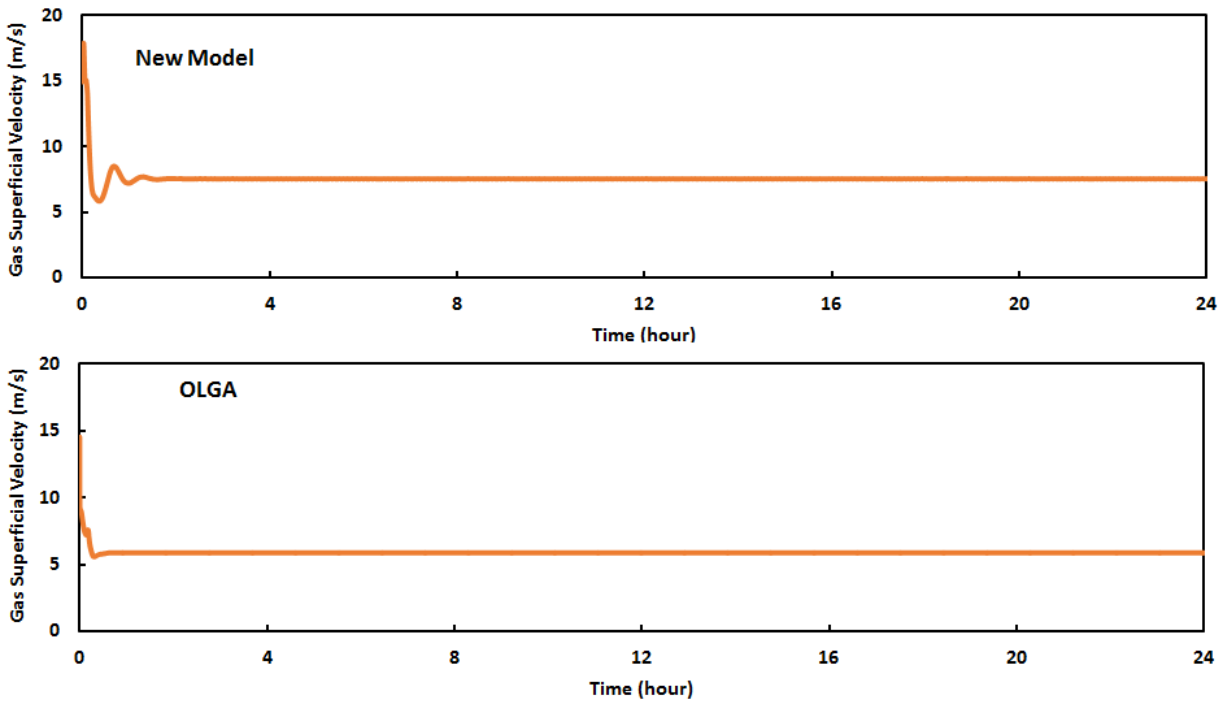

Figure 5-83: Severe Slugging in Horizontal Well, Outlet Gas Superficial Velocity Comparison with OLGA for 0.06 m Tubing Diameter

The new model and OLGA both predict stable flow. The new model gives a lower pressure at the bottom of the vertical section while agreeing very well with OLGA on the outlet velocities. The outlet superficial velocities increase substantially due to the decrease in the tubing diameter. The pressure, on the other hand, increases due to higher frictional pressure gradient.

Because the severe slugging primarily occurs due to the downward inclined lateral followed by the elbow, decreasing the lateral diameter alone is better economically and might solve the problem. The increase in liquid and gas velocities due to the decrease in lateral diameter creates high sweeping energy and therefore overcomes the liquid accumulation. Then the lateral tubing ID is decreased from 0.089 m (3.5 in) to 0.06 m (2.375 in) while keeping the tubing ID in the vertical section as 0.089 m. The pressure behavior, the outlet liquid superficial velocity, and the outlet gas superficial velocity are shown in Figures 5-84, 5-85 and 5-86, respectively.

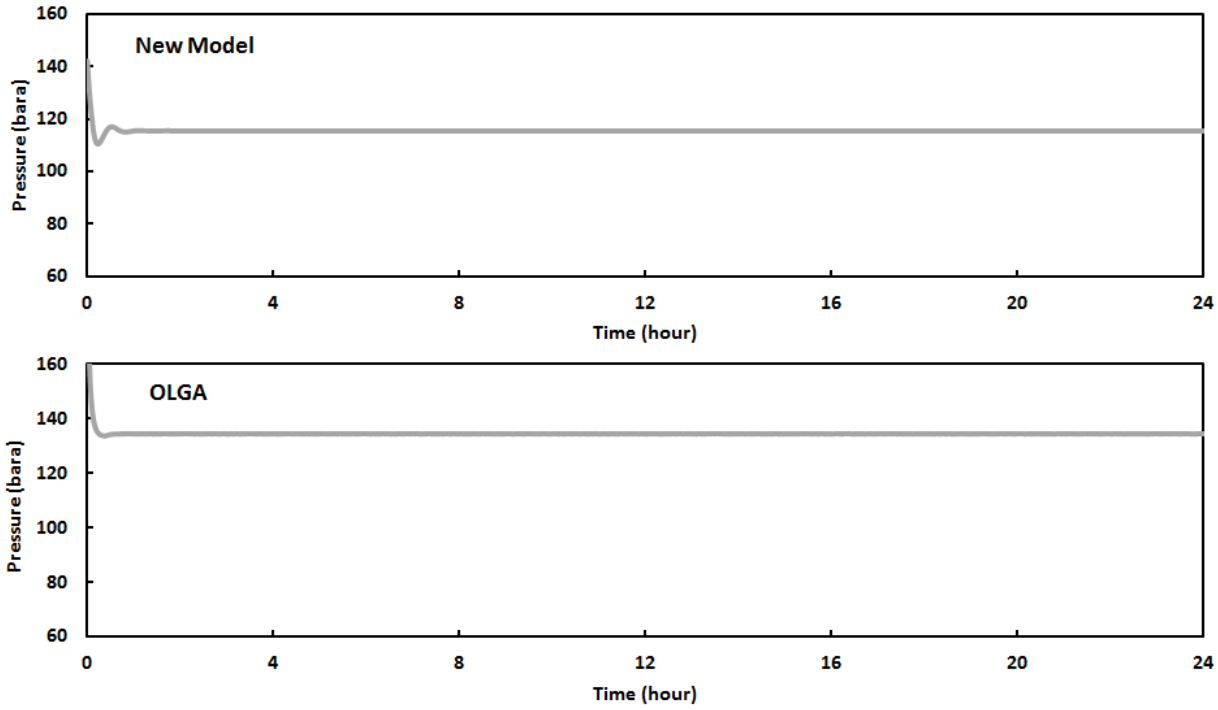

Figure 5-84: Severe Slugging in Horizontal Well, Bottom Pressure Behavior Comparison with OLGA for 0.089 m Vertical Tubing Diameter and 0.06 m Lateral Diameter

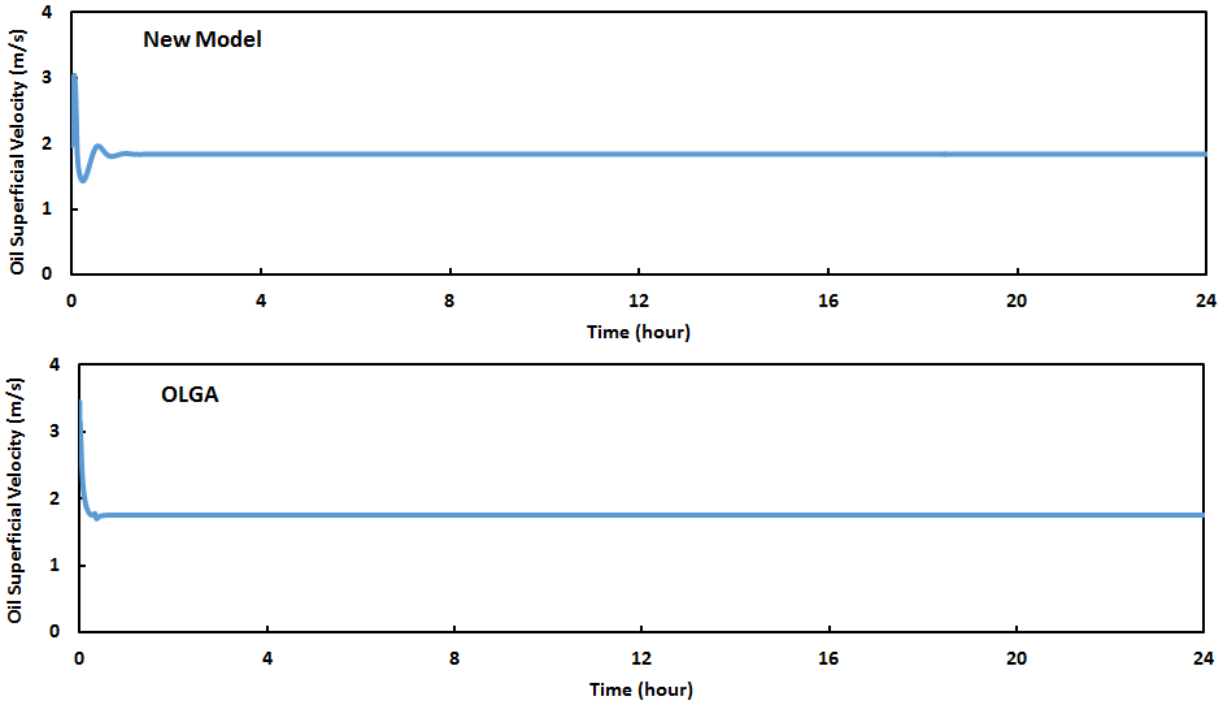

Figure 5-85: Severe Slugging in Horizontal Well, Outlet Oil Superficial Velocity Comparison with OLGA for 0.089 m Vertical Tubing Diameter and 0.06 m Lateral Diameter

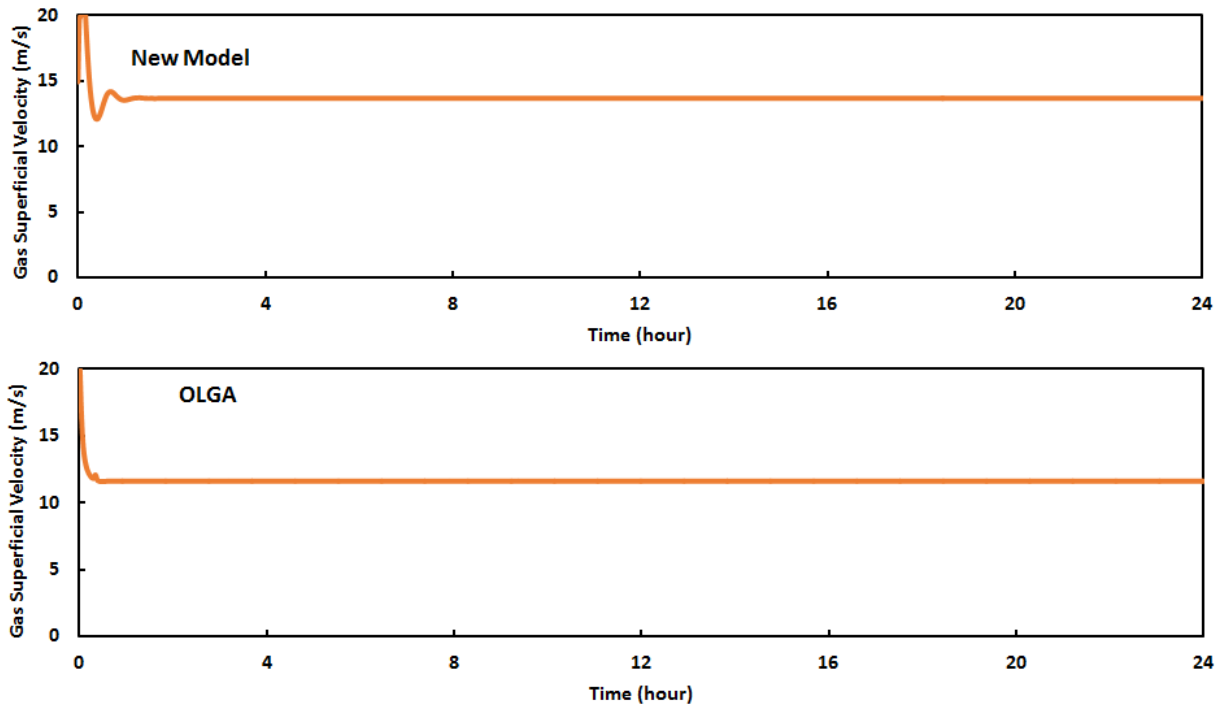

Figure 5-86: Severe Slugging in Horizontal Well, Outlet Gas Superficial Velocity Comparison with OLGA for 0.089 m Vertical Tubing Diameter and 0.06 m Lateral Diameter

The prediction results of both models show stable flow with significant decrease in bottom pressure. This solution is more practical and cost effective since only approximately half of the tubing needs to be replaced.

If the inflow performance is improved, the liquid and gas flow rates increase and, therefore, the severe slugging may be eliminated. The productivity index represented by the maximum oil flow rate for this two-phase flow well is the main factor in this stability control. For some wells, the inflow performance can be improved simply by stimulation jobs. Injecting an acid into the formation can reduce the skin, improve the damaged formation across the perforation, and as a result increase the inflow performance. Simulations are carried out with the maximum oil flow rate increase from 3800 STB/D to 4200 STB/D. The bottom pressure behavior, the outlet liquid superficial velocity, and the outlet gas superficial velocity are shown in Figures 5-87, 5-88 and 5-89, respectively.

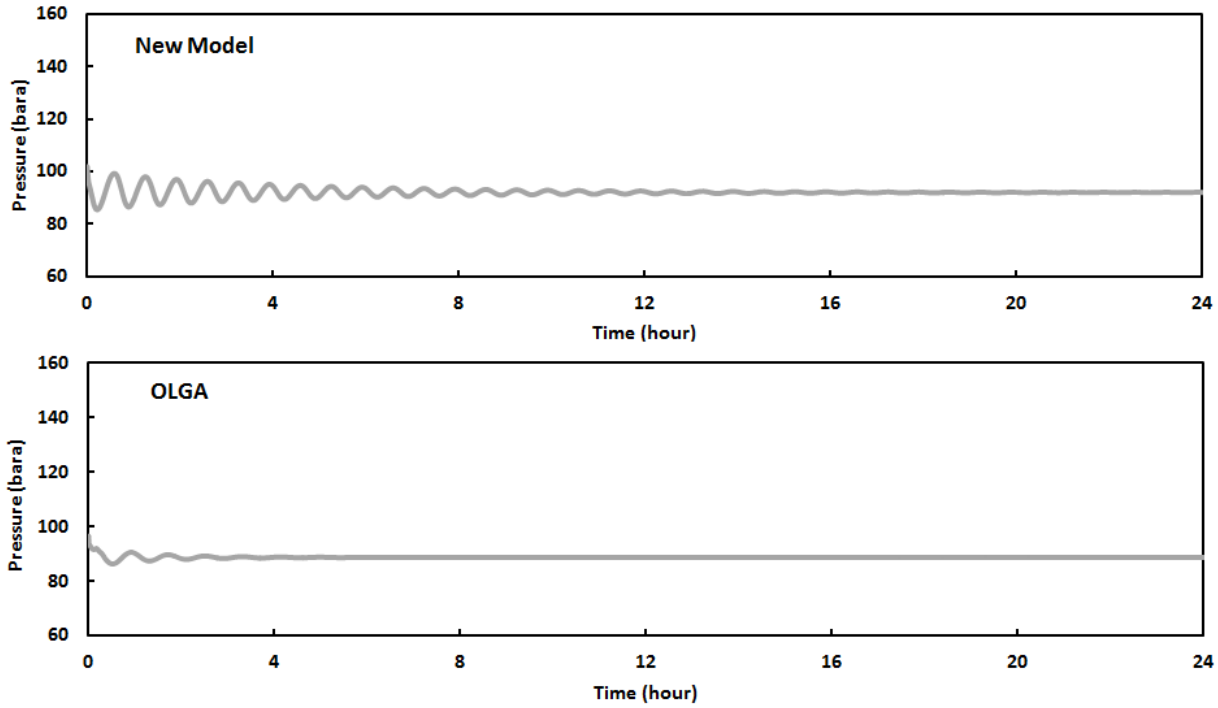

Figure 5-87: Severe Slugging in Horizontal Well, Bottom Pressure Behavior Comparison with OLGA for 4200 STB/D Maximum Oil Flow Rate

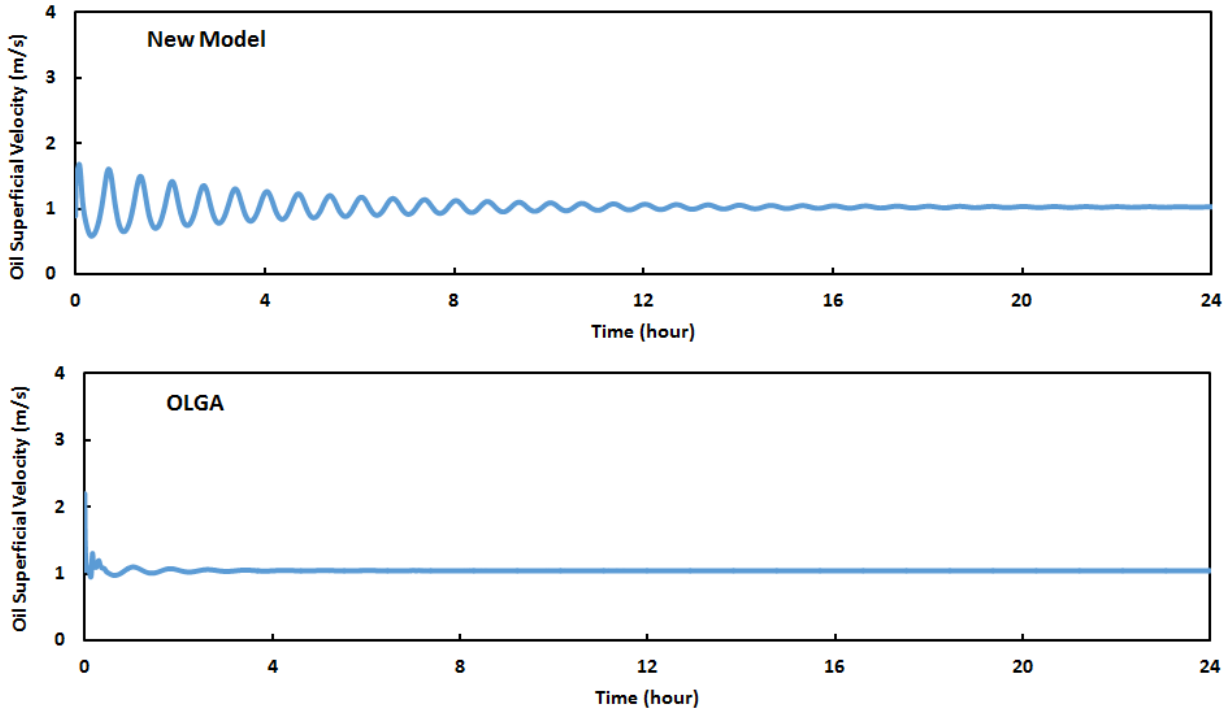

Figure 5-88: Severe Slugging in Horizontal Well, Outlet Oil Superficial Velocity Comparison with OLGA for 4200 STB/D Maximum Oil Flow Rate

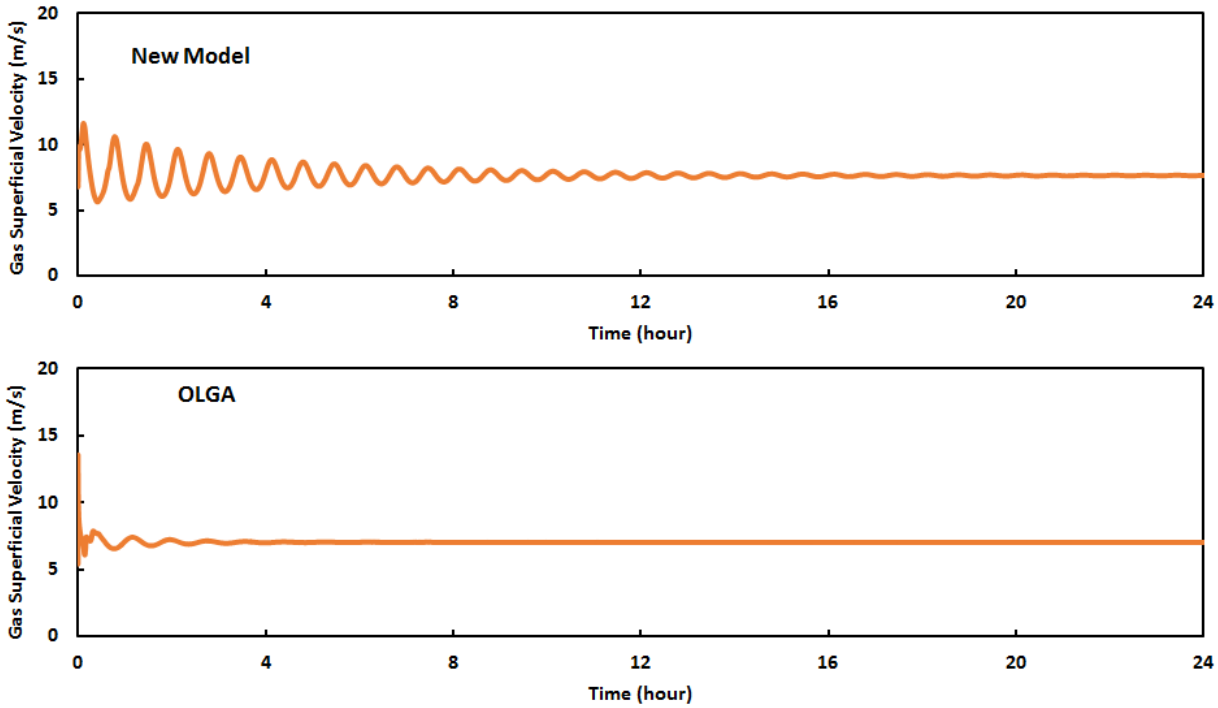

Figure 5-89: Severe Slugging in Horizontal Well, Outlet Gas Superficial Velocity Comparison with OLGA for 4200 STB/D Maximum Oil Flow Rate

The simulation results from the new model and OLGA show that a stable flow is also achievable if the reservoir performance is improved. In gas-lift operation, the casing heading can also be avoided by improving the productivity index. However, more practical and less expensive methods such as increasing the surface gas injection rate or decreasing the gas-lift port size are usually used. The stability controls for horizontal wells with severe slugging are limited, and the reservoir intervention if possible is a good option.

It is a common practice to drill further than the pay zone. This extra length is useful for running some types of lengthy logging tools and to avoid blocking the perforation interval in case a stuck tool is to be cut and dropped to the bottom. Moreover, it can also be used as a future contingency if the perforation interval needs to be changed without the need for expensive well re-entry and extension drilling. When the lateral length increases, the gas gets extra volume to pressurize and decompress which leads to a severe slugging cycle. It is also possible that a stable

horizontal well becomes unstable and behaves in fluctuation form if deeper perforation interval is needed and extension drilling is performed. In the next case, the lateral length is increased from 2500 m to 3000 m and the results are analyzed. The bottom pressure behavior, the outlet liquid superficial velocity, and the outlet gas superficial velocity for the increased lateral length are shown in Figures 5-90, 5-91 and 5-92, respectively.

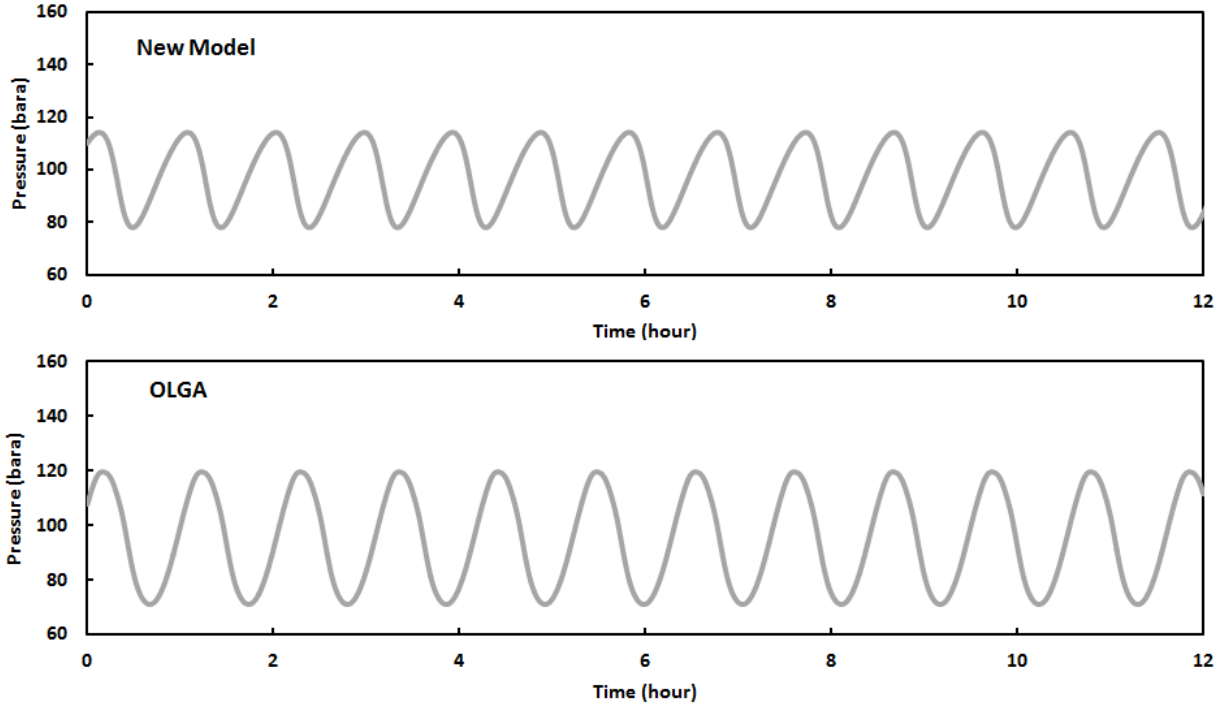

Figure 5-90: Severe Slugging in Horizontal Well, Bottom Pressure Behavior Comparison with OLGA for 3000 m Lateral Section Length

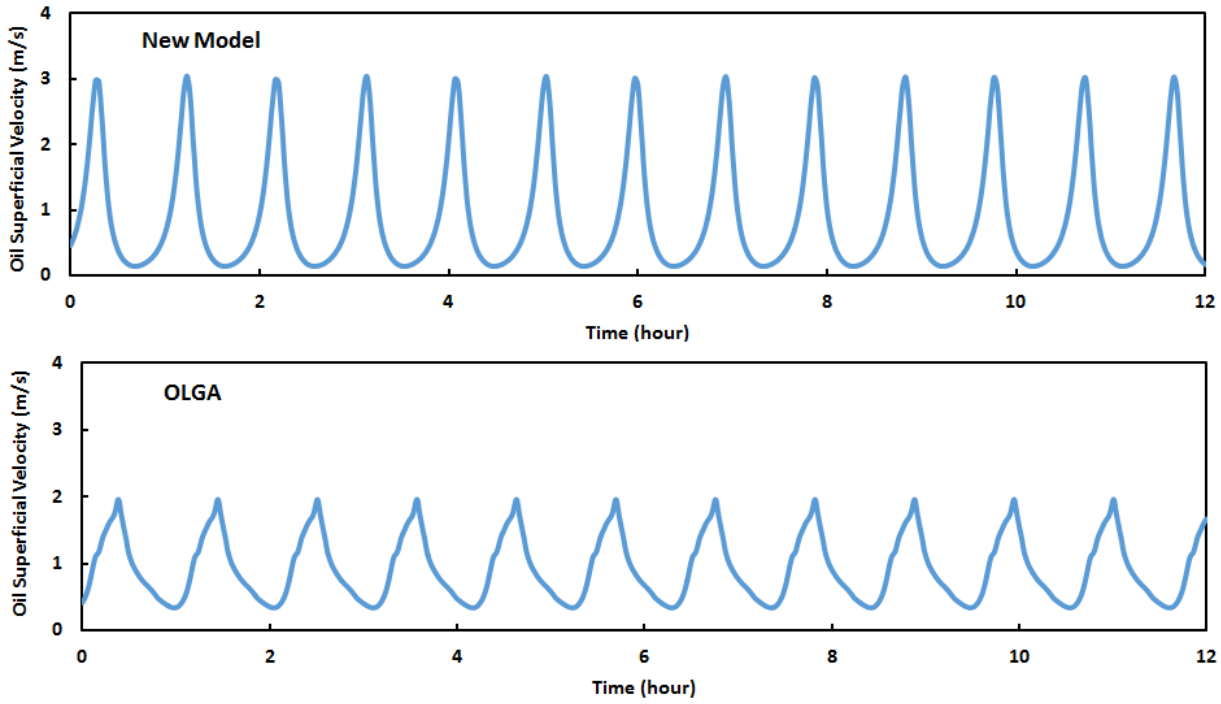

Figure 5-91: Severe Slugging in Horizontal Well, Outlet Oil Superficial Velocity Comparison with OLGA for 3000 m Lateral Section Length

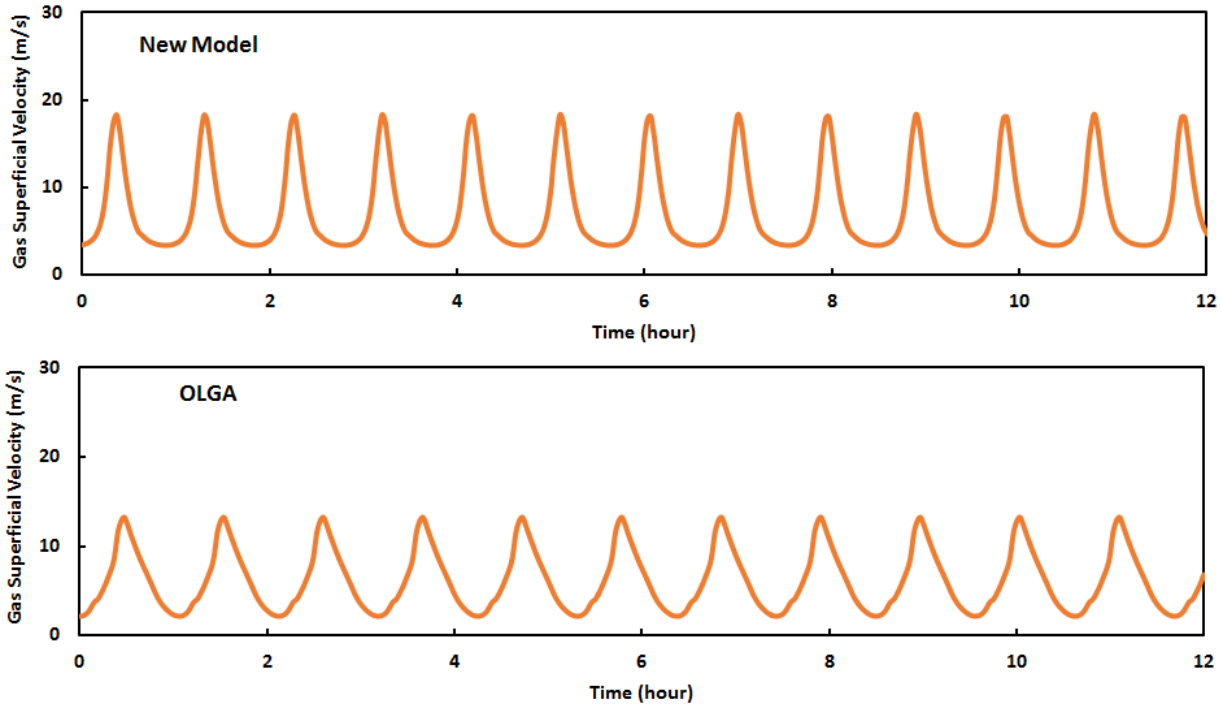

Figure 5-92: Severe Slugging in Horizontal Well, Outlet Gas Superficial Velocity Comparison with OLGA for 3000 m Lateral Section Length

The new model predicts slightly higher outlet velocities while both predict a longer severe slugging cycle compared with the base case. The higher gas superficial velocity predicted by the new model results in increased severity and minimum liquid velocity but does not yet lead to liquid fallback. Moreover, the high gas blowout may not only create severe slugging behavior but also generate large gas pockets that affect the surface separators and downhole pumps.

Decreasing the lateral section length becomes the logical option to be tested now. In some cases, when the lateral section is of an unnecessary length, it can be decreased by cement plugs. Moreover, cement plugs are useful if the perforation interval is changed and becomes closer to the wellbore. For the next case, the lateral section length is decreased from 2500 m to 2000 m keeping all the other inputs fixed. The bottom pressure behavior, the outlet liquid superficial velocity, and the outlet gas superficial velocity for the decreased lateral length are shown in Figures 5-93, 5-94, 5-95, respectively.

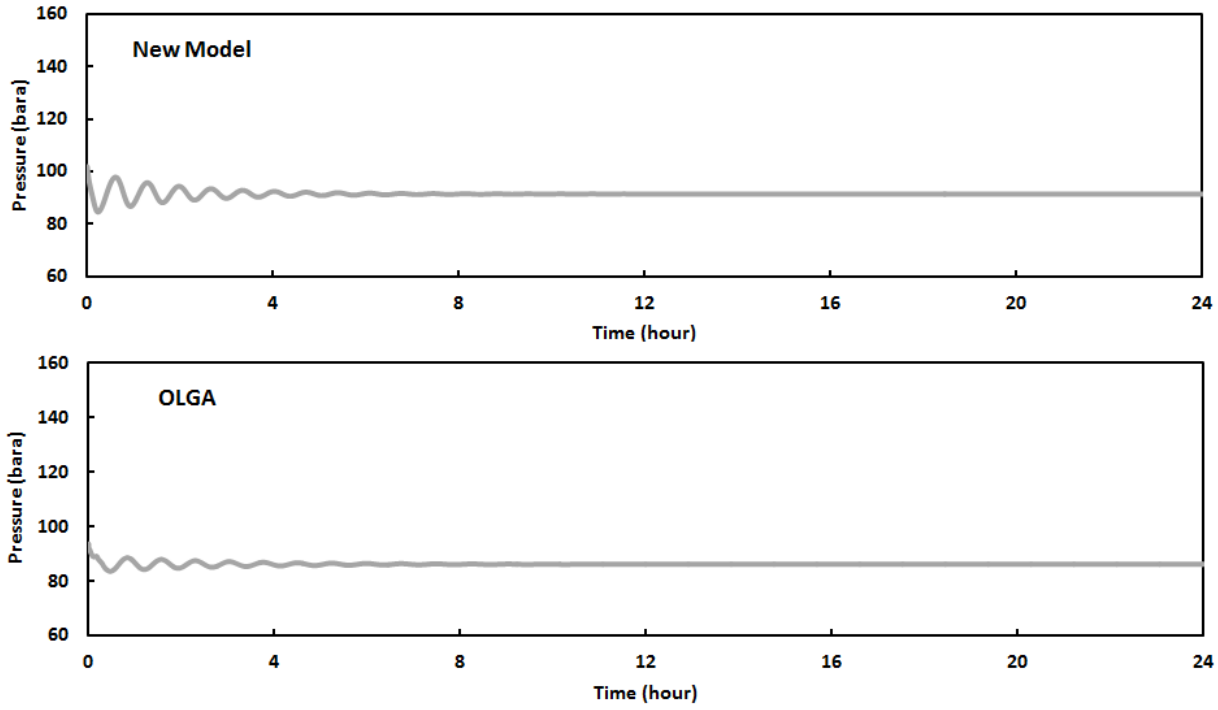

Figure 5-93: Severe Slugging in Horizontal Well, Bottom Pressure Behavior Comparison with OLGA for 2000 m Lateral Section Length

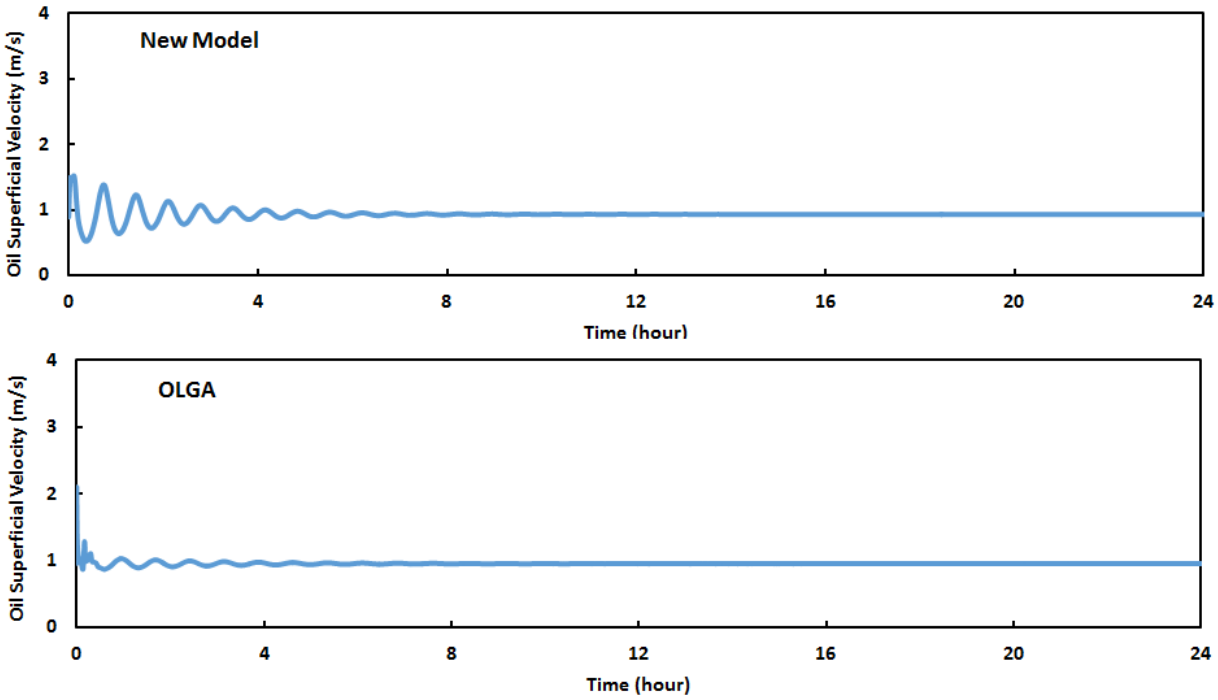

Figure 5-94: Severe Slugging in Horizontal Well, Outlet Oil Superficial Velocity Comparison with OLGA for 2000 m Lateral Section Length

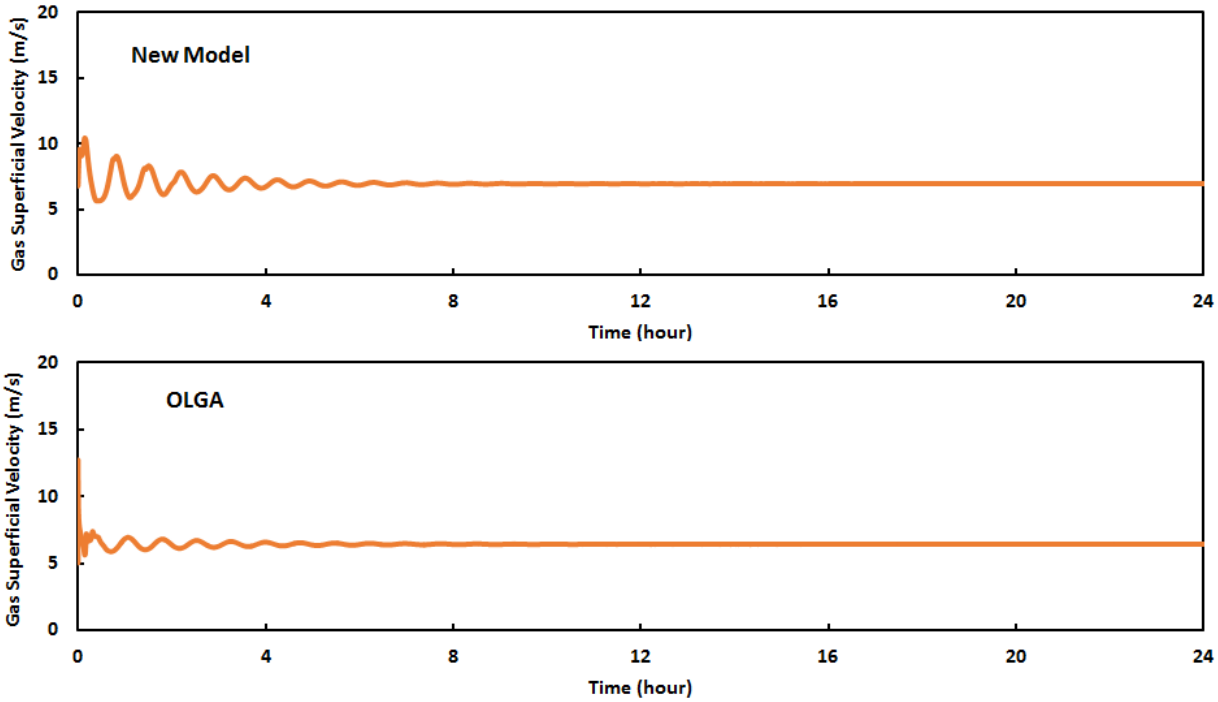

Figure 5-95: Severe Slugging in Horizontal Well, Outlet Gas Superficial Velocity Comparison with OLGA for 2000 m Lateral Section Length

The new model and OLGA simulation results predict stable flow and both agree well for all the calculated variables. All the stabilization techniques show effective results. Downhole well intervention is expensive and not always operationally feasible. Therefore, in real-world operation, the decision of the best stabilization technique is highly limited.

CHAPTER 6

CONCLUSIONS AND RECOMMENDATIONS

6.1 Conclusions

The objectives of this study on theoretical, numerical, and programming levels have been successfully met. A summary is presented below while the detailed conclusions are provided in the following sub-sections:

- In three-phase flow when the two liquids are separated, the two-phase models cannot be used and the new flow patterns must be considered. A new transient mechanistic model is developed based on mass and momentum conservation equations.
- A new numerical algorithm for solving the system of partial differential equations is presented and it shows a wide range of stability.
- The model is comprehensive and can be used to predict different steady-state and transient multiphase pipe flow behaviors. The model can also be used to generate detailed flow pattern maps for three-phase flow.
- The new transient model is verified with large-scale experimental results and commercial software simulations of commonly occurring transient phenomena and good agreement is observed.

6.1.1 Model Development

- Flow patterns are identified for three-phase pipe flows in horizontal and inclined pipelines. This study focuses on the most dominant and frequent flow patterns—three-

layer stratified flow, slug flow with stratified film and slug, and slug flow with stratified film and mixed slug.

- Use of three-fluid model instead of fully mixed or a drift-flux approximation especially for horizontal pipeline flow when all the phases are separated allows consideration of more physics which provides better predictions.
- In the new model, the slug unit is implemented by connecting the gas pocket and slug body regions using mass and momentum exchanges.
- Several steady-state closure relationships are replaced with transient conservation equations such as continuity and average holdup in the slug unit. This increases the number of variables with higher complexity, for capturing the transient behavior.

6.1.2 Numerical Scheme and Solution Algorithms

- The mass and momentum conservation equations are discretized using implicit finite difference schemes for better convergence and stability.
- The implicit solution allows the use of large time steps that make it economical to simulate deep wells and long pipelines.
- The stability of the implicit algorithm ensures the consideration of complex flow patterns without unnecessary simplifications.

6.1.3 Flow Pattern Transitions and Flow Pattern Maps

- Three-phase flow pattern maps were constructed based on gas-liquid flow pattern transitions and the oil and water mixing status. The flow pattern maps are useful for operating the flow within a safe margin if a specific flow pattern is required.

- At low water cut, the increase of water cut promotes stratification due to the extra energy required for the oil to disperse the water. The three-layer stratified flow and the slug flow with stratified film and slug become the dominant flow regimes instead of the stratified flow with fully mixed oil and water and slug flow with fully mixed oil and water.
- At high water cut, the water tendency to disperse the oil increases and expands the stratified flow with fully mixed oil and water. Moreover, the tendency for the liquid to disperse the gas reduces the stratified margin and increases the tendency of the slug flow.
- The slug flow with stratified film and mixed slug appears only for 40% water cut in a small area. This is because the turbulent energy in the slug body is higher than that in the liquid film of the gas pocket region.
- The criterion for predicting the mixing status between oil and water is based on a previous model that uses the maximum droplet size generated under local flow conditions as a benchmark. The model is modified to accommodate the presence of separated gas layer that affects the dispersion process by altering the liquid film holdup and velocity.

6.1.4 Steady State Perturbation and Sensitivity Analysis

- If the flow pattern is changed during the steady-state perturbation, the time it takes for stabilization may overcome the effect of the gravitational forces associated with the increase in inclination angle.
- The increase in cell length causes longer stabilization time in OLGA simulations but has less effect in the new model simulation.
- Increasing the time step does not affect the stabilization and cyclic period if they are within the CFL limit in both the new model and OLGA simulations.

6.1.5 Severe Slugging in Pipeline-Riser System

- The performance of the new model to simulate severe slugging phenomenon for three-phase flow has been confirmed through comparison with Beltran's (2005) experimental works, and the effects of water cut and the downward inclination angle are investigated.
- In severe slugging, increasing the gas superficial velocity can stabilize the flow. Before reaching the fully stable flow status, shorter severe slugging cycles, less pressure fluctuation at the bottom of the riser and the disappearances of slug production and gas blowout stages are observed.
- Since severe slugging only occurs when the flow pattern in the pipeline is stratified, using the new model of three-layer stratified flow instead of two-phase approximation gives better accuracy.
- The increase in water cut and pipeline downward inclination angle in severe slugging increases the time needed for the compressed gas to overcome the heavier liquid column in the riser and therefore leads to longer cycle.
- During the slug formation stage in three-phase severe slugging, the oil and water are separated in the riser and therefore the use of two-phase mixture approximation causes bigger error in results.
- The coexistence of oil and water in severe slugging occurrence in a pipeline-riser system creates a unique flow behavior. During slug formation and production stages, water may partially or fully block the oil in the pipeline creating higher water fraction in the riser and at the same time the oil in the riser segregates from the water. When the trapped oil in the pipeline is pushed through the bottom of the riser, liquid-liquid slugging is observed before the gas blowout stage.

6.1.6 Gas-Lift Instability Analysis

- The gas-lift casing heading process and its characteristics are analyzed with the new transient model and different optimization techniques are evaluated. Increasing the gas injection rate and decreasing the port size of the gas-lift valve are shown to be effective techniques for stabilizing the gas-lift instabilities.
- Increase of water cut in three-phase gas-lift casing heading increases the required gas injection rate for stable flow to overcome the heavier fluid in the tubing.
- Smaller gas-lift valve port size has a significant impact on well stability since it can suppress high gas oscillations. However, a small port size also causes a high pressure drop, resulting in a higher bottom hole pressure and a lower production rate.

6.1.7 Severe Slugging in Horizontal Wells

- Severe slugging that occurs in an offshore pipeline-riser system can also occur in an unconventional long horizontal well system. Although the slug production and severe gas blowout stages are absent, significant fluctuations of liquid and gas flow rates at the wellhead are generated due to the great length of the slug unit.
- Reducing the lateral tubing diameter, shortening the lateral section length, and improving the inflow performance are demonstrated to be good rectifying techniques for severe slugging in horizontal wells.

6.2 Recommendations

Below are several recommendations for further development of the model and validation.

- More experimental work and field data could be used for further model validations.

- Other elimination techniques for severe slugging such as gas lifting or choking and for gas-lift casing heading such as modified gas-lift valves can be tested.
- Most of the current simulators including this study assume constant wellhead pressure while in reality the pressure is fluctuating with the flow rates. The models in the literature for calculating the pressure drop at the surface valve for two-phase flow are outdated and need to be improved.
- This study considers the extreme cases of fully separated or fully dispersed oil and water. The partial dispersion that occurs during the transition needs to be considered.
- The new model in this study can be extended to accommodate the transient flow in pipeline networking.

NOMENCLATURE

English Letters

Symbol	Description
A	area
C_e	coefficient
d	pipe diameter
d	hydraulic diameter
d_{CB}	critical bubble diameter based on gravity and turbulent forces
d_{CD}	critical bubble diameter above which bubbles start to coalesce
d_{MAX}	maximum droplet diameter
F_E	liquid entrainment fraction
f	friction factor
f_O	oil fraction
f_W	water fraction
G_G	gas mass source
G_O	oil mass source
G_W	water mass source
g	gravity acceleration
H	holdup
H_{LC}	liquid holdup in gas core
H_{LS}	slug liquid holdup

H_{OC}	oil holdup in gas core
H_{WC}	water holdup in gas core
H_{WGS}	water holdup with entrapped gas in slug body
j	the sequence number of mesh cell
l	length
l	liquid
N_{Re}	Reynolds number
n	the sequence number of time step
p	pressure
p_r	average reservoir pressure
p_{wf}	flowing pressure at the bottom of the wellbore
q_o	oil flow rate
$q_{o,\max}$	maximum oil flow rate a well could theoretically deliver at zero p_{wf}
R_{FU}	film to slug unit length ratio
S	perimeter
t	time
v	velocity
v_D	drift velocity of gas bubbles
v_{SG}	superficial gas velocity
v_{SL}	superficial liquid velocity
v_{SO}	superficial oil velocity
v_{SW}	superficial water velocity
v_T	slug transitional velocity

W	mass flow rate
z	position

Greek Letters

Symbol	Description
α	gas-volume fraction in liquid of slug body, void fraction
ε	energy dissipation per unit mass
ϕ	volumetric phase fraction
θ	inclination angle from horizontal
μ	viscosity
ρ	density
σ	surface tension
τ	shear stress
Θ	wetted wall fraction

Subscripts

Symbol	Description
C	gas core, continuous
D	dispersed
F	liquid film
G	gas
I	interface, inversion
$I0$	oil-water interface in slug body of slug flow

I1	gas-oil interface in film region of slug flow
I2	oil-water interface in film region of slug flow
Int	internal
L	liquid
M	mixture
O	oil
OF	oil film
OS	oil phase in slug body
OW	oil-water
p	pipe
S	slug
U	slug unit
W	water
WF	water film
WS	water phase in slug body

BIBLIOGRAPHY

1. Açikgöz, M., França, F., and Laher Jr, R.T., 1992, "An Experimental Study of Three-Phase Flow Regimes," *Int. J. Multiphase Flow* **18** (3): 327.
2. Almudairis, F.B.A., 2014, "Modeling of Transient Operations and Instabilities in Gas Lift," M.S. Thesis, U. of Tulsa, Tulsa, OK.
3. Andritsos, N., and Hanratty, T.J., 1987, "Influence of interfacial waves in stratified gas-liquid flows," *AIChE J.*, **33** (3): 444-454.
4. Barnea, D., Shoham, O., and Taitel, Y., 1982, "Flow Pattern Transition for Vertical Downward Two-Phase Flow," *Chem. Eng. Sci.*, **37** (5): 741-746.
5. Beltran, C., 2005, "Severe Slugging Prediction for Gas-Oil-Water Flow in Pipeline-Riser Systems," M.S. Thesis, U. of Tulsa, Tulsa, OK.
6. Bendiksen, K.H., Malnes, D., Moe, R., and Nuland, S., 1991, "The Dynamic Two-Fluid Model OLGA: Theory and Application," *SPE Prod. Eng.* **6** (2): 171-180.
7. Bonizzi, M. and Issa, R. I., 2003, "On the Simulation of Three-Phase Slug Flow in Near Horizontal Pipes Using the Multi-Fluid Model," *Int. J. Multiphase Flow*, **29**: 1719–1747.
8. Brauner N., 2001, "The Prediction of Dispersed Flows Boundaries in Liquid-Liquid and Gas-Liquid Systems," *Int. J. Multiphase Flow*, **27** (5): 911-928.
9. Brauner, N., and Ullmann, A., 2002, "Modeling of Phase Inversion Phenomenon in Two-Phase Pipe Flows," *Int. J. Multiphase Flow*, **28**: 1177-1204.
10. Brinkman, H.C., 1952, "The Viscosity of Concentrated Suspensions and Solutions," *Journal of Chemical Physics*, **20** (4): 571.

11. Brodkey, R.S., 1967, "The Phenomena of Fluid Motions," Addison-Wesley Publishing Company, Massachusetts.
12. Courant R., Friedrichs, K., and Lewy, H., 1967, "On the partial difference equations of mathematical physics," *IBM J.*, **11** (2): 215- 234.
13. Fan, Y., 2005, "An investigation of low liquid loading gas-liquid stratified flow in near-horizontal pipes," Ph.D. Dissertation, U. of Tulsa, Tulsa, OK.
14. Hanich, L. and Thompson, C., 2001, "Validation of a Novel Algorithm for the Adaptive Calculation of Transient Stratified Flow of Gas, Oil, and Water in Pipelines," *Int. J. Numer. Meth. Eng.*, **51**: 579–607.
15. Hinze, J., 1955, "Fundamentals of the Hydrodynamic Mechanism of Splitting in Dispersion Process," *AIChE J.*, **1** (3): 289- 295.
16. Karami, H., 2015, "Low Liquid Loading Three-Phase Flow and Effects of MEG on Flow Behavior," Ph.D. Dissertation, U. of Tulsa, Tulsa, OK.
17. Keskin, C., Zhang, H.-Q., Sarica, C., 2007, "Identification and Classification of New Three-Phase Gas/Oil/Water Flow Patterns," SPE 110221, Presented at the SPE ATCE, Anaheim, California, November 11-14.
18. Khor, S.H., Mendes-Tatsis, M.A., Hewitt, G.F., 1997, "One-Dimensional Modelling of Phase Holdups in Three-Phase Stratified Flow," *Int. J. of Multiphase Flow* **23** (5): 885–897.
19. Oddie, G., Shi, H., Durlofsky, L.J., Aziz, K., Pfeffer, B., and Holmes, J.A., 2003, "Experimental Study of Two and Three Phase Cows in Large Diameter Inclined Pipes," *Int. J. of Multiphase Flow*, **29** (4): 527–558.

20. Pan, L., 1996, “High Pressure Three-Phase (Gas/Liquid/Liquid) Flow,” Ph.D. Dissertation, Imperial College, London, UK.
21. Pothapragada, V.K., 1996, “Transient Aspect of Unloading Gas-Lift Wells,” M.S. Thesis, U. of Tulsa, Tulsa, OK.
22. Sarica, C. and Shoham, O., 1991, “A Simplified Transient Model for Pipeline-Riser Systems,” *Chem. Eng. Science*, **46** (9): 2167-2179.
23. Scoggins, M.W., 1977, “A Numerical Simulation Model for Transient Two-Phase Flow in a Pipeline,” Ph.D. Dissertation, U. of Tulsa, Tulsa, OK.
24. Sharma, Y., 1985, “Modeling Transient Two-Phase Slug Flow,” Ph.D. Dissertation, U. of Tulsa, Tulsa, OK.
25. Shirdel, M. and Sepehrnoori, K., 2016, “Development of Transient Mechanic Three-Phase Flow Model for Wellbores,” SPE 180928, *SPE Journal*, **22** (1).
26. Sobocinski, D.P., 1955, “Horizontal, Co-Current Flow of Water, Gas-Oil and Air,” M.S. Thesis, University of Oklahoma, Norman, OK.
27. Taitel, Y. and Dukler, A.E., 1976, “A Model for Predicting Flow Regime Transitions in Horizontal and Near Horizontal Gas- Liquid Flow,” *AIChE J.* **22** (1): 47-55.
28. Taitel, Y., Barnea, D., and Brill, J. P., 1995, “Stratified Three-Phase Flow in Pipes,” *Int. J. Multiphase Flow* **21** (1): 53-60.
29. Taitel, Y., Shoham, O., and Brill, J., 1989, “Simplified Transient Solution and Simulation of Two-Phase Flow in Pipelines,” *Chem. Eng. Science*, **24** (6): 1353-1359.
30. Tang, Y., 1998, “Transient Dynamic Characteristic of Gas-Lift Unloading”. M.S. Thesis, U. of Tulsa, Tulsa, OK.

31. Woods, G.S., Spedding, P.L., Watterson, J.K. and Raghunathan, S., 1998, "Three-Phase Oil/Water/Air Vertical Flow," *Trans. IChemE* **76A**: 571–584.

32. Zhang, H.-Q., 2014, "A Unified Model for Transient Multiphase Flow in Wells and Pipelines," TUALP Advisory Board Meeting (ABM) Report, pp. 98-124.

33. Zhang, H.-Q., Wang, Q., and Brill, J. P., 2003, "A Unified Mechanistic Model for Slug Liquid Holdup and Transition Between Slug and Dispersed Bubble Flows," *Int. J. Multiphase Flow*, **29**: 97–107.

34. Zhang, H.-Q., Vuong, D.H., and Sarica, C., 2011, "Modeling High-Viscosity Oil/Water Cocurrent Flows in Horizontal and Vertical Pipes," SPE 135099, Presented at the SPE ATCE, Florence, Italy, September 20-22.

35. Zhang, H.-Q., Wang, Q., Sarica, C., and Brill, J.P., 2003, "Unified Model for Gas-Liquid Pipe Flow via Slug Dynamics – Part 1: Model Development," *J. Energy Res. Tech.* **125** (4): 266-273.

36. Zhang, H.Q. and Sarica, C., 2006, "Unified Modeling of Gas/Oil/Water Pipe Flow—Basic Approaches and Preliminary Validation," *SPE Project Facilities & Construction* **1**(2), pp. 1-7.

APPENDIX A

SETUPS FOR MODEL VERIFICATIONS

Table A-1: Three-Layer Stratified Flow Conditions

Pipe length (m)	40	Gas density (kg/m^3)	1.5
Outlet pressure (Pa)	200000	Oil density (kg/m^3)	850
Pipe diameter (m)	0.0508	Water density (kg/m^3)	1000
Gas superficial velocity (m/s)	0.1-2.5	Gas viscosity (kg/m-s)	0.0000189
Liquid superficial velocity (m/s)	0.01	Oil viscosity (kg/m-s)	0.01715
Water cut (%)	40-80	Water viscosity (kg/m-s)	0.001

Table A-2: Slug Flow with Stratified Film and Slug Conditions

Pipe length (m)	40	Gas density (kg/m^3)	1.5
Outlet pressure (Pa)	200000	Oil density (kg/m^3)	850
Pipe diameter (m)	0.0508	Water density (kg/m^3)	1000
Gas superficial velocity (m/s)	0.1-0.5	Gas viscosity (kg/m-s)	0.0000189
Liquid superficial velocity (m/s)	0.2	Oil viscosity (kg/m-s)	0.01715
Water cut (%)	40-60	Water viscosity (kg/m-s)	0.001

Table A-3: Low Liquid Loading Flow Conditions

Pipe length (m)	112.8	Gas density (kg/m^3)	1.9
Outlet pressure (Pa)	160000	Oil density (kg/m^3)	760
Pipe diameter (m)	0.1524	Water density (kg/m^3)	995
Gas superficial velocity (m/s)	9.5-22.6	Gas viscosity (kg/m-s)	0.000018
Liquid superficial velocity (m/s)	0.01	Oil viscosity (kg/m-s)	0.00127
Water cut (%)	20-80	Water viscosity (kg/m-s)	0.0009

Table A-4: Flow Pattern Maps Flow Conditions

Pipe length (m)	40	Gas density (kg/m^3)	1.5
Outlet pressure (Pa)	200000	Oil density (kg/m^3)	850
Pipe diameter (m)	0.0508	Water density (kg/m^3)	1000
Gas superficial velocity (m/s)	0.01-10	Gas viscosity (kg/m-s)	0.0000189
Liquid superficial velocity (m/s)	0.01-10	Oil viscosity (kg/m-s)	0.01715
Water cut (%)	20-60	Water viscosity (kg/m-s)	0.001